KATHOLIEKE UNIVERSITEIT LEUVEN
FACULTEIT DER TOEGEPASTE WETENSCHAPPEN
DEPARTEMENT WERKTUIGKUNDE
AFDELING PRODUKTIETECHNIEKEN,
MACHINEBOUW EN AUTOMATISERING
Celestijnenlaan 300B - B-3001 Leuven (Heverlee), Belgium

ROBOTIC FILAMENT WINDING OF ASYMMETRIC COMPOSITE PARTS

Jury :
Voorzitter :
Prof.dr.ir. J.Berlamont, vice-dekaan
Leden :
Prof.dr.ir. H. Van Brussel, promotor
Prof.dr.ir. I. Verpoest
Prof.dr.ir. J. De Schutter
Ing. P. Vanherck
Prof.dr.ir. J.P. Kruth
Prof.dr.ir. W. De Wilde (VUB)

Proefschrift voorgedragen tot
het behalen van het doctoraat
in de toegepaste wetenschappen

door

Johan Scholliers

U.D.C. 621.763:681.3*I29 December 1992

D/1992/5769/14
ISBN 90-73802-21-0

Graag had ik een woord van dank gericht aan de personen die dit doktoraatswerk hebben mogelijk gemaakt.

Vooreerst wens ik Prof. Van Brussel te danken, die mij de kans heeft gegeven dit onderzoek te doen, voor zijn steun en daadwerkelijke begeleiding.

Verder wil ik Paul Vanherck, bij wie ik steeds terecht kon voor alle technische problemen, bedanken. De leden van het leescommittee, Prof. Verpoest en Prof. De Schutter dank ik voor het kritisch nalezen van dit werk. De voorzitter en de leden van de jury, Prof. Berlamont, Prof. Kruth en Prof. De Wilde, wil ik danken voor hun bereidwillige medewerking.

Dit onderzoek werd mede gefinancierd door de firma Fabricom. Graag had ik hen, en vooral Mr. Van de Bruaene, hiervoor hartelijk bedankt.

Verder wens ik mijn collega's van de composietgroep op PMA *te danken voor de goede samenwerking : Mieke Lossie, Dirk Bastiaensen, Jonas de Carvalho en Begoña Bustinza. Mieke wil ik danken voor de talrijke discussies over het ontwerp van komposieten, Dirk voor zijn hulp bij het ontwerp van de wikkelmachine, Jonas en Begoña voor hun hulp bij het wikkelen. Mieke, Jonas, Wim en Dirk wil ik ook nog bedanken voor het nalezen van de tekst. Ook wil ik alle studenten bedanken die onderzoek hebben verricht in het kader van dit doktoraat.*

Een speciaal woord van dank ook aan Dr. Martine Wevers en Luk Peeters van het departement MTM *voor hun hulp bij het ultrasoon C-scannen.*

Ook wens ik mijn collega's aan de afdeling PMA *en de leden van de komposietgroep op* MTM *te danken voor de aangename werkatmosfeer.*

Tot slot wens ik nog Mervi, mijn ouders, familieleden en vrienden te danken voor hun steun en aanmoediging.

Johan Scholliers
Heverlee, November 1992

Abstract

Filament winding is a production technique for continuous fibre reinforced composite parts, in which impregnated fibre bundles are guided through a pay-out eye on a rotating mandrel. In the tape winding process a tape is used instead of separate fibre bundles.

A computer-integrated environment has been developed round the winding process, including design, production and quality control.

A program has been generated for the calculation of fibre paths on a part, which is designed in a CAD-system. A design methodology has been developed, which is not restricted to axisymmetric and almost-axisymmetric parts, but also applies to complete asymmetric parts.

A robotic tape winding cell has been constructed, which consists of a PUMA-762-robot and two external axes : the winding axis, that rotates the mandrel, and the pay-out eye axis, which allows to maintain a constant band width. Starting from the data of the fibre paths, a collision-free off-line robot program is generated. To avoid collisions, a heuristic collision control method has been developed. A tape wound T-piece has been designed and produced.

For quality control, a robotic ultrasonic C-scanning cell has been constructed.

Samenvatting : Gerobotiseerd wikkelen van asymmetrische composietvoorwerpen

Inleiding

Vezelversterkte kunststoffen worden steeds meer toegepast omwille van hun laag gewicht, hoge specifieke sterkte en stijfheid en goed chemische bestendigheid. Het ontwerp van composietstructuren verschilt sterk van het ontwerp van metalen componenten door het anisotrope karakter van composietmaterialen. Deze anisotropie kan gebruikt worden om de eigenschappen van de structuur aan te passen aan de wensen van de klant.

Voor een nauwkeurige produktie van composietstructuren werden een aantal geautomatiseerde processen ontwikkeld zoals (draad)wikkelen, bandwikkelen, bandplaatsing, pultrusie,... In het (draad)wikkelproces worden een aantal vezelbundels, die met hars geïmpregneerd zijn, door een wikkeloog op een roterende mal geleid. Een alternatief voor het (draad)wikkelproces is het bandwikkelproces, waarbij een band gebruikt wordt in plaats van vezelbundels. Dit proces vereist minder investeringskosten, daar slechts één afwikkeleenheid vereist is, maar heeft als nadeel dat de band gemakkelijk rimpelt.

Opdat het produktieproces nauwkeurig zou zijn, moet de vezel foutvrij op de mal geplaatst worden, op de plaats die berekend werd. Deze voorwaarde legt beperkingen op aan het verloop van de vezelpaden, en beperkt zo de vrijheid in het ontwerp van de composietstruc-

tuur. Het ontwerp is hierdoor een compromis tussen hetgeen optimaal is volgens sterkte- en stijfheidsvereisten en hetgeen wikkelbaar is. Het ontwerp van een gewikkelde structuur vereist hierdoor een coördinatie van de sterkteberekeningen en de berekening van de vezelpaden.

Dit werk beschrijft de constructie van een computer-geïntegreerde wikkelomgeving, die zowel het ontwerp, de produktie als de kwaliteitscontrole omvat. Voor het ontwerp wordt het ontwerp van de mal met een CAD-systeem, de sterkteberekeningen met een eindige-elementenpakket en de berekening van vezelpaden met eigen toepassingsprogramma's gecoördineerd.

Een gerobotiseerde wikkelinstallatie werd ontwikkeld, bestaande uit een PUMA-762 van Unimation en een externe as. De installatie werd aangepast voor het bandwikkelen door het toevoegen van een rotatievrijheid in het wikkeloog. Uitgaande van de vezelpaden wordt een off-line robotprogramma gegenereerd, dat in de robot geladen wordt.

Kwaliteitscontrole gebeurt met een gerobotiseerde ultrasone techniek.

Hoofdstuk 1 : Wikkelen

1.1 Fabricatie van composietstructuren

De basismaterialen voor composietmaterialen zijn vezels (glas, koolstof, aramide) en het matrixmateriaal, meestal een polymeerhars. Voor sterk belaste structuren worden vooral continue vezels gebruikt. Harsen worden onderverdeeld in twee klassen : thermoharders (epoxy, polyester,...) en thermoplasten (PEEK,polypropyleen,...). Thermoharders worden nog steeds het meest gebruikt. De vezels kunnen apart gebruikt worden (als vezelbundels, banden of weefsels), of vezel en hars kunnen reeds samengevoegd zijn (bv. prepreg, een reeds gedeeltelijk uitgehard materiaal).

Het fabricatieproces van composieten bestaat uit vier stappen : impregnatie, laminering, consolidatie en uitharding.

Impregnatie kan plaatshebben voor of tijdens het fabricatieproces. Impregnatie tijdens fabricatie heeft het voordeel dat de materiaalkost sterk wordt gereduceerd, maar de procesparameters dienen goed onder controle gehouden te worden om een reproduceerbare kwaliteit te bekomen.

Voor de **laminering** kunnen verschillende technieken gebruikt worden, zoals wikkelen, bandplaatsing,.... *Wikkelen* is een produktieproces voor continue vezelversterkte composieten, waarbij met hars geïmpregneerde vezelbundels onder gecontroleerde spanning door een wikkeloog op een roterende mal geleid worden. *Bandwikkelen* gebruikt een band in plaats van een aantal parallelle vezelbundels. Bij bandplaatsing *tape laying* wordt een band op een mal geplaatst en aangedrukt. *Vezelplaatsing* is een combinatie van wikkelen en bandplaatsing : vezelplaatsing gebruikt parallelle vezelbundels, drukt deze aan op de mal, en kan tijdens het proces de bandbreedte wijzigen door vezelbundels toe te voegen of weg te nemen. Bij *pultrusie* worden met hars geïmpregneerde vezels door een matrijs getrokken. De technieken waarbij de impregnatie tijdens het proces gebeurt (wikkelen en pultrusie) zijn de goedkoopste, door de geringe materiaalkost. Pultrusie is de goedkoopste methode, maar is voornamelijk beperkt tot structuren met constante doorsnede.

Voor een nauwkeurige plaatsing van de vezels tijdens het wikkelen mogen de vezelbundels niet slippen op het oppervlak. De dwarskracht op de vezel moet daarvoor kleiner zijn dan de maximale wrijvingskracht tussen de vezel en het onderliggende materiaal. De slipneiging λ wordt gedefinieerd als de verhouding tussen de dwarskracht en de normaalkracht op de vezel. De stabiliteitsvoorwaarde wordt dan :

$$|\lambda| \leq \mu$$

met μ de statische wrijvingscoëfficiënt. Wanneer $\lambda = 0$, werkt er geen dwarskracht op de vezel, en komt het vezelpad overeen met een *geodeet* op het oppervlak. Een stabiel vezelpad dat afwijkt van een geodeet wordt een *semi-geodeet* genoemd. Op convex/concave oppervlakken kan *brugvorming* optreden, i.e. het loskomen van de vezel van het oppervlak.

Tijdens het bandwikkelen en bandplaatsing zijn alleen geodeten toegelaten, om rimpelen van de band te vermijden. Vezelplaatsing laat grotere afwijkingen van de geodeten toe, maar vereist grote investeringskosten.

Tijdens **consolidatie**, die vaak vervat is in de laminering of de uitharding, wordt van de afzonderlijke lagen een compact materiaal gevormd, zonder luchtbellen en delaminaties.

Thermohardende harsen vereisen een **uithardingscyclus** om hun intermoleculaire netwerkstructuur te bekomen, wat tot lange fabrica-

tietijden leidt. Thermoplasten moeten daarentegen alleen gesmolten en vervormd worden onder hoge temperatuur en druk. Tijdens het wikkelen van thermoplasten wordt de thermoplastische prepreg gelast aan het reeds gewikkelde materiaal, door het hars lokaal te smelten en aan te drukken.

1.2 Het Wikkelproces

Een wikkelmachine bestaat uit een voedingseenheid (afwikkeleenheid, harsbad en spanningsregeling), een voedingsoog, en een aandrijfas voor de mal. De meeste wikkelmachines zijn gebouwd volgens het draaibankprincipe : de mal wordt op de spindel gemonteerd, het voedingsoog op de dwarse slede. Wikkelmachines zijn geëvolueerd van eenvoudige twee-assige machines met tandwieloverbrengingen tot complexe 7-assige computer-gestuurde machines. Door de slede van de wikkelmachine door een industriële robot te vervangen wordt de flexibiliteit verhoogd en kunnen de investeringskosten verminderd worden, aangezien robots in veel grotere series geproduceerd worden. De mal moet zo ontworpen zijn dat zij na het uitharden verwijderd kan worden en dat zij niet te veel vervormt tijdens het wikkelen en uitharden. De uiteinden van de mal moeten zo ontworpen worden dat het vezelpad kan terugkeren, eventueel door gebruik van eindkappen of stralenkransen.

Tijdens het wikkelen moeten de vezel-hars-verhouding en de interlaminaire druk zo constant mogelijk gehouden worden. De vezel-hars-verhouding wordt vooral beïnvloed door de impregnatie, de interlaminaire druk vooral door de vezelspanning en de kromtestraal van het pad. Indien een vaste afwikkeleenheid gebruikt wordt, ondergaat de vezel veel richtingsveranderingen. De spanning in de vezel stijgt bij iedere richtingsverandering. Om een constante vezelspanning te bekomen, moet de spanning gecontroleerd worden aan het uiteinde van het wikkeloog, wat evenwel zeer moeilijk is. In de praktijk wordt de spanning meestal gecontroleerd aan de afwikkeleenheid, waardoor de spanning in het wikkeloog echter niet constant is.

Aan de afdeling PMA werden twee wikkeleenheden ontwikkeld : een twee-assige machine voor het wikkelen van axisymmetrische voorwerpen, en een gerobotiseerde wikkelinstallatie. De gerobotiseerde cel bestaat uit een zesassige PUMA-762 en een externe as (wikkelas), die de mal roteert. Het wikkeloog wordt op de robotpols bevestigd.

Daarnaast werden ook een impregnatiebad en spanningsinstallaties ontworpen voor zowel inwendige als uitwendig afwikkelbare bobbijnen en voor kleine bobbijnen met banden.

Hoofdstuk 2 : Computer-geïntegreerde Wikkelomgeving

De toenemende complexiteit van malgeometrieën vereist het gebruik van geavanceerde programmatuur voor het ontwerp en de produktie van gewikkelde structuren. Een computer geïntegreerde omgeving dient rond het wikkelproces ontwikkeld te worden om ontwerp en produktie te automatiseren en de ontwerp- en produktie-kosten te drukken.

2.1 Wikkelomgeving

De wikkelomgeving omsluit zowel het ontwerp, de produktie als de kwaliteitscontrole. Het ontwerp bestaat uit drie taken : het ontwerp van de mal, de berekening van de sterkte, en het ontwerp van de vezelpaden. Voor het ontwerp van de mal wordt een CAD-systeem gebruikt en voor de sterkteberekeningen een eindige-elementenpakket. Voor de berekening van vezelpaden werd het programma **CAWAR** ontwikkeld. Informatie dient uitgewisseld te worden tussen de verschillende pakketten. Voor de berekening van de vezelpaden heeft **CAWAR** de mathematische beschrijving van de mal in het CAD-model nodig. De vezelpaden, die in **CAWAR** berekend worden, worden voorgesteld in het CAD-systeem. Met behulp van de FEM-preprocessor in het CAD-systeem wordt het invoer-bestand voor het eindige-elementenpakket gegenereerd. Uit de eindige-elementenberekeningen worden de optimale vezelrichtingen bepaald, die in het programma **CAWAR** kunnen ingevoerd worden. De laminaatopbouw van het eindige-elementenmodel wordt bepaald uitgaande van het verloop van de vezelpaden. Het invoer-bestand van het eindige-elementenpakket wordt dan automatisch aangepast.

Uitgaande van de vezelpaden wordt een off-line machineprogramma opgesteld. Eerst worden de posities van het wikkeloog bepaald, dan de snelheid in de verschillende posities en tenslotte de gegevens die naar de machine doorgestuurd worden. Het programma wordt gesimuleerd

in het simulatieprogramma IGRIP.

Voor de kwaliteitscontrole werd, in samenwerking met het departement MTM, een gerobotiseerde ultrasone C-scan techniek ontwikkeld. De programmatuur, die hiervoor ontwikkeld werd, is analoog aan de wikkelprogrammatuur : eerst wordt het pad bepaald en dan de posities van de robot.

2.2 Programmatie in een CAD-omgeving

Zowel voor het wikkelen als voor het scannen wordt de geometrie van het voorwerp beschreven in een CAD-systeem. De berekening van het robotpad gebeurt in een toepassingsprogramma, dat met het CAD-systeem moet communiceren.

Toepassingsprogramma's kunnen ofwel in het CAD-systeem geschreven worden, ofwel kan informatie uitgewisseld worden met behulp van neutrale formaten. Programmeren in het CAD-systeem kan op twee manieren : met behulp van de grafische programmeertaal van het systeem (bv. GRIP in Unigraphics) ofwel door gebruik van een neutrale programmeer-interface (bv. BM-interface). De grafische programmeertaal is systeem-afhankelijk en bestrijkt niet al de mogelijkheden van het CAD-systeem. De neutrale programmeer-interface vereist daarentegen een open CAD-systeem. Neutrale formaten zijn ontwikkeld voor de uitwisseling van tekeningen tussen verschillende systemen. IGES is het meest verspreide gestandaardiseerde neutrale formaat.

Een toepassingsprogramma dat een neutraal formaat gebruikt, moet eerst de nuttige informatie in het bestand zoeken, en dan omzetten naar het interne formaat van het programma. Voor de invoer (en de uitvoer) kan een programma in het CAD-systeem gebruikt worden, dat via bestanden informatie met het toepassingsprogramma uitwisselt.

Het programma **CAWAR** berekent vezelpaden voor een voorwerp dat ontworpen werd in een CAD-systeem. De geometrische informatie van het oppervlakkenmodel wordt uit een IGES-bestand geëxtraheerd. **CAWAR** berekent naast vezelpaden ook de robotpaden, de sequenties van de paden en de gegevens die naar de robot moeten doorgestuurd worden.

2.3 Gerobotiseerd Ultrasoon C-scannen

Voor de kwaliteitscontrole wordt een gerobotiseerde ultrasone puls-echo C-scan techniek met waterstraaltransmissie gebruikt. De ultrasone transducer is in een sproeikop geplaatst, die op de pols van de PUMA-762-robot bevestigd wordt. De sproeikop wordt loodrecht op het oppervlak geplaatst. Een veer tussen sproeikop en robotpols compenseert fouten in de beweging van de robot. Uitgaande van een CAD-beschrijving van het voorwerp, wordt, met behulp van de BM-interface, een raster van punten en normalen op het oppervlak geplaatst. De hiermee overeenstemmende robotposities worden berekend, en naar de robot doorgestuurd. Tijdens het scannen wordt een interpolatie tussen de rasterpunten uitgevoerd om de gewenste resolutie te bereiken. De meetresultaten worden binnengelezen in de PC en naar de VAX-computer doorgestuurd, waar de resultaten op een werkstation grafisch worden weergegeven. Het scannen is op dit ogenblik nog traag, daar slechts één punt per robotcyclus wordt ingelezen, maar de snelheid kan opgevoerd worden door, evt. met behulp van een andere computer, meerdere punten per cyclus in te lezen.

Een geïmpacteerde plaat, een gewikkelde cilinder en een composieten auto-onderdeel werden gescand. Goede resultaten werden bekomen voor gladde oppervlakken met constante dikte. De resultaten voor gewikkelde structuren waren niet zo goed, omwille van de ruwheid van het gewikkelde voorwerp en diktevariaties.

Hoofdstuk 3 : Ontwerp van Gewikkelde Voorwerpen

Het ontwerp van een gewikkeld voorwerp bestaat uit het ontwerp van de malgeometrie en het ontwerp van de vezelpaden. De geometrie van het voorwerp kan volledig gedetermineerd zijn, ofwel kan het ontwerp van de geometrie een geïntegreerd deel van het ontwerp van de gewikkelde structuur zijn. Het ontwerp van de mal wordt in dit werk niet behandeld.

Tijdens het (draad)wikkelen mogen de vezels niet slippen, tijdens bandwikkelen mogen de banden niet rimpelen. Draadwikkelen laat afwijkingen van geodeten toe, bandwikkelen niet.

3.1 Berekening van Vezelpaden

3.1.1 Literatuuroverzicht

Vezelpaden worden in de literatuur op twee manieren berekend : analytisch en door benadering van het oppervlak. De analytische oplossing van een geodeet op een omwentelingsoppervlak resulteert in het oplossen van een integraal, alle andere gevallen tot het oplossen van één of twee differentiaalvergelijkingen. De benaderende oplossing bestaat erin het oppervlak te benaderen door driehoekige vlakke elementjes.

3.1.2 Semi-geodetische Vezelpaden

In dit werk wordt de analytische methode gebruikt voor het berekenen van de vezelpaden. Uitgaande van de differentiaalgeometrie worden de twee volgende vergelijkingen afgeleid :

$$\begin{cases} \vec{c} \cdot \vec{b} &= -\lambda \vec{c} \cdot \vec{n} \\ \vec{c} \cdot \vec{t} &= 0 \end{cases}$$

met $\vec{t}$ de eenheidstangent aan de kromme, $\vec{n}$ de normaal op het oppervlak, $\vec{b} = \vec{t} \times \vec{n}$ de binormaal, en $\vec{c} = \frac{d\vec{t}}{ds}$ de krommingsvector, met s de afgelegde weg op het pad. Uit dit stelsel wordt een stelsel van twee tweede-orde differentiaalvergelijkingen afgeleid. Deze differentiaalvergelijkingen worden numeriek opgelost in het programma `CAWAR`. De startvoorwaarden zijn het startpunt, de raaklijn en de slipneiging.

3.1.3 Optimaal Vezelpad

Uitgaande van een eindige-elementenberekening worden de optimale wikkelhoeken bepaald. Deze hoeken worden in het programma `CAWAR` ingevoerd. Het vezelpad wordt volgens de optimale wikkelhoek geplaatst, en in elk punt worden slipneiging en brugvorming getest. Als de slipneiging te groot is, wordt deze beperkt en het punt opnieuw berekend. Treedt brugvorming op, dan worden de laatste punten van het pad herrekend met maximale slipneiging, tot brugvorming niet meer optreedt.

3.2 Ontwerp van Vezelpaden

Een voorwerp moet zodanig ontworpen worden dat het zo licht en zo sterk mogelijk is, en zo uniform mogelijk bedekt is.

3.2.1 Isotrope Spanningsberekening

Als startpunt voor het laminaatontwerp wordt een eindige-elementenberekening uitgevoerd op een isotroop model en de optimale wikkelhoeken worden afgeleid.

3.2.2 Selectie van de Vezelpaden

De literatuur beperkt zich meestal tot het ontwerp van buisvormige structuren, i.e. voorwerpen met een centrale as. Voor deze voorwerpen wordt een vezelpad gezocht, dat over de hele omtrek herhaald wordt. Tijdens dit doctoraatswerk werd een methode ontwikkeld die ook voor volledig asymmetrische voorwerpen mogelijk is.

De methode die gebruikt wordt voor het selecteren van de vezelpaden, wordt bepaald door de vorm van de mal en het basismateriaal (vezelbundels of band).

Indien het voorwerp rotatiesymmetrisch is, dan kan een vezelpad over de hele omtrek herhaald worden. Een gelijkaardige methode wordt toegepast voor buisvormige structuren : een wikkelpatroon wordt gevormd door een basispad over de hele omtrek te herhalen. Het basispad wordt in de twee-dimensionele parametervoorstelling van het oppervlak over een constante afstand verschoven volgens de parameter die overeenkomt met de omtreksrichting. Het basispad moet zo gekozen worden dat nergens op het voorwerp slip of brugvorming optreedt.

Indien een dergelijk basispad niet kan gevonden worden, moet elk vezelpad afzonderlijk berekend worden. De vezelpaden die mogelijk zijn op het voorwerp worden eerst onderzocht. Daarvoor worden "kaarten" gemaakt, die, in functie van de startpositie en startraaklijn (en evt. slipneiging) de mogelijke vezelpaden op het voorwerp aangeven. Vezelpaden, waarbij brugvorming optreedt, worden geschrapt. Eén vezelpad wordt als basispad gekozen. Dit basispad wordt verplaatst over de bandbreedte, zolang slip of brugvorming niet optreden. Het basispad wordt zo gekozen, dat een zo breed mogelijke band van parallelle vezelpaden ontstaat.

Tijdens bandwikkelen zijn alleen geodeten toegestaan. Hierdoor kunnen volledig parallelle vezelpaden niet gevonden worden. De vezelpaden moeten zo gekozen worden dat spleten en overlappingen tussen twee aangrenzende vezelpaden zo klein mogelijk zijn.

3.2.3 Volgorde van de Vezelpaden

Na het bepalen van het verloop van de vezelpaden, dient de volgorde waarin de vezelpaden gewikkeld worden, bepaald te worden. Deze padvolgorde beïnvloedt de sterkte, vooral als er buigspanningen in het voorwerp optreden. De vezelpaden moeten steeds starten aan de stralenkrans, waar het vorige vezelpad geëindigd is. De overspanning op de stralenkrans mag niet te klein zijn, om te vermijden dat de vezels van de pinnen afglijden, maar mag ook niet te groot zijn, om materiaalverlies te minimaliseren. De rotatierichting van het vezelpad rond de as van de stralenkrans blijft bij voorkeur behouden, om te vermijden dat de vezel van de stralenkrans schuift.

3.2.4 Laminaatopbouw en Sterkteberekening

Na het bepalen van de padvolgorde wordt de laminaatopbouw in het eindige-elementenpakket bepaald, en een eindige-elementenanalyse op het composietmodel uitgevoerd. Indien de sterkte onvoldoende is, wordt het vezelpaden-ontwerp aangepast, ofwel worden supplementaire versterkingen (bv. matten) voor of na het wikkelen aangebracht.

3.3 T-stuk

Tijdens dit doktoraatswerk werd een composiet T-stuk ontworpen en gewikkeld. Het T-stuk (Fig. 1) wordt gemodelleerd als 8 verschillende oppervlakken. Aan de drie uiteinden van de mal zijn stralenkransen bevestigd.

Het T-stuk werd gewikkeld met 25-mm brede glasvezelbanden. Hierdoor zijn alleen geodeten toegelaten.

Een spanningsberekening werd eerst uitgevoerd op een isotroop model. Deze berekening wees uit dat de grootste spanningen optreden in de vlakke stukken (oppervlakken 7 en 8 in Fig. 1). Kaarten werden vervaardigd om de geodeten die op het T-stuk mogelijk zijn na te gaan. Het grootste probleem in het vezelpadenontwerp is het grote percentage vezelpaden waar brugvorming optreedt, als gevolg van de convex-concave afronding (torus 4 en 5). De nadruk tijdens het ontwerp van het gewikkeld T-stuk ligt hierdoor vooral op de keuze van de wikkelpaden, zo dat de mal volledig bedekt wordt. Een aantal patronen werd geselecteerd, die bestaan uit een aantal quasi-parallelle

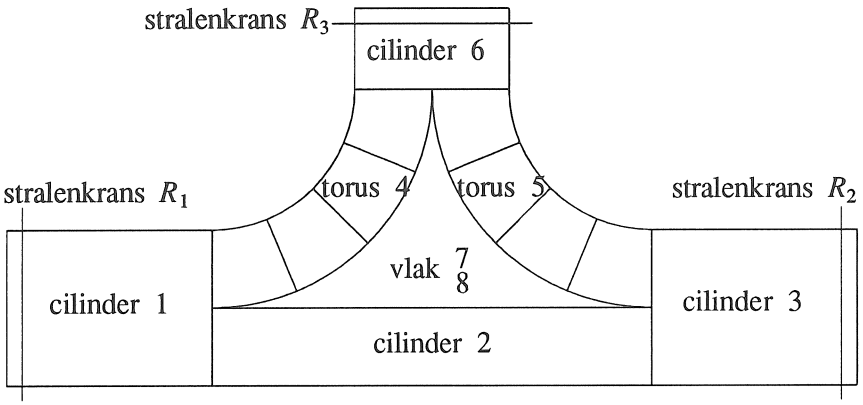

Figuur 1 : T-stuk

geodeten, en die een zo breed mogelijke band vormen. Een eindige-elementenberekening werd op een composietmodel uitgevoerd als controle van de sterkte.

Hoofdstuk 4 : Gerobotiseerd Bandwikkelen

Bandwikkelen vereist een kleinere investeringskost, aangezien slechts één spanningsregelaar vereist is. Banden rimpelen daarentegen zeer gemakkelijk door hun geringe stijfheid in de dwarsrichting, en moeten dus met de nodige voorzichtigheid behandeld worden.

De gerobotiseerde wikkelcel, die bestaat uit een PUM-762-robot en een externe as voor de rotatie van de mal, werd aangepast voor het wikkelen met banden.

4.1 Ontwerp van de Gerobotiseerde Bandwikkeleenheid

De taakvereisten voor het bandwikkelproces zijn :

- het uittreepunt van de vezel in het voedingsoog moet op de raaklijn aan het vezelpad gelegen zijn.
- de breedte van de band moet constant zijn.
- botsingen zijn niet toelaatbaar.

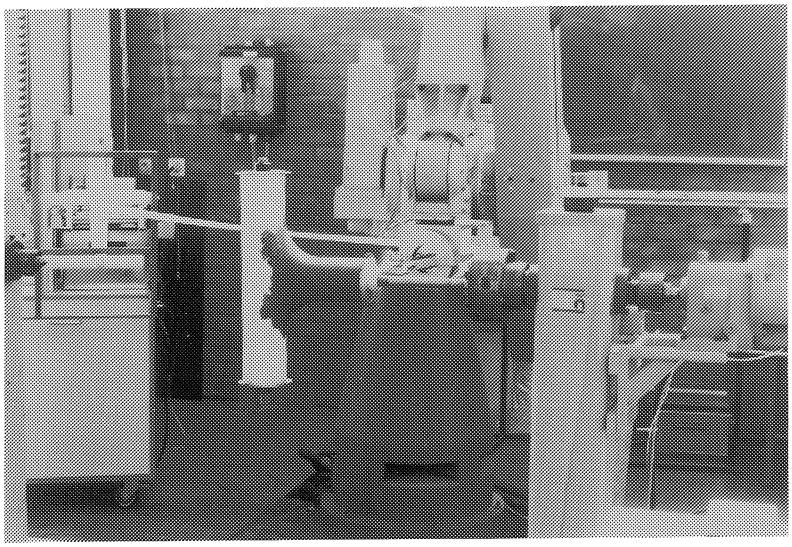

Figuur 2 : Gerobotiseerde bandwikkelcel

- de band mag niet rimpelen. De bandtorsie, i.e. de rotatie van de vezel rond zijn lengteas mag daarvoor niet te groot worden.
- de band moet steeds onder spanning staan.

Om aan alle vereisten te voldoen, inclusief botsingsvermijding, zijn 6 vrijheidsgraden nodig.

Aan de wikkelinstallatie werd een rotatieas in het wikkeloog rond de voedingsrichting toegevoegd, om een constante bandbreedte te kunnen garanderen (Fig. 2). De wikkelcel heeft hierdoor in totaal 8 vrijheidsgraden, ofwel 2 redundante vrijheidsgraden. Deze redundantie wordt opgelost door twee rotatievrijheidsgraden van de robotpols niet te gebruiken. De normaal op de robotflens wordt steeds verticaal naar beneden gericht. De as van het wikkeloog is hierdoor steeds horizontaal. De zesassige robot zou hierdoor vervangen kunnen worden door een goedkopere vierassige robot.

Aan het uiteinde van het wikkeloog wordt de band tussen twee rollen geleid. De band moet zo goed mogelijk gecentreerd zijn in deze rollen. Door de geringe stijfheid in de dwarsrichting, kan de band niet in de dwarsrichting geleid worden. De neiging van de band om te slippen tussen de rollen wordt zo klein mogelijk gehouden door de twee rollen zo goed mogelijk tegen elkaar te drukken. Het wikkeloog werd zo ontworpen, dat een zo groot mogelijke torsie tussen de ingang en het

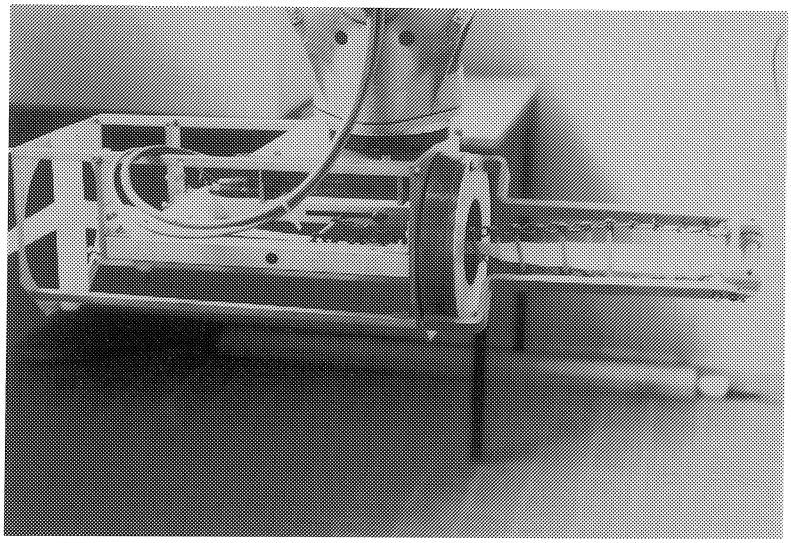

Figuur 3 : Wikkeloog

uittreepunt van het wikkeloog kan opgeslagen worden, door gebruik van een flexibele ladder (Fig. 3). De ladder is flexibel voor torsie, en kan een bandtorsie van 360° opnemen zonder rimpelen van de band. Torsies tussen de ingang van het wikkeloog en het impregnatiebad worden vermeden door de band op die plaatsen over twee verticale staven te leiden.

4.2 Sturing van de robotinstallatie

De PUMA-762 is een robot van de eerste generatie, wiens programmeertaal niet rechtstreeks toelaat een externe as synchroon met de robotassen te bewegen. De ALTER-mode van de PUMA-762 laat echter wel toe het pad te wijzigen tijdens de beweging. Een externe PC stuurt in deze mode om de 28 ms posities door naar de robot. Deze mode wordt ook gebruikt voor het wikkelen. Na het sturen van de gegevens naar de robot worden de externe assen aangestuurd. Het sturingsalgoritme voor de externe assen is gebaseerd op een combinatie van feed-forwardsturing en terugkoppeling.

Een elektrische controlekring is ontworpen voor het detecteren van fouten. Indien een fout gedetecteerd wordt, worden de robot en de externe assen in de laatst doorgestuurde positie gehouden.

Hoofdstuk 5 : Off-Line Robotprogramma

In het vorige hoofstuk werd het ontwerp van de wikkelmachine besproken. Dit hoofdstuk behandelt de generatie van het off-line robot programma voor het bandwikkelen. De generatie van het off-line robotprogramma bestaat uit drie delen : de berekening van de posities van de robotpols (het pad), van de snelheid van de robotpols (het traject = posities en tijdsinformatie), en de generatie van de gegevens die naar de robot moeten doorgestuurd worden. De detectie en vermijding van botsingen, één van de belangrijkste problemen bij het wikkelen van convex-concave structuren, wordt in het volgende hoofdstuk apart behandeld.

5.1 Robotpad

Het vezelpad wordt eerst ingelezen, eventueel rekening houdend met een symmetrietransformatie. Het pad achter de stralenkransen wordt bepaald.

Het uittreepunt in het wikkeloog moet op de raaklijn aan het vezelpad gelegen zijn. De vrije lengte wordt constant gehouden, om terugwikkelen van de band in de uittreerollen te vermijden. De oriëntatie van de as van het wikkeloog wordt bepaald door een strategie, bv. de as van het wikkeloog wordt gealigneerd met de raaklijn aan het vezelpad. De oriëntatie van de uittreerollen wordt bepaald, zo dat de bandbreedte constant blijft. Een correctie wordt dan uitgevoerd op de positie van het uittreepunt : de berekeningen werden tot hiertoe uitgevoerd voor het werkelijk uittreepunt, dat geen vast punt is in het wikkeloog, maar is functie van de relatieve positie van de raaklijn t.o.v. de as van het wikkeloog. Uitgaande van de oriëntatie van de raaklijn aan het vezelpad en van het wikkeloog wordt de positie van het referentie uittreepunt, dat een vast punt is in het wikkeloog, berekend.

De hoekpositie van de wikkelas wordt berekend, zo dat de as van het wikkeloog horizontaal is. Vervolgens wordt de rotatie rond de as in het wikkeloog bepaald, zo dat de normaal op de robotflens verticaal naar beneden gericht is. Door de geometrie van de flexibele ketting is deze oogrotatie beperkt tot 360°. Torsies kunnen evenwel veel groter worden, bv. tijdens het wikkelen rond een cylinder wiens as loodrecht op de wikkelas staat. Torsies kunnen op twee manieren gereduceerd

worden : door een "torsiecompensatiebeweging", en door torsies op te slaan achter de stralenkransen.

De torsiecompensatiebeweging bestaat erin zowel de mal als de robotpols over 360° rond de wikkelas te draaien, zo dat het teken van de oogrotatie verandert. Deze beweging is alleen maar mogelijk als de mal alleen in de vaste kop is opgespannen. In dit geval is er een gebied, waar de robot in zijn beweging rond de wikkelas niet door de mal gehinderd wordt.

Te grote torsies kunnen achter de stralenkransen opgeslagen worden. Tijdens de beweging achter de stralenkransen wordt het oog over een veelvoud van 180° geroteerd, zo dat de torsie die tijdens het vorige wikkelpad werd opgebouwd, gereduceerd wordt, en dat de torsies tijdens het volgende vezelpad zo laag mogelijk zijn.

5.2 Traject

De snelheid van de robot dient zo bepaald te worden dat de totale wikkeltijd zo kort mogelijk is, zonder de maximum snelheden en versnellingen van de gelederen te overschrijden. De snelheid van de vezel dient zo constant mogelijk te zijn, om een egale kwaliteit te bekomen.

De posities van de robotgelederen worden berekend met behulp van inverse kinematica. Daarna wordt de maximaal toegelaten snelheid in elk punt van het robotpad bepaald. Deze maximum toegelaten snelheid wordt bepaald door de richtingsveranderingen in het robotpad. Vervolgens worden de posities, die op constante tijdsintervallen naar de robot moeten doorgestuurd worden, berekend.

Na een transformatie naar de cartesische ruimte worden de gegevens omgezet in een geheel formaat en doorgestuurd naar de PC, die de robot aanstuurt.

5.3 T-stuk

Een T-stuk werd met een 25-mm brede band gewikkeld. De belangrijkste problemen die optreden bij het wikkelen van dit T-stuk zijn het vermijden van botsingen tussen het wikkeloog en de mal, en het vermijden van te grote bandtorsies. Om dit laatste probleem te kunnen oplossen, wordt de mal alleen in de vaste kop opgespannen.

Voor het uitvoeren van de berekeningen van het robotpad wordt getest of de torsiecompensatiebeweging wel kan uitgevoerd worden.

Indien dit niet het geval is wordt de positie van de mal of de wikkelmachine aangepast.

Hoofdstuk 6 : Botsingsvermijding

Botsingen kunnen tijdens het wikkelen optreden o.a. tussen wikkeloog en mal in convex-concave voorwerpen, wanneer de vrije lengte te klein is bij licht gekromde oppervlakken, en in de smalle ruimte tussen de stralenkransen en de vaste kop.

In de literatuur wordt veel aandacht besteed aan het zoeken van een botsingsvrij pad voor pick-and-place operaties en voor mobiele robots, en aan het bepalen van het pad voor redundante robots, maar er zijn maar weinig artikels over botsingscontrole wanneer de taak t.o.v. een oppervlak gedefinieerd is.

Tijdens dit doctoraatswerk werd een heuristisch botsingsvermijdingsalgoritme voor het wikkelen ontwikkeld. De meest voorkomende botsingen (i.e. botsingen tussen enerzijds wikkeloog en robotpols, en anderzijds mal, klauwen en vaste en losse kop) worden nagegaan en vermeden.

Botsingen kunnen in twee klassen verdeeld worden : degene die onafhankelijk zijn van de positie van de wikkelas (i.e. botsingen tussen het wikkeloog en de mal) en degene die wel afhankelijk zijn van de positie van de wikkelas (de rest van de botsingen). Botsingsvermijding wordt gespreid over twee fasen : eerst worden botsingen tussen de mal en het wikkeloog vermeden in het malassenstelsel, dat vast verbonden is aan de mal; in een tweede fase worden de rest van de botsingen (i.e. botsingen tussen de robotpols en de mal en botsingen met de steunen) en de bereikbaarheid van de positie van het wikkeloog door de robot gecontroleerd in het wikkelassenstelsel, dat vast verbonden is aan de wikkelmachine. In beide gevallen worden eerst alle punten op botsingen gecontroleerd, daarna wordt de methode bepaald die gebruikt wordt om botsingen te vermijden, dan worden botsingsvrije posities bepaald, en het pad vereffend.

Het wikkeloog wordt gemodelleerd als een cilinder. De oriëntatie van de uittreerollen heeft hierdoor geen invloed op het optreden van botsingen. Botsingen kunnen dan getest worden door de afstand tussen de as van de cilinder en het oppervlak na te gaan. Botsingsdetectie geschiedt in verschillende fasen : eerst wordt (indien mogelijk) getest

of het centrum van de basis van de cilinder binnen een omhullend oppervlak rond de mal gelegen is, dan wordt (voor elk deeloppervlak van de mal) een test uitgevoerd op een omhullende cilinder rond het oppervlak, en, indien een botsing met de omhullende cilinder optreedt, wordt de afstand tussen de cilinder en het oppervlak getest. Indien het oppervlak een eindvlak heeft, wordt nog een test uitgevoerd op botsingen met dit eindvlak.

Bij het vermijden van botsingen wordt een onderscheid gemaakt tussen "schrammen" en "doorboren". Indien eerst voor alle punten van de botsingszone een botsingsvrije positie bepaald wordt, en het pad dat de botsingsvrije posities verbindt continu is, spreekt men van *schrammen*. *Doorboren* wordt daarentegen gekenmerkt door een discontinuïteit in het pad dat de botsingsvrije posities verbindt. Het pad is niet botsingsvrij in de discontinuïteit : het wikkeloog beweegt dwars door de mal heen.

Bij het schrammen wordt een vereffend pad bekomen door het pad, dat de botsingsvrije posities verbindt, uit te vlakken. Dit is niet mogelijk bij het doorboren : dan wordt een "via-positie" in het midden van de botsingszone bepaald.

Doorboren treedt in het malassenstelsel op als de raaklijn aan het vezelpad door het oppervlak snijdt en de zin van de normaal in het botsingspunt plots van teken verandert. In de via-positie wordt de as van het wikkeloog evenwijdig met de langsas van het oppervlak gebracht. In het wikkelassenstelsel is het mogelijk dat het eindpunt van het wikkeloog in de halfruimte achter de wikkelas rond de mal beweegt. Dit wordt vermeden door een rotatie van 360° of 180° rond de wikkelas.

Botsingen kunnen in het malassenstelsel vermeden worden door de vrije lengte of de oriëntatie van de as van het wikkeloog aan te passen. Alvorens botsingsvrije posities te bepalen, wordt nagegaan welke aanpassingen mogelijk zijn, en de meest gunstige wordt geselecteerd. Botsingen in het wikkelassenstelsel kunnen vermeden worden door de oriëntatie van de as van het wikkeloog (in een horizontaal vlak), de rotatie rond de wikkelas of de vrije lengte aan te passen. Het wikkeloog wordt eerst geroteerd in een horizontaal vlak. Indien geen oplossing gevonden wordt, wordt de rotatie rond de wikkelas aangepast, en, indien nodig, de vrije lengte.

Voor elk verschillend botsingstype en elke verschillende aanpas-

singsmethode werden aparte routines ontwikkeld. Op basis van de geometrische informatie van de botsing wordt een nieuwe positie berekend, zo dat de afstand tussen het wikkeloog en het (benaderde) oppervlak gelijk is aan een veiligheidsafstand. Botsingen worden iteratief vermeden : na het zoeken van een nieuwe positie, worden botsingen opnieuw gecontroleerd, en, zo nodig, opnieuw vermeden, waarbij de veiligheidsafstand te vergroot wordt.

Het verkrijgen van een vloeiend pad gebeurt eveneens iteratief. De afwijking tussen het oorspronkelijk pad en het botsingsvrij pad wordt gekarakteriseerd door een "correctie". Als vereffend pad wordt een parabolische functie voorgesteld. De tweede afgeleide aan het pad wordt beperkt. Uitgaande van een startwaarde, wordt voor elk punt van het botsingsinterval een correctie voorgesteld. Indien dit niet tot een botsingsvrije positie leidt, wordt, met behulp van de botsingsvermijdingsroutines, een nieuwe botsingsvrije positie bepaald. Indien de tweede afgeleide in het botsingsinterval niet steeds binnen de gewenste grenzen blijft, wordt een nieuwe iteratie uitgevoerd, rekening houdende met de nieuwe afwijkingen.

Het heuristische algoritme onderzoekt evenwel niet alle botsingen, maar alleen de botsingen die het meest frequent voorkomen. Botsingen tussen het wikkeloog en de robotgelederen, botsingen tussen de robotgelederen en de mal, en botsingen tussen het einde van het wikkeloog en de steunen van de machine zijn niet gemodelleerd. Deze botsingen komen echter maar zelden voor. Deze botsingen zouden in het algoritme kunnen geïncorporeerd worden, maar dit zou de complexiteit van het algoritme en de rekentijd gevoelig doen stijgen. Sommige botsingen kunnen in rekening gebracht worden door het geometrisch model van bv. de robotpols of de steunen aan te passen. Voor de bereikbaarheid wordt alleen getest of de positie van de robotpols binnen het werkbereik van de robot gelegen is, niet of de gewrichtsvariabelen binnen de grenzen blijven. Hierop wordt een test uitgevoerd tijdens het bepalen van het traject. Indien de grenzen van een gewrichtsvariabele overschreden worden, wordt nagegaan of er geen alternatieve configuratie van de robot mogelijk is.

De niet-gemodelleerde botsingen worden getest in het simulatieprogramma IGRIP. De posities van de robot en de beide externe assen worden naar IGRIP doorgestuurd, en de beweging van de robot wordt gesimuleerd. Indien een botsing optreedt, bv. tussen de ingang van

het wikkeloog en de robotarm, wordt de positie van de wikkelmachine gewijzigd.

Besluit

Dit doctoraatswerk behandelt de generatie van een computer-geïntegreerde omgeving rond het wikkelproces, die zowel ontwerp, produktie als kwaliteitscontrole omsluit.

Het belangrijkste deel van het ontwerp van een gewikkeld voorwerp is de berekening en de selectie van de vezelpaden. Een computerprogramma werd ontwikkeld dat vezelpaden, zowel geodetische als semi-geodetische kan berekenen op een voorwerp, dat gemodelleerd is met een CAD-oppervlakken-model.

Een ontwerpmethode voor vezelpaden werd ontwikkeld, die niet alleen voor axisymmetrische en bijna-axisymmetrische voorwerpen geldig is, maar ook voor asymmetrische voorwerpen, en zowel voor draad- als voor bandwikkelen.

Het bandwikkelen is veel meer restrictief dan het draadwikkelproces, daar alleen geodeten toegelaten zijn. Hierdoor is het veel moeilijker een egale bedekking te bekomen, aangezien twee banden nooit volmaakt parallel aan elkaar gelegd worden.

Een gerobotiseerde bandwikkelinstallatie werd ontwikkeld, die bestaat uit een PUMA-762-robot en twee externe assen : de as die de mal roteert en een rotatie in het wikkeloog rond de voedingsrichting, die een constante bandbreedte toelaat. De robot en de assen worden gestuurd vanuit een PC, die op constante tijdsintervallen sturingsgegevens naar de robot en de externe assen doorstuurt.

Uitgaande van de gegevens van de vezelpaden wordt een off-line robotprogramma gegenereerd. De generatie van het off-line programma bestaat uit drie fasen : de berekening van de posities van de robot, de berekening van de snelheid en het bepalen van de sturingsgegevens van de robot. Tijdens de berekening van de robotposities worden botsingen tussen enerzijds het wikkeloog en de robotpols, en anderzijds de mal, de klauwen en de steunen van de wikkelmachine vermeden met behulp van een heuristisch botsingsvermijdingsalgoritme. Bandtorsies worden gecontroleerd met een aangepaste beweging van robot en mal, en door torsies op te slaan achter de stralenkransen.

Voor kwaliteitscontrole werd een gerobotiseerde ultrasone puls-

echo C-scan techniek met waterstraaltransmissie ontwikkeld : een ultrasone transducer wordt in een sproeikop, die op de robotpols gemonteerd is geplaatst. De transducer beweegt volgens parallelle krommen loodrecht op het oppervlak. De C-scan techniek werkt goed voor voorwerpen met een constante dikte. Gewikkelde voorwerpen stellen evenwel problemen door de ruwheid van het oppervlak en de niet-constante dikte.

Een bandgewikkeld T-stuk werd ontworpen en vervaardigd. Het grootste probleem bij het ontwerp van het T-stuk is het verkrijgen van een volledige bedekking. Sterkteberekeningen werden uitgevoerd ter controle van de sterkte. Een T-stuk werd met banden gewikkeld.

List of Symbols

Notations

$\vec{v}, \vec{a}_b$ geometrical vector in 3D-space

$\vec{r}_p$ position vector of point p

$L_p = (p, \vec{v})$ line, starting in point p with direction $\vec{v}$ and infinite length

$\mathcal{P}$ plane

$\{a\} = \{a; \vec{t_a}, \vec{n_a}, \vec{b_a}\}$ frame in point a, with $\vec{t_a}$ as x-axis, $\vec{n}_a$ as y-axis and $\vec{b}_a$ as z-axis

${}_a x, {}_a y, {}_a z$ coordinates in frame $\{a\}$

$\mathbf{a} = [a_1\ a_2 \dots a_n]^T$ array, coordinate column vector

${}_a\mathbf{v} = [{}_a v_x\ {}_a v_y\ {}_a v_z]^T$ geometrical vector $\vec{v}$ with respect to frame $\{a\}$

$\mathbf{A} = [\mathbf{a}_1\ \mathbf{a}_2 \dots \mathbf{a}_n]$ matrix

${}_o\mathbf{A}$ matrix $\mathbf{A}$ with respect to frame $\{o\}$

${}^o_a\mathbf{T}$ transformation matrix from frame $\{o\}$ to frame $\{a\}$

$$
{}^o_a\mathbf{T} = \begin{bmatrix} {}^o_a\mathbf{R} & {}_o\mathbf{a} \\ \mathbf{0}_{1\times 3} & 1 \end{bmatrix} = \begin{bmatrix} [{}_o\mathbf{t}_a & {}_o\mathbf{n}_a & {}_o\mathbf{b}_a] & {}_o\mathbf{a} \\ 0 & 0 & 0 & 1 \end{bmatrix}
$$

$$
= \begin{bmatrix} {}_o t_{a,x} & {}_o n_{a,x} & {}_o b_{a,x} & {}_o a_x \\ {}_o t_{a,y} & {}_o n_{a,y} & {}_o b_{a,y} & {}_o a_y \\ {}_o t_{a,z} & {}_o n_{a,z} & {}_o b_{a,z} & {}_o a_z \\ 0 & 0 & 0 & 1 \end{bmatrix}
$$

$\mathbf{Rot}(x, \varphi)$ transformation matrix for a rotation over an angle φ about the x-axis.

$$
\mathbf{Rot}(x, \varphi) = \begin{bmatrix} \mathbf{R}_{x,\varphi} & \mathbf{0}_{3\times 1} \\ \mathbf{0}_{1\times 3} & 1 \end{bmatrix} = \begin{bmatrix} 1 & 0 & 0 & 0 \\ 0 & \cos\varphi & -\sin\varphi & 0 \\ 0 & \sin\varphi & \cos\varphi & 0 \\ 0 & 0 & 0 & 1 \end{bmatrix}
$$

$\vec{a} \cdot \vec{b}$	internal product of two geometrical vectors
$\|\vec{a}\|$	norm of a geometrical vector
$\vec{a} \times \vec{b}$	cross product of two vectors

Fibre Path

s	parameter along the fibre path
$\Gamma_i(s)$	fibre path on mandrel surface
Γ_{i-1}^{i}	linking fibre path (behind the pin rings) between fibre path Γ_{i-1} and Γ_i
u, v	surface parameters
S	surface
$\vec{s}(u,v)$	position vector of surface point
$\vec{s}_u = \frac{\partial \vec{s}(u,v)}{\partial u}$	: derivative of surface in u-direction
$\vec{t}$	unit tangent
$\vec{n}$	outwards directed normal
$\vec{b}$	binormal
$\vec{c}$	curvature vector
$\vec{f_t}$	fibre tension
$\vec{f_r}$	winding force per unit length on mandrel surface
$\vec{f_n}$	normal force per unit length on mandrel surface
$\vec{f_b}$	transversal force per unit length on mandrel surface
$\vec{f_w}$	Coulomb friction force
T	magnitude of fibre tension
p_i	interlaminar pressure on mandrel surface
λ	slippage tendency
β	slippage angle
μ	coefficient of friction between fibre and mandrel
α	winding angle
r	radius, distance from point to winding axis
c_c	constant in equation of Clairaut
w	width of fibre band
t	thickness of one layer
n_p	number of fibre paths along circumference
R_j	pin ring
$C(\theta)$	base curve of pin ring
$p_0, p_1, p_{c1}, p_{c2}, p_2, p_e$	points on linking path (Fig. 3.7)
θ	radial coordinate, coordinate along the base curve of the pin ring

$\Delta\theta$	span of fibre path on pin ring the base curve of the pin ring
$\Delta\theta_m$	minimum span on pin ring
$\Delta\theta_a$	span on pin ring at which contact with end shaft occurs
r_a	radius of pin ring end shaft, radius of mandrel shaft
r_p	base radius of pin ring
w_p	width of pin ring : distance between edge and pins

Robot Path

Υ_i	path of pay-out eye
Υ_{i-1}^{i}	linking path of pay-out eye between Υ_{i-1} and Υ_i behind the pin rings
f	point of the fibre path
e	delivery point
re	reference delivery point, on the rotating axis in the pay-out eye
rf	centre of robot flange
rw	centre of robot wrist
o	origin of winding coordinate system, on winding axis
$q_1, q_2, \ldots q_8$	control points of the linking path Υ_{i-1}^{i} (Fig. 5.5)
$\vec{v}$	pay-out eye axis
$\vec{a}$	axis of the delivery rolls
$\vec{w}$	winding axis
$\vec{z}$	z-axis of robot base coordinate system, directed vertical upwards
l_f	free length
φ	angle of winding axis
ψ	angle of pay-out eye
η	twist angle
ψ_c	corrective rotation of pay-out eye
l_{fm}	minimum free length
η_{max}	maximum twist angle
γ_z, γ_y	z-y-Euler angles
${}_c\mathbf{S}$	symmetry transformation matrix

The possible coordinate systems are (cf. Fig. 5.1) :

$\{c\}$	CAD-coordinate system
$\{m\} = \{o; \vec{w}, \vec{n_m}, \vec{b_m}\}$	mandrel coordinate system
$\{w\} = \{o; \vec{w}, \vec{n_w}, \vec{z}\}$	winding coordinate system
$\{b\}$	robot base coordinate system

The possible frames are (cf. Fig. 5.2) :

$\{f\} = \{f; \vec{t}, \vec{n}, \vec{b}\}$	frame in a point of the fibre path, corresponds to the Frenet-trihedron
$\{e\} = \{e; \vec{v}, \vec{n_e}, \vec{a}\}$	frame in the delivery point e
$\{re\} = \{re; \vec{v}, \vec{n_e}, \vec{a}\}$	frame in the reference delivery point re
$\{e'\}$	frame in the delivery point e
$\{h\} = \{re; \vec{v}, \vec{z}, \vec{b_h}\}$	frame in re with horizontal tape
$\{rf\}$	frame attached to the robot flange

Robot Trajectory

$\xi = i + \lambda$	setpoint (i : integer ; $0 \leq \lambda 1$)
n	number of joints (+ external axes)
$\mathbf{q}_i$	$= [q_{i,1} \dots q_{i,n}]^T$: input pose
$\mathbf{b}_j$	output pose
$\mathbf{q}_i\mathbf{q}_{i+1}$	segment
$\mathbf{q}(s)$	path in joint space
s	path length
v	path velocity
a	path acceleration
$\dot{\mathbf{q}}(s)$	$= \frac{d\mathbf{q}}{ds}$: joint velocity
$\ddot{\mathbf{q}}(s)$	$= \frac{d^2\mathbf{q}}{ds^2}$: joint acceleration
$\dot{\mathbf{q}}_M$	maximum joint velocity
$\ddot{\mathbf{q}}_M$	maximum joint acceleration
A_{max}	maximum reference acceleration
$\mathbf{q}_i^*$	scaled input pose (base : acceleration)
ϵ_M	maximum smoothing error for joints
ϵ_{max}	maximum reference smoothing error
$\mathbf{q}_i^s$	scaled input pose (base : smoothing error)
$\mathbf{c}_0, \mathbf{c}_1, \mathbf{c}_2$	control points of Bézier curve
v_M	maximum path velocity
a_M	maximum path acceleration
l	length of segment
Δt	time step
t_{cyc}	cycle time robot
t_{lag}	time delay between reaction of external axes and robot

Collision Control

*	(superscript) value after collision avoidance
Υ^*	path linking the (initial) collision-free positions
Υ^s	smoothed collision-free path
ζ_{ab}	angle between the vectors $\vec{a}$ and $\vec{b}$
be	base point of pay-out eye cylinder
bw	base point of robot wrist cylinder
$L_e = (be, \vec{v})$	axis of the pay-out cylinder
$L_w = (bw, \vec{z})$	axis of the robot wrist cylinder
r_e	pay-out eye radius
d_r	distance between base pay-out cylinder and reference delivery point re
l_e	length of pay-out eye
r_w	radius of robot wrist
l_{ew}	distance between delivery point re and robot wrist rw, measured in a horizontal plane
ζ_{ew}	angle between the link $re-rw$ and the pay-out axis, measured in a horizontal plane
x_s, y_s, z_s	coordinates of edge of head- and tailstock
r_r	radius of the spherical working envelope of the PUMA-762
τ	orientation of pay-out eye (in a horizontal plane)
λ_c	tool parameter at collision
c_t	collision point on tool axis
c_s	collision point on surface
δ_s	safety distance
Δl_f	change of the free length
$\Delta\varphi$	change of the angle of the winding axis
σ	sign
$\mathbf{c}_j$	correction in j
$\Delta\mathbf{c}_j$	$= \mathbf{c}_j - \mathbf{c}_{j-1}$: correction difference in j
$\Delta^2\mathbf{c}_j$	$= \Delta\mathbf{c}_j - \Delta\mathbf{c}_{j-1}$: correction difference in j
$\mathbf{c}_j^r$	$= \mathbf{c}_{j-1} + \Delta\mathbf{c}_{j-1}$: reference correction in j
ϵ	maximum deviation from reference correction
$\mathbf{c}_j^*$	correction according to collision-free position
$\mathbf{c}_j^{old}$	collision-free correction from previous iteration
$L_{j_{o,\sigma}} = (\mathbf{c}_{j_{o,\sigma}}, \Delta\mathbf{c}_{j_{o,\sigma}})$	smoothing line
L_{opt}	smoothing line
$L_{lim,\sigma}$	limit line during smoothing

xxx

Contents

Introduction

Fibre reinforced composites with continuous reinforcement and polymer matrix are technical important materials due to their low weight combined with a high strength and stiffness. These materials are especially valuable in transport applications, e.g. in aircraft and automotive structures. Other advantages of fibre reinforced plastics are their good corrosion and chemical resistance, properties which are used in the chemical industry for the storage and transport of fluids and gasses.

The design of composite structures differs strongly from the design of metal structures, due to their anisotropic character. Strength and stiffness are function of the material lay-up, and can be tailored to the requirements of the costumer.

As the use of composites increases, enormous demands are placed on the existing labour intensive manufacturing techniques to meet the required volume, reduce the cost and increase quality [52]. To meet this demand automated manufacturing techniques have been developed to replace the current labour intensive techniques. The production of high performance composites requires an accurate placement of the fibres in the directions, desired by the costumer. Filament winding is one of the production techniques for high performance, continuous fibre reinforced composites, which allows the fibres to be placed, by automated means, with a high degree of precision. In the filament winding process a bundle of reinforcements is pulled, under controlled tension, through a pay-out eye on a rotating mandrel in previously prescribed patterns.

An alternative to filament winding is tape winding. The basic material in filament winding is a collimated band of individually tensioned fibre bundles, whereas tape winding uses a single tape of material. The use of tapes results in lower investment costs, since only one fibre delivery unit is necessary. Tapes wrinkle however easily under transversal

forces, which have therefore to be kept as low as possible.

The fibre paths cannot be chosen freely. In order to obtain an accurate fibre placement, the fibres must be placed and remain on the desired positions. The fibre path has therefore got to meet a stability criterion. The design of a filament wound part will be a compromise between what is optimal according to strength considerations and what is possible, taking account of the restrictions imposed on the winding path.

The first winding machines were two-axis gear controlled machines, which allowed only to wind axisymmetric surfaces, like cylinders and pressure vessels. With the demand for more complex geometries, computer-controlled filament winding machines, with up to seven axes, were developed. These machines are produced in very small quantities, and are therefore very expensive. Investment costs can be reduced, and flexibility increased, by the use of a robot instead of a filament winding machine. A robotic tape winding cell with a PUMA-762 robot and two external axes has been developed within the framework of this thesis.

The increasing complexity of the part geometry requires the use of advanced software tools for the design and production of wound parts. In the framework of this thesis a computer-integrated environment has been developed round the winding process. The environment encompasses design, production and quality control of the filament wound part. The main design problem is the selection of the fibre paths. A computer program **CAWAR** has been developed for the calculation of the fibre paths, starting from a CAD-surface model. The data from the fibre paths are then used to generate an off-line robot program. Quality control is performed with an ultrasonic technique. A robotic C-scanning cell has been developed in collaboration with the department MTM.

Chapter 1 discusses the filament winding process and relates it to the other manufacturing techniques for continuous fibre reinforced plastics. The wet winding process is discussed more thoroughly.

Chapter 2 deals with the generation of the computer integrated winding environment. The program **CAWAR** calculates fibre and robot paths, based on a CAD-surface model of the part. Similar software is used for the control of the robotic C-scanning cell.

The design of a filament wound part and, more specifically, the calculation and selection of fibre paths is discussed in chapter 3. The

major design problem is the selection of the fibre paths, so that a part with an optimal quality is obtained. A design methodology is developed which is not restricted to axisymmetric parts and parts which are approximately axisymmetric, but applies also to asymmetric parts. The design process is illustrated with the example of a tape wound T-piece.

Chapter 4 describes the design and the control of the robotic tape winding cell. Tapes are very sensitive to transversal forces. A special pay-out eye has been developed which is capable to guide the tape to the mandrel without wrinkling. The main problem in the control of the robotic winding cell is the synchronization between the robot and the external axes. The PUMA-762 is a relatively old robot and its controller is, opposed to more recent robot controllers, not directly capable of synchronizing the robot with an external axis.

The generation of the off-line robot program is discussed in chapters 5 and 6. Chapter 5 describes the different phases in the calculation of the poses of the robot path and the velocity along the robot path. As a case study, the production of a tape wound T-piece will be discussed.

During the calculation of the robot path all the interactions between the robot and the environment have to be detected and avoided. Collision avoidance is one of the most difficult steps in the construction of the robot paths. Collisions are avoided with an heuristic approach, which is discussed extensively in chapter 6.

Chapter 1

Filament Winding : a Manufacturing Technique for Composites

1.1 Introduction

Filament winding is a process for the fabrication of fibre reinforced composite structures, in which continuous resin-impregnated reinforcements (glass, carbon or aramid) are pulled through a pay-out eye on a rotating and removable mandrel along previously prescribed paths. The basic filament winding machine resembles a converted lathe : the spindle rotates the mandrel, and the pay-out eye, that is mounted on the transverse carriage, moves back and forth (Fig. 1.1).

The first sections of this chapter describe the fundamentals of the production of continuous fibre reinforced plastics : the basic materials (fibres and resins), the material forms (roving, tape, prepreg,...) and the different steps in composite materials processing. Filament winding is then compared with other methods to produce continuous fibre reinforced composites, such as tape laying and pultrusion. The next section describes the different steps and the process parameters in filament winding : fibre impregnation, tension control, mandrel design, cure cycle,... The last section discusses the winding machines developed at the division PMA (Production Engineering, Machine Design and Automation) of K.U.Leuven.

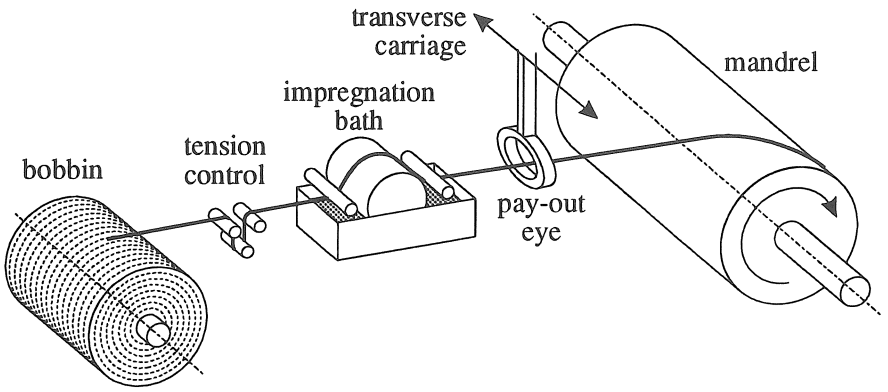

Figure 1.1: Basic filament winding machine

1.2 Materials

A composite material is composed of fibrous material held in place by a matrix material. A distinction is made between short fibre reinforced composites and continuous fibre reinforced composites. For high performance applications continuous fibres are generally used.

The fibres provide most of the tensile and compressive strength and stiffness in a continuous fibre reinforced composite. The matrix keeps the fibres in the proper position, helps to distribute the load, protects the fibres from adverse environmental effects, controls electrical and chemical properties and provides interlaminar shear strength [73]. Matrix materials are generally polymers, ceramics and metals. Polymer matrices are by far the most common.

1.2.1 Fibres

The most common reinforcing materials are glass fibre, carbon fibre, and aramid fibre.

Glass fibre has a low cost, good dimensional stability, moderate tensile strength and modulus and is easy to handle [73]. Glass fibre is available in several types : E, S and C-glass. E-glass is the cheapest form, is easy to handle and has a medium stiffness, but a poor chemical resistance. S-glass is more expensive but has a better stiffness and strength. C-glass has a good chemical resistance in corrosive environments. Glass fibre has a large elongation at failure (Table 1.1).

Material	Tensile Strength	Tensile Modulus	Elongation to Failure	Density	Specific Tensile Strength	Specific Tensile Modulus	Filament Diameter	Thermal Expansion Coefficient
Unit	MPa	GPa	%	g/cm^3	$10^6 m^2/s^2$	$10^6 m^2/s^2$	μm	$10^{-6}/K$
E-Glass	3447	72.4	4.8	2.60	1.35	28	3 – 25	5
S-Glass	4585	86.9	5.4	2.55	1.80	34	3 – 25	4
C-Glass	3100	71	3.5	2.45	1.27	29	3 – 25	7.2
Aramid	3617	62	4	1.44	2.51	43	12	–4
HM-Aramid	3445	186	1.8	1.44	2.39	129	12	–4
HT-Carbon	3996	227	1.3	1.75	2.28	130	7	–0.3
HST-Carbon	4100	234	2.0	1.78	2.30	131	6	–0.3
IM-Carbon	5133	275	1.5	1.73	2.96	159	6	0
HM-Carbon	2482	358	0.6	1.81	1.38	198	7	–0.8
Polyethylene	2585	117	2.6	0.97	2.66	121	27–38	< -9

Table 1.1: Properties of fibres [13, 73]

Material	Tensile Strength	Tensile Modulus	Elongation to Failure	Density	Compression Strength	Maximum Temperature
Unit	MPa	GPa	%	g/cm^3	GPa	°C
Room T Cured Epoxy	50 – 70	2 – 3	2 – 6	1.1 – 1.3	80 – 100	70 – 100
Heat Cured Epoxy	70 – 90	2.5 – 3	2 – 5	1.2 – 1.4	120 – 180	100 – 180
Polyester	50 – 60	2 – 3	2 – 3	1.2	60 – 80	60 – 80
Phenolic	50 – 60	5 – 11	1.2	1.2 – 1.3	120 – 130	100 – 125

Table 1.2: Properties of thermosetting resins [40]

Aramid (Kevlar, Twaron) has a larger specific strength and stiffness than glass, has a small density and a large impact resistance, but is more expensive than glass, absorbs more easily water, and has relatively poor shear and compression properties [73]. The high modulus aramid fibre (e.g. Kevlar 49) is most frequently used as reinforcement.

Carbon fibre, which is more expensive, is available in a wide variety : HM (high modulus), HT (high tensile strength), HST (high strain), IM (intermediate modulus, intermediate strength).

Polyethylene (PE) is a new fibre, which is very light and tough, but which has a large creep, a bad temperature resistance, and is expensive.

The application of more than one reinforcement (hybrid composites) may have advantages in terms of cost and product performance [95].

1.2.2 Matrix Materials

Polymer matrix materials can be divided in two classes : thermosetting and thermoplastic materials. They differ in their final intermolecular structure : the molecular chains of the thermosetting materials are interconnected with chemical bonds (cross-links), the thermoplastic chains not. Thermosets require cure to achieve cross-linking, and cannot be remelted due to this cross-linking. Thermoplastics are heated, moulded to the desired shape, and then resolidified to achieve their solid form.

Table 1.3 compares the characteristics of thermoplastic and thermosetting matrix materials. Thermosets require much longer processing times than thermoplastics, due to their long cure cycle. The processing temperatures and pressures for most thermoplastics are much higher than for thermosets, due to the high melt viscosity. Thermoplastics have generally a lower strength and stiffness than thermosets, but an improved damage tolerance and environmental resistance.

Thermosetting resins are still the principal matrix material for composite applications, but the use of thermoplastics is increasing.

1.2.2.1 Thermosetting Resins

The solidification of thermosetting resins starts when the resin components are mixed. As with most liquids, the resin viscosity decreases

	Thermoset Fiberite 931 Epoxy	Thermoplastic ICI APC-2 PEEK
Melt viscosity	low	high
Fibre impregnation	easy	difficult
Prepreg stability at $-18°C$	6 – 12 months	indefinite
Processing cycle	1 – 6 hours	15 sec – 6 hours
Processing temperature	177°C	370°C
Mechanical properties	good	good
Environmental durability	good	exceptional
Damage tolerance (toughness)	average	good

Table 1.3: Comparison between thermosetting and thermoplastic matrix materials [95]

when the temperature rises. As the chemical reaction continues, the resin viscosity increases due to the growing cross-link density. The resin changes from a liquid over a rubbery to a solid state in the gel point. Beyond the gel point, almost no resin flow, and hence no void diffusion and further consolidation of the composite, can occur. The cure is then typically 40 % to 60 % completed and the final shape and thickness are fixed [95]. Further exposure to higher temperatures or additional time is required to increase the cross-link density of the network and the stiffness of the polymer and to achieve maximal properties.

Three stages are defined in the cure of thermosets :

1. A-stage, which is a liquid or sticky solid prepolymer.
2. B-stage is a tacky fusible solid. The gel point is not yet reached.
3. C-stage is a fully cured cross-linked structure.

The most common thermosets are epoxy, polyester, vinyl ester, polyimide and phenolic resins (Table 1.2).

Epoxy is the most common matrix material for advanced composites. It contains no volatiles, has a good adhesion, good strength, low shrinkage, and a relatively good thermal and chemical stability [95].

Polyester is the major matrix material for non-critical applications, due to its lower cost, compared with epoxy. Polyester has a low initial viscosity that allows easy wet-out of the reinforcement and is easy to manufacture, while epoxies have a relatively high viscosity and slow cure [40]. Polyester has however a high exothermic cure with a high

shrinkage. Vinyl ester has a better chemical resistance and is more expensive than polyester, but cheaper than epoxy.

Phenolics have a high heat resistance, especially under oxidizing conditions [40]. Phenolics are however difficult to handle, and have poor mechanical properties due to the high void content. Polyimides and bismaleimides (BMI's) have a heat resistance up to 300°C [40].

1.2.2.2 Thermoplastic Resins

Thermoplastics which are used in composite materials are a.o. PEEK (polyether-etherketone), PPS (polyphenylene sulfide), PEI (polyether-imide) and PP (polypropylene). Thermoplastics are particularly used in applications where fatigue life, damage tolerance and large strains are important design criteria.

1.2.3 Material Forms

The fibres can be delivered as fibre bundles or as weaves. Fibre and resin can be delivered together, e.g. as an already impregnated material.

1.2.3.1 Dry Material Forms

A single fibre is usually called a *filament.* An untwisted bundle of continuous filaments is called a *tow* or *strand* [95]. A twisted bundle of continuous filaments is called a *yarn.* Several tows are collected in a parallel bundle, called a *roving.* During manufacturing several rovings are collocated, forming a band of material.

The rovings are delivered on bobbins, which can be internally or externally unwinding. Internally unwinding bobbins, which have a centre pull, have the advantage that no tension is required for unwinding. Manufacturers deliver bobbins which unwind internally without fibre twisting.

The size of glass fibre roving is denoted in *tex* (g/1000 m) or *denier* (g/9144 m) [83]. Typical sizes are 600, 1200 and 2400 tex. The size of carbon and aramid rovings is often denoted in the number of filaments per roving, e.g. a 3K (3000) carbon fibre roving.

Tows and yarns can be woven to give, respectively *woven roving* and *cloth* [40]. Weaves are deliverable in rolls of various widths. When the width is larger than 305 mm [25], they are referred to as *broad*

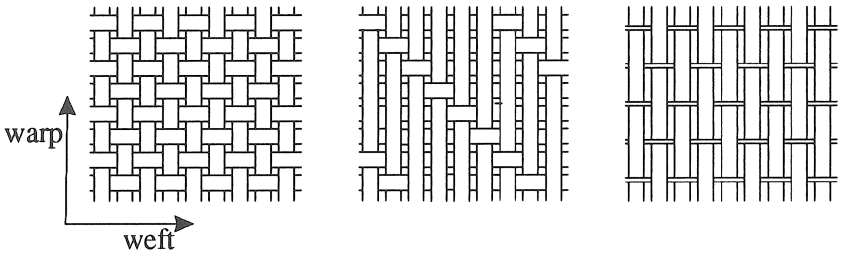

Figure 1.2: Material forms
(a) Plain weave (b) Satin weave (c) Unidirectional

goods, otherwise as *tapes*. The ratio of the number of filaments across the weave roll (*weft* direction) to the number along the roll (*warp* direction) can be easily varied from almost unidirectional, to equal warp and weft. Unidirectional weaves have only a few weft filaments, that can be the same material as the warp filaments or a low-cost fibre (e.g. nylon), to keep the weave together. A variety of weave patterns is possible [95] : e.g. a *plain weave*, where a warp filament goes alternatively over and under one weft filament, and a *satin weave*, where a warp filament goes over three or four and under one weft filament in an (ir)regular pattern (Fig. 1.2).

1.2.3.2 Pre-impregnated Material Forms (Prepregs)

A prepreg is a ready-for-use composite raw material, produced by pre-impregnating the reinforcement with the matrix. Thermosetting prepregs are B-staged, and a release paper is provided at both sides of the (tacky) prepreg. Thermosetting prepregs are stored at a temperature of about $-20°C$, at which their usable life is about 6 to 12 months. Thermoplastic prepregs are stiff and boardy at room temperature, have no tack and can be stored for an unlimited time. Prepregs are produced in different basic forms : roving (towpreg), tape and broad goods. Tapes and broad goods may be either unidirectional, held together by the resin, or woven.

1.2.3.3 Post-impregnated Material Forms

Here fibres and resin are combined but not yet impregnated. Post-impregnated material forms include e.g. intermingled yarns, in which the thermoplastic resin is shaped into fibres, which are intermingled with the reinforcement fibres, and thermoplastic powder impregnated woven cloth [37]. Post-impregnated materials are only used for thermoplastic resins : when the material is pressed and heated, the thermoplastic fibres melt and coat the reinforcement fibres.

1.3 Fundamentals of Composites Manufacturing

The manufacturing process of a continuous fibre reinforced part consists of the four major steps : *impregnation*, *lamination*, *debulking* and *cure*. Resin is applied to the fibre during the impregnation process, which can be a part of the manufacturing process, or be done by the material supplier. The part is built up during the lamination process, by e.g. winding round a rotating mandrel or by placing the material on a fixed mould. The part is then debulked, i.e. a monolithic material is formed from single plies by applying pressure, and cured to obtain a solid structure. Thermoplastic matrices do not require cure, but require higher processing temperatures and pressures.

The material parameters, that are of importance during manufacture are : drape, tack, resin flow and gel time [25].

Drape is the ability of the material to form to complex tools [25]. Drape defines the minimum curvature of the fibre path.

Tack is the adhesion of prepregs to tool surfaces and other layers of prepregs [25]. The tack should be high enough to allow the prepreg to adhere to the mould or preceding plies, but low enough to remove them from the release paper and guiding systems without loss of resin.

Flow is the amount of resin squeezed from a specimen as it cures between press plates. Some resin flow is desirable to fuse successive plies and to bleed out volatiles, but excessive flow will result in an inhomogeneous resin content and in fibre migration.

Gel Time is the time a specimen has to remain between heated plates until the gel point is reached. When the gel point is reached before lay-up, the prepreg becomes stiff and cannot be handled anymore.

1.3.1 Impregnation

Since the fibres are produced separately from the matrix, the matrix has to be combined with the fibre at a certain stage in the manufacturing process. The resin must be thoroughly integrated with the fibres, the air between the filaments must be expelled and fibres which stick to each other separated. Impregnation should be homogeneous, so that in a later stage no significant resin flow is required to obtain a uniform resin distribution.

The fibres can be impregnated with resin before, during or after the production process.

1.3.1.1 Impregnation in process (Wet Processing)

The resin is applied to the fibre during processing. The impregnation takes place in an impregnation bath, which is placed between the unwinding bobbins or rolls and the laminating device. Wet processing has the following advantages [73] :

- Low material cost.
- Large flexibility for the manufacturer by free choice of resin and fibre.

The disadvantages are :

- Bad reproducibility of manufacture, since the resin content depends on many factors, which may change during manufacture.
- Unclean manufacturing by superfluous resin.
- Frequent cleaning of resin bath and fibre guiding systems.
- Environmental and workshop loads by solvent gasses from resin.

1.3.1.2 Prepreg Processing

The fibre is impregnated with resin by the manufacturer. The advantages of prepreg processing are [73] :

- clean manufacturing.
- high processing speeds possible.
- excellent quality control and reproducibility in fibre volume fraction, uniformity and band width control.
- relative high tack.

The disadvantages are :

- high material cost : the price of prepregs is in the order of twice the price of wet processing materials [52, 95].
- ageing of the prepreg, resulting in a limited storage time.
- the flexibility in the choice and variation of resin systems and reinforcing fibres is limited to the commercially available prepregs.

1.3.1.3 Wet Rerolled Processing

A controlled length of fibre is impregnated with a controlled volume of resin, rewound on a bobbin without B-staging, and then used promptly or refrigerated [73]. Quality control can be performed away from the manufacturing operation. Rerolling can be a very cost-effective method to produce pre-impregnated rovings.

1.3.1.4 Impregnation after processing (Dry Processing)

The impregnation is done after processing, by e.g. Resin Transfer Moulding (RTM) or Structural-Reaction-Injection-Moulding (S-RIM) technique. In RTM a thermosetting resin is injected – at low pressures – into a cavity, which has the shape of the desired part and is filled with the fibre preform. S-RIM is similar to RTM and is used for highly reactive resins : the resin consist of two components, which are injected separately under high pressure into a mixing chamber and then directly in the tool. The mould is often put under vacuum to remove entrapped air from the reinforcement. The reinforcement is wetted out by the pressure of the injection. The design of the mould is very critical : the mould must be constructed in such a way, that the resin can reach all areas and that a uniform impregnation takes place. The resin must have a very low viscosity, and the fibre preform must be permeable enough, in order to penetrate fully the preform, without leaving dry areas.

1.3.2 Lamination

The three principal laminating processes for continuous fibre-reinforced composites are winding, laying and pultrusion. In the winding process the reinforcing material is guided by a delivery eye or roll onto a rotating mandrel under controlled tension. In the laying process the material is placed on a surface and immediately consolidated. In pultrusion, the material is pulled through a die.

The properties of the composite material depend strongly on the orientation of the fibres. It is therefore very important that the position of the laid-down material corresponds to the desired position. The requirements, which are imposed on the path, depend on the form of the reinforcement.

1.3.2.1 Rovings : Slippage Prevention

During winding, the only external force which acts on the fibre is the fibre tension. The fibre tension $\vec{f}_t$ leads to a force $\vec{f}_r = \frac{d\vec{f}_t}{ds}$ per unit length on the mandrel surface, which is directed towards the centre of curvature of the fibre path. The resultant force $\vec{f}_r$ can be split in two components : the normal force $\vec{f}_n$, perpendicular to the surface and the transversal force $\vec{f}_b$, tangential to the mandrel surface (Fig. 1.3).

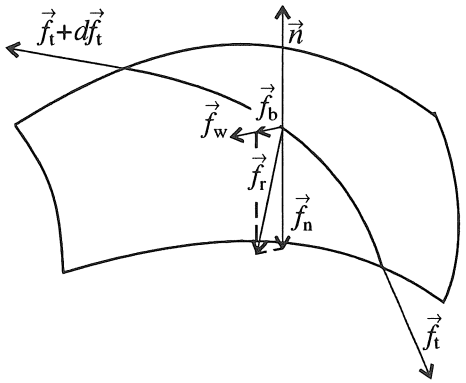

Figure 1.3: Stability condition for fibre path

In order to obtain an accurate and reproducible fibre lay-down, the fibre may not slip on the surface. The *slippage angle* β [2] is defined as the angle between the forces $\vec{f}_r$ and $\vec{f}_n$, and the *slippage tendency* λ

[24] as the ratio between the transversal force $\vec{f}_b$ and the lateral force $\vec{f}_n$:

$$|\lambda| = |\tan\beta| = \frac{\left\|\vec{f}_b\right\|}{\left\|\vec{f}_n\right\|} \tag{1.1}$$

The fibre will slip if the transversal force $\vec{f}_b$ is larger than the maximum friction force between the fibre and the material underneath. The magnitude of the friction force $\vec{f}_w$ equals :

$$\left\|\vec{f}_w\right\| = \mu \left\|\vec{f}_n\right\| \tag{1.2}$$

with μ the static coefficient of friction. The stability condition

$$\left\|\vec{f}_b\right\| \leq \left\|\vec{f}_w\right\| \tag{1.3}$$

can then be written as :

$$\left\|\vec{f}_b\right\| = |\lambda| \left\|\vec{f}_n\right\| \leq \mu \left\|\vec{f}_n\right\| \tag{1.4}$$

or :

$$|\lambda| \leq \mu \tag{1.5}$$

If the transversal force is zero ($\vec{f}_b = \vec{0}$), the resultant force $\vec{f}_r$ on the surface is normal to the surface. The fibre path corresponds then to a *geodesic*. A geodesic is defined as a curve, for which the second order derivative is perpendicular to the surface [69]. It is also the curve which traces the shortest distance between two points on a surface [69]. Some examples : a geodesic on a sphere corresponds to a meridian circle, on a plane to a straight line, on a cylinder to a helix.

If only geodesics are used for winding, the term *geodesic winding* is used, otherwise, if fibre paths are allowed to deviate from geodesics, the term *non-geodesic winding* or *semi-geodesic winding* is used. The restriction to geodesics simplifies the calculation of the fibre paths, but reduces the design freedom : once the starting conditions are defined, the rest of the trajectory is fixed.

The coefficient of friction can be measured on a sphere [2] or ellipsoid [110] by winding hoop windings with decreasing diameter, until the fibre slips on the surface. The values measured for the friction coefficient between mandrel and fibre vary from 0.20 (wet roving on a

wet surface) [2] to 0.39 (dry with PTFE spray on mandrel) [110]. Dry winding allows higher friction coefficients than wet winding [2]. In practice slippage is likely to be unpredictable. Prepreg systems have, due to their higher tack, a higher coefficient of friction than wet resin systems, and allow therefore a larger deviation from the geodesics.

The normal force $\vec{f_n}$ provides the interlaminar pressure p_i, which is needed to compact the laminate :

$$p_i = \frac{\left\| \vec{f_n} \right\|}{w} = \frac{T\kappa_c}{w} \tag{1.6}$$

with w the width of the tape, κ_c the curvature of the fibre path and T the fibre tension.

If a consolidation pressure is applied at the contact point, much larger deviations from the geodesic are allowed [12]. The pressure prevents the fibre to slip in the lay-down point, and the consolidated material allows higher transversal forces.

The stability condition has to be valid for each fibre of the roving band, also for the outer edges. The requirement that the fibres at the edge of the band may not slip limits the width of the roving band. The band width is a function of the mandrel curvature normal to the fibre path. The maximum band width for a geodesic path is [107] :

$$w_{max} = \frac{2}{\kappa_g} \arctan \mu \tag{1.7}$$

with κ_g the curvature in the direction normal to the fibre path.

1.3.2.2 Tapes : Natural Path

The fibres in a roving band, which are independently tensioned, can move longitudinally with respect to each other. This is not possible in a tape. If the difference between the lengths of the edges of the tape becomes too large, the path of the longitudinal fibres will change so, that the difference between the lengths of the paths is minimized : the tape will slip, wrinkle or lift off from the surface, which will have a negative effect on the strength of the part. The path of the middle of the tape should be such that the difference between the lengths of the edges is minimized. Such a path is called a *natural path* [98]. A path, where all the fibres have the same length, can only be generated

over a complete surface when the surface is developable. The development of the path results in a line, which is also the development of a geodesic (cf. Appendix A.2). Tornincasa [98] defines the natural path on a surface as the envelope of the natural paths on the locally tangent developable ruled surfaces. The fibre path obtained in this way corresponds to a geodesic.

So, in order to place tapes accurately, only geodesics are allowed.

1.3.2.3 Broad Goods

The formation of complex shaped parts from continuous fibre broad goods depends mainly on in-plane shear (Trellis effect) [4]. This shear can be induced by manual pressing and shaping during lay-up, or by the interactions between the mandrel and the mould. Due to in-plane shear, the orientation of the fibres changes (Fig. 1.4).

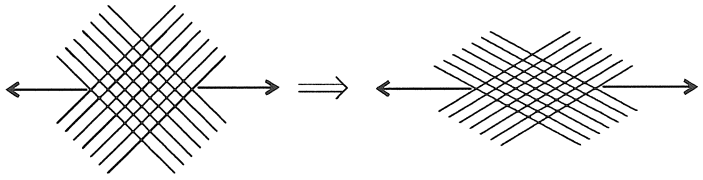

Figure 1.4: Trellis effect

The Trellis effect is limited by the maximum deformation angle which depends on the thickness of the fibres, the density of the fabric and the weave pattern. A plain weave is the most resistant to in-plane shear, a satin weave is more pliable and conforms easily to complex surfaces [95]. Two-directional weaves are more deformable than unidirectional tapes and broad goods, due to their higher dimensional stability. When the maximum deformation angle is reached, further deformation of the fabric causes local buckling of the fibres, and wrinkling of the fabric.

1.3.2.4 Fibre Bridging

When the surface is not completely convex, the fibre may lift off from the surface, taking a shorter way through the air. This is called *fibre bridging*. To prevent fibre bridging, the resultant force $\vec{f_r}$ must be directed towards the material side of the surface, in the opposite

direction of the outwards directed normal $\vec{n}$:

$$\vec{n} \cdot \vec{f_r} \leq 0 \tag{1.8}$$

with $\vec{n}$ the outward directed normal to the surface.

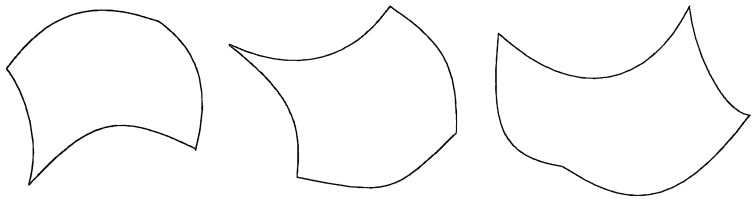

Figure 1.5: Convex, convex/concave and concave surface

If the fibre tension is the only force applied, complete concave surfaces cannot be produced. Convex/concave surfaces (Fig. 1.5) can only be produced if, for each point of the fibre path, the centre of curvature of the fibre path lies at the material side of the surface.

1.3.3 Debulking

After lamination, a monolithic material must be formed from single plies. In order to ensure material integrity, a certain interlaminar pressure should be set up.

Debulking is the process of densifying and forming a monolithic material from single fibre bundles and plies [83], hereby removing voids and delaminations between layers. After debulking no interfaces between the layers should be detectable.

Debulking is usually accomplished through the application of pressure and heat in a bag or mould.

The debulking step can, for thin laminates, be combined with cure by applying pressure during cure, in e.g. an autoclave. Thicker parts require intermediate debulking steps during lay-up, resulting in a substantial cost increase. Carbon-epoxy ply lay-ups are typically compacted once every 10 to 20 ply lay-ups [83]. Evaluations of the aerospace industries have demonstrated that in many cases debulking requirements can be accomplished at room temperature or eliminated through the mechanical lay-up and immediate compaction during lam-

ination [83]. In this case, a compaction pressure is applied during lamination in the lay-down point by means of a compaction roll.

1.3.4 Cure of Thermosetting Resins

Thermosets require cure to achieve cross-linking. The cure cycle consist of three phases : B-staging, normal cure and postcure.

B-staging The resin is heated until the chemical reaction starts, but cure is stopped before the gel point is reached. The resin is then still soft to the touch and exhibits some tack. Excess resin can be removed with plastic paddles before proceeding to cure.

Normal cure The resin changes from the B-stage to completely hard, so that the part can be removed without damage.

Postcure The residual stresses, which are induced in the composite part during cure, are decreased and the mechanical properties of the composite are improved [95].

Heat and pressure are applied during cure. Curing devices are autoclaves, vacuum curing ovens, etc.

Dependent on the temperature of cure, a distinction is made between room temperature and high temperature curing resins. Room temperature curing resins are easier to handle, because no heat has to be applied, and allow the application of cheaper mandrel materials, like polyurethane and nylon polymers. As a general rule [61], the temperature of cure is somewhat below the maximum temperature capability of the composite. Room temperature cured resins will perform only slightly above room temperature.

The cure of polyesters is performed at room temperature. Heat cured epoxy resins are cured in autoclaves, presses or ovens with simultaneous application of pressure. Typical cure temperatures are 120°C and 177°C, the latter for aerospace applications [40].

1.3.5 Thermoplastic Processing

The high melt viscosity and the high melting point of thermoplastics make impregnation very difficult, so that almost always pre- or post-impregnated material forms are used. Thermoplastic prepregs are stiff and miss the drape of thermosetting prepregs, so that cold lay-up is

limited to flat plates. To fuse the plies, only heating to the melting point, applying contact pressure to consolidate and cooling to solidify, is required. Due to the lack of drape, high pressures are needed to form complex parts. Post-impregnated materials are drapable and flexible, but, due to the high melt viscosity, require much longer times above the melting point and higher pressures to effect impregnation during forming [37]. Due to the high temperatures, which are necessary to melt the thermoplastic resin, thermal expansion becomes more critical in the mould design.

Stacked thermoplastic plies are transformed into a laminate in a hot press. In the forming phase, thermoplastic resins are heated to temperatures well above the glass transition temperature (amorphous matrices) or close to the melting point (semi-crystalline) to soften the matrix.

1.4 Laminating Techniques for Continuous Fibre Reinforced Parts

This section will discuss the laminating techniques for the production of continuous fibre reinforced structures. The choice of both the laminating technique and the curing process depends on the required properties of the finished part. Elements which influence the selection are part shape and dimensions, lot size, required strength, cost, familiarity with processing techniques,etc. [83]. The various manufacturing techniques for fibre-reinforced plastics may be classified according to the form of the reinforcement (roving, tape, broad goods) and the method of lamination (winding, laying, ...). All techniques can be automated.

1.4.1 Filament Winding

Filament winding is a process for the fabrication of fibre reinforced composite structures, in which continuous resin-impregnated reinforcements are pulled, under controlled tension, through a pay-out eye on a rotating and removable mandrel along previously prescribed paths. The fibre tension provides the pressure, necessary to compact the laminate. The part is cured after winding and the mandrel is then removed.

The basic filament winding machine resembles a converted lathe :

the spindle rotates the mandrel, and the pay-out eye, that is mounted on the transverse carriage, moves back and forth (Fig. 1.1).

Filament winding employs a bundle of dry or prepreg rovings. If dry rovings are used, the fibres can be impregnated in process (wet winding) or after winding (dry winding). Most winding is performed wet. Dry wound parts are slightly impregnated with a binder to maintain the shape of the preform, and impregnated after winding e.g. by means of the RTM-technique [50]. In prepreg winding, the mandrel or the prepreg is preheated in order to obtain the necessary degree of tack and resin flow [40]. Prepreg winding is not so common, due to the lack of "roving prepregs".

1.4.1.1 Applications of Filament Wound Structures

Filament winding is used for the production of parts with closed surfaces. Most parts are axisymmetric, since these parts exploit best the advantages of filament winding. Filament wound parts are hollow, since an internal mandrel is used.

Filament wound parts are used in various sectors [42] :

- military aerospace : rocket motor cases, launch tubes, helicopter rotor blades
- civil aerospace : pressure vessels, aircraft structures, prototype of the Beech starship fuselage
- automotive : drive shafts, leaf springs, steering columns [108]
- machine construction : flywheels
- sports : fishing rods, baseball bats, paddles, bicycle frames
- chemical : storage and processing tanks, pressure vessels [59], reinforced pipes
- energy : wind turbine blades

Filament winding is also used for the production of semi-finished parts, mostly circular or rectangular hollow tubes, which are commercially available in a wide variety of fibre-resin combinations and winding angles.

1.4.1.2 Thermoplastic Winding

During winding, a thermoplastic prepreg is heated to the thermoplastic softening point just before being wound on the mandrel, and consolidated to the part (Fig. 1.6). Thermoplastic winding can be seen as a continuous welding process, in which the prepreg is welded onto the previously wound material.

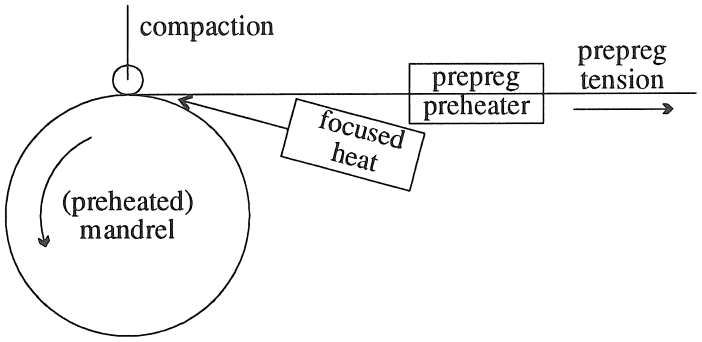

Figure 1.6: Thermoplastic winding

The heating of the prepreg is the most critical step in the fabrication process : the prepreg has to be heated from room temperature to the softening point of the thermoplastic resin in a short time. The size and location of the melt zone are critical : the zone must be large enough to allow full consolidation between the incoming tape and the substrate, but not to large to allow tape slippage [111]. The heating energy must be localized to maintain accuracy of the melt zone size, controllable to achieve a good quality, and intense enough to achieve acceptable transfer rates [111]. Several heating methods have been investigated in literature : infra-red radiators, inert gas (e.g. nitrogen) flameless torches, ultrasonic and laser radiation, hot iron contact,... [1, 72, 111]. Laser heating gives the best results, but the control of the laser beam poses serious problems and a considerable investment is required [1]. Heating by inert gas (e.g. nitrogen) is the least costly method, but offers only low heat transfer rates [111]. A preheater, mostly an infrared radiator, is used to preheat the tape, in order to reduce the energy required in the contact point.

The prepreg must be cooled and consolidated at the point of contact. Consolidation pressure can be applied either by fibre tension

or pressure from rollers. Prepreg and mandrel are above the melting point of the matrix at the point of contact, but cooling is rapid due to the relative low capacity of the heated area [37]. The mandrel can be heated to assist consolidation and to limit the power of the focused heat.

Automated Dynamics has developed a commercial thermoplastic processing head for winding cylinders, which uses a low pressure nitrogen torch to heat the thermoplastic prepreg, and a consolidation roller, which has the ability to cut and restart the prepreg [38].

Experimental set-ups with robots have been realized by Peters (laser heating, with a flexible tube to guide the laser beam [72]) and Steiner [41, 94] (nitrogen gas heating).

Thermoplastic filament winding allows high transverse forces on the fibre, since the prepreg is immediately welded to the previously wound material. This gives a great freedom in the fibre path design. By means of a correctly designed consolidation system concave parts can be produced [41].

1.4.2 Braiding

Braiding is a technique derived from the textile industry. In a tubular braiding machine, a number of yarn carriers are mounted on a ring of (rotating) horn gears (Fig. 1.7a). When the horn gears rotate, the yarn carriers are passed from one horn gear to another. Two sets of yarn carriers move on wavelike circles in opposite directions round the mandrel (cf. maypole dance) (Fig. 1.7b), and produce a woven layer on a central mandrel as the mandrel moves through the ring. Braiding has the advantage that a large number of yarns are processed at the same time, so that production time decreases. Braiding results in a more weavelike structure than filament winding. Due to the interlacing of the fibres, the coefficient of friction is larger than in filament winding, so that larger deviations from the geodesic fibre path are allowed [62], and better interlaminar properties are obtained [49]. Braiding can handle more complex shapes than filament winding [49]. Braiding is mainly used for the production of net shape preforms of tubular parts, which are impregnated with the RTM process.

A extension of the (two-dimensional) braiding process is three-dimensional braiding, where the horn gears are mounted in a square grid instead of in a ring.

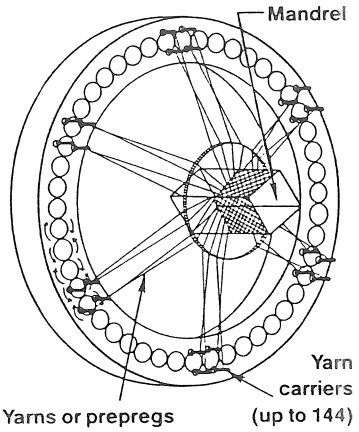

Figure 1.7: Braiding machine [26]

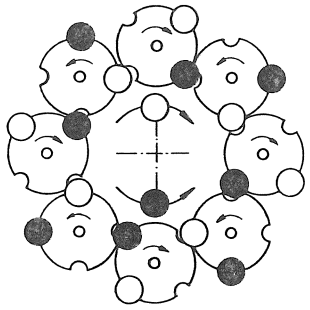

Motion of yarn carriers [63]

1.4.3 Tape Winding

Tape winding uses a unidirectional tape, instead of separate rovings. The tape winding technique is originally developed by General Dynamics for prepreg tapes [45]. The tape winding machine of General Dynamics is discussed in section 4.3.1.

Prepreg tape is currently the best supplied product form, providing a better fibre collimation, less fibre damage and a better control of band width, ply thickness and resin content than other composite product forms. The better quality of the tape results in better properties with respect to shear and compression (up to 30 % better than filament wound parts [45]). Fabrication times for both filament winding and tape winding are identical [45].

Prepreg tapes are very sensitive to transverse compressive forces. Even small compressive forces cause the tape to wrinkle. Tape is therefore also sensitive to tape twisting, i.e. a rotation about the length axis of the tape : the tape will fold together when this twist becomes too large.

The tape is also hard to centre. A roving in a roving bundle can be centred by means of combs, but these transverse guiding systems induce transverse compressive forces in the tape, and are therefore not allowed.

As a guideline [45], the ratio of the tape width to the mandrel's nominal diameter should not exceed 1/25 when winding over double

curved surfaces like end domes.

1.4.4 Tape Laying

Prepreg tapes are placed by a tape placement head on a male or female mould in adjacent bands. There are two systems of tape-laying machines : single and double stage tape-laying machines. A single stage tape laying machine cuts the prepreg tape, lays a specified length, cuts the end angle, indexes one tape width and repeats the cycle in the inverse direction (Fig. 1.8). A major problem is that the tape should be cut without cutting the release paper, that guides the tape to the lay-down position. To avoid this problem, Goldsworthy [36] has developed a two-stage tape-laying system, in which the tapes are cut, checked on flaws, placed on a release paper and stored in a tape reel cassette on a separate tape-processor. The cassette is placed in the tape placement head, which lays the tape on the mould and consolidates it.

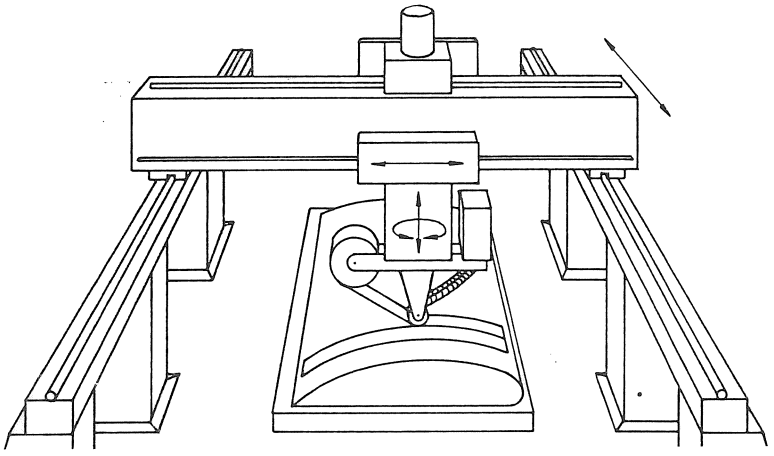

Figure 1.8: Tape-layer [63]

Tape laying machines are very large, due to the various functions which are combined in the tape placement head. Tape laying is mainly used in the aerospace industry for the manufacture of panels with large curvatures, like wing skins.

1.4.5 Fibre Placement

Fibre placement is a synergic blend of filament winding and tape laying, which eliminates some of the drawbacks and limitations of these methods. Fibre placement is an automated process in which individual, independently tensioned, rovings are fed into a processing head, where they are collimated into a tape-like band, and compacted directly on a mandrel [29] (Fig. 1.9). The compaction pressure is delivered by an elastomeric roller, which is kept normal to the mandrel surface as the fibres are placed. The rovings are delivered at low tension. The fibre placement machine is able to change the width of the roving band by individual roving cut/start mechanisms. Fibre placement is applicable to both thermosets and thermoplastics.

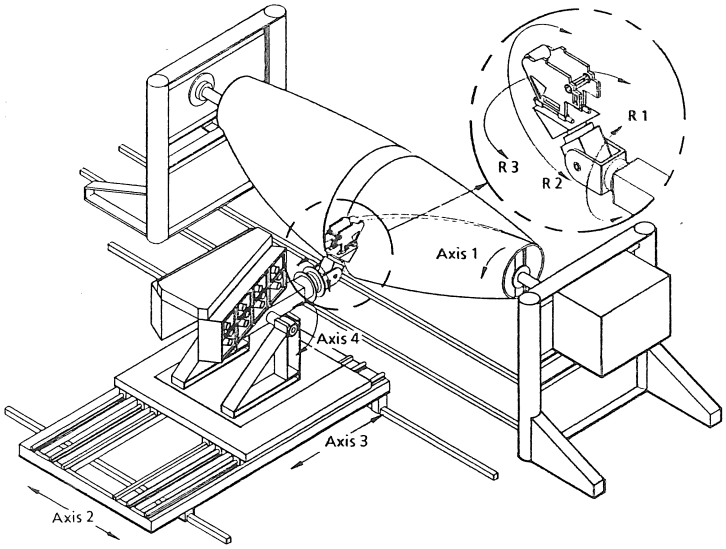

Figure 1.9: Fibre placement machine (Hercules) [3]

Opposed to filament winding, fibre placement does not rely on fibre tension to consolidate the material. Opposed to tape laying and tape winding, fibre placement does not start directly with a collimated tape, but uses independently tensioned fibres. Due to the compaction, independent fibre feeding and material tack, the material can be placed in highly non-geodesic fibre paths and onto concave surfaces [3, 12]. Fibre placement provides the designer with the capability to design a laminate without constraints of geodesics and constant band width.

Fibre placement machines are however very expensive.

1.4.6 Wrapping

Wrapping or rolling [78] is an alternative method to winding for producing reinforced tubes. The prepreg material to be wrapped is laid on a flat table without tension. The mandrel is then rolled over the material (Fig. 1.10). Compaction of the material during wrapping is accomplished by contact pressure between mandrel and material. There are two wrapping methods : convolute and spiral wrapping. In convolute wrapping a number of rectangular sheets of material, equal to the desired number of circumferential layers or plies, is wrapped in one time round the mandrel. In spiral wrapping, plies are cut in parallellograms, and rolled on the surface, so that one complete layer all over the surface is obtained. Wrapping is the most efficient for cylinders with diameters up to 150 mm [78].

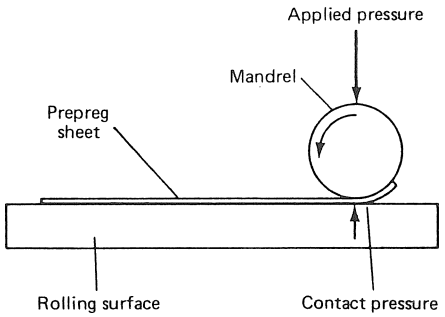

Figure 1.10: Wrapping [78]

1.4.7 Ply Lamination

Manual wet lay-up is the oldest and simplest, but very labour-intensive way to produce composites. The dry reinforcement (mostly fabric or mat) is cut by hand, laid in the mould and the resin is applied by hand or with a spray gun. The resin is distributed uniformly with a roller. This sequence is repeated for the following layers. The part is cured in an oven or an autoclave.

This method is very labour-intensive, and asks for automation. Automated lay-up or ply lamination systems use prepreg plies consisting

of unidirectional or woven prepreg fabrics in various sizes. Automated ply lamination consists of three steps :

Ply cutting The plies are cut from wide sheets with a reciprocating Gerber knife [83], water jet or laser [40]. The tables, on which the plies are cut, can be stationary or can be transferred from the cutting machine to the transfer machine by a table transporting device [30].

Ply transfer The plies are extracted from the cutting table by a vacuum hand, which is manipulated by a robotic arm [30] and laid down in the mould.

Consolidation A roller head presses the ply onto the mould. The ply transfer and consolidation functions can be combined in a computer controlled roller head, which rolls gently over the cut ply, introducing vacuum into it to pick it up, moves towards the lay-down table where the roller rotates and presses the ply unto the mould [30].

1.4.8 Pultrusion

Pultrusion is a continuous process for manufacturing composites, which is used for the production of reinforced structures with constant cross sections. Continuous reinforcements (rovings, tapes,...) are pulled through a resin bath, combined and pulled through a forming die. The die forms the cross section and squeezes out excess resin. There are three methods to cure a pultruded part [83] :

- continuous cure of the part in a free state in a tunnel oven (Fig. 1.11)
- the part is cured statically by external heating of the (split) die. After cure, the next discrete length is brought into the die. A variation of this process is *pulforming*, where a curved die is used to make curved profiles, e.g. automobile leaf springs [83].
- the material is heated while passing through the shaping die.

The parts are cut to their final size after cure. The main advantage of pultrusion is the high fabrication speed, with a high material usage, and high fibre volume fractions ($\approx$70%). Pultrusion is however limited to parts with constant cross sections.

The *pulwinding* process [86] is a combination of pultrusion and filament winding, in which the pultrusion process provides axial reinforcements and radial or helical reinforcements are provided by rotating ring-eyes.

1.4.9 Comparison of the manufacturing techniques

Filament winding, tape winding, tape laying and fibre placement are compared in Table 1.4.

	Filament Winding	Tape Winding	Tape Laying	Fibre Placement
Non-geodesic paths	limited by slip	no	no	yes
Concave surfaces	no	no	yes	yes
Strongly curved surfaces	yes	no	no	yes
Changing band width	no	no	no	yes
Compaction	fibre tension applied	fibre tension applied	yes	yes

Table 1.4: Comparison between manufacturing methods [12]

Krolewski [52] has investigated the effect of automation on part cost in the aerospace industry in the U.S. in 1985. Fig. 1.12 compares the cost and Fig. 1.13 the cycle times for a flat part for various manufacturing methods[1].

Those processes, which use raw materials (i.e. filament winding and pultrusion) offer significant savings. Pultrusion is the most cost effective method, due to the relatively low equipment and material cost and a high production rate, but is severely limited in part geometry and fibre orientation. Labour costs can be relatively small compared with material costs. Krolewski states that the other automated techniques are probably not cost effective, due to the low part volumes in the aerospace industry, the high cost of the automated equipment and the only marginal gains expected in scrap and rework reduction.

The comparison is made for a simple geometry. The complexity of the part and the lay-up strongly influence the cost and the cycle

[1] The filament wound part is wound on a cylindrical mandrel, cut and then cured on a flat tool.

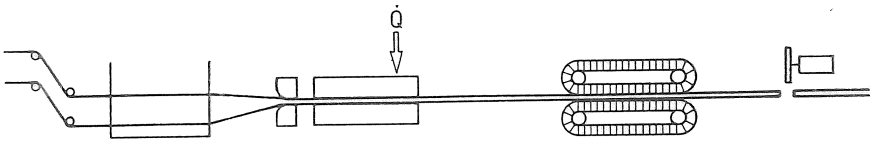

Figure 1.11: Pultrusion with tunnel oven cure[63]

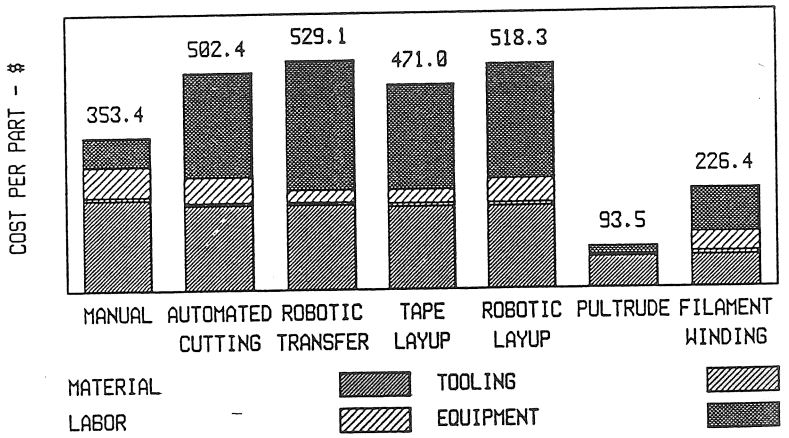

Figure 1.12: Cost for a 0.40-m^2, 24-ply part for an annual production of 2000 parts in the U.S. in 1985 [52]

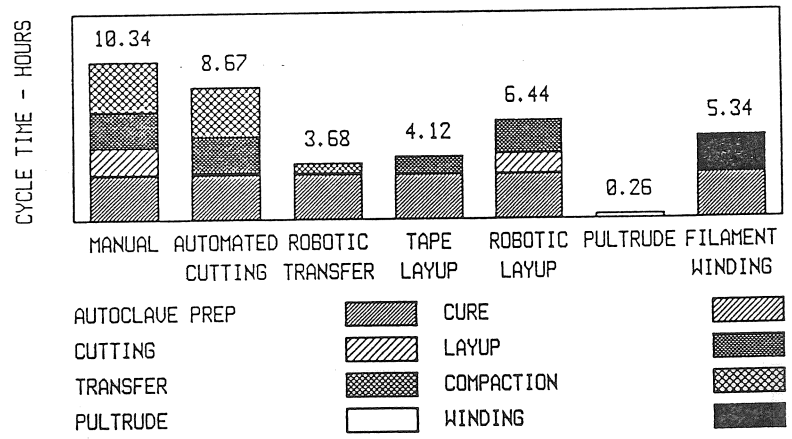

Figure 1.13: Cycle time for a 0.40-m^2, 24-ply part for an annual production of 2000 parts [52]

time. For filament winding the cost increases due to the use of more complex winding machines and more expensive mandrels and mandrel materials. The production time depends on the material lay-up : the production rate of hoop winding is significantly higher than the production rate of low angle helical winding, because helical winding demands more movements of the transverse carriage than hoop winding to wind the same amount of fibre.

Tape winding is a good alternative for filament winding : since one tape is used instead of independent rovings, investment costs for the fibre delivery system are reduced. Tapes are however more difficult to handle, since they easily wrinkle, and paths are limited to geodesics. Fibre placement is a promising technique, but requires very high investment costs.

1.5 The Filament Winding Process

The different steps in the winding process are given in Fig. 1.14. The quality of a filament wound part is influenced by a lot of parameters :

- initial resin viscosity and initial resin content
- initial degree of cure of the resin
- fibre tension
- accuracy of fibre placement
- winding speed (mandrel velocity and transverse carriage velocity)
- cure cycle (B-staging, cure, postcure)

The values of the process parameters must be selected prior to winding, and controlled during winding. They have to be selected in such a way, that the final part meets all the requirements. The mechanical properties of the wound part can be derived from the theoretical data of fibre and resin. But, if the production of the filament wound part is not completely under control, the properties of the wound part can vary up to 50 % [35]. The process requirements are [35, 54] :

- few fibre damage
- the desired fibre volume fraction

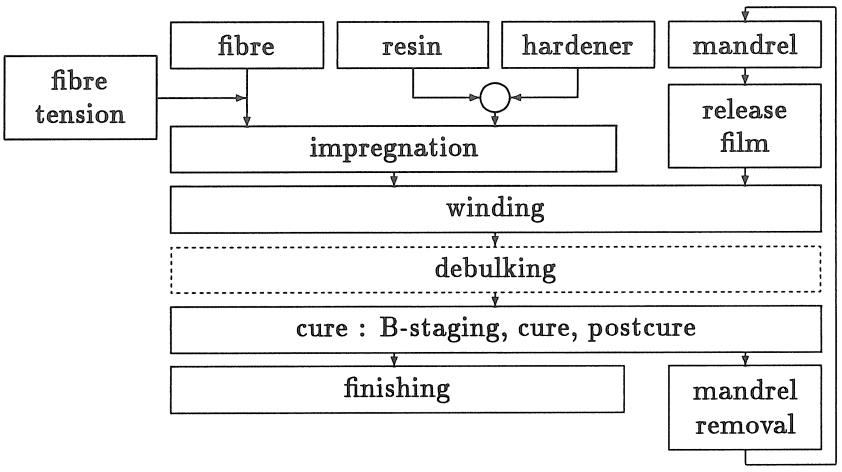

Figure 1.14: Filament winding cycle

- an accurate fibre lay-down and uniform fibre distribution
- low porosity. The composite will be porous through the presence of voids. The filament winding process generates many possible void sites between fibres at roving crossovers. The void content of filament wound parts ranges from 3 to 8 % [27]. A high void content decreases the interlaminar shear strength, and indirectly the compressive strength and the resistance to buckling [83].
- the part may not be damaged during manufacture and cure. Damage may occur due to the residual stresses which are caused by temperature variations. This is especially a problem for thick cylinders and pressure vessels.
- a uniform and complete cure. The temperature may never exceed the maximum allowed temperature [54].
- the part should have the desired properties of strength, stiffness, and shape.
- the manufacturing time should be as short as possible

1.5.1 Winding Pattern

Most of the shapes to be wound are axisymmetric, although every closed surface (except concave surfaces) can be wound. For axisym-

metric parts, a fibre path is repeated all over the circumference. A *winding pattern* is a combination of adjacent fibre paths, which cover the mandrel uniformly. A winding pattern on an axisymmetric surface is defined by the trajectory of the fibre path and the winding sequence.

1.5.1.1 Fibre Paths

The fibre path on an axisymmetric surface is characterized by the *winding angle* α [2, 59], i.e. the angle between the tangent to the fibre path and the generatrix of the surface of revolution, measured in the tangent plane to the surface (Fig. 1.15).

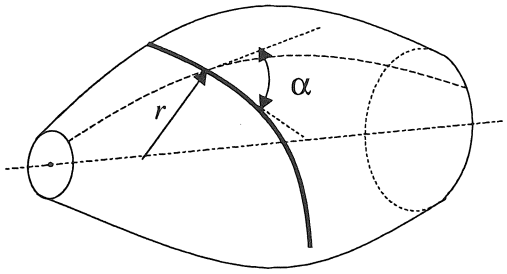

Figure 1.15: Winding angle on a surface of revolution

Geodesic Fibre Paths on Surfaces of Revolution For a surface of revolution, a geodesic meets the equation of Clairaut (cf. Appendix A.1) :

$$r \sin \alpha = c_c \tag{1.9}$$

with r the radius, α the winding angle, and c_c a constant for the geodesic.

Hoop Winding or circumferential winding (Fig. 1.16a) : the fibre bands are wound adjacent to each other, almost perpendicular to the mandrel axis ($\alpha \approx 90°$). Each full rotation of the mandrel, the payout eye advances over the band width, giving complete coverage as the winding progresses.

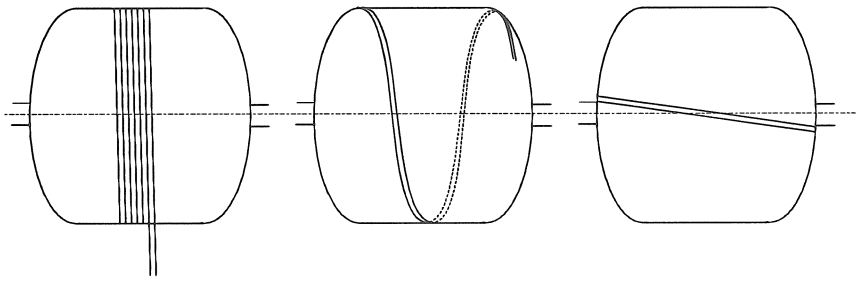

Figure 1.16: Classical fibre paths
(a) Hoop winding (b) Helical fibre path (c) Polar fibre path

Helical Fibre Path (Fig. 1.16b) : a path generated by a two-axis filament winding machine, with a constant velocity ratio between the spindle and the transverse carriage. For cylinders, a path with a constant winding angle is obtained.

Polar Fibre Path (Fig. 1.16c) or planar fibre path : a fibre path that lies in a plane, which is tangent to the polar opening at one end of the part and tangent to the opposite side of the polar opening at the other end. It is mainly used in pressure vessels with length-to-diameter ratios of < 1.8 [73].

1.5.1.2 Winding Sequence

The individual fibre paths have to be combined, so that the whole part is covered. A series of two consecutive fibre paths is called a *winding circuit* : the first fibre path crosses the mandrel from the opening at one end of the part to the opening at the other end, and the second fibre path returns towards the first opening. The next circuit is, for a axisymmetric mandrel, identical to the first but shifted over the circumference of the mandrel.

The time sequence of fibre lay-down in a cross section of a mandrel is called winding sequence, and is denoted as the ratio of two integers $\frac{m}{n}$ (m and n may not have a common divisor).

Two approaches exist, depending on whether or not the band width is taken into account. Lossie [59] ($\frac{m_1}{n_1}$) takes the band width into account. The denominator equals n_p, the global number of fibre paths along the circumference. The second circuit is shifted over a fraction

$\frac{m_1}{n_p}$ of the circumference with respect to the first circuit (e.g. $\frac{3}{8}$-th in Fig. 1.17)

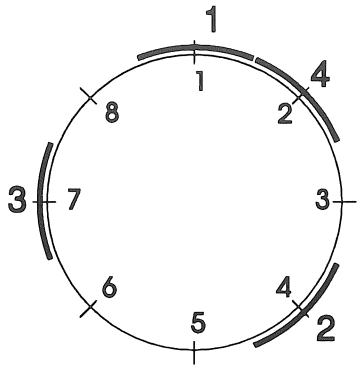

Figure 1.17: Winding sequence : $\frac{m_1}{n_1} = \frac{3}{8}$ (Lossie), $\frac{m_2}{n_2} = \frac{1}{3}$ (Weck)

Weck [109] ($\frac{m_2}{n_2}$) does not take the band width into account : the n_2+1-th circuit is adjacent to the first sequence. Each circuit is therefore shifted over a fraction $\frac{m_2}{n_2} \pm \frac{1}{n_2 n_p}$, with respect to the previous circuit (e.g. winding sequence $\frac{1}{3}$ in Fig. 1.17).

1.5.2 Filament Winding Machines

A filament winding machine consists of :

- an unwinding creel, that can be mounted on the transverse carriage or be stationary
- a tension control unit, that induces a constant tension in the fibre
- an impregnation bath
- fibre guiding systems and the pay-out eye, which is mounted on the carriage of the filament winding machine
- a mandrel support structure (headstock and tailstock), and spindle

1.5.2.1 Mechanical Winding Machines

The oldest filament winding machines are gear-controlled. Transmission gears control the velocity relation between mandrel and pay-out eye. By changing the gears a new winding pattern is obtained. Mechanical winders are mostly limited to two degrees of freedom, and are particularly suited for large production runs of simple axisymmetric components like cylinders and pressure vessels. There are two basic versions : helical winding machines and polar winding machines.

Helical winding machines resemble converted lathes (cf. Fig. 1.1). The mandrel is mounted on the spindle (winding axis), and the pay-out eye and the roving delivery system on the transverse carriage. The pitch of the helical winding pattern is controlled by the transmission gears. The axis is mostly horizontal, but sometimes vertical [73] : this has the advantage that the weight goes through the axis of rotation, minimizing mandrel deflections.

Polar winding machines are developed for the production of dome-ended pressure vessels with small polar openings and low winding angles. The pay-out eye, which is mounted on an arm, moves on a circle while the mandrel rotates slowly. The eye moves in a plane which is tangent to both polar openings. The (polar) fibre paths lie adjacent to each other : while the arm makes one cycle, the mandrel is indexed over the band width.

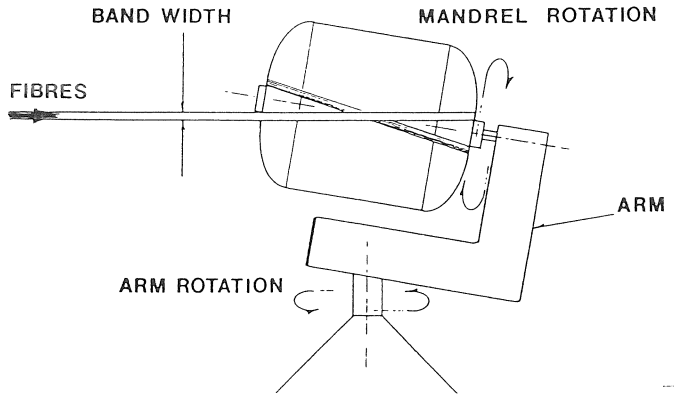

Figure 1.18: Tumble winder[85]

In the tumble winder both movements are performed by the mandrel, and the pay-out eye is stationary [83] (Fig. 1.18).

1.5.2.2 Numerically Controlled Filament Winding Machines

The use of computers in the control of filament winding machines makes it possible to control each axis independently, so that more complex parts, including non-axisymmetric parts, can be wound.

Filament winding machines may have up to 7 axes : the rotation of the mandrel, three translations (transverse carriage and horizontal and vertical cross-feed) and three rotations for the pay-out eye.

All filament winding machines work with bands, consisting of up to 40 rovings. For wide bands, a rotation of the pay-out eye about the fibre feeding axis necessary to maintain a constant band width when the winding angle changes. This rotation can be computer controlled, but also controlled automatically, based on force measurements in the pay-out eye [39].

The impregnation bath is in most cases mounted on the transverse carriage, and the creel with the unwinding bobbins is stationary. If the part is very large, the creel follows the motion of the transverse carriage.

For large parts multiple pay-out eyes are placed in a (translating) ring, which encloses the (rotating) mandrel. Several rovings are pulled through the pay-out eyes and wound at the same time [47].

1.5.2.3 Robotic filament winding machines

Several set-ups have been realized in which an articulated robot is used for filament winding. The pay-out eye is, in all set-ups, mounted on the end flange of the robot and the impregnation bath is stationary. The articulated robot replaces the carriage in a cartesian filament winding machine. Robots have several advantages :

- Robots have more programming capabilities than conventional filament winding machines. Robots are therefore better suited to wind complicated parts.
- The use of robots leads to automation of the whole production process. The robot could moreover be used for other tasks than winding, like mandrel positioning and transfer, and quality control of the composite after cure, with e.g. ultrasonic C-scan.

- The kinematic construction of an articulated robot is better suited to wind complex structures : the inertia of the rotational joints is less than the inertia of the prismatic joints in a cartesian filament winding machine. An articulated robot allows therefore higher winding speeds than a cartesian filament winding machine.
- The price of a robotic filament winder is less than the price of a conventional filament winding machine (ratio 2:3 [65]), since robots are produced in much larger series than filament winding machines.

Robots have however the following disadvantages :

- The accuracy of an industrial articulated robot is generally less than the accuracy of a cartesian filament winding machine. The accuracy can be improved by the application of a calibration technique [103].
- It is often very difficult to synchronize an off-the-shelf robot controller of the first generation with the mandrel drive.
- An articulated robot uses only a small sector of its working envelope. The impregnation bath has to be placed so, that the fed fibre does not interact with the robot. The impregnation bath has therefore to be placed next to the robot, resulting in a severe fibre direction change in the pay-out eye. This problem can be avoided by mounting the robot on the ceiling.

In the most common robotic filament winding set-up [10, 39, 65, 72] a simple pay-out eye is attached to the end flange of the robot. The mandrel is rotated by an external axis, that is synchronized with the robot.

Kirberg [47] (IKV-Aachen) mounts a ring-type pay-out eye, with multiple fibre bundles, on the robot flange. The ring moves through a fixed mandrel. This set-up is very useful to wind S-shaped air ducts.

Automated Dynamics has developed a winding head that attaches to an industrial robot (Unimation Series 6000) for filament winding on a stationary mandrel [113]. This winding head has two translational degrees of freedom, and carries the unwinding bobbins. Due to the fixed mandrel winding time is reduced, but wet winding is not possible.

Elliman [28] (Univ. of Nottingham) uses the robot to assist a cartesian winding machine. An adhesive applicator tool is mounted on the robot. An adhesive is applied to the mandrel just before (dry) fibre contact, at points where normally fibre slippage will occur. In this way, large deviations from geodesics are allowed.

1.5.2.4 Continuous Filament Winding Machines

Continuous working filament winding machines have been developed for the production of endless tubes, which are afterwards cut to the desired length. Two systems have been developed : the Henschel-Finsai system and the Drostholm process.

Henschel-Finsai for the reinforcement of an extruded thermoplastic tube with a helical wound layer and an axial layer. The pay-out eyes are mounted in a ring, which rotates around the axially moving tube [34].

Drostholm An endless steel belt is wound on a cylindrical mandrel. The steel belt moves axially by a helical guide when the mandrel rotates. The composite is wound and cured on the steel belt. The fibre delivery system is stationary [33].

1.5.3 Tooling

One of the big advantages of filament winding over other composite manufacturing techniques is the simplicity of the required tooling. The winding mandrel, that provides the part with an accurate internal geometry, is mostly the only major tool. Mandrel design can be as simple or as complex as the part requires. The basic requirements for the mandrel are [73, 93] :

- The mandrel must be strong enough to support its own weight and the weight of the applied composite while resisting the pressure from the fibres during winding and cure.
- It must be dimensionally stable and should have a coefficient of expansion appropriate to the reinforcement used.
- It may not be so heavy that unwanted bending in the winding axis is induced, thereby adding uncertainty to the fibre path.

- It should be easily removable.
- Cost should be appropriate to the value of the component and the number of items to be fabricated.

1.5.3.1 Mandrel Design

For cylindrical parts *solid removable tube mandrels* are employed. The wound part is pushed or pulled off from the mandrel with a hydraulic cylinder after cure. Steel is preferable to aluminium and copper, due to its better wear resistance and lower coefficient of thermal expansion. Mandrel surface finish is important to ease mandrel removal. A small taper along the length of the cylinder is also beneficial. For high processing temperatures graphite mandrels with low thermal expansion are used [73]. A hollow tube can be used to save weight, but if the thickness of the tube is too small or not uniform, out-of-round parts can be produced [93].

Many parts, like pressure vessels, have small openings at the end, so that solid mandrels cannot be used. Several techniques and materials are applied :

- *segmented (or collapsible) mandrels.* They are used for high production volume applications, since they are very expensive but reusable.
- *spider-plaster mandrels.* A spider frame from metal rods forms a removable or collapsible structure. Plaster is added, cured and machined to the size of the mandrel on a lathe.
- *inflatable rubber mandrels.*
- *dissolvable mandrels* :
  - foams (e.g. polystyrene). They have poor mechanical properties, but are a cheap solution for room temperature curing prototypes [59].
  - water-soluble sand mandrels. The sand is kept together by adding a PVA (polyvinylalcohol) binder. The mandrel is cast in halve female moulds, pressed, and then cured. Both halves of the mandrel are assembled and bonded. The mandrel is removed by pumping hot water through the tooling.
  - soluble salts and low melting temperature alloys. These materials can be recycled after cure.

Irremovable liners are used as mandrels for winding pressure vessels. The liner, that can be either metal, plastic or rubber, prevents the vessel from leaking. This results in a lightweight structure that combines the high specific strength of the composite with a thin, impermeable liner to contain high pressure, low-molecular weight gas, such as helium or hydrogen. If the liner cannot sustain the winding stresses, the mandrel is filled with sand or pressurized.

If the shape contains concave surfaces, and is therefore not windable, a *rubber bladder*, which is inflated to the approximate required part diameter during winding, is used as mandrel. After winding, a female mandrel is placed round the composite part, and gas is pumped into the bladder which applies an internal pressure on the part and moulds it to the contour of the female mandrel [93].

1.5.3.2 Mandrel Ends : Domes, Pin Rings,...

Filament winding uses a continuous band of rovings. Special provisions have to be taken at the mandrel ends, so that the fibre path can return. If the winding angle at the mandrel end is high enough, it is possible to return in a relatively small space by *non-geodesic winding* (cf. appendix A.1.4). End joints are then often integrated in the winding process [59, 73]. If the winding angle is too low, *end domes* – which can be conical or spherical – or *pin rings*, are attached to the mandrel ends. These pin rings or end domes are cut away after cure. Pin rings have the advantage that they offer a complete freedom in the choice of the return fibre path, opposed to end domes where the slippage condition has to be taken into account.

1.5.3.3 Mandrel Preparation

A release material, i.e. a wax or a release tape (e.g. teflon), is applied to the mandrel prior to winding, in order to avoid adherence of the resin to the mandrel and to ease faultless mandrel removal. An adhesive system is applied if bonding of the mandrel to the composite is desired, e.g. for the liner of a vessel.

1.5.4 Fibre Impregnation

The requirements of the impregnation process are :

- to allow a high and constant fibre volume fraction (typically 50 to 70 % [107]).
- to avoid air absorption. Entrapped air and volatiles can lead to voids in the finished structure which are harmful to its properties.
- to allow high winding speeds.

The resins which are used in the wet winding process, have to meet the following requirements :

- Resin viscosity should be in the range of 0.35 – 1.5 Pa·s [95]. Resin viscosity should be high enough to coat well without dripping from the fibres or migrating on the mandrel. If the resin is however too thick, the fibres are poorly wetted or become entangled when passing through the resin bath [95].
- Pot life should be as long as possible, preferably longer than 6 hours [73]. Gelation may not occur before completion of the winding.
- Toxicity should be low, for safety of the operators. It is preferable that no solvents are used in the resin system, since they may be hazardous and difficult to remove during cure.

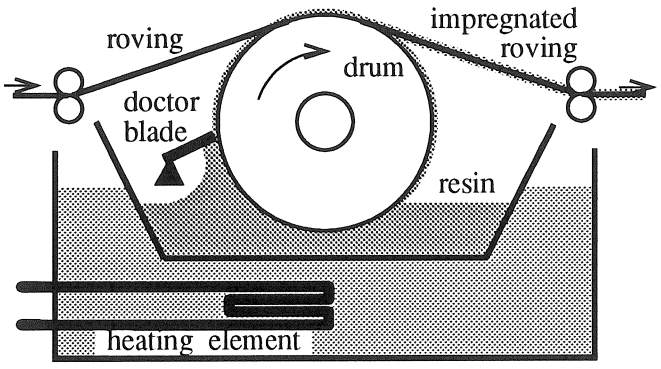

Figure 1.19: Impregnation bath

Wet impregnation can either be accomplished by pulling the reinforcement through a resin bath or over a roller, which contains a controlled volume of resin (Fig. 1.19). In the latter case the fibres force the roller to rotate. A layer of resin, the thickness of which is

controlled by a doctor blade, adheres to the roller. Additional scraping rolls scrape the excess resin from the fibre, which leads to a lower resin content, and remove entrapped air and separate fibres which stick to each other. Scraping rolls induce however large tensions in the fibre.

For higher viscosity resins or higher winding speeds, the rovings pass over and under a series of transverse fingers, immersed in the resin bath [73]. This method leads to a higher resin content and a higher void content, due to frothing of the resin.

The resin content is influenced by many factors :

- resin viscosity, that depends on the temperature of the resin and the time the resin remains in the bath. Resin viscosity can be reduced by heating, although this usually shortens the life of the resin, as the higher temperature will accelerate the curing reactions [61].
- fibre tension. A higher fibre tension leads to a lower resin content, due to the decreasing porosity of the roving [107].
- thickness of resin layer on the impregnation roll.
- winding speed. The residence time of the rovings in the impregnation bath should be sufficiently long for proper fibre impregnation.

The first layers have to be resin-rich, since the outer layers push the resin out of the inner layers. It is therefore advisable to put a layer of resin on the mandrel prior to winding.

1.5.5 Tension Control

Fibre tension is a critical parameter in the impregnation and the consolidation process. The fibre tension on the mandrel provides the interlaminar pressure, which determines the monolithic integrity of the part [97]. Changes in the interlaminar pressure will cause variations in the resin distribution by affecting resin flow. In order to maintain a constant interlaminar pressure, the tension should be changed with changing fibre angle and mandrel diameter (cf. Eq. 1.6).

A higher fibre tension results, on the one hand, in a higher fibre volume fraction, a lower void content, and a better fibre alignment, and so in a lower laminate thickness and in a higher strength. But on the other hand, a higher fibre tension increases fibre damage, resulting

in a lower tensile strength. A higher fibre tension will also increase resin migration from inner to outer layers, and may cause wrinkling of the inner layers or deformations of the mandrel, due to the cumulative pressure of multiple fibre layers [77].

There is no consistency in the optimal fibre tension among manufacturers. Von Gellhorn [107] proposes a fibre tension of 6.25 N per 1000 tex for glass fibre, 3 N per 1000 filaments for carbon fibre, and 2.5 N per 1000 filaments for aramid fibre. According to Munro [65], the fibre tension should be 1% to 2% of the ultimate strength of the fibre (i.e. 13.5 N to 27 N for a 1000 tex E-glass fibre).

Fibre tension should be kept low before the impregnation bath to prevent damage of the dry fibres by abrasion. The tension may be increased after the impregnation bath, since the resin protects the fibre from abrasion.

To obtain a constant fibre tension on the mandrel, the tension should be controlled at the exit point of the pay-out eye, since the fibre tension increases with every change in the direction of the fibre. This is usually not possible, and tension is mostly applied to the fibre at the unwinding bobbin and measured before impregnation. Controlling tension before impregnation has the advantage that the tension control system is not contaminated with resin, resulting in an easier maintenance, but the induced tension should be low to prevent fibre damage. When tension is controlled before impregnation, it should be referred to as "pull-off force control", since the controlled fibre tension differs strongly from the tension at the mandrel.

The tension control system serves often also as a material buffer. In order to enable low angle winding, a post-tensioner, which also works as a buffer, is placed after the impregnation bath to take up slack [94].

Each individual roving should be tensioned independently, so that the fibres can move longitudinally with respect to each other during winding.

At externally unwinding bobbins the tension can be introduced tangentially at the bobbin, by controlling the torque of the unwinding motor. The tension level is set by a constant force (e.g. a pneumatic cylinder or a weight), which acts on a dancer arm [114]. Variations in the fibre feed will cause the dancer arm to move out of its neutral position. The torque of the unwinding motor is then controlled, so that the arm returns to its neutral position (Fig. 1.20). A constant

fibre tension can also be obtained by a motor which exhibits a constant torque in the direction opposite to the unwinding direction.

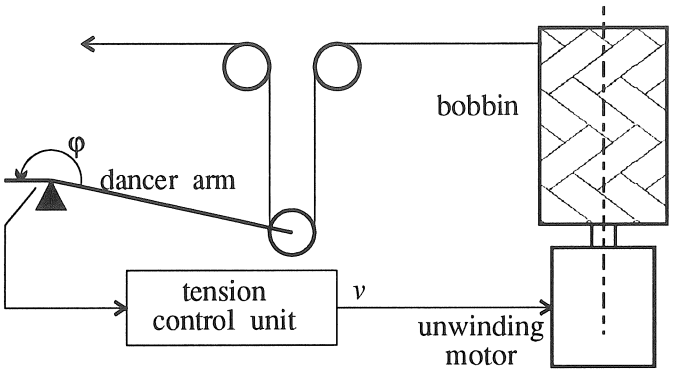

Figure 1.20: Tension control system

Internally unwinding bobbins can be unwound without fibre tension, but require a tension initiator. Initiating tension is very difficult, due to the large risk of fibre damage, which occurs when applying friction, and the abrasive action of the fibres on tension initiators.

1.5.6 Fibre Guiding Systems

The fibre guiding systems have to be designed in such a way that fibre damage is kept as low as possible, by a small surface roughness, a small coefficient of friction, a large wear resistance, large entry- and exit-radii and a large diameter [107].

The construction of the pay-out eye has to be such that the width of the roving band remains constant, independent of the winding angle. The roving band must be uniform, without gaps between individual rovings or rovings lying on top of each other.

Toroidal eyes, grooves or combs, which divide the band of rovings in separate rovings, can be used to guide the rovings. The material, which is used for the guiding systems, depends on the reinforcing material. High modulus fibres, like carbon fibre, are easily damaged, and require ceramic guiding systems. Glass fibre is less demanding, and allows also the use of metals, like brass and chromed steels [107].

Fixed guiding systems are preferable. When rotating guiding rolls are used, separate broken filaments may attach to the rotating rolls.

Rotating guiding rolls have however a lower friction than fixed guiding systems, so the tension increase will be smaller.

1.5.7 Debulking

A high interlaminar pressure is necessary to reduce voids and to obtain a complete compaction during cure. This interlaminar pressure can be provided by the fibre tension or by additional compaction processes. The fibre tension is however limited to prevent fibre damage. Compaction alone is not sufficient : a fibre tension is still needed to align the fibres, in order to increase the longitudinal strength [97].

If the interlaminar pressure, provided by the fibre tension and by the mandrel expansion during cure, is insufficient to provide proper debulking, additional debulking procedures are necessary.

Debulking can be provided by hoop windings, which absorb a part of the resin and compact the previous layers. These hoop windings are, if necessary, removed after compaction.

If the mandrel is flat, or the radius of curvature too large, supplementary interlaminar pressure must be supplied by other sources, such as an autoclave, vacuum bag, or shrink tape. A shrink tape is usually a teflon or polypropylene tape, which is wound with maximal tension round the surface, and which shrinks during cure (3–25% [75]). An exterior mould can be used, in combination with a rubber bladder : the part is wound on the bladder and pressurized against the exterior mould during cure [75].

1.5.8 Cure

During the first part of the cure, B-staging, the mandrel has to rotate continuously to avoid resin concentrations and the formation of resin drops at the bottom of the mandrel. Excess resin can be removed with plastic paddles after B-staging. Heat can be applied in an oven or by infrared lamps, which are placed near the filament winding machine. Heating with lamps has the drawback that non-cylindrical parts will heat unevenly : places which are closer to the lamps will heat more quickly than places far from the lamps. The temperature may never exceed the maximum allowed temperature, to avoid degradation of the resin.

For the normal cure, lamps, ovens and autoclaves may be used.

Autoclave cure results in a better surface quality than oven cure. A postcure can be performed after removing the mandrel, in order to reduce residual stresses.

1.5.9 Finishing

The quality of the inside surface of a wound part equals the quality of the mandrel surface, but the outside surface is typically rough and varies both in dimensions and appearance. The outside surface is not aesthetic and can produce a lot of noise in rotating applications.

Several techniques are used to finish the wound part [75] :

- Grinding with a diamond abrasive grinding wheel.
- Centreless grinding of cylindrical parts with a diamond abrasive.
- Sanding, e.g. in combination with grinding.
- Debulking techniques and pressurized cure (e.g. autoclave) produce a smooth outside surface

The part can be coated after finishing with e.g. an epoxy or elastomeric urethane coating or a metal film [75].

1.5.10 Simulation of the filament winding process

Various models have been developed to simulate the winding process of helical wound cylinders, a.o. by Calius [14], Lee [54], Tzeng [100] and Tarnopols'kii [97]. The models of Calius [14] and Lee [54] consist of the following submodels :

1. The **thermochemical submodel** describes the thermal and chemical processes which occur in the filament wound shell during winding and cure. This submodel provides temperature, viscosity and degree of cure, and the total time necessary to cure the part.

2. The **fibre motion submodel** provides the fibre and resin distributions and the fibre tension in function of time. The fibres move radially due to the radial inward force $\vec{f}_n$, resulting from the fibre tension. The only resistance against this motion is the drag, caused by the motion of the fibres through the viscous resin. The inward motion continues until the tension in the fibres is lost, the resin starts to gel or the fibre layer is fully compacted [100].

3. The **stress submodel** provides the residual stresses and strains. Once the part is cured, thermal stresses and deformations are introduced into it. These stresses and deformations are caused by temperature changes within the shell and by the forces exerted on the composite shell by the mandrel as it undergoes thermal expansion. This submodel calculates also where fibre breakage, delamination and matrix cracking occur due to residual stresses.

4. The **void submodel** provides an estimate of the porosity. Voids are modelled as spherical bubbles which are trapped between layers during winding. The diameter of the void is determined from the radial equilibrium of forces at the void-composite interface.

5. The **strength submodel** calculates the burst strength and elongation of the cylinder at failure.

1.6 Filament Winding Equipment at PMA

Two filament winding machines have been developed at the division PMA : a numerically controlled filament winding machine with two degrees of freedom for axisymmetric parts and a robotic winding unit, which is able to wind complex asymmetric parts.

1.6.1 Filament Winding Machines

1.6.1.1 Two-axis Numerically Controlled Machine

A small low-cost filament winding machine with 2 axes has been developed at PMA to wind axisymmetric parts [59] (Fig. 1.21). The first axis of this machine is the mandrel drive, the second axis is an oscillating arm, on which the pay-out eye is fixed. The pay-out eye describes a circular path in a vertical plane parallel to the mandrel axis. The length of the oscillating arm can be adjusted in function of the dimensions of the mandrel. The inertia of the arm is very small compared with the inertia of the carriage in a conventional cartesian filament winding machine, so that higher winding speeds can be obtained. The velocities of both axes are controlled in such a way that even for complex axisymmetric parts constant winding speeds are obtained [17]. With this machine cylinders, pressure vessels and spinning pots have been

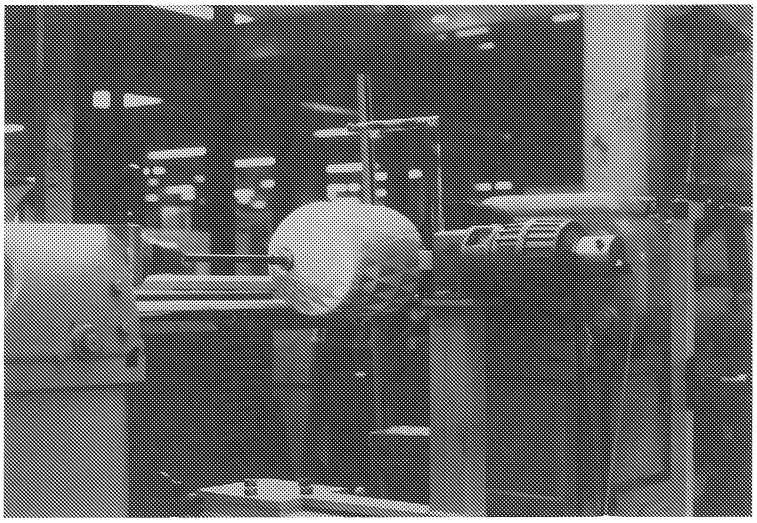

Figure 1.21: Two-axis numerically controlled filament winding machine

wound successfully [59]. The calculation of the positions of the pay-out eye and the control of the axes is discussed extensively in Appendix B.

1.6.1.2 Robotic Filament Winding Cell

A robotic filament winding cell has been developed for the production of asymmetric shapes. The robotic cell consists of a stationary fibre feeding unit (tension control unit and impregnation bath), a robot, on which the pay-out eye, that pulls the fibre onto the mandrel, is mounted, and a mandrel support unit with the mandrel drive (Fig. 1.22). The robot is an articulated PUMA-762 from Unimation, with six degrees of freedom, and off-line programmable in the VAL-II language. The pay-out eye, which is mounted on the end flange of the robot, consists of two toroidal ceramic eyelets. The eyelets are directed in such a way that the fibre does not meet any sharp edges.

The mandrel support structure consists of the head- and tail-stock. The mandrel drive and the chuck are mounted on a headstock, the centre point on a tailstock. Both head- and tail-stock can be moved along a linear slide. The whole structure can be moved with respect to the robot, in order to make optimal use of the working envelope of

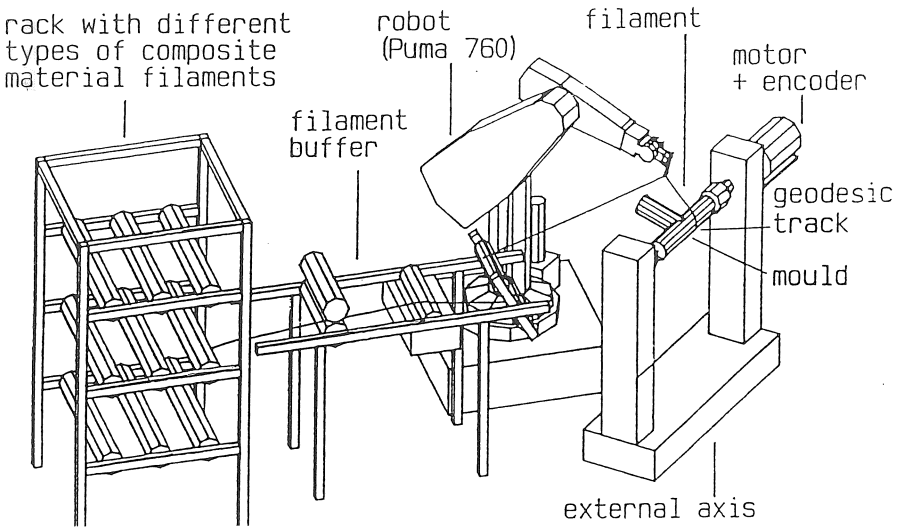

Figure 1.22: Robotic filament winding cell

the robot.

The robotic filament winding cell has been adapted to enable tape winding. The basic material is a 25-mm wide unidirectional glass fibre tape. The tape is impregnated during winding, so that this process can be described as a "wet tape winding" process. A rotation of the delivery rolls about the feeding direction is added to the pay-out to maintain a constant band width. The robotic tape winding cell is discussed extensively in section 4.3.2.

1.6.2 Impregnation Bath

The fibre is pulled over a drum, which contains a metered volume of resin, controlled by a doctor blade.

The resin bath meets the following design requirements [21] :

- easy maintenance. The number of elements making contact with the resin is as small as possible, and these elements are easily dismounted and cleaned.
- the volume of the resin bath is as large as possible, to reduce refilling operations during winding. The minimum amount of resin for proper impregnation is as small as possible.

- the bath can be used both for rovings and for tapes.
- the bath contains a heating element to reduce resin viscosity.

The resin bath [21] consists of a drum, which rotates freely in the bath, a doctor blade, a roller, which rests upon the drum and allows to impregnate the upper side of the tape, and some scraper rolls (Fig. 1.23). These scraper rolls induce however high forces in the fibre and increase so the risk of fibre damage [21].

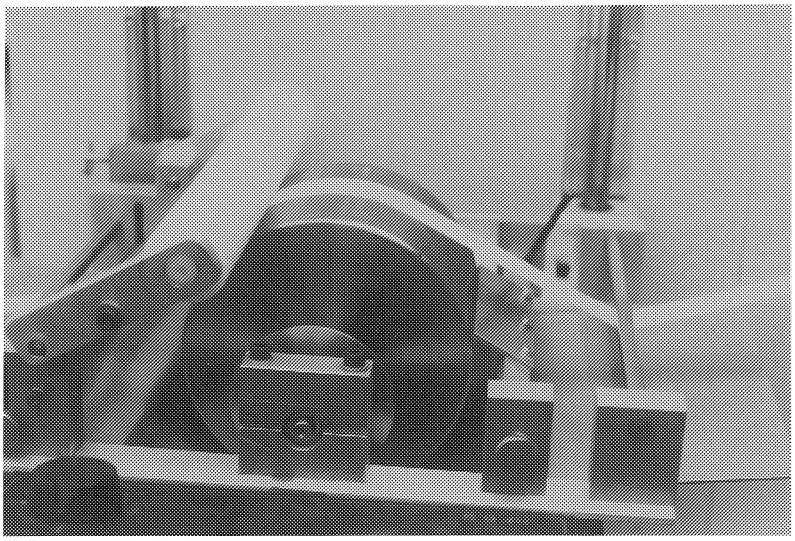

Figure 1.23: Impregnation bath

1.6.3 Tension Control Units

Tension is controlled at the unwinding motors. It is rather a pull-off force control than a fibre tension control, since tension in the fibre raises due to the multiple direction changes. A constant fibre pull-off force will lead to a constant impregnation.

1.6.3.1 Externally Unwinding Bobbins

The roving passes round two rollers which are mounted on the ends of a dancer arm (Fig. 1.24). The desired pull-off force is set by a mass, which exhibits a constant moment on the dancer arm. In equilibrium the moment of the roving forces compensates the constant moment

of the mass. Variations in the fibre tension change the position of the dancer arm. The position of the dancer arm is measured with a potentiometer, and fed back to the motor control. The speed of the unwinding motor is proportional to the deviation from the equilibrium position.

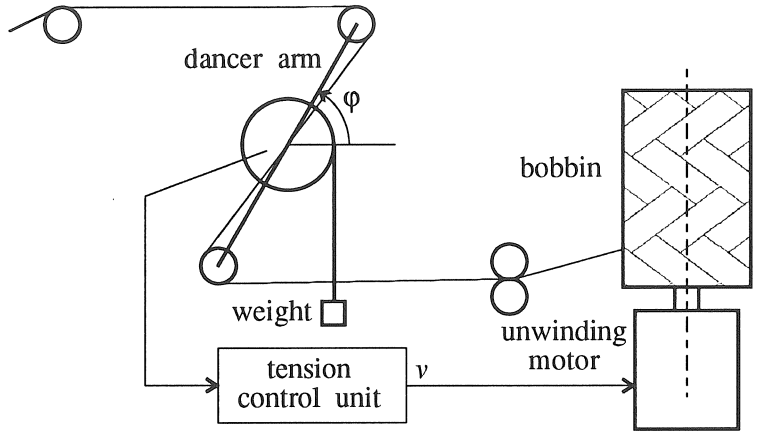

Figure 1.24: Dancer arm tension control system

The dancer arm works also as a buffer between the pay-out eye, and the unwinding motor. The length of the dancer arm has to be large enough to compensate for accelerations of the roving. The slack, which can be taken up during rewinding is however limited. Unacceptable forces are induced in the roving when the motor does not react on the signal of the potentiometer.

1.6.3.2 Internally Unwinding Bobbins

Internally unwinding bobbins, which have a centre pull, do not need a force to unwind. A constant tension has to be initiated in the roving. Several problems occur during tension initiation :

- If the roving is clamped, e.g. between two leaf springs or two steel rollers, the rovings are severely damaged.
- Rovings slip easily, even over rubber rolls, so that it is difficult to introduce tension by applying friction.
- When rotating systems are used, broken filaments adhere easily to the rotating rolls, and hinder the fed roving.

A solution has been found by using two soft profiled rubber rollers [21] (Fig 1.25). Due to the profile, the roving is continuously clamped and released, so that it will not adhere to the rollers. A constant torque is applied to one of the rollers, so that a constant tension is initiated in the roving. The fibre must however be dry. Traces of oil or resin will reduce the friction between roving and rolls, so that the fibre will slip over the rolls, and no tension is induced. The rewinding capacity is therefore limited to the distance between the impregnation bath and the tension initiator.

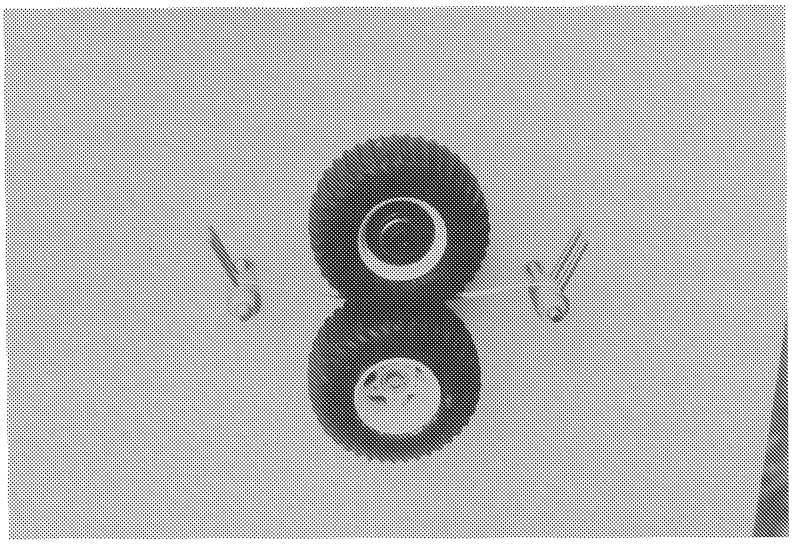

Figure 1.25: Tension control system for internally unwinding bobbins

1.6.3.3 Tension Control Unit for Tapes

The 25-mm wide glass fibre tapes, which are used in the robotic tape winding process are delivered in small bobbins containing 50 m tape. The bobbin is mounted on the shaft of a DC-motor with a permanent magnetic field. This motor is driven with constant current, and hence with a constant torque. The fibre pull-off force is then inverse proportional to the radius of the bobbin.

In order to obtain a constant pull-off force, the motor torque has to be adapted in function of the radius. A pivoting arm, at the end of which a roller is attached, rests on the bobbin (Fig. 1.26). The position

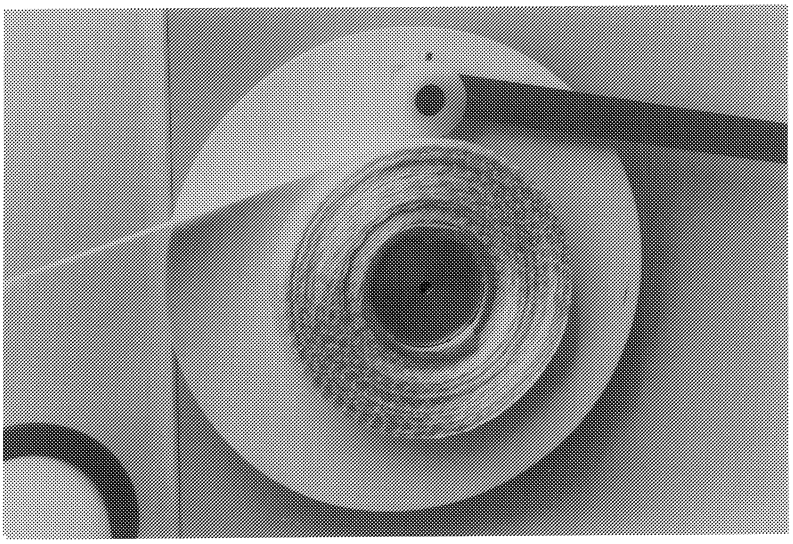

Figure 1.26: Tension control system for tapes

of the arm, which is a function of the bobbin radius, is measured with a potentiometer. The position of the potentiometer is fed back to the motor control, which adapts the motor current.

The applied tension is kept low to reduce fibre damage and to reduce the forces which act on the impregnation bath and the pay-out eye. The forces in the pay-out eye have to be limited due to the limited load capacity of the robot (200 N [122]).

1.7 Conclusions

The basis of the filament winding process is the high-speed precise lay-down of continuous reinforcements in prescribed patterns. The trajectory of the fibre path can however not be determined freely : in order to obtain an accurate fibre placement, the fibres must be placed along slip-free trajectories. The continuous lay-down of fibres leads to automation.

The main advantages of the filament winding process are [73] :

- Low capital cost, due to the elimination of an expensive autoclave. For many applications a simple mechanical winder is sufficient, reducing further capital cost.

- Low material cost, since fibre and resin can be used in their lower cost form rather than as prepreg.
- Low labour input, due to the automation of the process.
- Low tooling costs, since only an inner mandrel is necessary.
- The highly repetitive nature of fibre placement for axisymmetric surfaces
- The capacity to use continuous fibre over the whole component area.
- High material usage, due to the capacity to use the fibres optimally.
- High fibre volume fraction possible.
- Large structures can be built, larger than any autoclave.
- Joints can be easily included in the winding process [73].

The main disadvantages are :

- The key process parameters (resin content, fibre tension) are difficult to control when winding complex parts. Control of the key parameters is important, in order to obtain a part with a high and reproducible quality.
- The laminate quality is generally lower than that of an autoclave-cured part, due to the limits on fibre tension. A higher void content and a lower shear and compressive strength result.
- Poor external surface, which may hamper aerodynamics or aesthetics.
- The trajectory of the fibre paths is limited to semi-geodesics. The tape winding process is even more restrictive and allows only geodesics. In convex/concave surfaces fibre bridging can occur, and collisions between the pay-out eye and the mandrel.
- The fibre path can only be changed abruptly by pins. Pins have to be located in a section of the part that is cut away after curing.
- The shape of the mandrel, or the mandrel material, has to be such that the mandrel is removable. Concave parts cannot be wound directly, and require the use of an inflatable mandrel and forming after winding [93, 95].

Filament winding is a cost-effective method to produce closed high performance composite structures. Tape winding is a good alternative for filament winding : since one tape is used instead of independent rovings, investment costs for the fibre delivery system are reduced. Tapes are however more difficult to handle, since they easily wrinkle, and the trajectory of the fibre paths is limited to geodesics. Fibre placement is a promising technique, but requires very high investment costs.

Chapter 2

Computer Integrated Winding Environment

2.1 Introduction

Filament winding allows to place the fibres with a highly reproducible degree of precision, and has therefore become a widely used technique for the production of high quality composite structures. The calculation of the fibre and machine paths of a filament wound part requires however considerable mathematical effort. Due to the increasing complexity of the part geometry, advanced software tools are required for the design and production of filament wound parts.

The labour-intensive part design, development and production costs can be reduced by automation of the design and the production. This requires the creation of a computer integrated environment round the winding process, which includes design, production and quality control of the wound part. The design of a filament wound part includes the design of the shape and the design of the fibre paths. The programs which are utilized during the design phase are : CAD/CAM systems to model the shape of the part, finite element analysis programs to calculate stresses and strains in complex composite structures, and special application software to calculate fibre paths. In the production phase the machine path is calculated, based on the data of the fibre paths. Quality control is performed with an automated ultrasonic technique.

This chapter describes, after a literature survey, what this computer integrated environment should encompass. The next section

discusses the techniques to write application programs in a CAD-environment. These techniques are applied to two processes : robotic filament winding and robotic ultrasonic C-scanning.

2.2 Literature Survey

Several software packages have been developed for the design and production of filament wound parts, e.g. CADFIL [64], CADMAC [110] and CADFIBER [47]. CADFIBER from IKV-Aachen is an integrated program for composite materials, consisting of four modules : materials data bases, construction and dimensioning, process simulation (filament winding and SMC) and quality assurance. The manufacturers of filament winding machines, e.g. Baer [7] and En-Tec (FiberGrafix) [115] provide software for the calculation of fibre paths and machine paths on simple geometries.

All these packages have their own graphics for the representation of surfaces and fibre paths. Some programs have links with commercial CAD-systems for the definition of the shape of the surface (CADMAC). Some packages have interfaces to Finite Element systems (CADFIL, CADMAC, FiberGrafix).

All these packages are practically limited to "tubelike" (or "almost axisymmetric") surfaces, i.e. closed surfaces with a central spine and an almost constant cross-sectional shape. For such surfaces a winding pattern is formed by repeating a basic fibre path all over the circumference, so that the fibres are spread equally over each cross section normal to the spine [47, 64]. The angle of the fibre path, and thus the thickness and the lay-up, can be derived at each point of the part from the winding pattern and the number of fibre paths per cross section (cf. Appendix A.3). Hence, the input for finite element calculations can directly be derived from the winding pattern.

Asymmetric shapes, where the shape of the cross section varies strongly, like branched mandrels, are difficult to handle with these programs. Opposed to tubelike surfaces, a single winding pattern that covers the asymmetric part completely cannot be found. Each fibre path must be separately designed, resulting in a large amount of data for complete part coverage. The lay-up and the thickness differ in each point of the part, depending on the fibre paths that pass over the element.

The position of the pay-out eye is defined by the intersection of the tangent to the fibre path with an enveloping control surface [47, 115] or by maintaining a constant distance between mandrel and pay-out eye [110]. Some programs [2, 110] check on collisions between mandrel and pay-out eye, which are e.g. possible in convex/concave areas.

2.3 Computer Integrated Winding Environment

2.3.1 Computer Integrated Design of Wound Parts

2.3.1.1 Design Tools

The design of a wound part includes both the design of the part shape and the design of the fibre paths. Different tools are used for the design of the geometry, the strength analysis and the calculation of fibre paths.

Design of the Part Geometry The shape is designed with the surface modeller of a CAD-system. The shape can be completely predetermined, or the design of the shape can be an integral part of the winding design. In the latter case, the shape of the part and the fibre paths have to be designed so, that all the fibres are uniformly stressed, and that these stresses are as low as possible. If an outside shape is defined, the shape of the mandrel depends on the thickness of the wound part, and thus on the wound lay-up.

The CAD-systems which were used within this work are CDM-300 from Kongsberg, ANVIL-5000 from MSC and Unigraphics-II from McDonnell Douglas.

The CAD-surface model is also used to fabricate the mandrel or the mould, in which the mandrel is cast, on a CNC-machine.

Strength analysis Several techniques can be used to calculate stresses in composite materials :

Netting analysis assumes that only the fibres take up all the load, and that all the fibres are equally loaded. Netting analysis is employed for e.g. the generation of end domes of pressure vessels [59].

Laminate plate theory [99] for the calculation of the strength and stiffness of laminates.

Finite Element Analysis (FEA) allows to calculate stresses in a mesh of anisotropic (e.g. laminated composite) elements. The forces acting on each element are calculated by the Finite Element Analysis, the stresses in the different plies of the composite element are calculated with the Laminate Plate Theory. The FEA-programs available at the division PMA are SYSTUS from Framatome and NASTRAN from MSC.

Generation of fibre paths In order to obtain an accurate and reproducible lay-down, fibre paths must correspond to semi-geodesics. A computer program **CAWAR** has been developed to calculate fibre paths on a part, that is described in a CAD-system.

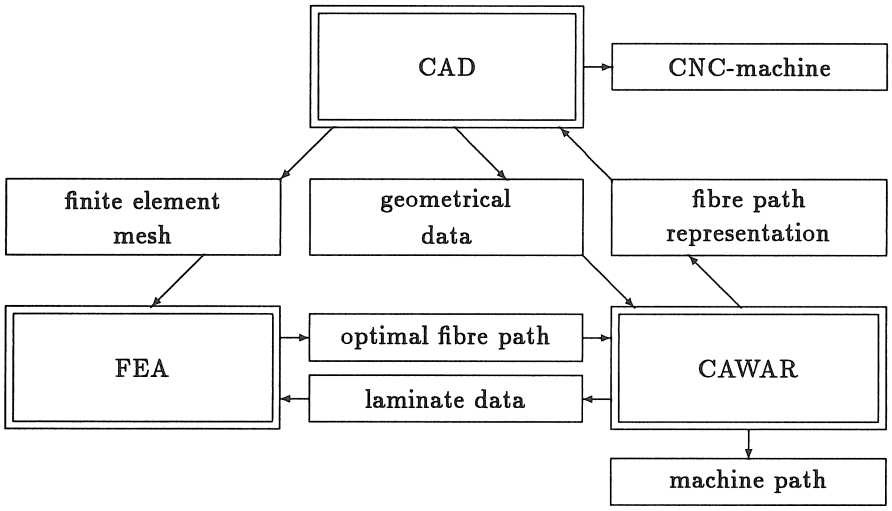

Figure 2.1: Integration of CAD, FEA and CAWAR

2.3.1.2 Integration of Design Tools

The tools which are used for the design of the wound part (CAD, FEA, **CAWAR**) have to be integrated (Fig. 2.1). Information must be exchanged between the different design tools :

Finite Element Mesh The finite element mesh (of e.g. Nastran) can be created by the FEA-preprocessor of a CAD-system (e.g. Unigraphics). This ensures that the geometry in the FEA-system corresponds to the CAD-surface model.

Geometrical Data The program CAWAR needs the mathematical description of the surfaces for the calculation of the fibre paths. The geometrical data of the surfaces are extracted from the CAD-system and inputted in the application program.

Fibre Path Representation The program CAWAR has no own graphic possibilities. The fibre paths, which are calculated in CAWAR are represented in the CAD-system.

Optimal Fibre Path The winding angles, desired to obtain a part with an optimal strength, are derived from the results of the finite element analysis. The method, which is used for the calculation of the optimal winding angles is principal stress design [99] : the fibres are aligned with the principal stress directions [20, 24, 64].

This method is very efficient, but is limited to single load design [99]. Another possibility is to use netting analysis, starting from the principal stresses [73]. Netting analysis calculates the optimal angle α of a symmetric laminate with an equal amount of fibres in the α and the $-\alpha$ direction, under the assumption that all the fibres are equally loaded [73]. Consequently, netting analysis provides only good results if the principal stress directions correspond to the axial and the circumferential direction and if both principal stresses have an equal sign.

The optimal winding angles in the elements of the finite element mesh are inputted in the program CAWAR to calculate the optimal fibre path [20].

Laminate Data In order to be able to perform a composite finite element analysis, the data of the fibre paths have to be translated towards laminate data (i.e. ply angles and ply thicknesses) for the elements of the finite element mesh. A distinction is made between tubelike and asymmetric parts. For tubelike parts, the laminate data

are derived for each element, starting from the data of one basic fibre path. For asymmetric parts, the program LUPGEN, developed by Lossie [59], calculates the laminate data for each element, starting from the data of all the individual fibre paths. The input file for the FEA-program is updated with the new laminate data [20].

2.3.2 Computer Integrated Production of Wound Parts

Winding machines can be programmed in several ways : by teaching the machine how to wind the part, by calculating the path during the process by the controller of the winding machine, or off-line, by a program developed on an external computer.

Application Software Most suppliers of filament winding machines [7, 115] provide application programs for winding standard shapes, such as cylinders and pressure vessels. The operator just inputs the required component parameters such as diameter, length, winding angle, winding speed,... and the controller of the winding machine generates the required machine path [65].

Teach-in The operator leads the pay-out eye physically through the winding process, teaching it how to lay the fibre along the desired path, and records its position at regular time intervals [39]. A collision-free control program is generated, which can be repeated by the machine. The teaching operation is however very time consuming and occupies the machine for a large amount of unproductive time. Another drawback is that it is almost impossible for the operator to teach the desired winding pattern accurately. Since teach-in programs are developed with dry fibres, which have significantly higher friction with the mandrel than wet-resin, the lay-up may not be stable [64]. Furthermore, teach-in is done statically what can lead to severe machine and fibre accelerations when the program is run dynamically. Regions with high accelerations can be removed by smoothing the path with sophisticated and highly interactive software packages [115].

Off-line The machine program is generated away from the machine on an external computer. An off-line program is generated in several steps :

- Calculation of the positions of the pay-out eye and the rotations of the spindle on the external computer, starting from the data of the fibre paths, so that all the task requirements are fulfilled. All possible collisions between the pay-out eye and the mandrel have to be foreseen and avoided.
- Calculation of the path velocity : the machine motions have to be optimized to minimize winding time without violating any constraints on accuracy, velocity and acceleration.
- Generation of the off-line machine program. The program can be simulated in a graphical robot simulation system, like IGRIP or ROBCAD, to check if the task is performed correctly.
- Downloading the off-line program in the machine controller.

The advantages of off-line programming are that the work of the operator is reduced to a minimum, that the machine is freed for production runs only, and that fibre placement is more accurate. Off-line programming allows to integrate the machine in a CAD-environment.

2.3.3 Computer Integrated Quality Control of Wound Parts

In the quality control phase, ultrasonic C-scanning is used to check the composite material on defects. A robotic ultrasonic C-scanning cell has been developed, in collaboration with the department MTM. An ultrasonic transducer is mounted on the end flange of the robot, and scans the surface at a constant distance normal to the surface. An off-line robot program is generated, starting from a CAD-description of the part. The measuring data of the ultrasonic transducer are visualized on a computer screen after execution of the robot program. The ultrasonic technique is discussed more in detail in section 2.7.

2.4 Surface Related Robot Programming

Winding, scanning and machining are tasks in which the motion of the tool is related to the surface geometry of the part. Performing a task on a surface involves two steps : the generation of paths on the surface, and the calculation of the position of the tool, according to the task requirements (e.g. aligning the tool with the normal to the surface).

2.4.1 Surface Paths

2.4.1.1 Surface Representation

A curve in $\mathbb{R}^3$ is in a CAD-system represented as a function Γ of a parameter s [69] :

$$\Gamma(s) : I \subset \mathbb{R} \rightarrow \mathbb{R}^3 : s_0 \leq s \leq s_1 \rightarrow \Gamma(s) = \begin{bmatrix} x(s) \\ y(s) \\ z(s) \end{bmatrix}$$

The functions $x(s), y(s)$ and $z(s)$ are called the coordinate functions of the curve Γ.

A surface is most commonly described by the mapping[1] $S(u, v)$ [69] :

$$S(u,v) : D \subset \mathbb{R}^2 \rightarrow \mathbb{R}^3 : \begin{cases} u_0 \leq u \leq u_1 \\ v_0 \leq v \leq v_1 \end{cases} \longrightarrow \mathbf{s}(u,v) = \begin{bmatrix} x(u,v) \\ y(u,v) \\ z(u,v) \end{bmatrix}$$

Surfaces which are implemented in CAD-systems include surfaces of revolution, ruled surfaces, Coons-, Bézier-, B-spline surfaces [31, 81],... As an example, a surface of revolution, which is generated by rotating a planar curve $C(u) = [x(u) \quad r(u) \quad 0]^T$ about the x-axis, is represented by :

$$\mathbf{s}(u,v) = [x(u) \quad r(u)\cos v \quad r(u)\sin v]^T \tag{2.1}$$

u is the parameter along the generatrix (axial parameter), v is the parameter along the circumference (circumferential parameter).

A curve $C_2(s) = [u(s)\ v(s)]^T$ in $\mathbb{R}^2$ can be mapped on the surface $S(u, v)$, thus defining a curve $\Gamma(s)$ on the surface S (Fig. 2.2).

2.4.1.2 Frenet-trihedron

A Frenet-trihedron [79] is attached to each point f of the curve Γ on the surface S. The Frenet trihedron consists of three orthonormal vectors : the unit tangent $\vec{t}$, the outwards directed normal $\vec{n}$, and the binormal $\vec{b}$ (Fig. 2.3).

---

[1] $\vec{s}$ is the position vector of a point on the surface, s stands for the array representing the coordinates of the position vector $\vec{s}$ (cf. p. xxv).

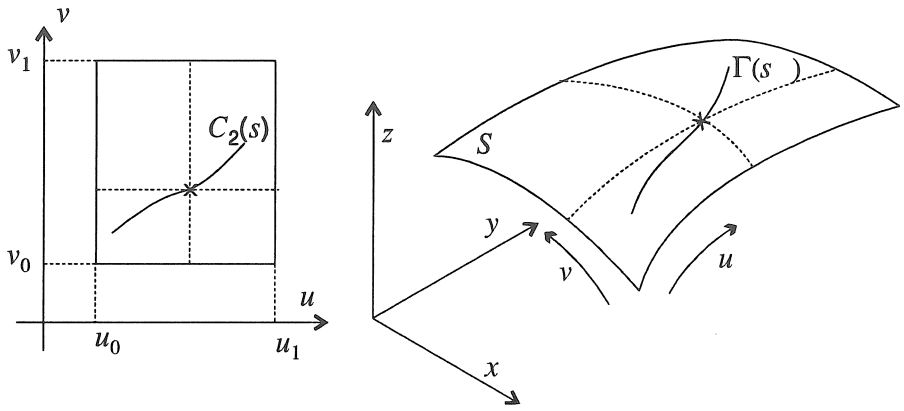

Figure 2.2: Curve on a surface

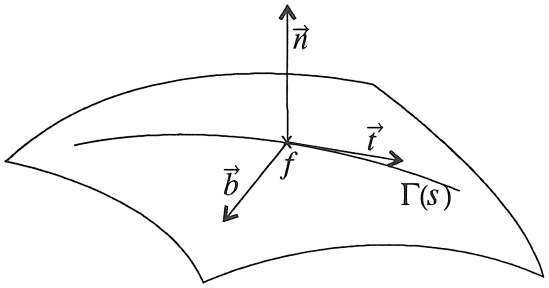

Figure 2.3: Frenet trihedron

The Tangent $\vec{t}$ is defined as :

$$\vec{t}(s) = \frac{d\vec{\Gamma}(s)}{ds} = \frac{\partial \vec{s}(u,v)}{\partial u}\frac{du}{ds} + \frac{\partial \vec{s}(u,v)}{\partial v}\frac{dv}{ds} = \vec{s}_u\frac{du}{ds} + \vec{s}_v\frac{dv}{ds} \qquad (2.2)$$

If the length of the tangent differs from 1, the tangent has to be normalized.

The *natural parametrization* is the parametrization in which the parameter s corresponds to the path length on the curve. The length of the tangent is then always 1. For a natural parametrization, the following relation has to be fulfilled :

$$\vec{t}\cdot\vec{t} = 1 \implies \frac{d(\vec{t}\cdot\vec{t})}{ds} = 0 \text{ or } 2\vec{t}\cdot\frac{d\vec{t}}{ds} = 0 \qquad (2.3)$$

The Outwards Directed Normal $\vec{n}$ to the surface S is the normalized cross product of two non-coincident vectors in the tangent plane at S, e.g. $\vec{s}_u$ and $\vec{s}_v$, the derivatives in the u- and the v-direction :

$$\vec{n} = \pm \frac{\vec{s}_u \times \vec{s}_v}{\|\vec{s}_u \times \vec{s}_v\|} \tag{2.4}$$

The sign depends on the material side of the surface.

The Binormal $\vec{b}$ is the cross product of the unit tangent $\vec{t}$ and the normal $\vec{n}$:

$$\vec{b} = \vec{t} \times \vec{n} = \vec{b}_u \frac{du}{ds} + \vec{b}_v \frac{dv}{ds} \text{ with } \begin{cases} \vec{b}_u &= \vec{s}_u \times \vec{n} \\ \vec{b}_v &= \vec{s}_v \times \vec{n} \end{cases} \tag{2.5}$$

The tangent $\vec{t}$ and the binormal $\vec{b}$ are function of $u, v, \frac{du}{ds}$ and $\frac{dv}{ds}$. The normal $\vec{n}$ depends only on u and v.

If the curve $\Gamma(s)$ is naturally parametrized, the vector $\vec{c} = \frac{d\vec{t}}{ds}$ is, according to (2.3), always normal to the tangent $\vec{t}$ to Γ_s. The vector $\vec{c}$ is called the *curvature vector*, and is directed towards the centre of curvature of the curve [69]. The curvature vector equals :

$$\vec{c} = \vec{s}_u \frac{d^2u}{ds^2} + \vec{s}_v \frac{d^2v}{ds^2} + \vec{s}_{uu} \left(\frac{du}{ds}\right)^2 + 2\vec{s}_{uv} \frac{du}{ds}\frac{dv}{ds} + \vec{s}_{vv} \left(\frac{dv}{ds}\right)^2 \tag{2.6}$$

The curvature κ_c of Γ at f corresponds to the length of the curvature vector [69].

2.4.2 Machine Path

The pose of the tool is represented by a frame $\{e\} = \{e; \vec{t}_e, \vec{n}_e, \vec{b}_e\}$, with as origin the end point e of the tool and consisting of the three orthonormal vectors $\vec{t}_e, \vec{n}_e$ and $\vec{b}_e$. The position of the frame $\{e\}$ in a coordinate system, e.g. the machine base coordinate system $\{b\}$, is given by the homogeneous transformation matrix ${}^b_e\mathbf{T}$. This transformation matrix consists of a transformation matrix ${}^b_e\mathbf{R}$, and the position vector ${}_b\mathbf{e}$ [18] (cf. p. xxv) :

$$ {}^{b}_{e}\mathbf{T} = \begin{bmatrix} {}^{b}_{e}\mathbf{R} & {}_{b}\mathbf{e} \\ \mathbf{0}_{1\times 3} & 1 \end{bmatrix} = \begin{bmatrix} [{}_{b}\mathbf{t}_{e} & {}_{b}\mathbf{n}_{e} & {}_{b}\mathbf{b}_{e}] & {}_{b}\mathbf{e} \\ 0 & 0 & 0 & 1 \end{bmatrix} \tag{2.7} $$

$$ = \begin{bmatrix} {}_{b}t_{e,x} & {}_{b}n_{e,x} & {}_{b}b_{e,x} & {}_{b}e_{x} \\ {}_{b}t_{e,y} & {}_{b}n_{e,y} & {}_{b}b_{e,y} & {}_{b}e_{y} \\ {}_{b}t_{e,z} & {}_{b}n_{e,z} & {}_{b}b_{e,z} & {}_{b}e_{z} \\ 0 & 0 & 0 & 1 \end{bmatrix} \tag{2.8} $$

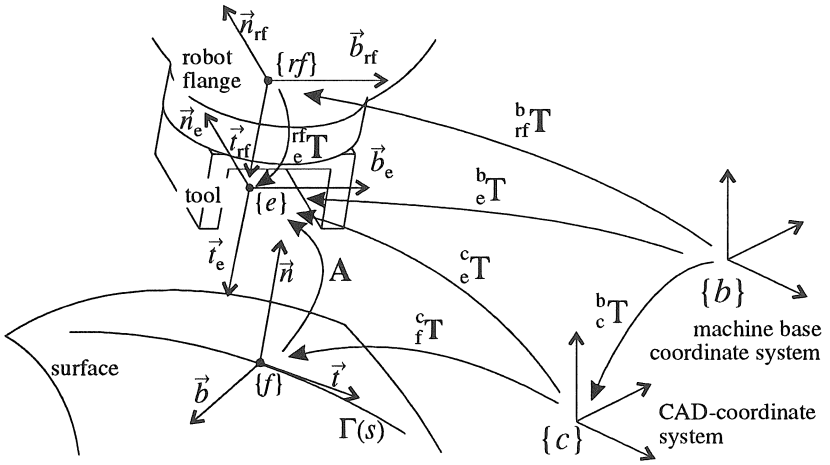

Figure 2.4: Position of the robot tool

The task requirement defines the pose of the tool frame $\{e\}$ with respect to the Frenet trihedron in f. The Frenet trihedron $\{f\} = \{f; \vec{t}, \vec{n}, \vec{b}\}$ is defined in the CAD-coordinate system $\{c\}$, and represented by the transformation matrix ${}^{c}_{f}\mathbf{T}$. The tool $\{e\}$ is defined relatively to the end flange of the robot $\{rf\}$ by ${}^{rf}_{e}\mathbf{T}$. The relation between the Frenet trihedron $\{f\}$ and the tool $\{e\}$ is given by the transformation matrix $\mathbf{A} = {}^{f}_{e}\mathbf{T}$. The position of the tool in the CAD-coordinate system equals (Fig. 2.4) :

$$ {}^{c}_{e}\mathbf{T} = {}^{c}_{f}\mathbf{T}\ {}^{f}_{e}\mathbf{T} = {}^{c}_{f}\mathbf{T}\ \mathbf{A} \tag{2.9} $$

The position of the tool in the coordinate system $\{b\}$, attached to the robot base equals :

$$ {}^{b}_{e}\mathbf{T} = {}^{b}_{c}\mathbf{T}\ {}^{c}_{e}\mathbf{T} = {}^{b}_{c}\mathbf{T}\ {}^{c}_{e}\mathbf{T} \tag{2.10} $$

The transformation matrix ${}^{b}_{c}\mathbf{T}$ represents the position of the CAD-coordinate system in the coordinate system attached to the robot base.

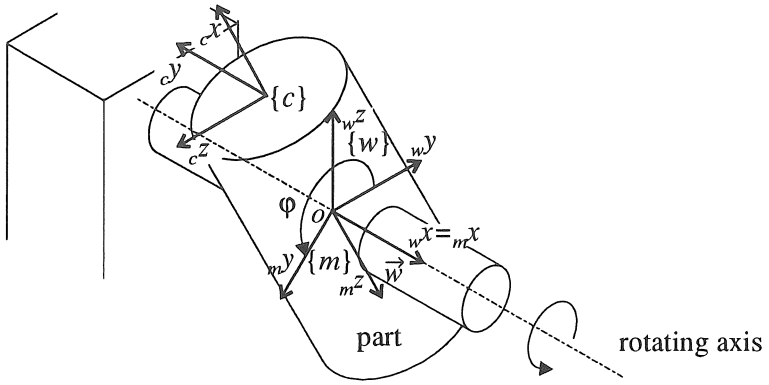

Figure 2.5: Mandrel and winding coordinate system

The position of the end flange of the robot equals :

$$ {}^{b}_{rf}\mathbf{T} = {}^{b}_{c}\mathbf{T}\ {}^{c}_{e}\mathbf{T}\ {}^{e}_{rf}\mathbf{T} = {}^{b}_{c}\mathbf{T}\ {}^{c}_{e}\mathbf{T}\ {}^{rf}_{e}\mathbf{T}^{-1} \tag{2.11} $$

For some applications, like filament winding and scanning of cylindrical parts, an external axis is added to rotate the part. Two supplementary coordinate systems are then defined : the mandrel coordinate system $\{m\}$, which is attached to the part, and the winding coordinate system $\{w\}$, which is attached to the machine (Fig. 2.5). The x-axis of both coordinate systems corresponds to the rotating axis $\vec{w}$. The origin o of both coordinate systems lies on the rotating axis. At the start of the motion, both coordinate systems coincide. The pose of the tool in the winding coordinate systems equals :

$$ {}^{w}_{e}\mathbf{T} = \mathbf{Rot}(x, \varphi)\ {}^{m}_{c}\mathbf{T}\ {}^{c}_{e}\mathbf{T} \tag{2.12} $$

with φ the angle of the rotating axis. The pose of the tool in the machine base coordinate system $\{b\}$ is :

$$ {}^{b}_{e}\mathbf{T} = {}^{b}_{w}\mathbf{T}\ \mathbf{Rot}(x, \varphi)\ {}^{m}_{c}\mathbf{T}\ {}^{c}_{e}\mathbf{T} \tag{2.13} $$

2.5 CAD-based programming

Some surface-related tasks, like 3-axes machining, are implemented in CAD-systems : the CAD-system calculates first the path of the tool tip, and then the positions of the tool centre point.

When the task is not implemented in the CAD-system, the task has to be programmed in the CAD-system, or in an external application program. There are two possibilities to program a task in the CAD-system : in the system's graphical program language, or in a higher programming language with a neutral programming interface. If an external application program is used, the geometrical information has to be extracted from the CAD-system through a neutral interface format.

2.5.1 Programming in the CAD-system

2.5.1.1 Graphical Program Languages

Most CAD-systems have a graphical language in which application programs can be developed, e.g. GRIP in Unigraphics, and GRAPL in both ANVIL-5000 and CDM-300.

The main disadvantage of these languages is that they are system-dependent, so that programs cannot be transported easily to other CAD-systems. If the application has to work on several CAD-systems, a new graphical program has to be written for every CAD-system.

The graphical program language supports mostly only a subset of the CAD-manipulations and some additional logical, in- and output, and program control manipulations. Manipulations which are possible in one graphical language may not be possible in another graphical language, so that the application cannot be translated to another CAD-system [82].

2.5.1.2 Neutral Programming Interface

Application programs can be written in a system-independent way by using a set of standardized functions for the use of the graphical and interactive possibilities of the CAD-system. These standardized functions are converted by a neutral programming interface to specific system-dependent calls into native CAD-routines. An example of such a neutral programming interface is the Brite Modesti (BM)-interface [43]. The BM-interface consists of two parts : one part has to be linked to the application program and is independent of the CAD-system, the other part is linked to the CAD-system, and has to be decoded for each different CAD-system. The application program is started in the CAD-system. The communication between application programs and

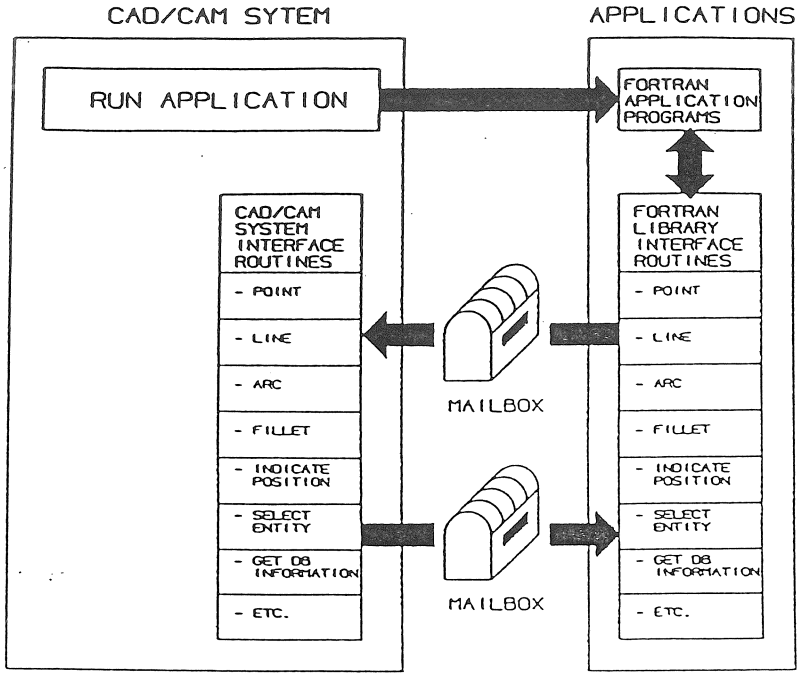

Figure 2.6: BM-interface [43]

CAD-system passes via mailboxes : e.g. if the user program wants to create a point in the CAD-system, it writes a request for generating a point and the coordinates of the point in a mailbox. The other process reads the data through the mailbox and returns a data base pointer through a second mailbox (Fig. 2.6).

The application programs which are created in this way are completely independent of the CAD-system. The CAD-part of the interface has to be decoded for each CAD-system, and requires therefore an open CAD-system.

2.5.1.3 Files Containing Points and Lines

The output of an application program, which creates e.g. fibre paths, can be stored in a file as a list of point coordinates. This file can be read in two ways in the CAD-system :

- by a small user-written program in the CAD-system (GEO).

- by the use of the BULK-DATA I/O interface of some CAD-systems, like ANVIL-5000 and CDM-300. The BULK DATA I/O interface allows to read a file containing points and lines, which are described in an APT-like format, e.g. for a point :

```
P = POINT/ 241.00 , 20.41 , -50.40
```

2.5.2 Neutral Interface Formats

The wide variety of CAD-systems and other computer aided applications created the necessity to exchange product definition data between CAD-systems and applications. To transfer data from one system to another, special interface software has been developed. Data can be transferred by special system-to-system translators (e.g. the GFEM-interface from Unigraphics to Nastran), or by neutral interfaces [44]. Neutral interfaces are more interesting than translators, since they are system-independent.

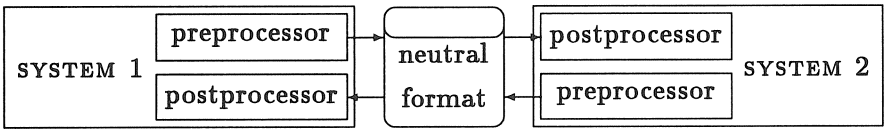

Figure 2.7: Communication between CAD-systems with neutral format

The preprocessor of the CAD-sending system converts the data from the system's database native format into the neutral file format, the postprocessor of the receiving system restores the data from the neutral format in the system's internal format (Fig. 2.7). The neutral file format contains all the data necessary to regenerate the part, both geometrical and non-geometrical data, such as dimensions, views, drawings,... The most widely spread standardized neutral interface formats nowadays are IGES, SET and VDAFS [44]. This section briefly discusses the most important characteristics of the neutral interfaces IGES and VDAFS.

2.5.2.1 IGES

IGES [91] ("Initial Graphics Exchange Specification") was the first standard to appear. To ensure hardware independency and a good

readability, IGES consists of a very simple physical data format : files are organized sequentially, with a fixed record length of 80 characters in ASCII-code. An IGES-file consists of five sections :

start section : contains a man-readable text with general information.

global section : contains information needed by the postprocessor to handle the file. This section defines e.g. the delimiters and the unit measuring system used by the preprocessor to describe the data.

directory entry section : contains data common to all the CAD-entities, such as entity type, layer, name and pointer to the definition coordinate system. This section contains two lines per entity in a fixed format.

parameter section : contains, in free format, all the parameters associated with each entity. Links between directory and parameter section are realized with forward and backward pointers.

terminate section : contains the total number of lines in each previous section.

IGES has however some drawbacks :

- IGES-files are very large. The IGES-file contains all the data, both geometrical and non-geometrical, of the CAD-model. The fixed format in the directory section and the fixed record length of 80 characters cause a low packing density and enlarge the volume of the file.
- Most CAD-systems support only a subset of the data which are described in the standard [44]. Not all the entities which are implemented in the CAD-system can be handled by the system's IGES-preprocessor. So is the CDM-300 system able to generate B-spline surfaces but not to output them to an IGES-file [19]. This leads to a non-complete regeneration of a part in an other CAD-system, and poses limitations on the use of application programs.
- The meaning of the various parameters differs for each entity. Each entity must therefore be handled by the postprocessor in a different way during reading, which leads to complex conversion routines.

- The references between directory entry section and parameter section result in a complex workpiece description, so that error-free transfer of geometrical data is often not accomplished. These references make reading data in an IGES-file very time-consuming.
- Due to the poor quality of some processors [44] conversion errors, syntax errors and errors caused by differences in implementation can occur during IGES-data transfer.

2.5.2.2 VDAFS

VDAFS ("Verein der Automobilindustrie - Flächenschnitstelle") [124] has been developed for (and is limited to) the exchange of geometrical data of free form surfaces and curves. All surfaces consist of patches, which are polynomials in the surface parameters u and v :

$$\mathbf{s}(u,v) = \sum_{k=0}^{n_v-1} \sum_{j=0}^{n_u-1} \mathbf{a}_{jk} u^j v^k \tag{2.14}$$

VDAFS supports only a limited number of entity types (point, point sequence, point vector sequence, circle, curve, surface, curve on surface, trimmed surface and composite surface) and some organizational elements, allowing the grouping of elements and comments. VDAFS-files are, like IGES, sequentially ordered with fixed length records of 80 ASCII-characters. The elements are described in an APT-like data format.

The main advantage of VDAFS is that data processing is simplified due to the unique (polynomial) representation of free form curves and surfaces. A drawback is that simple curves and surfaces are transformed into much more complicated curves and surfaces. VDAFS is limited to polynomial surfaces, and cannot represent NURBS (Non-Uniform Rational B-Spline Surfaces) [31] exactly.

2.5.2.3 Programming Using Neutral Formats

An application program, which uses a neutral format to extract the geometrical data from the CAD-system, has to read the appropriate data in the neutral format, and convert these data into the program's internal format. The neutral format contains all the geometrical and

non-geometrical data of the part, but only the data of the entities of interest have to be extracted. In order to be able to recognize these entities, they have to be named in the CAD-system prior to the creation of the neutral format.

Small programs in the CAD-system can be used as an interface between the CAD-system and the external application program (Fig. 2.8). These programs are used for the selection of the input variables in the CAD-system in a user-friendly way, and for the representation of the output paths [10, 19].

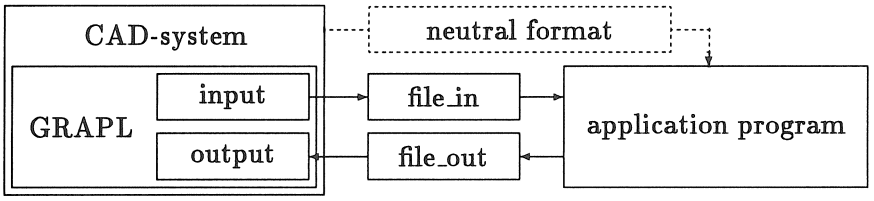

Figure 2.8: Interfacing an application program by means of a graphical program

2.6 Computer Program CAWAR

A computer program **CAWAR** (Computer Aided filament Winding of Asymmetric parts using Robots) has been developed for the calculation of fibre paths and robot paths. The program **CAWAR** is written in the C-language on a VAX-computer.

The part is designed in a CAD surface modeller.

The fibre paths are calculated by numerically solving a set of differential equations (cf. section 3.2.3). For the solution of this set of differential equations, the points and the first and second order derivatives to the surface have to be evaluated. The geometrical data of the CAD-surfaces have therefore to be made available to the program **CAWAR**. A neutral interface format is used to transfer the data from the CAD-system to **CAWAR**. IGES is used since it is the most widely spread neutral interface format.

The program reads first the surface data in the IGES-file and converts them into the program's internal format. **CAWAR** calculates then consecutively fibre paths, fibre path sequences, robot paths and path

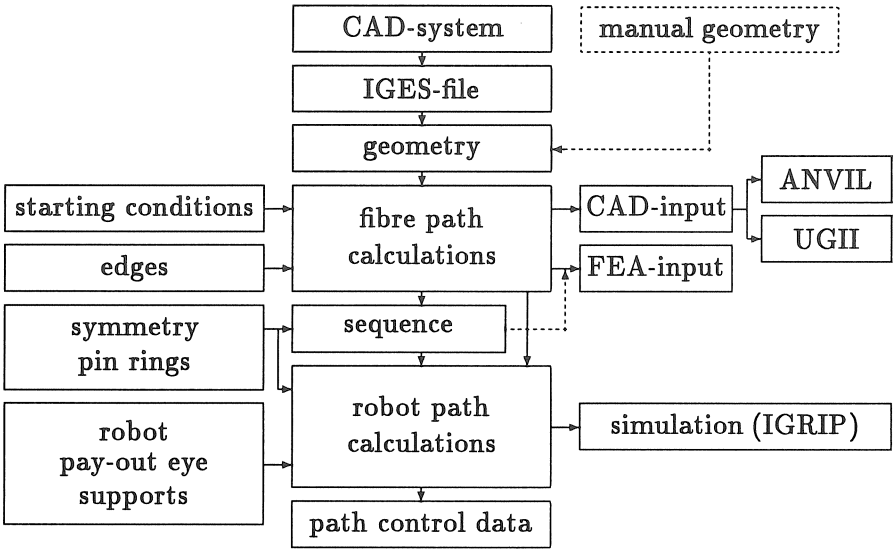

Figure 2.9: Structure of program CAWAR

control data (Fig. 2.9). The input for the program is completely menu-driven. The amount of input, which has to be entered by the operator, is kept as low as possible, by the use of default input values and initialization files. CAWAR consists of four calculation modules, two input modules (input variables and initialization files) and an output module.

2.6.1 IGES-postprocessor and geometry storage

An IGES-file makes the geometrical data of the CAD-system available for the application program CAWAR. To automate reading the surfaces in the IGES-file, the names of the surfaces have to be numerals in ascending order : the first surface has to be named "1.", the second surface "2.",... The generation of the names can either be done manually or by a small program in the CAD-system.

CAWAR extracts the data from the IGES-file in two phases : first the directory entry section is scanned for surfaces, then the data of the surfaces are read in the parameter section, and converted into CAWAR's own internal format. Each different IGES-entity type is stored in a different record structure, which contains all the data, needed

to evaluate the entity. Surfaces are stored in a record of the type SURFACE, curves in a record of the type CURVE. The components of these records are : entity type, limits of the variables, definition coordinate system and a pointer to an entity type dependent record, e.g. REVOL_SURF for a surface of revolution and RULED_SURF for a ruled surface (Fig. 2.10). These record structures contain pointers to records of the type CURVE, to describe the generating curves.

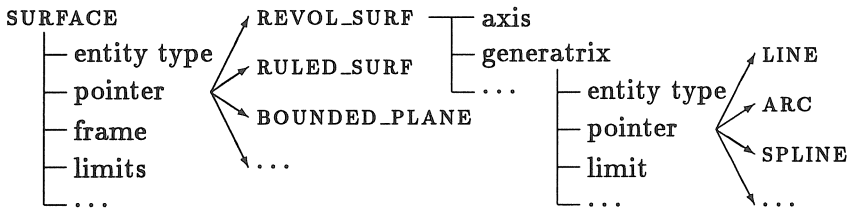

Figure 2.10: Storage of surfaces in CAWAR

Simple surfaces, like cylinders can be inputted directly, without the need to design the part in a CAD-system.

2.6.2 Modules of CAWAR

2.6.2.1 Fibre Path Calculation

The program CAWAR is able to calculate geodesics, semi-geodesics with a constant slippage tendency and constant angle paths on an asymmetric part. The calculation method is described in chapter 3.

2.6.2.2 Fibre Path Sequence

The sequence in which the fibre paths have to be wound on the mandrel has to be defined prior to the calculation of the robot paths. The construction of fibre path sequences is subjected to several requirements, which are discussed in section 3.4.

2.6.2.3 Robot Path Calculation

CAWAR calculates the robot path for a specified fibre path sequence. During the calculation of the robot path, collisions between, on the one hand, the pay-out eye and the robot wrist, and, on the other hand, the

mandrel and the mandrel support structure, are continuously checked and avoided by the use of a heuristic method. The calculation of the poses of the robot path is discussed in section 5.2, collision avoidance in chapter 6.

2.6.2.4 Generation of path control data

The position-time relationship is calculated for the poses of the robot path, so that the winding time is minimized without violating any velocity or acceleration constraints. The path control data are then transformed to the format, required by the robot control program. These data are downloaded in the PC, which controls the winding process. The generation of path control data is discussed in section 5.3.

2.6.2.5 Default input values

The default input values give the operator at the start of the program a guideline for choosing the process parameters and allow to run the program in batch mode. Default values include the directories to store files, tolerances, creation of monitoring files, distances between points, distance between mandrel and pay-out eye, maximum winding speed,...

2.6.2.6 Initialization files

The initialization files, which are used in CAWAR contain information on the mandrel, which cannot be extracted from the CAD-system, and information on the winding machine. Initialization files can be divided in two groups : machine and part dependent initialization files. The machine dependent files contain information on the geometry of the robot, the pay-out eye and the mandrel support structure. The part dependent files contain information on the edges of the part (where the fibre paths start and the pin rings are attached), on the material side of the surfaces, the part set-up, symmetry of the part and the geometry of the pin rings.

2.6.2.7 Output

CAWAR has several output possibilities. Fibre paths, sequences, robot paths and path control data are stored in binary files for further cal-

culations, and can be converted into an ASCII-format. Other output possibilities are :

Fibre Path : CAD-input The fibre path can be represented in a CAD-system. The file format depends on the CAD-system : for CDM-300 and ANVIL-5000 the BULK DATA I/O format is used, for Unigraphics a text file is generated, which is inputted in the GRIP-program `GEO`. The fibre path can be represented as a series of points, as a curve consisting of connecting lines, as a number of parallel curves or as a mesh of curves.

Fibre Path : FEA-input The data of the fibre path are used to generate the laminate data of the finite element mesh. For tubelike parts, the ply angles and thicknesses are calculated for each element, and the input file for the finite element mesh is updated with the new laminate data [20]. For asymmetric parts, the points and the tangents of all the fibre paths and the fibre path sequence are written to a file, which is inputted in the program `LUPGEN` [59] to calculate the laminate data.

Robot Path : IGRIP-input The robot program can be simulated in the graphical robot simulation system IGRIP. The poses of the robot end flange and the angles of the two external axes are written to a file, which is read by the program `WIKKEL_PUMA` (cf. section 6.7.1).

2.7 Robotic Ultrasonic C-scanning

2.7.1 Ultrasonic Inspection of Composite Materials

Ultrasonic techniques are commonly used for quality control of composite materials. An ultrasonic wave, with a frequency in the range of 0.4 – 25 MHz, is propagated by a piezo-electric crystal through the specimen, reflects at defects and at surfaces, and is received by the receiving transducer [106] (Fig. 2.11). A pulse generator generates a short ultrasonic pulse at regular time intervals. Flaws are detected by monitoring the time-of-flight and/or the signal strength of the returning echoes. Defects that can be detected are delaminations and

three-dimensional voids. Matrix cracks which are perpendicular to the surface cannot be detected.

Dependent on the equipment, different displays are possible : A-scan (amplitude of the signal received in function of the time for a measurement in a point), B-scan (measurement of a cross section) and C-scan (measurement of a surface). To obtain the C-scan, the whole surface is scanned by tracing lines which are adjacent to each other.

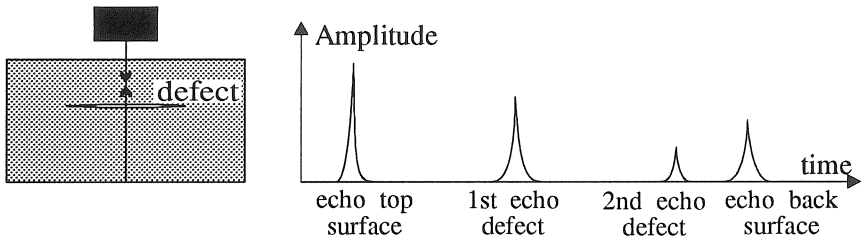

Figure 2.11: Ultrasonic signal (A-scan)

In order to obtain a good transmission from the piezo-electric transducer to the composite material, an ultrasonic coupling medium is used, like oil or water. This coupling medium must be permanently present between transmitter and receiver to avoid supplementary reflections. There are two methods of coupling : both specimen and transducers are immersed in a water bath, or a water jet is used as the coupling medium between transmitter, specimen and receiver.

The transducer should be placed normal to the surface, otherwise the reflections will not be detected by the receiver.

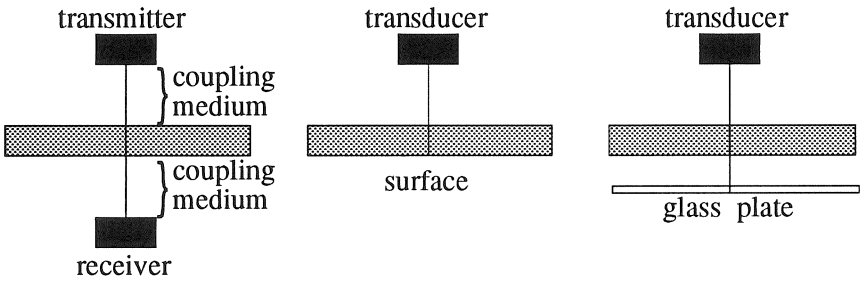

Figure 2.12: Scanning methods
(a) through-transmission (b) pulse-echo (c) glass plate reflection

The *through-transmission*-technique uses two compatible transducers to find defects (Fig. 2.12a), by capitalizing on the phenomenon that sound waves propagate faster through a solid, flaw-free medium than they do through defects [96]. The distance between transmitter and receiver has to be constant. This can be realized by linking both transducers mechanically, or by moving them by two cooperating machines. The latter technique is implemented in the AUSS-system of McDonnell Douglas [119], where a gantry with two robot arms is used to scan large aircraft structures (Fig. 2.13).

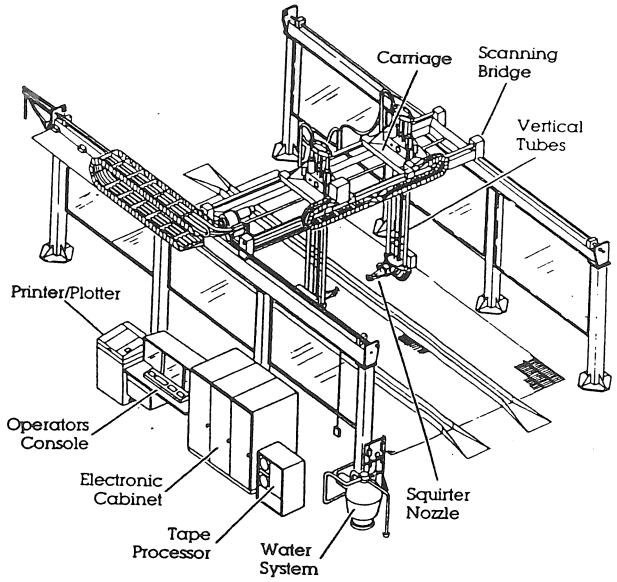

Figure 2.13: Robotic ultrasonic through-transmission (AUSS) [119]

The most common method of ultrasonic testing is the *pulse-echo* method, in which transmitter and receiver are combined (Fig. 2.12b). The receiver records the reflection of a sound wave from a surface or defect. The echoes are shown on an oscilloscope display at a time delay equivalent to twice the distance between the transmitter and the reflecting surface (Fig. 2.11). The pulse-echo method can be used for in-service inspection of composites, e.g. with the MAUS-system of McDonnell Douglas [120], an apparatus that is moved manually over a wetted surface. The data can be processed in two ways : the conventional 2-D technique uses only the peak amplitude in a preset time

interval, and the high frequency 3-D technique uses all the information on time-of-flight and amplitude, and can distinguish flaws at different depths. The preset time interval in the 2-D technique corresponds to the echo of the bottom surface. This echo will be maximal if there are no defects in the material. This technique is however limited to parts with constant thickness.

The *reflector-plate* technique is a variation of the pulse-echo method, which uses a glass plate which is positioned below the specimen (Fig. 2.12c). The sound waves pass twice through the material, which makes this method especially sensitive to flaws [96].

2.7.2 Robotic Implementation

A robotic C-scan cell has been developed with the PUMA-762 robot, which is used for winding. The method applied is the pulse-echo method with water jet coupling [105]. The ultrasonic transducer is mounted in a squirter, which is attached to the robot wrist (Fig. 2.14). Water is continuously fed between the transducer and the exit of the squirter, so that a continuous layer of water is generated between the transducer and the surface.

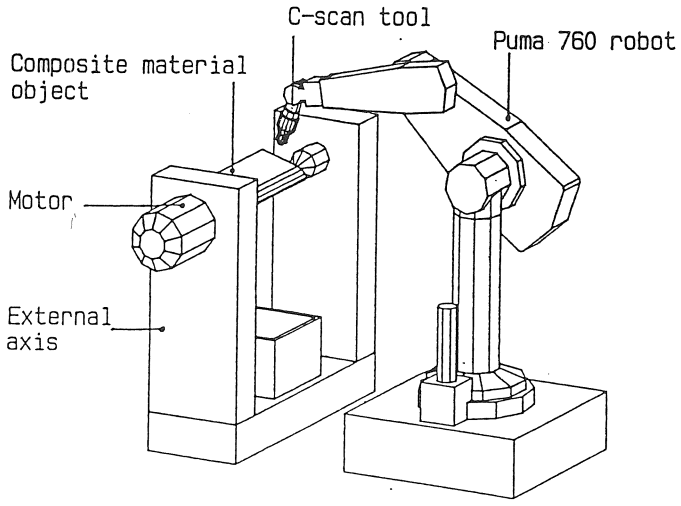

Figure 2.14: Scanning cell

The measuring device is a Krautkrämer-Branson USIP-12. An "electronic gate" converts the amplitude of the largest echo within

a preset time interval to a voltage, which is sent to the PC. The time gate is positioned at the echo of the bottom surface. The reference for the time gate is set to the echo of the top surface, so that small variations in the distance between the transducer and the surface do not influence the output value. Since the echo of the bottom surface has to remain in the time gate, the thickness of the part must be constant, and the surface roughness may not be too large.

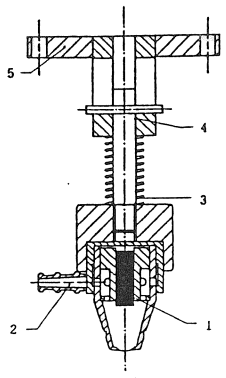

1. Piezo-electric transducer
2. Water supply
3. Flexible spring
4. Sliding fit
5. Robot attachment

Figure 2.15: Squirter

The squirter is brought into contact with the part in order to obtain a constant distance to the surface. A spring is installed between the transducer and the robot wrist, allowing a relative motion between the squirter and the robot wrist (Fig. 2.15), to take inaccuracies in the robot path into account. The squirter rests on a small film of water in between the squirter and the part. Small variations in the thickness of this water film have no influence on the measuring data, since the reference pulse of the electronic gate corresponds to the echo of the top surface.

When the part has a closed surface, the robot is not able to align the squirter with the normal all over the surface due to its limited working envelope. The external axis, which is used to rotate the mandrel during winding, is in this case used to rotate the part during C-scanning.

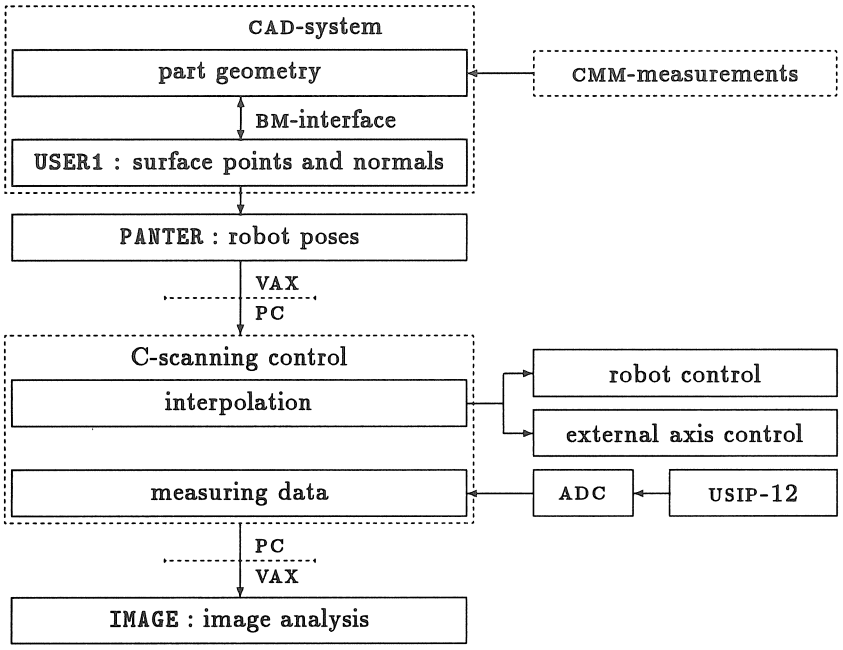

Figure 2.16: Robotic ultrasonic C-Scanning programming

2.7.3 Programming

The programming of the robotic ultrasonic C-scanning unit consists of four steps : the generation of a mesh of points on the surface, the calculation of a mesh of robot poses, the control of the C-scanning process and the image analysis (Fig. 2.16).

2.7.3.1 Surface Points and Normals

The geometry of the part is defined in a CAD-system. The CAD-description of the part can be derived from measurements on a 3D-coordinate machine [105]. An application program USER1 [105] in the CAD-system selects the section of the surface to be scanned, the scanning pattern and generates a mesh of points and normals on the surface. USER1 is written in FORTRAN and uses routines of the BM-library.

Several scanning patterns are possible : scanning along paths with constant u-parameter (Fig. 2.17a) or along paths with constant v-parameter (Fig. 2.17b), with or without use of the external axis. The

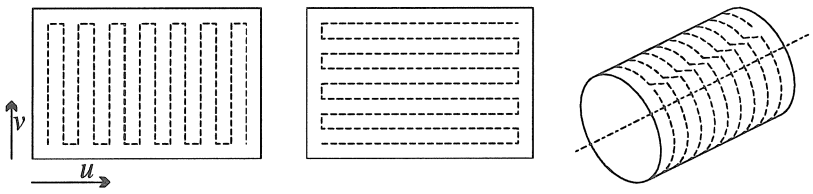

Figure 2.17: Scanning patterns.
(a) ct. u-paths (b) ct. v-paths (c) cylindrical

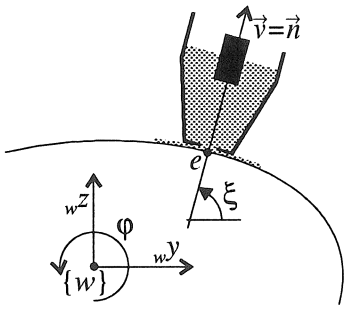

Figure 2.18: Position of the robot tool

best way to scan e.g. a surface of revolution is to follow paths with constant u-parameter, with use of the external axis (Fig. 2.17c) : the robot does not move during one rotation of the external axis.

2.7.3.2 Robot Poses

A mesh of poses of the robot tool is calculated in the program PANTER, starting from the mesh of surface points and normals.

The tool is axisymmetric, and can be represented as a line $L_e = (e, \vec{v})$, with e the end point of the tool and the vector $\vec{v}$ directed towards the robot wrist. The end point e coincides with the point on the surface, the vector $\vec{v}$ with the outwards directed normal to the surface. The position of the tool axis is uniquely defined if the external axis is not used. If a rotation about the external axis is allowed, a redundancy occurs. The end point e is then restricted to a plane through the external axis, that makes an angle ξ with the horizontal plane (Fig 2.18). The position of the point e after rotation

over an angle φ about the external axis is :

$$ {}_w\mathbf{e} = \mathbf{Rot}(x,\varphi)_m\mathbf{e} = \begin{bmatrix} {}_me_x \\ {}_me_y\cos\varphi - {}_me_z\sin\varphi \\ {}_me_y\sin\varphi + {}_me_z\cos\varphi \end{bmatrix} \tag{2.15} $$

The angle with the horizontal plane equals ξ :

$$ \frac{{}_we_z}{{}_we_y} = \frac{{}_me_y\sin\varphi + {}_me_z\cos\varphi}{{}_me_y\cos\varphi - {}_me_z\sin\varphi} = \tan\xi \tag{2.16} $$

The angle φ of the external axis equals :

$$ \varphi = \xi - \arctan\left(\frac{{}_me_z}{{}_me_y}\right) \tag{2.17} $$

Since the tool is axisymmetric, the rotation of the robot tool about the tool axis $\vec{v}$ can be chosen freely. The rotation of the tool is minimized by placing the vector $\vec{n}_e$, which is normal to the tool axis $\vec{v}$, parallel to a plane (with normal $\vec{a}$) :

$$ \vec{n}_e = \frac{\vec{a}\times\vec{v}}{\|\vec{a}\times\vec{v}\|} \tag{2.18} $$

Starting from the orthonormal vectors $\vec{v}$ and $\vec{n}_e$ the frame $\{e\} = \{e;\vec{v},\vec{n}_e,\vec{v}\times\vec{n}e\}$, which is attached to the tool is constructed.

2.7.3.3 Robot Control

The mesh of robot poses, which are calculated on the VAX-computer, are downloaded in the PC, which controls the scanning process. The control of the PUMA-762 will be discussed extensively in section 4.4 : a PC sends every time cycle (28.8 ms) path control data to the robot and the external axis. The PC reads also every time cycle the analog output signal of the USIP-12, and converts it into a 12-bit digital value by a MetraByte A/D-board, which is plugged into the PC.

The poses, where the robot is sent to, are interpolated between the mesh of robot poses. The distance between the measuring points has to approximate the diameter of the ultrasonic transducer (e.g. 0.1 mm). The ultrasonic measuring data are stored in the memory of the PC and sent back to the VAX-computer after scanning.

2.7.3.4 Image Analysis

An image analysis of the measured data is performed on a VAX-workstation by the program **IMAGE**. This program uses routines of the GKS-library, which is an internationally standardized library for the generation of 2D-graphics. **IMAGE** reads the data, measured by the ultrasonic transducer, and stores them in a matrix. This matrix is drawn on screen, using different colours to represent different amplitude levels. Other output options are two-colour "damage level"-plots – with one colour for the amplitudes below the selected damage level, and the other colour for the values above the damage level – and plots of the normal and the cumulative amplitude distributions.

2.7.4 Experimental Results

The robotic ultrasonic C-scanning technique has been tested on different parts : a.o. a flat impacted plate, a wound cylinder, and a sculptured SMC-surface.

2.7.4.1 Impacted Plate

The impacted plate was chosen as a test part, to be able to compare the results with the conventional two-dimensional C-scanning equipment at the department MTM. A sector of 50 mm $\times$ 50 mm has been scanned. The distance between the measured points is 0.293 mm, resulting in a matrix of 167 $\times$ 167 data. Fig 2.19 shows the measuring results. The signals in the damaged zone (red colour) are smaller than the signals in the undamaged zone (blue colour). Fig 2.20 gives a damage level plot. The results were comparable with the results obtained at MTM [105].

2.7.4.2 Wound Cylinder

A glass fibre reinforced tube with a diameter of 90 mm and a winding angle of 45° has been scanned with the use of the external axis (over a length of 20 mm. A matrix of 980 $\times$ 76 data is obtained. Fig. 2.21 depicts the measuring results. The matrix is represented as a square. The horizontal scale in Fig. 2.21 is therefore 13 times larger than the vertical scale. The angle between the fibres and the horizontal axis is $\approx 4.4°$. The results are however hard to interpret. This is mainly due

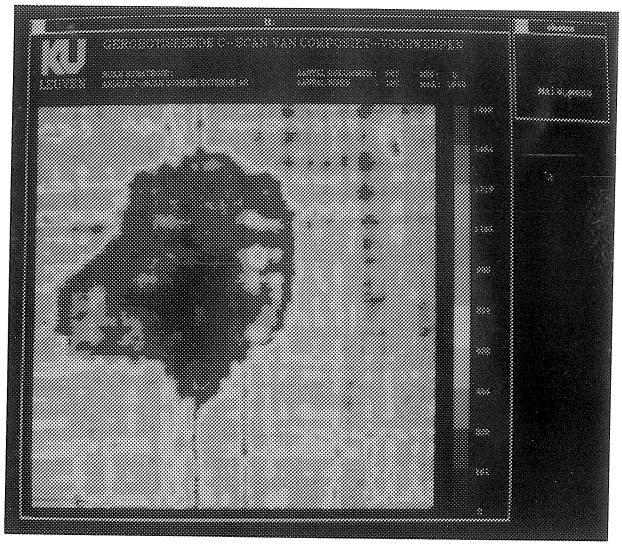

Figure 2.19: Colour plot of impacted plate [105]

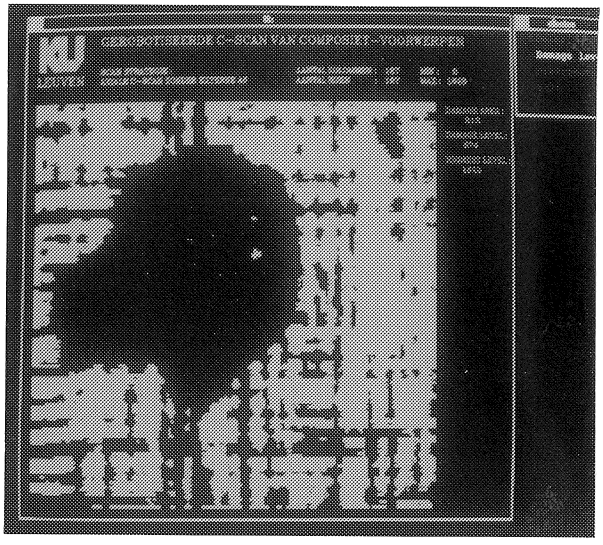

Figure 2.20: Damage level plot of impacted plate [105]

to the roughness of the wound tube, which leads to dispersion of the ultrasonic wave.

2.7.4.3 Sculptured Surface

A part of a composite car hood (a sector of 20 mm × 20 mm), with random oriented continuous fibres, has been scanned. The measuring results are shown in Fig. 2.22. In the lower right corner an artificial triangular fault has been introduced into the part.

2.7.4.4 Conclusions

The robotic ultrasonic C-scanning works well for composite laminates. Wound parts pose difficulties, due to the rough outside surface and variations in part thickness. The implemented scanning process is slow, but the scanning time can be decreased by the use of a second PC to measure data at regular small time intervals. The method remains however restricted to parts with constant thickness.

Due to the long cycle time of the robot, robotic C-scanning is a relatively slow process. The scanning time can be reduced by reading multiple ultrasonic data per robot time cycle. Reading should take place under a timer interrupt without disturbing the communication with the robot, or on a second PC which communicates with the control PC. The image analysis could be performed on the second PC in real-time.

2.8 Conclusions

A computer integrated environment has been constructed round the filament winding process. This environment includes design, production and quality control. Design is an integrated process, requiring the use of CAD-, FEA-programs and application programs for the calculation of fibre paths. The program CAWAR has been developed for the calculation of fibre paths and robot paths on parts, which are described in a CAD-surface modeller. CAWAR extracts the data from the CAD-program by an IGES-file. The production consists of : calculation of a collision-free robot path, the derivation of the position-time relationship and the actual control of the winding process. Quality control is performed with a robotic ultrasonic C-scanning technique, which uses software

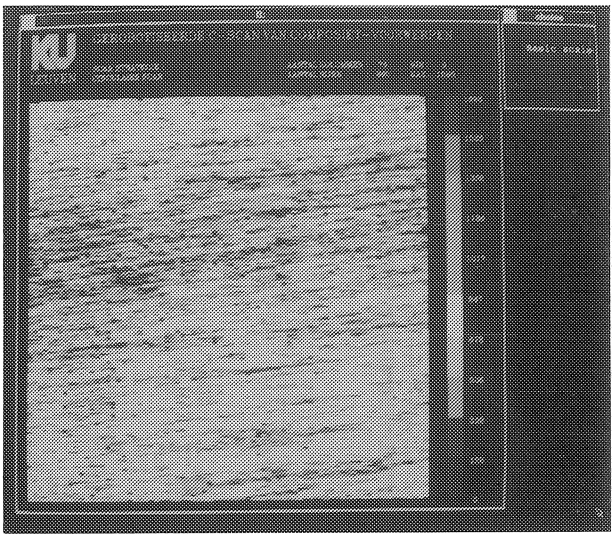

Figure 2.21: Colour plot of wound cylinder [105]

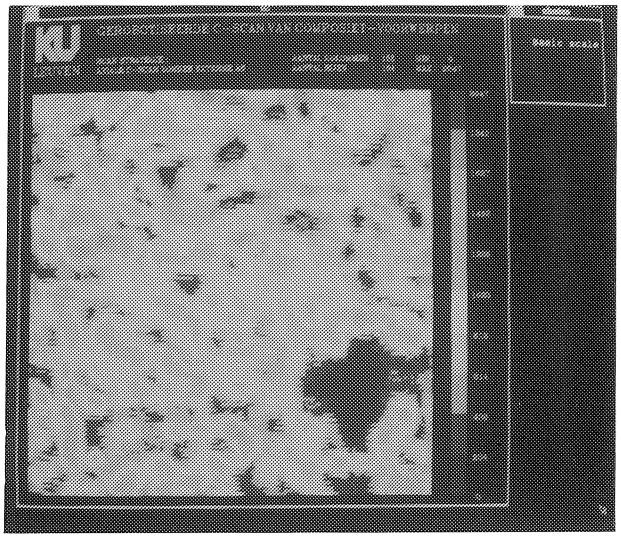

Figure 2.22: Colour plot of sculptured surface [105]

similar to the winding process. The scanning pattern is defined in a CAD-system, the robot path is calculated and sent to the robot, and the measuring data are sent back to the host computer for an image analysis.

Chapter 3

Design of Wound Parts

3.1 Introduction

The design of a filament wound part consists of two main parts : the design of the shape and the design of the fibre paths.

The shape can be completely determined by imposed design requirements or the design of the shape can be an integral part of the winding design. The design of the shape is not discussed in this work.

The fibre paths cannot be chosen freely, since they are subjected to requirements to prevent fibre bridging and fibre slippage or tape wrinkling. The design of a filament wound part is therefore a compromise between the optimal design, according to strength and stiffness, and the restrictions imposed by the winding process.

The method used to design the fibre paths depends on the shape of the part (axisymmetric, tubelike, asymmetric) and the basic material (rovings or tapes) used. Axisymmetric and tubelike parts require only a single fibre path as basis for the coverage pattern. This fibre path is repeated all over the circumference, forming a complete layer of material. Such a single path cannot be found for an asymmetric shape : each fibre path must then separately be designed, so that a large amount of data is necessary to cover the part completely. The design of the fibre paths, so that a part with an optimal strength and uniform thickness is obtained, is the main problem in the design stage.

This chapter discusses first the methods to calculate fibre paths, and the implementation in the program CAWAR. The next section deals with the design of fibre paths, which is illustrated with the design of a

tape wound T-piece. The last section discusses the generation of fibre path sequences.

3.2 Fibre Path Calculation

This section discusses the calculation of fibre paths. First an overview is given of the methods which are used in literature. The method, based on differential geometry, is extensively described. The next sections describe the calculation of semi-geodesic fibre paths in the program CAWAR. The last section describes the calculation of fibre paths at pin rings, which are attached at the ends of the mandrel.

3.2.1 Literature Survey

There are two basic methods to calculate fibre paths : by deriving analytically the equation of the fibre path or by subdividing the part in simple surfaces.

Analytical Method This method is based on differential geometry. One or two differential equations are derived for the geodesic or semi-geodesic. These equations are solved numerically.

Geodesics on surfaces of revolution meet the simple equation of Clairaut (1.9). The path trajectory is obtained by solving an integral [2]. A closed analytical form can be derived for cylinders, cones and spheres [2].

The equations for semi-geodesics are derived by Li [55] for a surface of revolution (cf. Eq. 2.1) :

$$\mathbf{s}(u,v) = [x(u) \quad r(u)\cos v \quad r(u)\sin v]^T$$

The calculation of geodesics on surfaces of revolution is discussed in Appendix A.1. Di Vita [24] derives the equation for a semi-geodesic on a generalized surface of revolution :

$$\mathbf{s}(u,v) = [x(u) \quad r(u,v)\cos v \quad r(u,v)\sin v]^T$$

Korn [51] derives a system of differential equations for a geodesic on a general surface. Lloyd-Thomas [58] derives one differential equation for a semi-geodesic.

Approximation Surfaces of revolution are subdivided in cylindrical and conical segments [59]. Geodesics on these surfaces are lines in the developed cylinders and cones.

Asymmetric surfaces are approximated by a triangular mesh in CADFIBER [47] and CADFIL [64]. The part is first defined by a set of cross sections. The cross sections are approximated by series of points. A triangular mesh is then generated between these points.

The fibre path is always a straight line on a (flat) triangular patch[1]. The change in fibre path direction at the edge of two patches has to be such, that the force along the edge is smaller than the friction force.

3.2.2 Calculation of Semi-Geodesic on a Surface

The analytical method has the advantage that the geometry of the CAD-model can directly be used, and is therefore used in this work.

The fibre follows a path $\Gamma(s)$ on the surface $S(u,v)$. If s corresponds to the path length (natural parametrization), the tangent $\vec{t}$ has unit length, or (Eq. 2.3) :

$$\frac{d\vec{t}}{ds} \cdot \vec{t} = 0 \quad \text{or} \quad \vec{c} \cdot \vec{t} = 0 \tag{3.1}$$

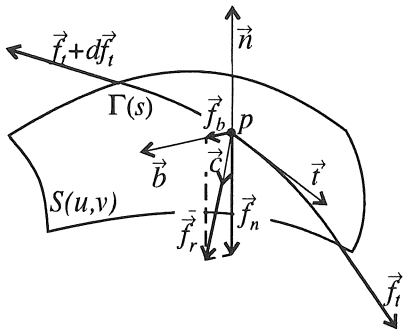

Figure 3.1: Forces acting on the fibre path in p

The forces (per unit length) $\vec{f}_r$, $\vec{f}_n$ and $\vec{f}_b$, which act on the fibre in the point p (cf. section 1.3.2.1), can be written in function of the unit

[1] The normal force $\vec{f}_n = \vec{0}$ on a plane. According to (1.4) the force $\vec{f}_b = \vec{0}$, and thus $\frac{d\vec{t}}{ds}$. The fibre path is therefore always a straight line on a plane.

tangent $\vec{t}$, the normal $\vec{n}$ and the binormal $\vec{b}$ of the Frenet trihedron in p (Fig. 3.1) :

$$\vec{f}_r = \frac{d\vec{f}_t}{ds} = \left\|\vec{f}_t\right\| \frac{d\vec{t}}{ds} = T\vec{c} \tag{3.2}$$

$$\vec{f}_n = -\left(\vec{f}_r \cdot \vec{n}\right)\vec{n} = -T\left(\vec{c} \cdot \vec{n}\right)\vec{n} \tag{3.3}$$

$$\vec{f}_b = \left(\vec{f}_r \cdot \vec{b}\right)\vec{b} = T\left(\vec{c} \cdot \vec{b}\right)\vec{b} \tag{3.4}$$

with $T = \left\|\vec{f}_t\right\|$ the fibre tension. The slippage tendency λ is in Eq. (1.1) defined as the ratio between the transversal and the normal force :

$$\lambda = \frac{\vec{c} \cdot \vec{b}}{-\vec{c} \cdot \vec{n}} \tag{3.5}$$

or :

$$\vec{c} \cdot \vec{b} = -\lambda \vec{c} \cdot \vec{n} \tag{3.6}$$

The curvature vector $\vec{c}$ is function of the second derivatives $\frac{d^2u}{ds^2}$ and $\frac{d^2v}{ds^2}$ (Eq. 2.6). The other vectors are only function of $u, v, \frac{du}{ds}$ and $\frac{dv}{ds}$ (cf. Eq. 2.2,2.4 and 2.5). The set of equations (3.1) and (3.6) :

$$\begin{cases} \vec{c} \cdot \vec{t} &= 0 \\ \vec{c} \cdot (\vec{b} + \lambda \vec{n}) &= 0 \end{cases} \tag{3.7}$$

can be written as :

$$a_{11}\frac{d^2u}{ds^2} + a_{12}\frac{d^2v}{ds^2} = b_1 \tag{3.8}$$

$$a_{21}\frac{d^2u}{ds^2} + a_{22}\frac{d^2v}{ds^2} = b_2 \tag{3.9}$$

with :

$$\begin{aligned} a_{11} &= \vec{s}_u \cdot \vec{t} \\ a_{12} &= \vec{s}_v \cdot \vec{t} \\ a_{21} &= \vec{s}_u \cdot \left(\vec{b} + \lambda \vec{n}\right) \\ a_{22} &= \vec{s}_v \cdot \left(\vec{b} + \lambda \vec{n}\right) \\ b_1 &= -\left[\vec{s}_{uu}\left(\frac{du}{ds}\right)^2 + 2\vec{s}_{uv}\frac{du}{ds}\frac{dv}{ds} + \vec{s}_{vv}\left(\frac{dv}{ds}\right)^2\right] \cdot \vec{t} \\ b_2 &= -\left[\vec{s}_{uu}\left(\frac{du}{ds}\right)^2 + 2\vec{s}_{uv}\frac{du}{ds}\frac{dv}{ds} + \vec{s}_{vv}\left(\frac{dv}{ds}\right)^2\right] \cdot \left(\vec{b} + \lambda \vec{n}\right) \end{aligned}$$

This is a set of two equations which can be solved for $\frac{d^2u}{ds^2}$ and $\frac{d^2v}{ds^2}$ with the method of Cramer :

$$\frac{d^2u}{ds^2} = \frac{a_{22}b_1 - a_{12}b_2}{a_{11}a_{22} - a_{12}a_{21}} = f_1\left(u, v, \frac{du}{ds}, \frac{dv}{ds}\right) \tag{3.10}$$

$$\frac{d^2v}{ds^2} = \frac{a_{11}b_2 - a_{21}b_1}{a_{11}a_{22} - a_{12}a_{21}} = f_2\left(u, v, \frac{du}{ds}, \frac{dv}{ds}\right) \tag{3.11}$$

The system of differential equations (3.10) and (3.11) is solved numerically. The path is completely determined by the u and v-parameters in the starting point, and the derivatives $\frac{du}{ds}$ and $\frac{dv}{ds}$ in the starting point, which are defined by the starting tangent.

For a geodesic, the curvature vector $\vec{c}$ is perpendicular to the surface, or, in other words, to two arbitrary vectors in the tangent plane. The set of equations (3.7) is then replaced by :

$$\begin{cases} \vec{c} \cdot \vec{s}_u &= 0 \\ \vec{c} \cdot \vec{s}_v &= 0 \end{cases} \tag{3.12}$$

These equations were solved for a surface of revolution by Bryon and Van Aelst [10].

3.2.3 Calculation of Fibre Paths in CAWAR

The program CAWAR is able to calculate geodesics, semi-geodesics and constant angle paths on parts which are composed of several surfaces. The mathematical description of the surfaces is extracted from the IGES-file.

The program reads the starting conditions, which are entered by the user and calculates then the points of the fibre path on the surface (Fig. 3.2). Points are calculated at constant path length intervals Δs. Tests are performed for fibre bridging and to check if the point is still within the surface limits. If the point lies outside the surface, the surface on which the fibre path proceeds is selected. The starting conditions for the new surface are derived and the fibre path on the new surface is calculated.

3.2.3.1 Numerical solution of the differential equations

The system of differential equations (3.10) and (3.11) is solved numerically with the D02BAF-routine from the NAG software library.

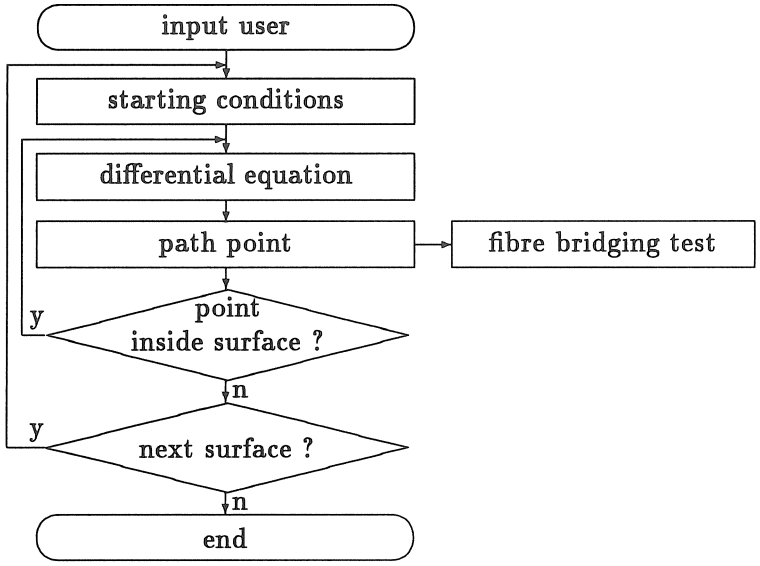

Figure 3.2: Calculation of semi-geodesics in CAWAR

This routine solves a system of first order differential equations with a Runge-Kutta-Merson method [121]. The system of two second order differential equations is therefore transformed into the set of four first order differential equations, with $x_1 = u, x_2 = v, x_3 = \frac{du}{ds}, x_4 = \frac{dv}{ds}$:

$$\begin{aligned} \frac{dx_1}{ds} = \frac{du}{ds} &= x_3 \\ \frac{dx_2}{ds} = \frac{dv}{ds} &= x_4 \\ \frac{dx_3}{ds} = \frac{d^2u}{ds^2} &= f_1(x_1, x_2, x_3, x_4) \\ \frac{dx_4}{ds} = \frac{d^2v}{ds^2} &= f_2(x_1, x_2, x_3, x_4) \end{aligned} \tag{3.13}$$

3.2.3.2 Starting Conditions

The starting conditions of the set of differential equations (3.13) are the parameters u,v and their derivatives $\frac{du}{ds}$ and $\frac{dv}{ds}$ in the starting point. The tangent vector in the starting point has to have unit length. The slippage tendency λ is given a constant value (0 for a geodesic).

The starting point lies mostly along the edge of a surface, which

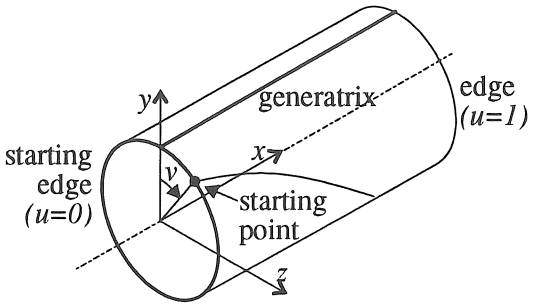

Figure 3.3: Starting point and starting edges on a cylinder

corresponds to a curve with constant u- or v-parameter. The starting point is defined by the edge and the parameter along the edge. For example : in a surface of revolution (2.1), u is the parameter along the generatrix, and v the angle along the circumference between the point and the generatrix (Fig. 3.3). The starting point is defined by the starting edge (i.e. $u = 0$ or $u = 1$) and the angle v.

The starting tangent is defined by the winding angle. This winding angle is defined on p. 34 for surfaces of revolution. This definition has to be extended towards asymmetric surfaces.

Kirberg [47] defines the winding angle for a surface with a central spine (Fig. 3.4) : the winding angle in a point p is the angle, measured in the tangent plane $\mathcal{T}$, between the tangent $\vec{t}$ and the plane $\mathcal{P}$, which is formed by the normal $\vec{n}$ to the surface in p and the tangent $\vec{t}_s$ to the spine, in the projection p_s of the point p on the spine. The winding angle is given by :

$$\alpha = \arccos\left(\frac{\vec{t}\cdot\vec{t}_s}{\sqrt{1-(\vec{t}_s\cdot\vec{n})^2}}\right) \tag{3.14}$$

The winding angle in this definition depends on the definition of the central spine.

This definition cannot be used if a central spine cannot be defined (e.g. for branched mandrels). The winding angle is in this case defined as the angle between the curve with constant v-parameter in p and the fibre path (Fig. 3.5) :

$$\alpha = \arccos\left(\frac{\vec{t}\cdot\vec{s}_u}{\|\vec{s}_u\|}\right) \tag{3.15}$$

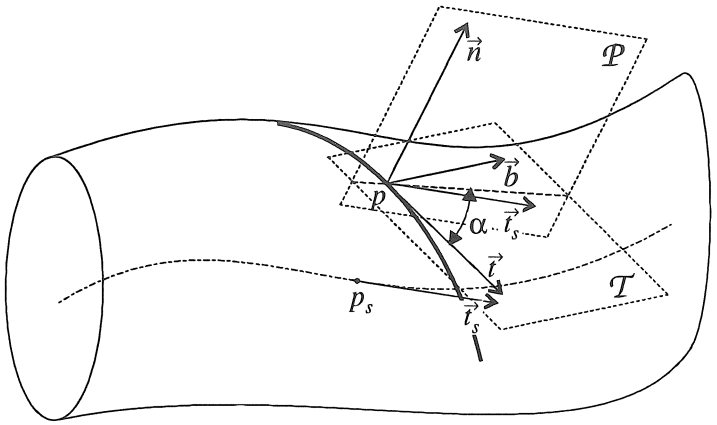

Figure 3.4: Definition of the winding angle for a surface with a central spine

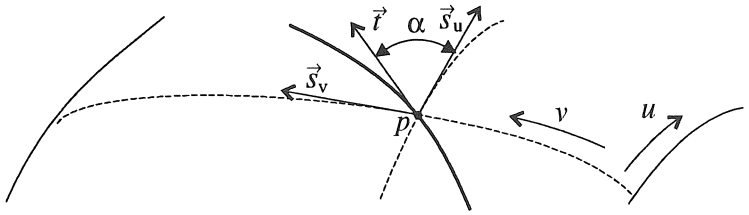

Figure 3.5: Definition of the winding angle for a general surface

The winding angle in this definition depends on the surface parametrization.

3.2.3.3 Check on Fibre Bridging

If the path has a reverse curvature in p, the fibre will not remain on the surface, but take a shorter way through the air. At each point of the fibre path, fibre bridging is checked with Eq. (1.8), which, with Eq. (3.3), can be written as :

$$\vec{c} \cdot \vec{n} \leq 0 \tag{3.16}$$

3.2.3.4 Surface Selection

At each point p of the fibre path, a test is performed to check if the surface limits ($u_0 \leq u \leq u_1$ and $v_0 \leq v \leq v_1$) are not exceeded (Fig. 3.2). If the surface limits are exceeded, the point p is placed at the boundary of the surface by interpolation between the two last points.

If the part consists of more than one surface, the surface on which the path proceeds, has to be selected. For all surfaces S_i, the distance d_i between the last point p of the fibre path and the surface is calculated. If d_i equals zero, the fibre path continues on the surface S_i.

The distance d_i corresponds to the minimum of the distance between p and a point s on the surface S_i :

$$d_i^2 = \min_{u,v} \|\vec{r}_p - \vec{s}_i(u,v)\|^2 = \min_{u,v} (\vec{r}_p - \vec{s}_i(u,v)) \cdot (\vec{r}_p - \vec{s}_i(u,v)) \quad (3.17)$$

The minimum d_i is searched with the E02LBF-routine from the NAG-library [121].

The parameters u and v in p on the new surface S_i are also obtained from the minimization routine. The derivatives $\frac{du}{ds}$ and $\frac{dv}{ds}$ in p are derived by decomposing the tangent $\vec{t}$ at p in $\vec{s}_u \frac{du}{ds}$ and $\vec{s}_v \frac{dv}{ds}$ (cf. Eq. 2.2).

This procedure can only be used if all surfaces are continuously linked in the CAD-surface model. If this is not the case, the user has to write a surface selection routine, which is linked to the main program. This routine has to calculate the number of the new surface and the new starting point and tangent, starting from the last point and tangent [82].

3.2.4 Optimal Fibre Path

The optimal winding angles α_{opt} at each point of the surface are derived from the results of a finite element analysis [20] (cf. p. 63). The fibre path should approximate the optimal winding angles $\alpha_{opt}(u,v)$ as well as possible, without violating the constraints on slippage and fibre bridging.

A starting point is chosen on the surface and its parameters u_0, v_0 ($\mathbf{y}_0 = [u_0\ v_0]^T$) are derived. The optimal winding angle $\alpha_{opt}(u_0, v_0)$

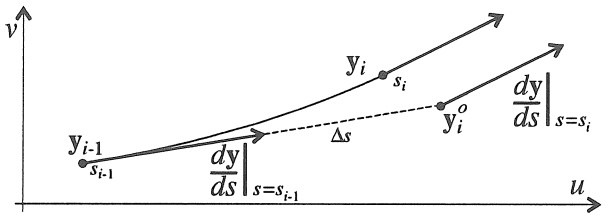

Figure 3.6: Calculation of the points of the optimal fibre path in the uv-mapping of the surface

in the starting point defines the starting tangent (or the derivative $\frac{d\mathbf{y}}{ds} = [\frac{du}{ds}\ \frac{dv}{ds}]^T$ for $s = s_0$).

The points of the fibre paths $\mathbf{y}_i = [u_i\ v_i]^T$ are calculated in two steps. A first estimation $\mathbf{y}_i^o = [u_i^o\ v_i^o]^T$ of the points of the fibre path is made by assuming that the derivative $\frac{d\mathbf{y}}{ds}$ is constant in the uv-mapping (Fig. 3.6) :

$$\mathbf{y}_i^o = \mathbf{y}_{i-1} + \Delta s \left.\frac{d\mathbf{y}}{ds}\right|_{s=s_{i-1}} \tag{3.18}$$

with Δs the iteration step. The derivative $\frac{d\mathbf{y}}{ds}$ in $\mathbf{y}_i$ is derived from the optimal winding angle $\alpha_{opt}(u_i^o, v_i^o)$ in $\mathbf{y}_i^o$. The point $\mathbf{y}_i$ is calculated, assuming that the derivative $\frac{d\mathbf{y}}{ds}$ changes linearly :

$$\mathbf{y}_i = \mathbf{y}_{i-1} + \frac{\Delta s}{2}\left(\left.\frac{d\mathbf{y}}{ds}\right|_{s=s_{i-1}} + \left.\frac{d\mathbf{y}}{ds}\right|_{s=s_i}\right) \tag{3.19}$$

At each point of the fibre path, the path is checked on slippage and fibre bridging. Both tests require the calculation of the curvature vector $\vec{c}$ (2.6). To be able to evaluate the curvature vector, the second derivative $\frac{d^2\mathbf{y}}{ds} = \left[\frac{d^2u}{ds^2}\ \frac{d^2v}{ds^2}\right]^T$ is needed. The second derivative is calculated from the difference between the derivatives at $\mathbf{y}_i$ and $\mathbf{y}_{i-1}$.

Fibre bridging is tested with Eq. (3.16), fibre slippage with with Eq. (3.5).

If slippage occurs at $\mathbf{y}_i$, the slippage tendency is limited to $\pm\mu$, and $\mathbf{y}_i$ is recalculated. If fibre bridging is detected, the last n points of the path are recalculated, and placed on a semi-geodesic curve with $\lambda = \pm\mu$. The value of n is increased as long as fibre bridging occurs [20].

3.2.5 Calculation of Fibre Path behind the Pin Rings

A pin ring consists of a number of pins which are mounted at the end of the mandrel. Pin rings allow sudden changes in the trajectory of the fibre path. Pin rings offer, opposed to end domes (cf. p. 42), a great freedom in the choice of the next fibre path that has to be wound.

The base curve of the pin ring corresponds to an edge of a surface in the CAD-model. The pin ring is modelled as a tabulated cylinder with as base the base curve of the pin ring, and as length w_p. The base curve is considered to be planar, so that the pin ring has a flat end plane. Usually an end shaft (with radius r_a) is provided in the centre of the pin ring, to support the mandrel in the head- or tailstock.

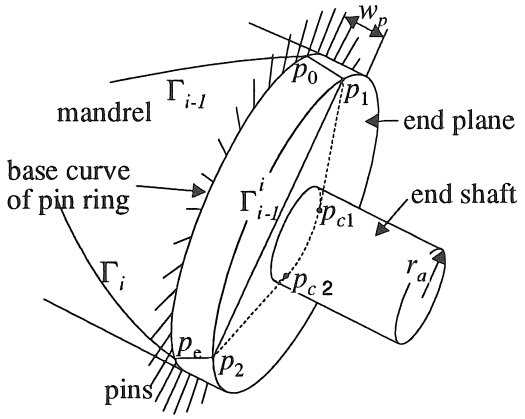

Figure 3.7: Fibre path behind a pin ring

In this section, the trajectory of the fibre path behind the pin ring is discussed. The minimum distance between the starting and the end point at the pin ring is derived : if this distance becomes too small, a stable fibre path cannot be found on the pin ring.

The fibre path Γ^i_{i-1} on the pin ring links the fibre paths Γ_{i-1} and Γ_i on the part surface. The path connecting the two points p_0, the end point of Γ_{i-1}, and p_e, the starting point of Γ_i, on the pin ring can be divided in three parts (Fig. 3.7) :

1. A path p_0p_1 at the outer surface of the pin ring, between the pins and the edge of the pin ring.
2. A path p_1p_2 across the end plane of the pin ring. This path consists of three parts when the path makes contact with the

end shaft : two lines $p_1p_{c_1}$ and $p_{c_2}p_2$, which are tangent to the end shaft and the circular arc $p_{c_1}p_{c_2}$, along the end shaft. The path is a straight line if there is no contact with the end shaft (Fig. 3.7).

3. A path p_2p_e at the outer surface of the pin ring, between the edge of the pin rings and the pins.

Position of the Points p_1 and p_2 on the Edge of the Pin Ring The assumption is made that the linking path Γ_{i-1}^{i} corresponds to a geodesic, across the edge of the pin ring. If the mandrel is developed into the end plane of the pin ring, the path Γ_{i-1}^{i} develops into a line (Fig. 3.8).

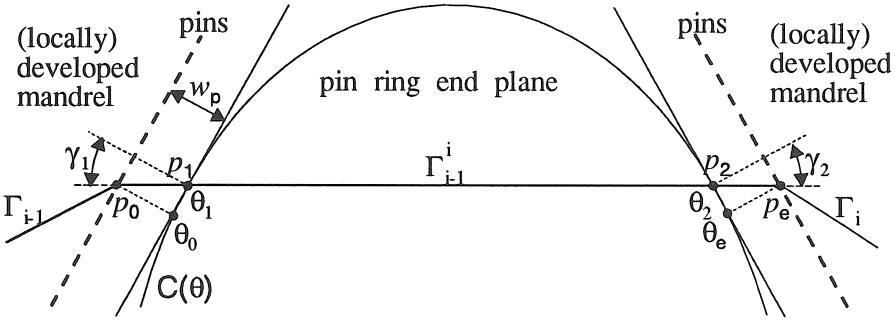

Figure 3.8: Developed fibre path behind a pin ring (without intersection with the end shaft of the pin ring) for a pin ring with a general cross-section

The base curve of the pin ring is a curve $C(\theta)$. The parameters at the points p_0, p_1, p_2 and p_e are, respectively, $\theta_0, \theta_1, \theta_2$ and θ_e. The parameters θ_0 in p_0 and θ_1 in p_1 differ, due to the angle γ_1 between the normal to the base curve $C(\theta)$ in p_1 and the developed fibre path (Fig. 3.8). The length l_{0e} between p_0 and p_e, measured along the base curve of the pin ring, equals :

$$l_{0e} = \int_{\theta_0}^{\theta_e} \left\| \frac{dC(\zeta)}{d\zeta} \right\| d\zeta = w_p \tan\gamma_1 + \int_{\theta_1}^{\theta_2} \left\| \frac{dC(\zeta)}{d\zeta} \right\| d\zeta + w_p \tan\gamma_2 \tag{3.20}$$

with w_p the distance between the pins and the edge of the pin ring. Eq. (3.20) can be solved iteratively.

In the common case of a pin ring with a circular cross section (with radius r_p), the angles γ_1 and γ_2 are equal due to symmetry (Fig. 3.9),

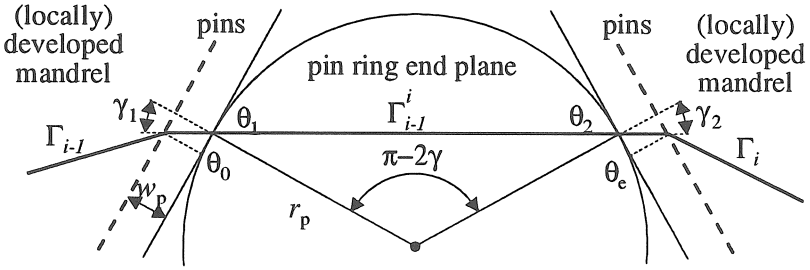

Figure 3.9: Developed fibre path on a pin ring with circular cross section

and $\theta_2 - \theta_1 = \pi - 2\gamma$ if there is no contact with the end shaft. Eq. (3.20) can then be written as :

$$l_{0e} = r_p \, \Delta\theta = r_p(\theta_e - \theta_0) = 2w_p \tan\gamma + r_p(\pi - 2\gamma) \tag{3.21}$$

or :

$$\Delta\theta = \theta_e - \theta_0 = \frac{2w_p}{r_p} \tan\gamma + \pi - 2\gamma \tag{3.22}$$

Eq. (3.22) is solved iteratively. The value of γ determines the position of p_1 and p_2.

The fibre path makes contact with the shaft when $\gamma_a = \arcsin\left(\frac{r_a}{r_p}\right)$. The span $\Delta\theta_a$ equals then :

$$\Delta\theta_a = \frac{2w_p}{r_p} \frac{r_a}{\sqrt{r_p^2 - r_a^2}} + \pi - 2\arcsin\left(\frac{r_a}{r_p}\right) \tag{3.23}$$

Minimum Span Eq. (3.22) has a minimum $\Delta\theta_m$ at $\gamma_m = \arccos\left(\sqrt{\frac{w_p}{r_p}}\right)$:

$$\Delta\theta_m = \frac{2}{r_p}\sqrt{w_p(r_p - w_p)} + \pi - 2\arccos\left(\sqrt{\frac{w_p}{r_p}}\right) \tag{3.24}$$

If the span $\Delta\theta$ is less than $\Delta\theta_m$, no stable fibre path can be found on the end plane of the pin ring. The fibre will slip from the end plane of the pin ring, and possibly lift off from the pins.

3.3 Fibre Path Design

This section describes the design of filament wound parts. First the general design methodology for wound parts is discussed, and then the design of the fibre paths is treated more in detail. As a case study, the design of tape wound T-piece is discussed.

3.3.1 Design of Wound Parts

The design of the fibre paths is based on two criteria : uniform coverage and optimal strength. The fibres should be placed adjacent to each other to obtain a uniform fibre distribution and a full coverage. To obtain an optimal strength, fibres are aligned as well as possible with the principal stress directions (cf. p. 63).

The design process consists of the following steps (Fig. 3.10) :

Step 1. Isotropic stress analysis A finite element analysis (FEA) is performed on an isotropic model in order to provide a starting point for building up the laminate.

Step 2. Fibre path design The fibre paths are selected with a design strategy, which depends on the global shape of the part (axisymmetric, tubelike, asymmetric) and the basic material (roving, tape). The design strategy is discussed extensively in section 3.3.2.

Step 3. Fibre path sequence The fibre paths are assembled in a fibre path sequence. The construction of the fibre path sequence is discussed in section 3.4.

Step 4. Determination of laminate lay-up The composite laminate lay-up is generated as input for the finite element model (cf. p. 63).

If the thickness of some elements is too small, supplementary fibre paths are generated or the existing fibre paths are adapted.

Step 5. Composite stress analysis A finite element analysis is performed on the composite part. If the requirements of strength and stiffness are not fulfilled, the lay-up is adapted by adding fibre paths or

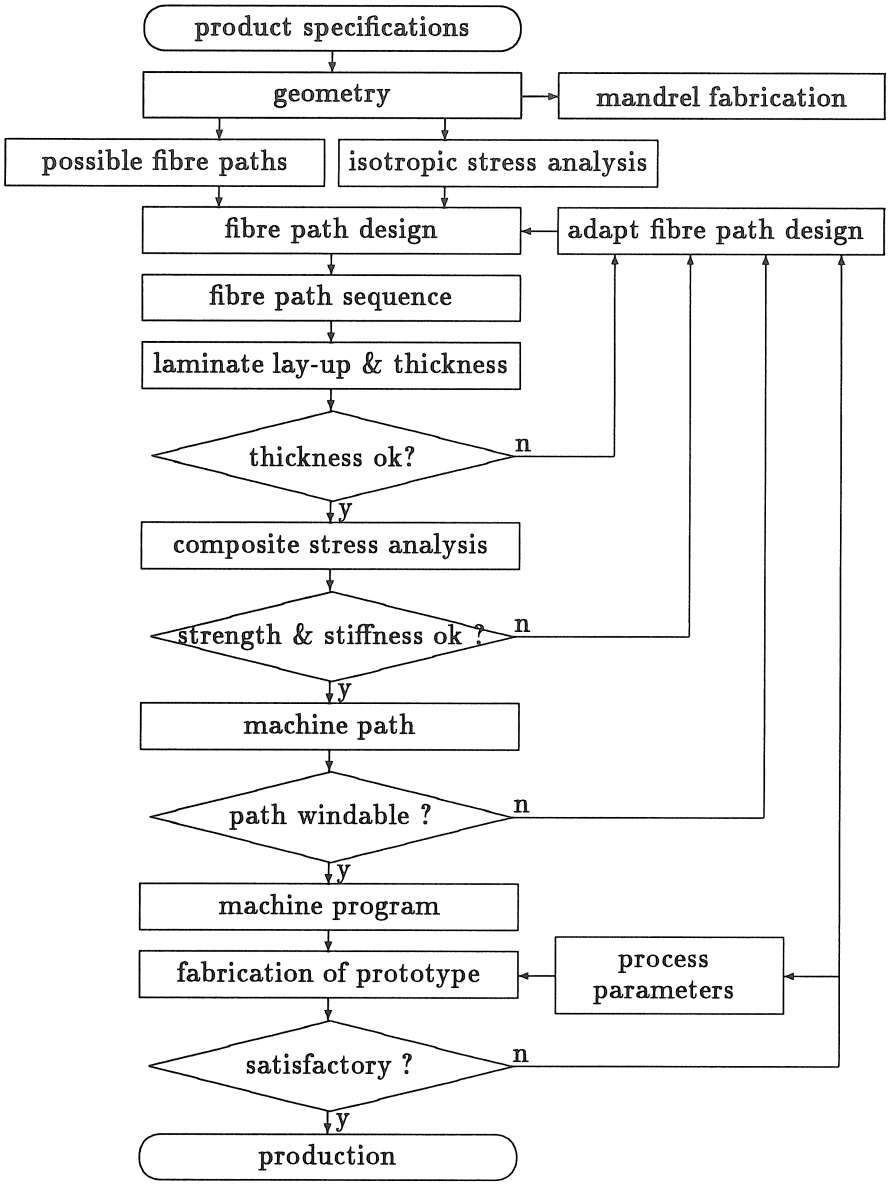

Figure 3.10: Design of a filament wound part

by changing the trajectory of the fibre paths. In zones where winding in the most loaded directions is not possible, e.g. in convex/concave zones, reinforcements are added before or after winding.

Step 6. Check on windability The positions of the pay-out eye are calculated. If the part has convex/concave areas, a solution may not be found if the tangent to the fibre path intersects the part, and the distance between the point of the fibre path and the intersection with the part is too small (cf. p. 198). If a path cannot be wound, the path is reversed. If the path can neither be wound backwards, it is removed from the lay-up and replaced by another path. If no alternative path can be found, the part has to be locally reinforced with weaves or mats.

3.3.2 Fibre Path Design Strategy

The fibre path design strategy of tape wound parts differs from the fibre path design strategy of filament wound parts. Tape winding allows only geodesics, whereas filament winding allows deviations from the geodesics. As a result, filament winding allows a better alignment with the optimal fibre directions. The method depends also on the shape of the part : axisymmetric, tubelike (or almost-axisymmetric) parts, or asymmetric parts with varying cross sections.

3.3.2.1 Filament Wound Parts

The optimal fibre directions, which are obtained by a finite element analysis in the isotropic part, are imported in CAWAR, and the fibre path is fit as close as possible to the optimal fibre path (cf. section 3.2.4). It is however not always possible to place the fibres in the desired directions, since these directions could be concave or thus not windable.

A uniform coverage is obtained by placing the fibres adjacent to each other. The approach, used to select the fibre paths, depends on the shape of the part.

Axisymmetric Parts A single fibre path is required as basis for the coverage pattern. The following paths are obtained by rotating the basic fibre path about the winding axis. The number of fibre

paths needed for complete coverage is calculated from the band width (cf. Appendix A.3).

Tubelike Parts These are parts which have a central spine, and an approximately constant cross-sectional shape, as e.g. cylinders, cones, pressure vessels, prisms,... The design of filament wound tubelike parts resembles the design of axisymmetric filament wound parts : a basic fibre path is repeated all over the circumference, in such a way that the fibres are spread equally over each cross section [47, 64]. The fibre paths are obtained by *circumferential shifting* of the basic fibre path, i.e. the fibre path is shifted, in the two-dimensional uv-mapping of the surface, over a constant distance in the circumferential direction, and then transformed back to the surface [64] (Fig. 3.11).

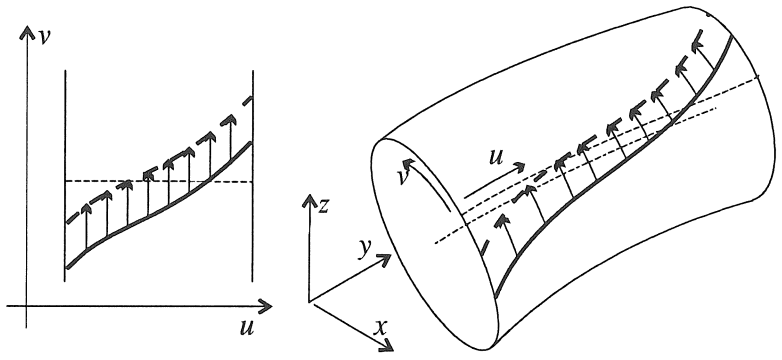

Figure 3.11: Circumferential shifting of a fibre path

If the spine direction of the surface $S(u,v)$ corresponds to the u-direction, and the circumferential direction to the v-parameter, the fibre paths $\Gamma_i(s) = [u_i(s)\ v_i(s)]^T$, obtained by circumferential shifting of a basic fibre path $\Gamma_0(s) = [u_0(s)\ v_0(s)]^T$, are :

$$\begin{cases} u_i(s) &= u_0(s) \\ v_i(s) &= v_0(s) + \frac{iV}{n_p} \end{cases} \tag{3.25}$$

with V the total span in the v-direction and n_p the number of fibre paths in each cross section.

The basic fibre path should be such, that for each derived fibre path the slippage tendency remains within limits.

Asymmetric Parts The above described strategy does not apply to asymmetric surfaces with continuously varying cross sections. A single fibre path, that can be repeated all over the surface, cannot be found. Each fibre path must be designed separately.

Trajectory Maps To get a better view on the fibre paths which are possible in the part, geodesics are calculated for different combinations of starting position and orientation (and possibly slippage tendency). These geodesics are symbolically represented by their surface sequence, i.e. the sequence of the surfaces or surface patches, in which the part is subdivided, where the fibre path passes. The starting point is moved along a curve, e.g. an edge of the part. The surface sequences are written in trajectory maps, which have in abscissa the starting position and in ordinate the starting winding angle. Trajectory maps are constructed for several starting curves, so that all possible geodesic trajectories are investigated.

If fibre bridging occurs, the fibre path is crossed in the trajectory map and excluded. This method is especially useful in parts with complex geometries, which have zones with reverse curvature where fibre bridging can occur.

Fibre Path Selection A geodesic path is chosen as a template for the coverage pattern. New fibre paths are derived by *parallel shifting*, i.e. by offsetting the basic fibre path over the band width w (Fig. 3.12). The points of the shifted path are obtained by calculating the end point of a geodesic with length w, which starts perpendicularly to the basic fibre path. The basic path is shifted as long as the slippage tendency remains within limits and fibre bridging does not occur. The basic fibre path has to be chosen in such a way, that an as wide pattern as possible is obtained.

Complete coverage is checked in the CAD-system, or by winding the part manually.

3.3.2.2 Tape Wound Parts

Tape wound parts allow only geodesics. A pattern of geodesics, that follows the principal stress directions as close as possible and the trajectory of which does not vary too much when the starting point is slightly changed, is selected.

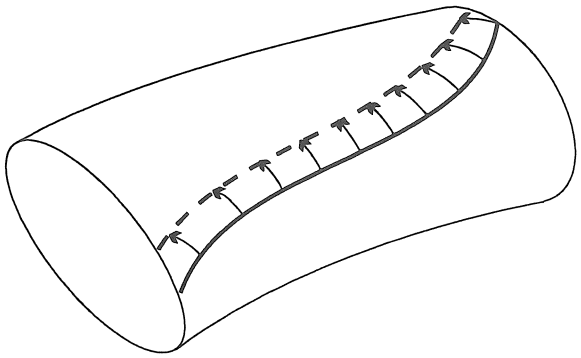

Figure 3.12: Parallel shifting of a fibre path

A uniform coverage is obtained by laying the fibres parallel to each other. Overlaps and gaps between adjacent tapes must be minimized in order to realize a path with a compact and uniform fibre distribution [98]. Complete parallel fibre paths can mostly not be constructed since only geodesics are allowed : the gap between two geodesics, which are adjacent at the start grows rapidly when they encounter areas which are not identical. Gaps and overlaps between adjacent fibre paths are minimized by demanding that the distance between two fibre paths equals the band width at two reference curves.

3.3.3 Case Study : a T-piece

Pipes have been manufactured in plastic materials for the past 20 years. Especially glass fibre reinforced plastics are interesting due to their corrosion resistant properties and inherent strength characteristics [76]. Glass fibre reinforced tubes are produced in large quantities by filament winding. The connections between pipes still pose problems. The aim of this study is to design and produce a T-piece by tape winding. The material used for tape winding is a 25-mm wide glass fibre tape. Since tapes are used, only geodesics are allowed in the fibre path design.

The shape of the composite T-piece differs from the shape of a metal T-piece. A conventional metal T-piece consists of two intersecting cylinders. The sharp edges between the two cylinders are very unfavourable for winding, since the tapes are wrinkled severely, which

might lead to fibre damage and voids [39]. The intersection of the two cylinders is therefore smoothed (Fig. 3.13). The fillet is convex/concave, which can lead to fibre bridging and collisions between the pay-out eye and the mandrel.

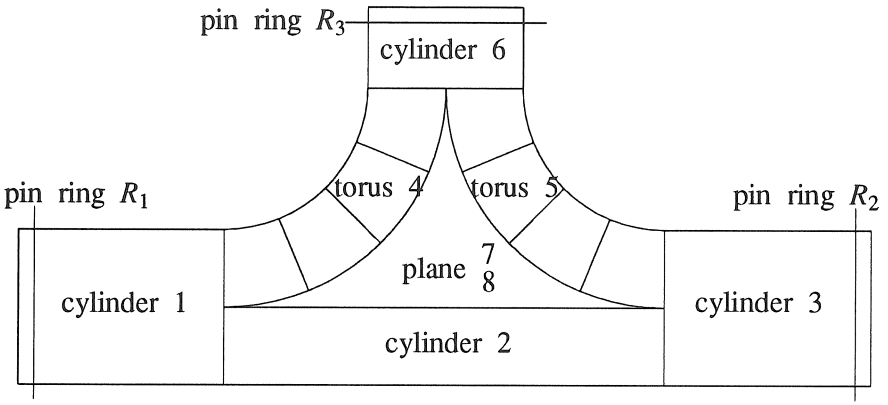

Figure 3.13: T-piece

3.3.3.1 Modelling of the T-piece

The T-piece cannot be modelled as one single surface in a CAD-surface modeller. It is modelled as 8 different surfaces : 4 cylinders (1,2,3,6), 2 torus segments (4,5) and 2 bounded planes (7,8) (Fig. 3.13). Pin rings are provided at the three ends of the T-piece : R_1 at the left edge of cylinder 1, R_2 at the right edge of cylinder 3, and R_3 at the upper edge of cylinder 6. The T-piece has two symmetry planes : the first plane contains the axes of cylinders 1 and 6, the second plane contains the axis of cylinder 6 and is perpendicular to the axis of cylinder 1.

3.3.3.2 Isotropic Stress Analysis

Stress calculations have been performed with the finite element code SYSTUS by M. Lossie [59]. For the isotropic model a steel part with a thickness of 3 mm is used. Fig. 3.14 shows the Von Mises stresses at the outside of the T-piece for a 1 MPa internal pressure, with clamped end sections [59, 82]. This plot shows high bending stresses in the planes 7 and 8. Special attention will have to be paid to the reinforcement of these zones.

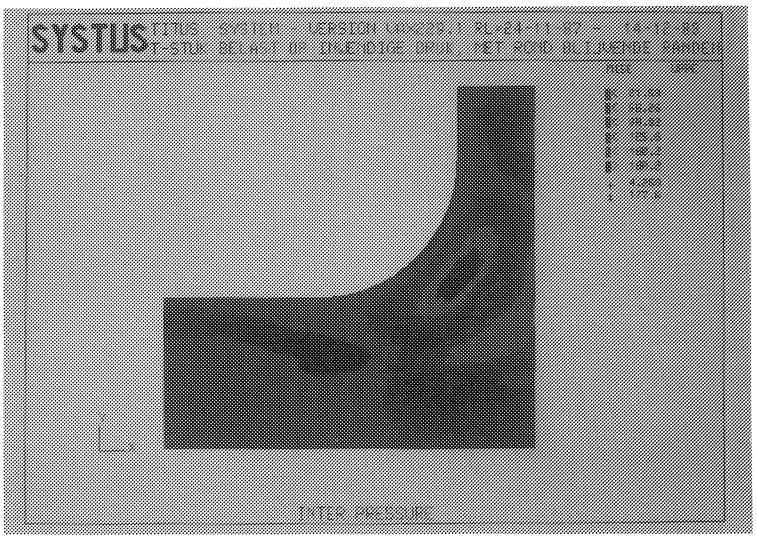

Figure 3.14: Von Mises stresses in a quarter of the T-piece, loaded with a 1 MPa internal pressure (clamped end sections)[59]

3.3.3.3 Trajectory Maps

Trajectory maps are generated for the lower edge of cylinder 6 and the right edge of cylinder 1 as starting curve. Fig. 3.15 shows a trajectory map with the lower edge of the vertical cylinder 6 as a starting curve. Geodesics are calculated for different combinations of starting positions and winding angles. The starting position needs only to be varied over a quarter of the complete circumference, due to the symmetry planes of the T-piece. The geodesics are represented by their surface sequence (cf. Table 3.1) If fibre bridging occurs, the geodesic must be excluded and its symbol in Fig. 3.15 is shaded. Three main families of trajectory types can be distinguished (Fig. 3.16) :

- The trajectory types K,L (surface sequence : 6 4 (7 2) 1 – Fig. 3.16a) and U,V (6 4 7 5 (8 2) 3 – Fig. 3.16b), that start at cylinder 6, and follow the inner ring of one of the torus segments towards the cylinder 1 or 3. Fibre bridging occurs in most of these geodesics.

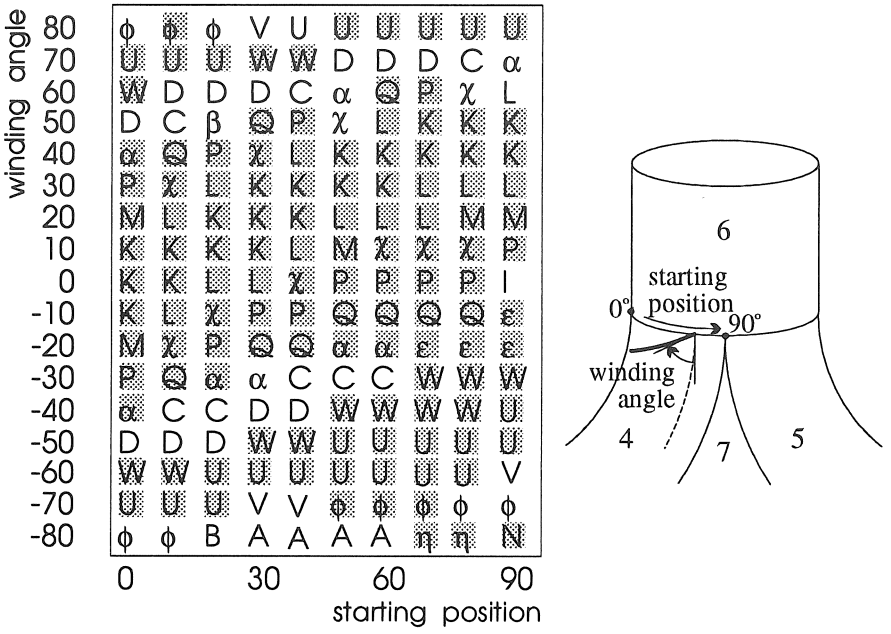

Figure 3.15: Trajectory map for T-piece. Fibre bridging occurs if the code is shaded

code	surface sequence	code	surface sequence
K	6 4 1	A	6 4 7 5 8 2 1
L	6 4 7 2 1	B	6 4 7 5 8 2 8 4 1
M	6 4 7 2 8 4 1	C	6 4 7 2 8 5 3
N	6 4 7 5 8 4 1	D	6 4 7 2 3
U	6 4 7 5 3	P	6 4 7 2 8 4 6
V	6 4 7 5 8 2 3	Q	6 4 7 2 8 5 6
W	6 4 7 2 8 4 1		
α	6 4 7 2 8 5 7...	ϵ	6 4 7 5 7 2 8...
β	6 4 7 2 8 5 8...	ϕ	6 4 7 5 8 2 7...
χ	6 4 7 2 8 4 7...	η	6 4 7 5 8 4 8...

Table 3.1: Codes used in trajectory map
Different codes refer to different surface sequences. An Arabic letter corresponds to one sequence, a Greek symbol to a group of sequences.

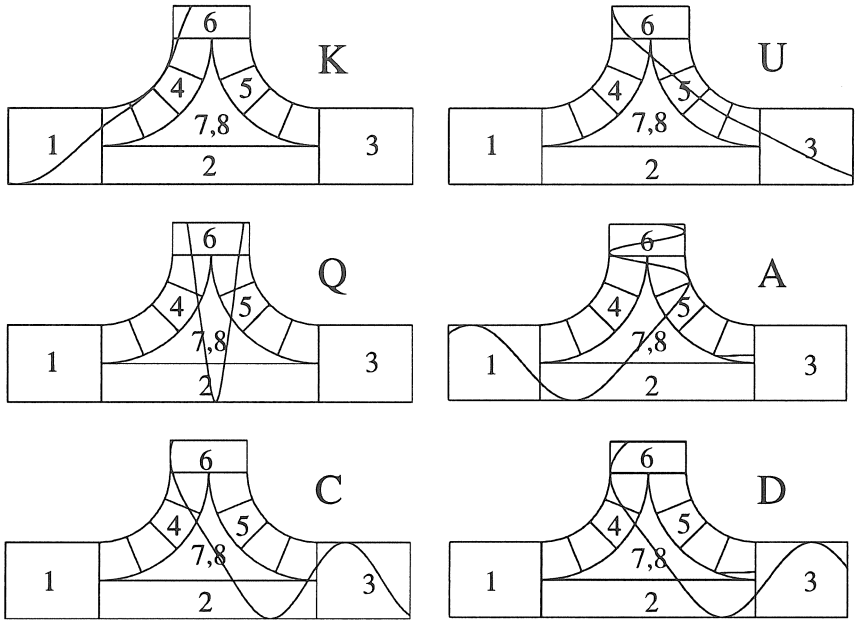

Figure 3.16: Geodesic trajectory types on a T-piece
(a) K (b) U (c) Q (d) A (e) C (f) D

- The trajectory types P (6 4 7 2 8 4 6 – Fig. 3.16c) and Q (6 4 7 2 8 5 6), that start with low winding angle at cylinder 6, go via a torus segment to cylinder 2 and return upwards to cylinder 6. Fibre bridging occurs in most of these geodesics in one of the torus segments.

- The trajectory types A,B (6 4 7 5 8 2 (8 4) 1 – Fig. 3.16d) and C,D (6 4 7 2 (8 5) 3 – Fig. 3.16e,f), that start with a relatively high winding angle, go via a torus segment diagonally over the plane towards the cylinder 1 or 3.

In Fig. 3.15, only 26 % of the geodesics are free from fibre bridging. The main problem is therefore the selection of bridging-free fibre paths, covering the surface completely. The results of the isotropic finite element analysis could therefore almost not be taken into account. Finite element analysis is in this application especially used as a verification tool, and to indicate where additional reinforcements have to be placed [59].

3.3.3.4 Fibre Path Selection

Only the trajectory types A,B,C,D give continuously positive results, so these trajectory types will certainly be needed in the final winding pattern to cover the vertical cylinder. The individual fibre paths of this family are selected in such a way that their mutual distance at two reference curves (the right edge of cylinder 1 and the lower edge of cylinder 6) equals the band width. This selection is done iteratively. A basic curve, in the middle of the band is chosen as a template. The starting position is shifted over the band width, measured along the right edge of cylinder 1 (i.e. over $\frac{w}{\cos\alpha_0}$, with w the band width and α_0 the winding angle at cylinder 1 in the starting point). The starting winding angle α_0^* of the new curve is adapted until the distance between the two fibre curves at the lower edge of cylinder 6 equals the band width. In this way a large band of almost-parallel geodesics is constructed (Fig. 3.17). The paths are not completely parallel : they converge in the top of torus segment 5, and diverge at the cylinders 1 and 6.

Due to the two planar symmetries of the T-piece, the data of each fibre path can be used four times in the final lay-up.

A second trajectory map is generated with the right edge of cylinder 1 as starting curve. A helical winding pattern is selected. The paths are chosen so, that their mutual distance at the right edge of cylinder 1 and at the left edge of cylinder 3 is equal. This winding pattern is extrapolated to cover the lower part of torus 5 (Fig. 3.18). For spots of the T-piece that are not covered by one of the two selected winding patterns, e.g. the top of the bounded planes and the middle parts of the torus segments additional geodesics are selected (Fig. 3.19).

3.3.3.5 Laminate Lay-Up and Composite Stress Analysis

The laminate data for the finite element analysis are calculated with the program `LUPGEN` [59]. The program calculates the contribution of a fibre path to the laminate thickness in each element. This information is used to calculate how many times a geodesic has to be repeated in the winding pattern. Additional geodesics are selected for elements that remain too thin. A uniform coverage is however difficult to obtain. The minimum value of the ratio between thickest and thinnest element

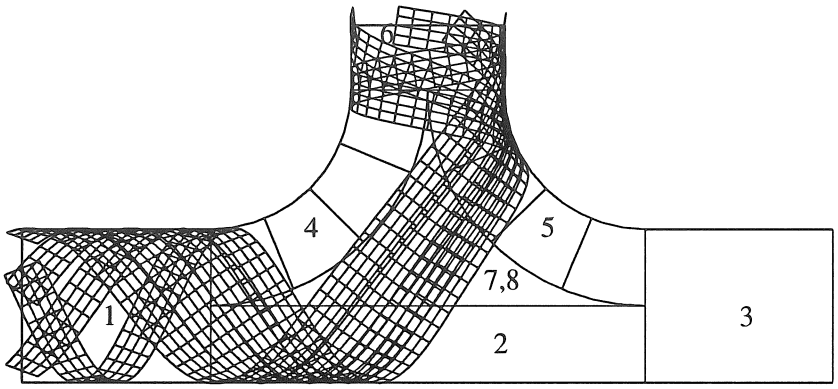

Figure 3.17: First pattern of quasi-parallel geodesic paths

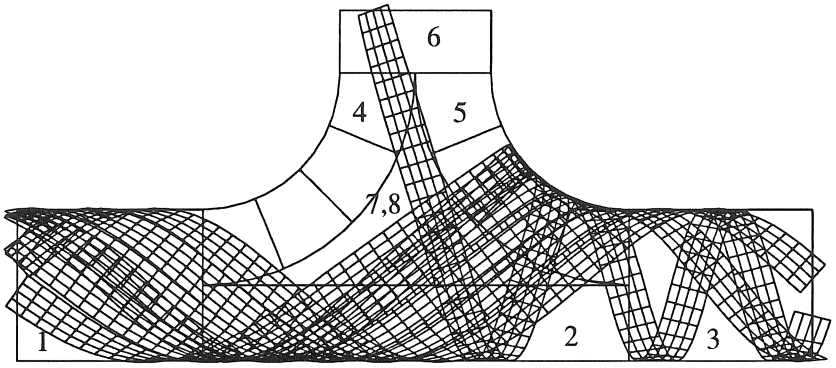

Figure 3.18: Second pattern of quasi-parallel geodesic paths

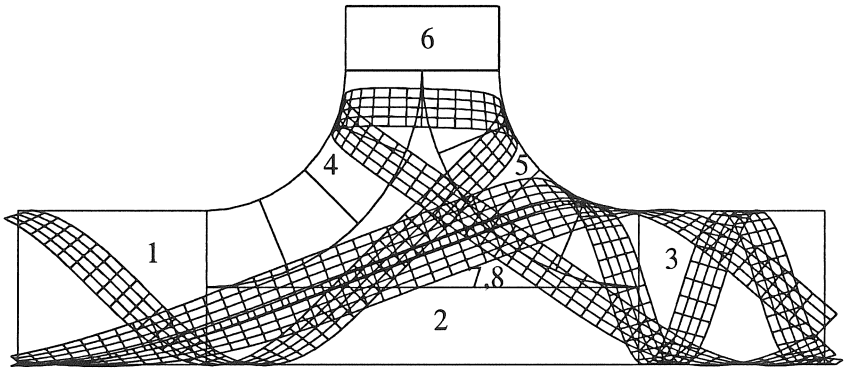

Figure 3.19: Additional geodesics

obtained is 4.3 [59].

A finite element analysis on the composite part is then performed to test the strength of the part [59]. The composite part is, like the metal part, subjected to a 1 MPa internal pressure. The most critical areas are still the planes 7 and 8. The most loaded layer in the most critical element will fail at a fraction 0.285 of the applied load [59]. To be able to sustain the applied load, the weakest zones have to be reinforced with additional well-oriented fibres.

3.4 Fibre Path Sequence

After the design of the fibre paths Γ_i, the sequence $\mathbf{v} = [\Gamma_1 \ldots \Gamma_i \ldots \Gamma_n]^T$ in which the fibre paths Γ_i have to be wound on the mandrel is defined. The sequence of the lay-down influences the properties of the wound part. If bending moments act on the composite shell, the stresses in the fibre paths depend on the position of the fibre in the laminate, and therefore on the sequence of the fibre paths. The sequence will then influence the global strength of the composite. The fibre path sequence determines also the degree of interweaving, which influences the strength and fatigue properties [59].

If end domes are used, the stability criteria must always be fulfilled, so the freedom in the construction of the fibre path sequence is limited. Pin rings allow sudden changes in the trajectory of the fibre path, and give therefore a much larger freedom in the construction of the fibre path sequence. The construction of the fibre path sequence is subjected to some requirements, which are discussed in this section.

3.4.1 Requirements for the Sequence

3.4.1.1 Continuity

The fibre path Γ_i must start at the pin ring R_j where the previous fibre path Γ_{i-1} ended.

Not every sequence $\mathbf{v}$, which is desired by the operator, can be wound : the array $\mathbf{n}_v = [n_{v,1} \ldots n_{v,j} \ldots n_{v,m}]^T$ (with m the number of pin rings), which consists of the number of occurrences of a pin ring R_j in the sequence $\mathbf{v}$, may maximal contain two odd elements, viz. the starting and the end pin ring.

An example : if the part has 3 pin rings, and the following 3 fibre paths have to be wound :

Fibre Path	Γ_1	from pin ring R_1	to R_2
	Γ_2	R_2	R_3
	Γ_3	R_1	R_2

The array $\mathbf{n}_v = [2\,3\,1]^T$. The starting pin ring has to be R_2 or R_3. If R_3 is chosen as starting pin ring, a possible sequence[2] is : $\mathbf{v} = [-\Gamma_2\ -\Gamma_1\,\Gamma_3]^T$.

3.4.1.2 Minimum span at the pin rings

The minimum span $\Delta\theta_m$ between the end point p_0 of Γ_{i-1} and the starting point p_e of Γ_i is given by Eq. (3.24). If the span is smaller, an additional turn around the axis of the pin ring is necessary. If the pin ring has no end shaft, a value less then the minimum value is never allowed.

3.4.1.3 Rotation direction

When tapes are used for winding, the difference between the path lengths of the edges of the tape should be as small as possible. Differences in the path length are compensated at the pins : after fixing the fibres behind the pins, the difference in path length cannot be compensated by contraction of the tape, so that the longer edges will lift off from the surface, which can lead to releasing from the pin rings. In the optimal case, the path $\Gamma_i\Gamma_i^{i+1}\Gamma_{i+1}$ is one geodesic, without discontinuities in the tangent at the pin rings. Allowing only this fibre path would nullify the freedom, demanded by the user. The path length differences are limited by demanding that the rotation direction about the axis of the pin ring is maintained (Fig. 3.20). The rotation direction of the mandrel remains in this case unchanged for tubelike parts, so that a constant mandrel velocity could be maintained. The linking motion behind the pin rings becomes also more complicated when the rotation direction changes.

[2]The minus sign before Γ_2 and Γ_1 indicates that the path will be wound backwards.

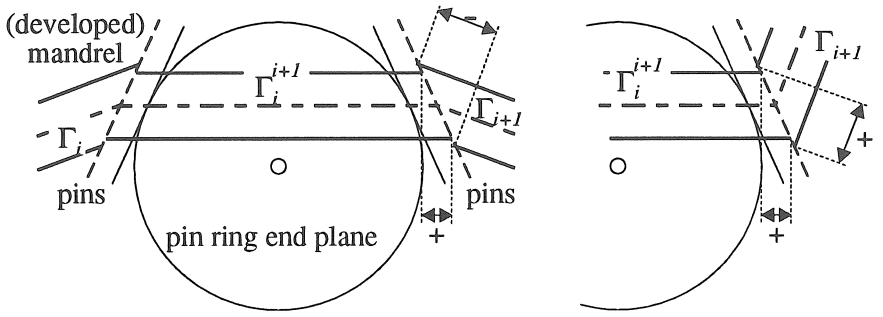

Figure 3.20: Differences in the path length between the lower and the upper edge of the tape

The fibre path is developed in the end plane of the pin ring (cf. Fig. 3.9). In Fig. (a) the rotation direction of the paths Γ_i, Γ_i^{i+1} and Γ_{i+1} about the axis of the pin ring is the same (clockwise), in Fig. (b) not (Γ_{i+1} counterclockwise). In Fig. (a) the differences in path length of the edges of the tape from Γ_i^{i+1} compensate each other, in Fig. (b) not.

3.4.1.4 Maximum span at the pin rings

To limit the amount of fibre at the end plane of the pin rings, the span between the p_0 and p_e is limited to the span $\Delta\theta_a$ at which the fibre makes contact with the end shaft of the pin ring (cf. Eq. 3.23).

3.4.2 Construction of the fibre path sequence

The operator inputs a desired sequence, and the program converts it into a feasible sequence. A test is first performed to check if the sequence can start from the desired starting pin ring. A test is performed if there is a pin ring which occurs only once in the fibre path sequence. If there is such a pin ring, the corresponding fibre path is put at the end of the sequence. Tests are then performed for all the fibre paths. If the starting or end pin ring correspond to the current pin ring, all the above mentioned requirements are checked. If all these requirements are fulfilled, this path will be the next path to be wound. If no solution is obtained, the last requirement (maximum span) is dropped, and all fibre paths are checked again to find a new solution. If then no solution is found, the requirement of constant rotation direction is dropped, and afterwards the requirement of minimum span, until a

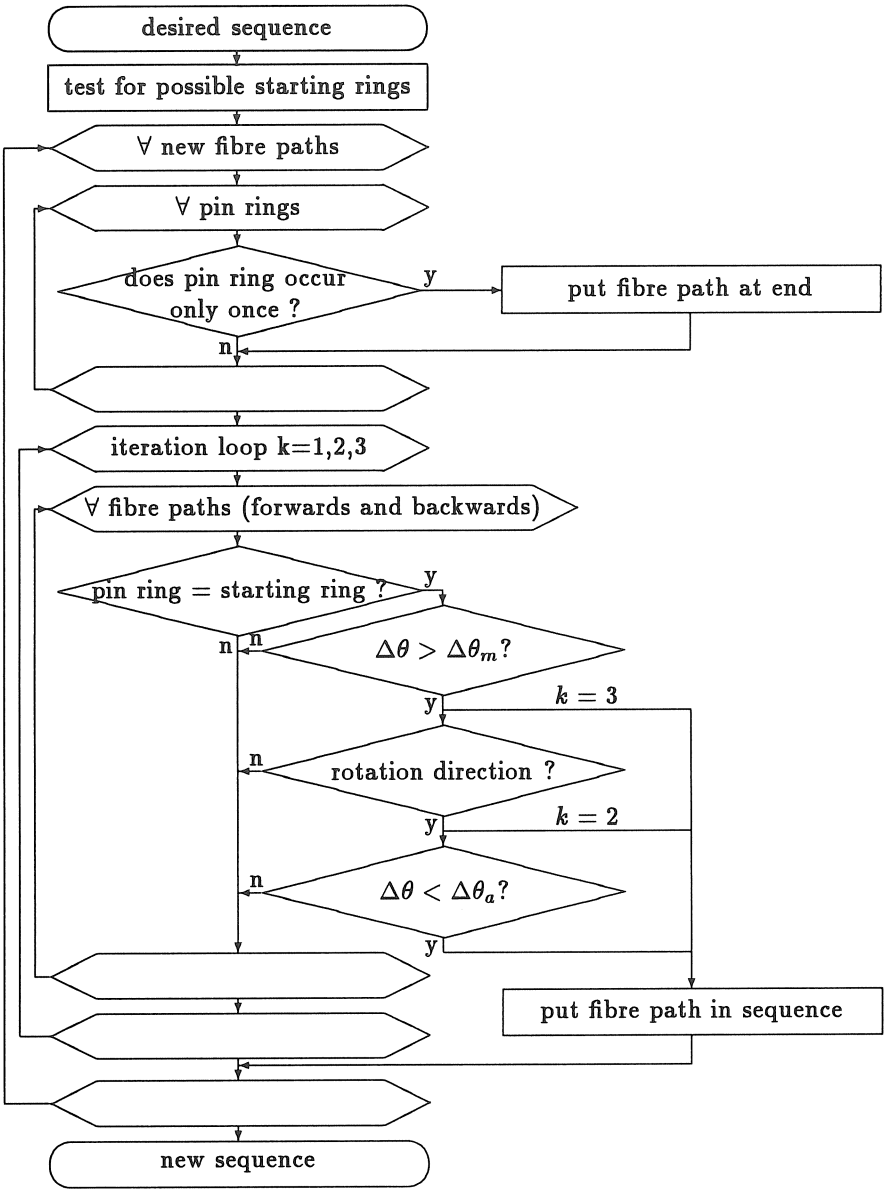

Figure 3.21: Algorithm for construction of fibre path sequence

solution is found.

3.5 Conclusions

This chapter described the design of filament wound parts. A program has been developed for the calculation of geodesic and semi-geodesic fibre paths, which is based on the solution of a system of differential equations.

The fibre paths have to be selected so that the part is as strong and uniformly covered as possible. As a starting point, the stresses are calculated in an isotropic part, and the optimal fibre angles are derived.

A design methodology has been developed for filament wound and tape wound parts. The design method depends strongly on the type of surface (axisymmetric, tubelike, asymmetric) and the basic material (roving, tape). Axisymmetric and tubelike parts require only a limited number of fibre paths which are repeated all over the circumference. Asymmetric surfaces require a lot of individual fibre paths.

Tape winding allows only geodesics, limiting so the opportunity to match the fibre paths to the optimal fibre paths, since the geodesic is completely determined by its starting point and starting orientation. Filament winding allows significant deviations from the geodesics without fibre slippage, so that the fibre paths can be better aligned with the optimal fibre directions, and a more uniformly covered part can be obtained.

The sequence in which the fibre paths are wound is defined, and the laminate lay-up determined. The stresses are then calculated in a composite material to check the strength of the part.

Chapter 4

Robotic Tape Winding Cell

4.1 Introduction

The first filament winding machines were gear-controlled lathe type machines with 2 axes. The growing demand for more complex parts, and the advent of computer-controlled machines, led to the development of computer-controlled filament winding machines. In most machines the mandrel is mounted on the spindle and the pay-out eye on the transverse carriage, which has up to six axes of control.

The pay-out eye can also be mounted on the end flange of a robot. Replacing the transverse carriage by a robot reduces the investment cost and increases the flexibility of the winding cell (cf. section 1.5.2.3).

A robotic filament winding cell has been developed at PMA (cf. section 1.6.1.2), which consists of a PUMA-762 robot and an external axis for the rotation of the mandrel (Fig. 1.22). This chapter will describe how this set-up has been adapted to enable winding with tapes.

Tape winding has some advantages over filament winding, like a lower investment cost, because only one delivery unit is needed, and the possibility to decrease the fabrication time. Tapes are however very sensitive to transversal forces. Special attention has therefore to be paid to tape guidance, tape centring and tape twisting.

This chapter discusses first the task requirements for the tape winding process. Two tape winding machines are discussed : the commer-

cial tape winding machine from General Dynamics and the robotic tape winding unit, developed at PMA. The control of the robotic tape winding unit is then discussed more in detail.

4.2 Task Requirements

4.2.1 Requirements for the Tape Winding Process

The task requirements for the tape winding process are :

1. The delivery point in the pay-out eye e must lie on the tangent $\vec{t}$ to the fibre path in the contact point f (Fig. 4.1) :

$$\vec{r}_e = \vec{r}_f + l_f\vec{t} \tag{4.1}$$

with $\vec{r}_e$ and $\vec{r}_f$ the position vectors of respectively e and f, and l_f, the free length, i.e. the distance between f and e.

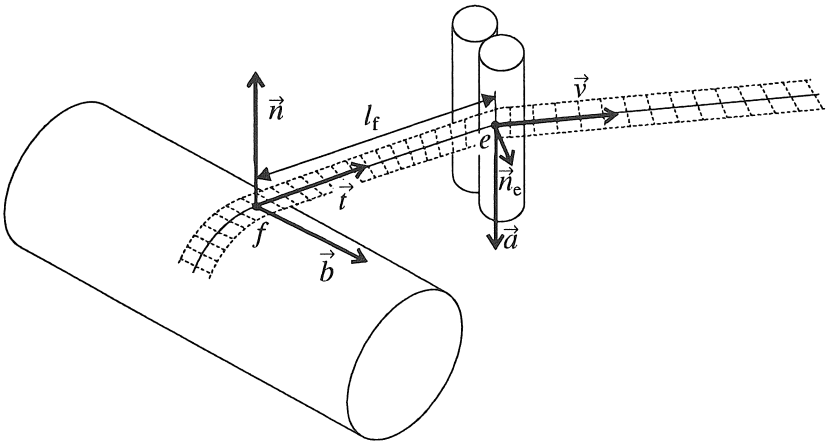

Figure 4.1: Position and orientation of the pay-out eye

2. All collisions have to be avoided. The collisions which are the most likely to occur are collisions between, on the one hand, the pay-out eye and the machine joints, and, on the other hand, mandrel and head- and tail-stock. Collisions between the pay-out eye and the machine joints are also possible.

   Collision between the pay-out eye and the mandrel occur in the winding process if the part has convex/concave areas, or if the

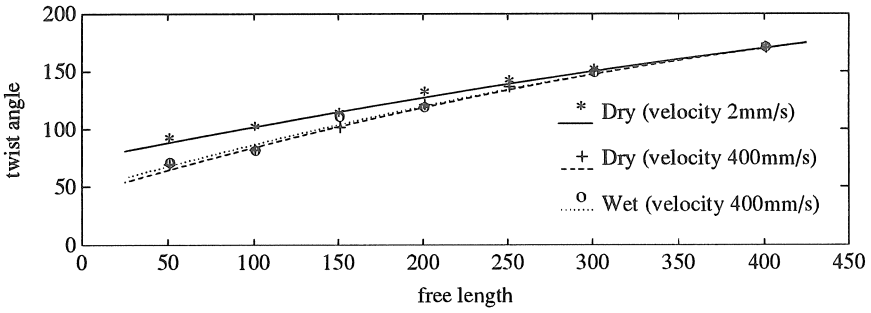

Figure 4.2: Maximum twist angle in function of the unsupported length for a 25-mm wide unidirectional E-glass tape

free length is too small in zones with large radii of curvature. Collisions with head- and tail-stock occur during the linking motion, if the distance between the pin rings and the stocks is small.

The position of the pay-out eye must lie within the working envelope of the winding machine.

3. The band width must be constant. A roll or a set of cylindrical rolls is used as delivery geometry. The axis $\vec{a}$ of these rolls is perpendicular to the pay-out axis $\vec{v}$, i.e. the feeding axis in the pay-out eye. To maintain a constant band width, the vector $\vec{a}$ must be normal to the tangent to the fibre path $\vec{t}$ [107] (Fig. 4.1) :

$$\vec{t} \cdot \vec{a} = 0 \tag{4.2}$$

The resultant force of the tape on the rolls, which is generated by the difference in orientation between the tangent $\vec{t}$ and the pay-out eye axis $\vec{v}$, is then perpendicular to the axis of the rolls $\vec{a}$, so that no slip occurs.

4. The tape must be delivered without folding or wrinkling. The tape will fold up if the tape twist angle, i.e. the rotation about the length axis of the tape, becomes too high. In axisymmetric structures the twist angle does not exceed 90°, but in asymmetric parts twists can become very large, e.g. when winding round a cylinder with an axis perpendicular to the winding axis [68]. The maximum allowable twist angle is function of the unsupported length (Fig. 4.2).

5. The tape should always be tensioned. Slack can occur during rewinding. Rewinding occurs in the delivery point, when the decrease of the free length is larger than the increase of the length of the wound fibre path, e.g. during the motion round the pin rings. Rewinding can also occur at the exit of the impregnation bath, when the pay-out eye moves towards the impregnation bath.

   The tensioning systems have to be designed so, that sufficient slack can be taken up. If slack cannot be taken up by the tensioning system, the position of the pay-out eye has to be calculated so, that rewinding does not occur.

4.2.2 Degrees of Freedom Necessary

Only two degrees of freedom are required to wind small roving bundles. It is possible to wind any complex convex shape with a simple two-axis filament winding machine. However, if the band width increases, an additional rotation of the pay-out eye about the feeding axis of the tape is required. Another translational axis is necessary to control the free length, in order to avoid folding of the tape and to maintain a good accuracy [15].

Collisions can be avoided by changing the free length or the orientation of the pay-out axis. In the extreme case the pay-out axis has to be aligned with the normal to the surface in convex/concave parts (cf. p. 222). Two additional degrees of freedom are therefore required to be able to change the orientation of the pay-out eye.

So, in order to avoid collisions efficiently, a machine with 6 axes is necessary.

4.3 Tape Winding Machines

Two distinct approaches are possible in tape winding :

- the unwinding bobbin is mounted on the transversal carriage. This limits the number of guiding systems, so that an accurate tension control and an easier control of tape twisting is obtained. The inertia of the transversal carriage is however increased, since the unwinding bobbin, and, in case of wet winding, also the impregnation bath, are mounted on the transversal carriage.

- a fixed unwinding bobbin and impregnation bath are employed. The number of guiding systems increases, resulting in a poor tension control, and a more difficult tape twisting control. The inertia of the transversal carriage is reduced, enabling fast complex motions of the pay-out eye.

This section compares two tape winding machines : the prepreg tape winding machine of General Dynamics, where the unwinding bobbin is mounted on the transversal carriage, and the robotic (wet) tape winding cell developed at PMA, with a fixed tape unwinding system.

4.3.1 Prepreg Tape Winding Machine

The tape winding machine developed by General Dynamics (Fig. 4.3) is a converted filament winding machine and consists of :

- 4 programmable machine axes : mandrel (spindle axis), transversal carriage (horizontal and in-feed axis) and delivery system (rotating axis).
- tape unwinding system. Tension is applied at the roll, on which the tape is delivered. A release paper removal removes the release paper from the prepreg. Almost frictionless guide components direct the tape towards the roller head assembly.
- the roller head assembly (Fig. 4.4) guides the tape untwisted towards the delivery roller. The assembly consists of four elements : the support frame, which can be fixed to the rotating axis or to the transversal carriage, the roller turning axis, a freely pivotal head and the delivery roller. The roller can rotate freely about a turning axis, which is mounted eccentrically to the rotating axis, so that the roller is purely responsive to winding forces. The rotating axis has to be programmed in such a way that the tape is delivered to the delivery head roller without twisting [46].
- the delivery head roller is the final controlling element. Its surface should provide adequate friction between roller and tape to avoid slippage and material damage. As surface material a polyurethane casting is chosen, because this material provides a good interface with the tape. The roller has a convex profile or a centering arch (Fig. 4.4), which have a recentring capability when the tape moves off centre [15].

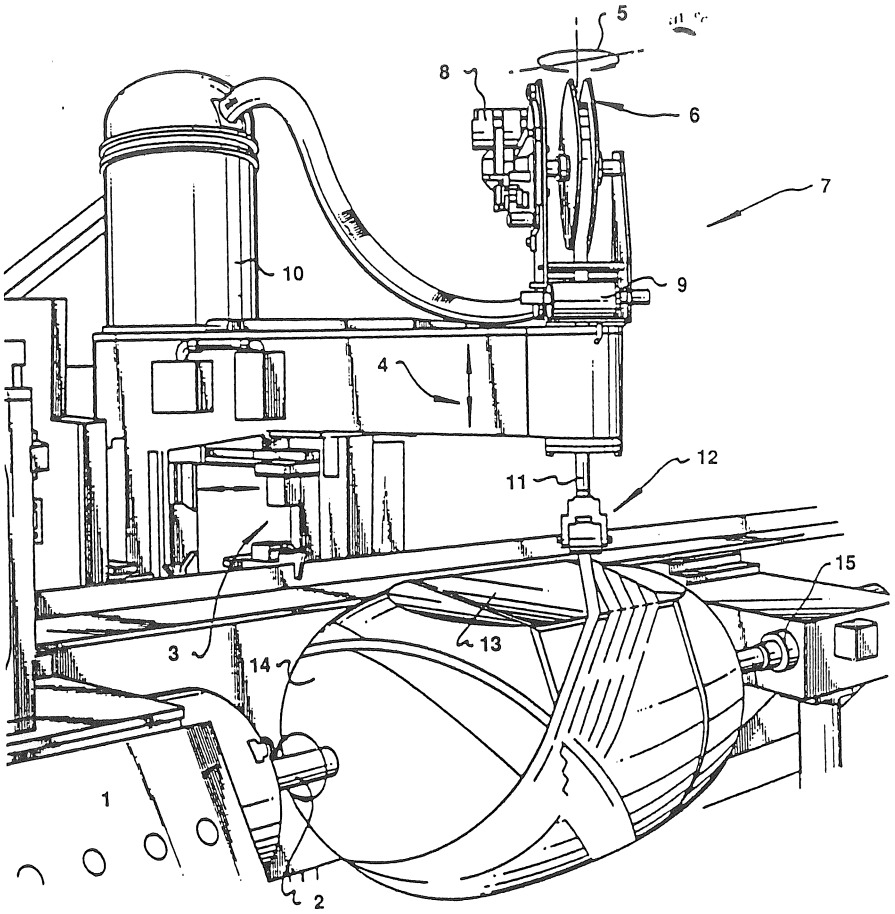

1. Programmable Controller
2. Spindle Axis
3. Horizontal Axis
4. In-Feed Axis
5. Rotating Axis
6. Packaged Tape
7. Creel
8. Tension Controller
9. Guide Components
10. Backing Paper Removal System
11. Roller Turning Axis
12. Delivery Head Roller
13. Mandrel Body
14. End Dome
15. Tail Stock

Figure 4.3: Tape winding machine (General Dynamics) [15, 46]

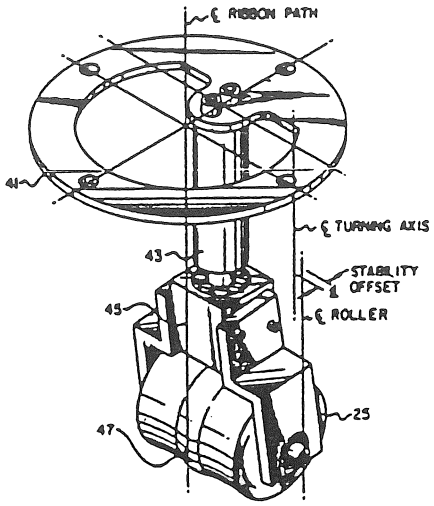

Figure 4.4: Roller head assembly of the General Dynamics tape winding machine [46]

Because this machine has only four degrees of freedom, the possibilities to avoid collisions are severely limited. This machine is therefore practically limited to convex parts.

4.3.2 Robotic Tape Winding Cell

The robotic filament winding cell, which is developed at PMA (cf. section 1.6.1.2), has been adapted to enable winding with tapes. The basic material is a 25-mm wide unidirectional glass fibre tape[1]. The tape is impregnated during winding, so that this process can be described as a "wet tape winding" process.

In order to maintain a constant band width, the pay-out eye is provided with a rotation about the feeding direction.

The robotic tape winding cell has 8 degrees of freedom : 6 degrees of freedom of the PUMA-762, the mandrel rotation, and the delivery roll rotation. The tape winding process fixes only 3 variables, and 3 supplementary degrees of freedom are necessary to avoid efficiently collisions. This results in a redundancy of two degrees of freedom.

[1]The tape is a plain weave of 4.6 EC-glass fibre rovings (1200 tex) per cm in the warp direction and 1.55 pair of EC-glass fibre rovings (34 tex) per cm in the weft direction. The weight of the tape is 600 g/m^2 [117].

The simplest solution to solve this redundancy is to fix two degrees of freedom : two rotations of the robot wrist are fixed by maintaining the normal to the robot end flange vertically downwards. The motions of the robot wrist and the risk of collisions between the robot and the mandrel are then reduced, and the resin does not drip on the robot joints. The pay-out axis is perpendicular to the normal to the robot end flange, and moves in a horizontal plane (Fig. 4.5).

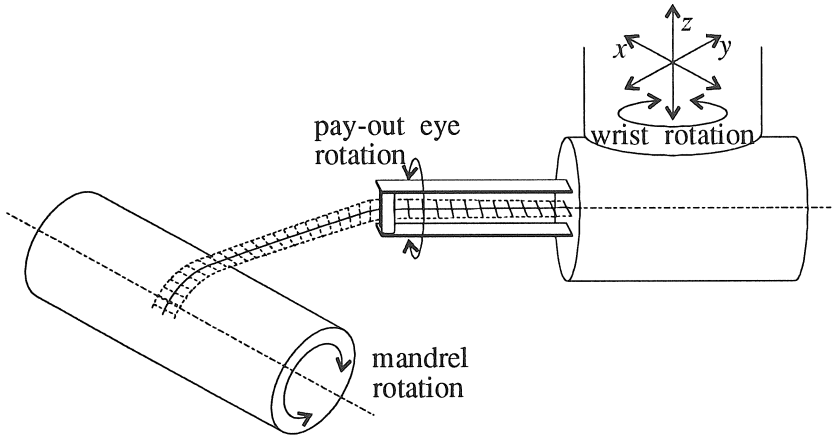

Figure 4.5: Position of the pay-out eye : the normal to the robot flange is directed vertically downwards, the axis of the pay-out eye is horizontal

Due to the redundancy, the PUMA-762 could be replaced by a cheaper robot with four degrees of freedom (e.g. SCARA-type robot). A robot which is mounted on the ceiling is also more appropriate than a robot which is mounted on the floor. A floor-mounted robot has as drawbacks that only a small part of the working envelope can be used for winding and that the delivery system has to be placed such, that the fibre does not make contact with the robot.

The pay-out eye, which is mounted on the robot end flange, consists of three sections :

- a delivery section, which is the last controlling element in the tape placement, and is therefore responsible for the accuracy of tape placement.
- a tape guiding system, which has to guide the tape without wrin-

kling through the pay-out eye.

- an entry section, which has to centre the tape in the guiding system without wrinkling.

The pay-out eye is developed for tape winding, but can easily be modified to wind with roving bundles. The rolls and bars, which are employed during tape winding, are then replaced by toroidal eyelets or combs.

4.3.2.1 Delivery Section

The delivery section consists of a pair of rolls, which guide the tape (Fig. 4.6). The rolls must be oriented so, that the band width remains constant.

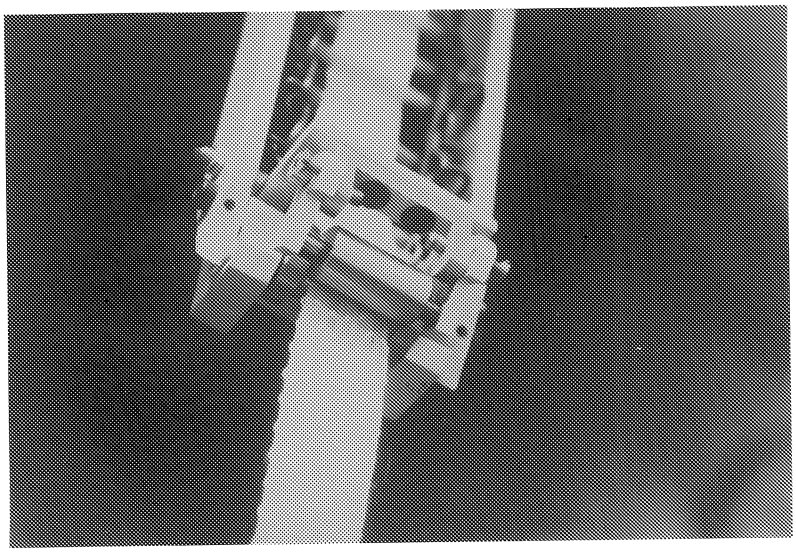

Figure 4.6: Delivery rolls

The tape must be centred in the delivery rolls without contracting. To keep the tape as well as possible in the centre, the resistance against moving out of centre should be as high as possible. A high friction force is therefore induced by pressing the two rolls against each other. One of the rolls has flanges at both ends, so that the tape cannot move out of the rolls (Fig. 4.6).

4.3.2.2 Tape Guiding System

The tape guiding system has to guide the tape from the entry section towards the delivery rolls without wrinkling. The tape guiding system must store as much tape twist as possible. Excessive fibre twists can be released behind the pin rings, which are mounted at the ends of the mandrel and are cut away after cure.

When the twist angle exceeds a critical value, which depends on the unsupported length of the tape (Fig. 4.2), the tape folds up, which leads to errors in tape placement. The tape must therefore be supported at several points to be able to store a large amount of tape twist without folding. Three guiding systems have been designed :

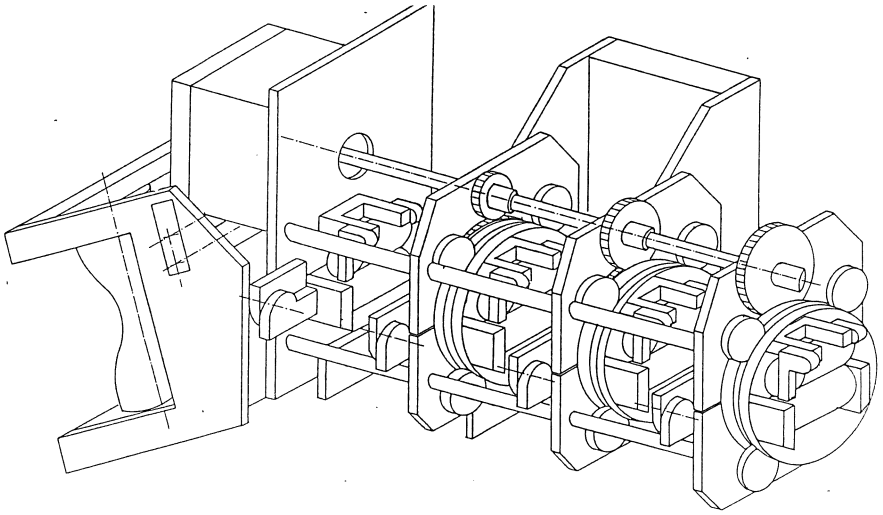

Figure 4.7: Pay-out eye with proportionally rotating rolls [67]

Proportionally Rotating Rolls The fibre is guided at four places between pairs of rolls : at the entry, at the delivery, and at two intermediate positions [67]. The entry rolls are fixed, the other rolls can rotate about the pay-out axis. The rotation of the delivery rolls is divided proportionally over the three pairs of rolls (Fig. 4.7) : by means of spur gears with different transmission ratios the first intermediate pair of rolls makes $\frac{1}{3}$-th, and the second $\frac{2}{3}$-th of the rotation of the delivery rolls. This design has the drawback that the number of

mechanical components is extremely high (170), resulting in a pay-out eye which is expensive and difficult to maintain.

Concentrated Proportional Rotation The number of mechanical components is reduced by grouping the gears in one housing and by connecting the rolls with arms to the gears [68] (Fig. 4.8). Internal gears transmit the rotation, allowing the tape to pass through the centre of the internal gear. A plastic tube, placed round the feeding axis, protects the gears from the resin.

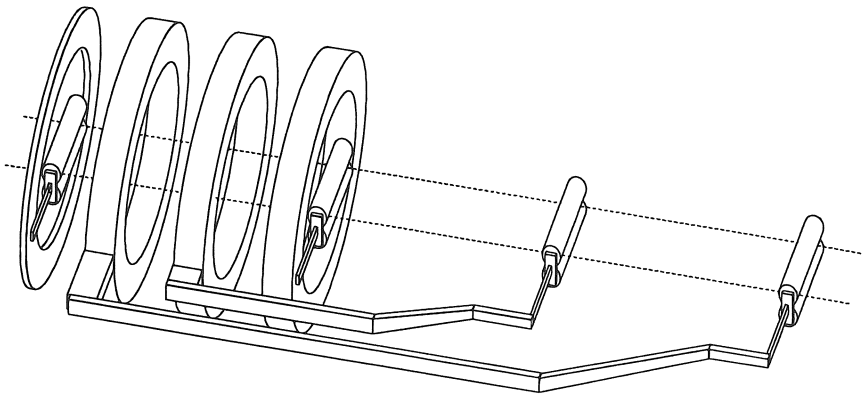

Figure 4.8: Pay-out eye with concentrated proportional rotation [68]

Flexible Ladder In the final design, a flexible ladder is used to guide the tape [68]. The ladder, which is flexible for torsion, consists of two chains which are connected with transversal bars, (Fig. 4.9). The tape is guided over and under the bars. The rotation of the motor is transmitted by internal gears. The delivery rolls and the end of the flexible ladder are connected with an arm to this internal gear. The tape twist is spread equally over the ladder during the rotation of the delivery rolls.

The number of bars and their mutual distance is chosen experimentally, so that the tape does not contract or fold when passing through the ladder at maximum tape twist [68]. Springs pre-stress the chains, and allow the axial length of the ladder to change during rotation of the delivery rolls. If no rotation is applied, the ladder is horizontal

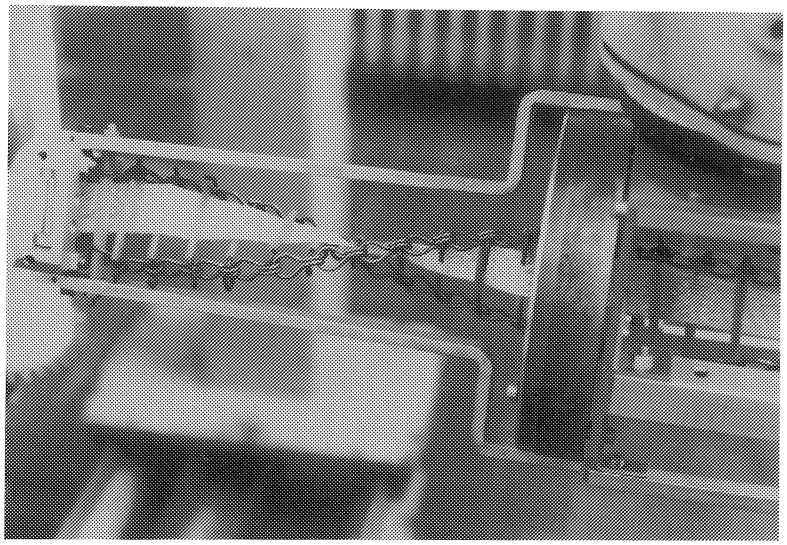

Figure 4.9: Flexible ladder

(Fig. 4.10). The number of mechanical components is reduced to a minimum (40).

The main disadvantage of the flexible ladder is the high friction force which acts on the tape while being pulled through the ladder. The friction can be decreased by using a material with a low coefficient of friction for the bars.

4.3.2.3 Entry Section

The geometry of the entry section has to be such that the tape is centred as well as possible in the tape guiding system, and that no twists occur between the impregnation bath and the guiding system.

The application of a constant orientation for the normal to the robot end flange allows to avoid tape twists between the impregnation bath and the guiding system by maintaining a constant tape orientation : the tape is guided over a vertical bar at the exit of the impregnation bath and enters the pay-out eye over a vertical bar (Fig. 4.11). The bar is then guided over a horizontal bar prior to entering the flexible ladder.

The horizontal and vertical bar in the pay-out eye centre the tape also in the guiding system. The vertical bar should be long enough to

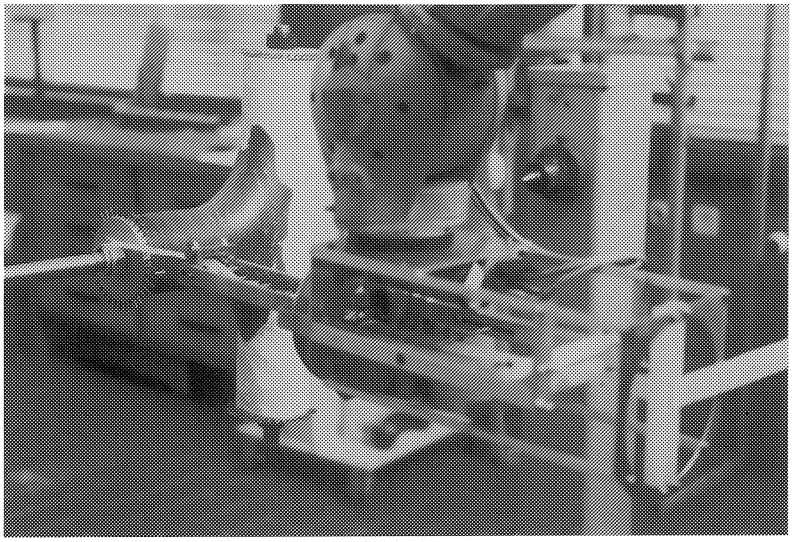

Figure 4.10: Pay-out eye with flexible ladder, attached to the PUMA-762

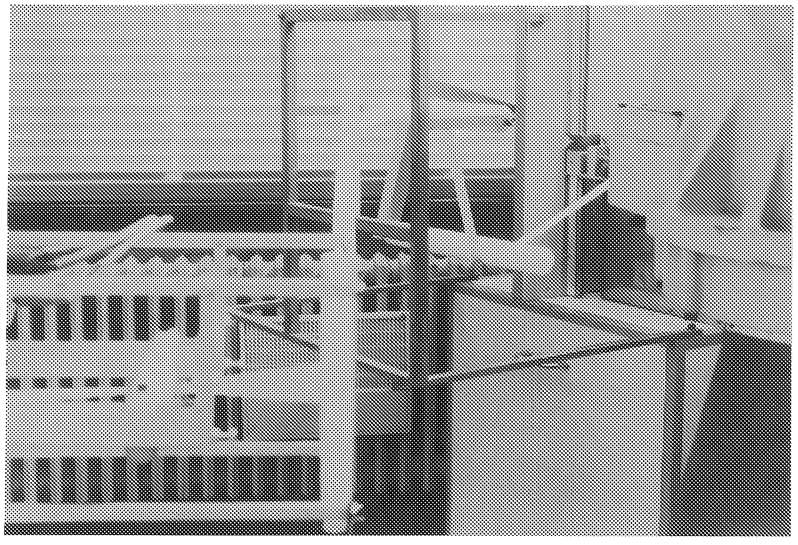

Figure 4.11: Entry section of the pay-out eye
The tape leaves the impregnation bath (behind the robot) over a lever and a vertical bar, and enters the pay-out eye first over a vertical bar, and then over a horizontal bar.

avoid that the tape makes contact with the flanges at the end of the bars, where it might fold up.

The tape must always be tensioned between the impregnation bath and the entry of the pay-out eye : if the pay-out eye moves towards the impregnation bath, the fibre will have to rewind in the impregnation bath. This is prohibited by the friction in the impregnation bath, so the tape will be slack. If the tape is slack, it can fold up at the ends of the entry bar or get stuck at protruding parts. A lever, which is placed after the impregnation bath, is used to maintain tension in the tape [94]. This lever serves both as a material buffer during rewinding, and induces tension in the tape, when the tension drops below a minimum level.

4.4 Control of the Robotic Winding Process

The calculation of the points of the machine path is discussed in section 5.2. Starting from these points, a machine program has to be generated. The programming language depends on the controller of the filament winding machine (e.g. WiMax [116], ISO/EIA [2]). These programs are mostly a list of points, with additional velocity information. Other machines require a list of positions at regular time intervals.

The last step in the winding process is the execution of the machine program. The robotic tape winding machine consists of 3 elements that have to be synchronized : the PUMA-762, the mandrel drive and the delivery roll rotation.

The PUMA-762 can be programmed in the VAL-II-language, which is a BASIC-like interpreter. VAL-II is also the name of the robot control system. The central processor of the robot is an LSI-11/73. The cycle time of the robot[2] is 28.8 ms : every 28.8 ms, the LSI-11 sends positioning commands to the servo boards of the robot joints [122].

Both mandrel and pay-out eye are driven by DC-motors. The position of the axes is read by encoders, which are mounted on the motor shaft.

[2]According to the manual of the PUMA-762 [122] the cycle time equals 28 ms. By verifying the cycle time by measuring the time of 10000 cycles with the clock of a PC, a cycle time of 28.8 ms has been obtained.

Two control methods have been investigated for the synchronization of the robot and the external axes : (i) by application of a program in the VAL-II-language and a motion control IC, and (ii) by controlling both robot and external axes by an external PC.

4.4.1 Control with VAL-II

A program in the VAL-II-language is written for the winding motion. The external axes are controlled with a HCTL-1000, a general purpose motion controller, which is mounted on a board, which is plugged into the robot controller. The VAL-II-program calculates the data that have to be sent to the HCTL-1000.

4.4.1.1 HCTL-1000

An interface board has been constructed for the control of the winding axis. This board is plugged into the LSI-11-bus of the robot controller, so that the HCTL-1000 can be programmed with VAL-II commands [6]. The interface board consists of bus-address decoders, which translate VAL-II addresses to HCTL-addresses, an encoder signal counter, the HCTL-1000 and a DAC, which converts the digital signal to an analog signal, that is sent to the motor amplifier.

The HCTL-1000 [118] can be programmed in different modes : position control (with maximum velocity), trapezoidal position control (position control with a trapezoidal velocity profile), proportional velocity control and integral velocity control (imposed velocity and constant acceleration) [92, 118]. The integral velocity mode of the HCTL-1000 is used to control the winding axis. The position control modes cannot be used, since the start and end velocities of each motion segment are zero. The HCTL-1000 is initialized at the start of the robot program, and new velocity settings ω_{set} are sent to the HCTL-1000 during motion (Fig. 4.12).

The control method with the HCTL-1000 has only been developed for the winding axis. For the control of the pay-out axis a similar interface circuit has to be added.

4.4.1.2 Control of the External Axis with the HCTL-1000

The main VAL-II program consists of a series of motion commands, the new positions of the winding axis, and calls to the synchronization

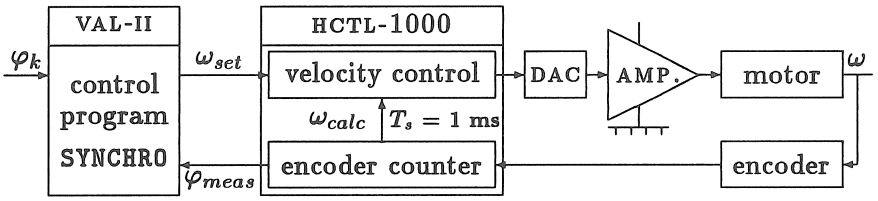

Figure 4.12: Control of an external axis with the HCTL-1000

subroutine SYNCHRO, e.g. (without control of the pay-out axis) :

```
MOVES REFER:TRANS( 226.16, 0.00, 152.80, 90.00, -90.00, -44.69)
ANGLE =    -84794
CALL SYNCHRO
MOVES REFER:TRANS( 153.37, 0.00,  99.17, 90.00, -90.00, -25.21)
ANGLE =    -60456
CALL SYNCHRO
```

The synchronization routine SYNCHRO calculates the velocity ω_{set} of the winding axis, based on the difference between the successive values of the mandrel angle, and the time needed for the robot motion between the corresponding robot positions.

To this end, this method needs a model for the motion of the robot between two positions. Experiments have been performed in which the position of the robot is monitored at regular time intervals, for various lengths of motion segments ℓ and velocity settings v_0. Starting from these measurements, a basic kinematic model of the PUMA-762 for straight line motion is derived. The results are given in the following table (with v_0 the VAL-II-velocity setting in MMPS (mm/s) and the length of the motion segment ℓ in mm) [6] :

Velocity Setting (MMPS)	$v_0 < 0.631\ell$	$v_0 > 0.631\ell$
Velocity Profile	Trapezoidal Profile	Triangular Profile
Acceleration (mm/s^2)	$a = 3.00v_0$	$a = 1.50v_0$
Max. Velocity (mm/s)	$v_{max} = 2.18v_0$	$v_{max} = \sqrt{a\ell}$

Fig. 4.13 shows the mean and the maximum velocity during the motion in function of the velocity setting. Remark the discontinuity at $v_{0d} = 0.631\ell$ MMPS : a velocity setting which is slightly lower than v_{0d} results in a higher mean velocity than a velocity setting which is slightly higher than v_{0d}.

The control with VAL-II has however some serious drawbacks :

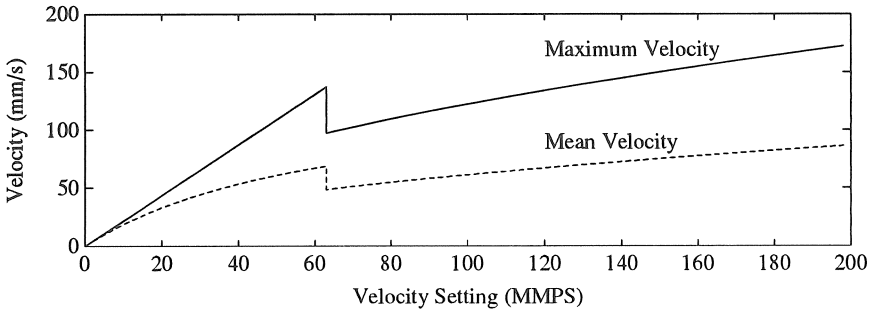

Figure 4.13: Mean and maximum velocity in function of velocity setting for a motion segment with length $\ell = 100$ mm

- The synchronization routine is a subroutine of VAL-II, and can only be called once per robot motion (`MOVES`) command. The time between two motion commands is large ($\approx$ 0.5 s), resulting in large tracking errors.
- The VAL-II memory is limited to 64 K, which is far too small to store all the data to wind a complex part.

4.4.2 Control from an External PC

4.4.2.1 ALTER Mode

VAL-II allows to communicate with an external system, by means of the Real-Time Path Control Mode or ALTER-mode. The ALTER-mode allows to change the robot path in function of sensory information while the robot is moving [57, 123]. In the ALTER-mode, the robot controller sends every 28.8 ms a request to an external PC for path control data. Within the next 16 ms the external computer has to send path correction data to the robot controller. After sending the data, the external computer calculates the data for the next interval and sends them after the next request. Data between robot controller and PC are transmitted via an RS-232C port at 19200 baud.

The main difference with the control with a VAL-II-program is that the generation of the robot trajectory and the low level control are now performed by the external PC instead of by the robot controller.

VAL-II program The path control data are calculated by a program which runs at the external PC. At the robot controller, the ALTER-mode is controlled by a small VAL-II-program [68, 105] :

```
ALTER(0,18)
MOVES HERE
FOR I = 0 TO 1000
    DELAY(899)
END
NOALTER
```

ALTER is activated with the `ALTER(0,18)` command[3] The ALTER-mode remains activated during the time defined by the `DELAY` command (1000×899 s). The ALTER-mode is ended by the `NOALTER` command or when no message is received from the external PC.

Path Control Data The path control data, which have to be sent by the PC to the robot controller, consist of six components : three displacements (dx, dy, dz) and three rotations (rx, ry, rz).

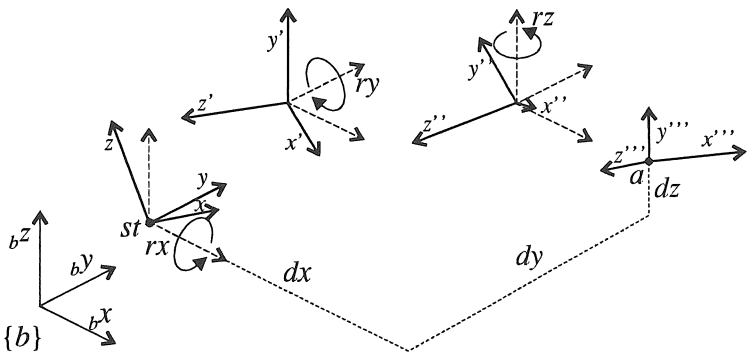

Figure 4.14: Path control data in ALTER-mode

The displacement components are referred to the starting position *st* :

$$[dx \quad dy \quad dz]^T = {}_b\mathbf{a} - {}_b\mathbf{st} \tag{4.3}$$

[3]In the ALTER(0,18) command, 0 designates the number of the serial port of the robot controller, and 18 the mode [57]. The mode is here : world coordinates, path modification, non-cumulative. ALTER has two different modification modes : cumulative and non-cumulative. In non-cumulative mode the altering data are referred to a fixed starting pose, in cumulative mode to the previous pose. Non-cumulative mode is used to control the winding and the scanning process.

with ${}_b\mathbf{a}$ the current position q of the robot end flange in the robot base coordinate system $\{b\}$.

The rotation components are the rotation about, successively, the x, y and z-axes of the robot base coordinate system $\{b\}$ between the orientation of the robot end flange in the starting pose $\{st\}$ and the current pose $\{a\}$:

$$[rx \quad ry \quad rz]^T = \mathbf{xyz}({}^{st}_{a}\mathbf{R}) = \mathbf{xyz}({}^{b}_{st}\mathbf{R}^T \, {}^{b}_{a}\mathbf{R}) \tag{4.4}$$

with $\mathbf{xyz(A)}$ the roll-pitch-yaw-angles about fixed x, y and z-axes [18] : the frame $\{st\}$ is first rotated over an angle rx about the x-axis of the robot base coordinate system $\{b\}$, then over an angle ry about the y-axis of $\{b\}$ and then over an angle rz about the z-axis of $\{b\}$ (Fig. 4.14).

During winding, the robot wrist rotates only about the vertical z-axis. Both the rx and ry values are zero.

Prior to sending, the path control data must be converted into a 16-bit integer format, by multiplication with the scale factors [123] :

for translations : 16.0000 (1/mm)
for rotations : 182.0444 (1/degree)

The complete message, which has to be sent to the robot controller, consists of three control bytes, followed by an exception code, the number of data bits transmitted, the path control data, two control bytes and a check byte [123].

4.4.2.2 Control of the External Axes

The PC, which sends the data to the robot controller, also controls the motion of the external axes. An in-house developed interface board sends analog signals to the two motor amplifiers of the external axes and reads the positions of the encoders.

After completion of the communication with the robot controller (i.e. 15 ms after the reception of the first byte from the VAL-II-message), the PC sends data to the external axes. The robot and the external axes do not react at the same moment : the external axis reacts almost immediately after sending the data, the robot starts reacting 45 ms

after the start of the signal[4]. The time delay between the reaction of external axes and robot is t_{lag} = 30 ms. The data, which are sent to the external axes, must therefore refer to a time t_{lag} before the data, which are sent to the robot. The time sequence for the ALTER-mode is given in Fig. 4.15.

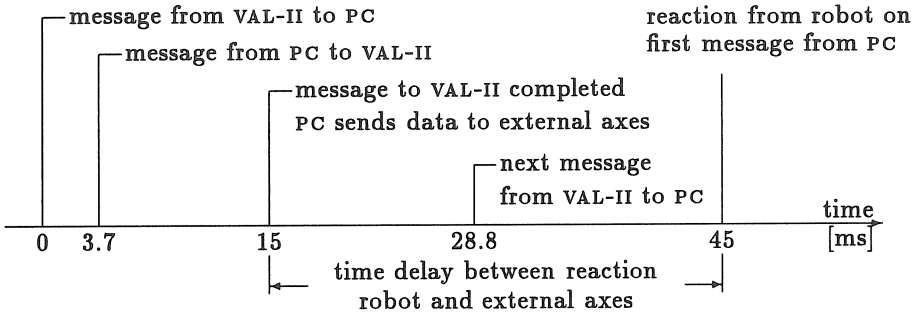

Figure 4.15: Time sequence in ALTER-mode

Interface Board An interface board has been constructed by Liao [56] for the communication between a PC and one or two DC-motors. For each motor, the digital output signal of the control program on the PC is converted with a 12-bit DAC into a voltage, which is sent to the motor amplifiers (Fig. 4.16). The signals of the encoders are counted by 16-bit TCTL-2000 - IC's, and stored in registers which are read by the control program.

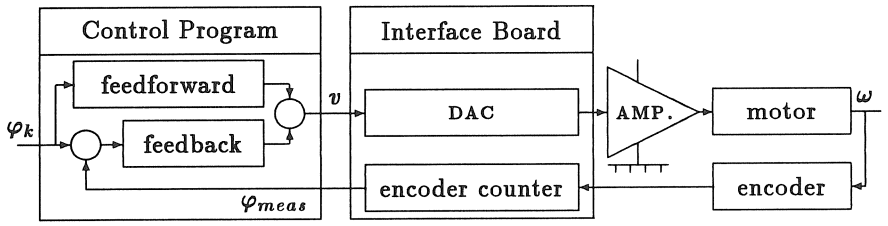

Figure 4.16: Control of an external axis with the interface board

[4]The time delay has been checked by applying a periodic motion to the robot, and by measuring the time between the start of the signal and the moment that the current in a motor joint starts to change.

Control of the External Axes The positions of the external axes are controlled with a combination of feedforward and feedback control (cf. Appendix B). A feedforward velocity signal is calculated from the difference between the calculated values of the external axis φ_{k+1} and φ_k. The feedback signal is proportional to the difference between the angle φ_{meas}, returned by the encoder, and φ_k.

4.4.2.3 Control Program

The communication between PC and robot passes via interrupt, in order to be able to pass data at the correct moment. The interrupt routine is activated at the receipt of a signal from the robot controller. The interrupt routine reads the message from the robot controller and sends a message from the PC to the robot controller. After execution of the interrupt routine, the execution of the main program is continued.

The control program consists of six layers [23] :

Application Layer This is the highest layer. The user can write his own application program, using functions which are similar to VAL-II-commands to perform robot motions.

Calculation Layer The data, which have to be sent to the robot, are calculated for the VAL-II-like functions.

Communication Layer This layer performs the synchronization between calculations and transmission under interrupt.

Format Layer This layer calculates the individual bytes which have to be sent to the robot.

Byte Layer This layer encapsulates the data with the ALTER-protocol, and performs the reception and transmission of data under interrupt.

Bit Layer This layer generates the individual bits of each byte that has to be transmitted (number of data bits, start bits, parity).

The winding application program consists of the following modules :

READ_DATA This module reads the data of the robot path, which is calculated on the VAX-computer. The output from the calculations on the VAX-computer is a file, which contains the successive

poses of the robot and the angles of the external axes at constant time intervals. The time step Δt is a multiple of the robot cycle $t_{cyc} = 28.8$ ms.

WIND_INIT Installation of the interrupt routine and resetting of the encoder counters. Reception of the first ALTER-message.

CONT_PATH Tracking of the path. Calculation of the data which have to be sent to the robot controller and the external axes. This is done every cycle. During testing, the program can be run at speeds which are an integer ratio $1/n_r$ of the nominal speed. The time interval between two successive input data is then $n_r \Delta t = n_c t_{cyc}$, with n_c the number of ALTER cycles.

The data $\mathbf{b}$, which are sent to the robot at $t = (in_c + j)t_{cyc}$ $(0 \leq j < n_c)$ are obtained by linear interpolation between the data $\mathbf{a}_i$ of the input file :

$$\mathbf{b} = \mathbf{a}_i + \rho(\mathbf{a}_{i+1} - \mathbf{a}_i) \quad \text{with} \quad \rho = \frac{j}{n_c} \tag{4.5}$$

Due to the time delay between the external axes and the robot, the data φ, that are sent to the external axes, refer to the time $t - t_{lag} = (in_c + j - \frac{t_{lag}}{t_{cyc}})t_{cyc} = (i^* + \rho^*)n_c t_{cyc}$, with i^* an integer and $0 \leq \rho^* < 1$ (Fig. 4.17) (with φ_i the input data) :

$$\varphi = \varphi_{i^*} + \rho^*(\varphi_{i^*+1} - \varphi_{i^*}) \tag{4.6}$$

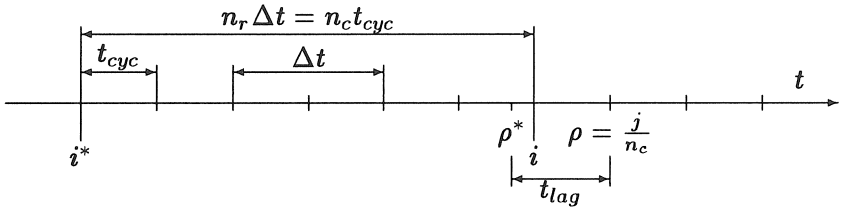

Figure 4.17: Time delay between robot and external axes ($n_c = 6$, $j = 1$)

4.4.2.4 Electronic Control Circuit

The application of an additional I/O board, which is added to the PC, allows to monitor external signals. This can be used to pause the

winding process when an error occurs, e.g. fibre breakage, to replace the unwinding bobbins or to fill the impregnation bath.

An electronic circuit, consisting of two serially placed switches, has been constructed in order to pause the process. The control program puts a constant voltage on this circuit and checks every cycle if the circuit is still closed. If the circuit is open, the program is paused. The ALTER-mode remains activated : robot and external axes are kept in the last transmitted positions.

4.5 Conclusions

This chapter described the design and control of a robotic tape winding cell. The cell consists of a PUMA-762 with six degrees of freedom, and a mandrel support structure with the mandrel drive. The pay-out eye, which is attached to the end flange of the robot, has an additional rotation, to be able to maintain a constant band width. A flexible ladder in the pay-out eye prevents tape wrinkling during rotation of the delivery rolls.

Only four degrees of freedom of the robot are used during winding : the normal to the robot end flange is kept vertically downwards. The axis of the pay-out eye is always horizontal. The robot could therefore be replaced by a simpler robot with four degrees of freedom.

The main problem in the control of the robotic cell is the synchronization between the robot and the external axes. The PUMA-762 is controlled in the ALTER or Real-Time Path Control Mode from VAL-II. An external PC sends every 28.8 ms motion commands to the robot and both external axes. An electronic circuit makes it possible to react on errors during the winding process.

Chapter 5

Off-Line Robot Winding Program

5.1 Introduction

Starting from the data of the fibre paths, an off-line machine program has to be generated. The generation of the robot program consists of several phases : the calculation of the points of the robot path, the calculation of the path velocity, and the construction of the robot program. The last two steps are often coupled, since the possibilities to control velocities depend on the control possibilities of the winding machine. The PUMA-762 is controlled in the ALTER-mode, and does not require the creation of a robot program, but a list of poses at equidistant time intervals.

The control of the filament winding process of an asymmetric part differs from the control of an axisymmetric part : when winding an axisymmetric part, a basic path is repeated continuously, by indexing the winding axis, opposed to an asymmetric part, which consists of a number of different fibre paths. Winding an asymmetric part requires therefore a substantial amount of data.

The first section of this chapter discusses the calculation of the points of the robot path. The next section treats the calculation of the robot trajectory and the generation of the path control data. The last section deals with the construction of the off-line program with the program CAWAR.

A distinction is made between a *point* or *position* and a *pose*. The

former terms refer to a point in space, whereas a pose refers to both a point in space and an orientation at that point [103].

A second distinction is made between the term *robot path* and *robot trajectory*. A robot path contains only poses, a robot trajectory also velocity information.

5.2 Robot Path

The robot path consists of the successive poses of the end flange of the robot, and the angles of the two external axes. This section describes the different steps in the calculation of the robot path :

Task Requirements The poses of the pay-out eye have to be calculated so, that all the task requirements (cf. section 4.2.1) are fulfilled. Some of the requirements are fulfilled by the design of the robotic tape winding cell, but the design of the robotic cell has led to additional requirements, which have to be taken into account during the calculation of the robot path.

1. The delivery point must lie on the tangent $\vec{t}$ to the fibre path in the contact point on the mandrel (cf. Eq. 4.1).
2. No collisions may occur. Collision control is an important step in the calculation of the robot path, and is treated separately in chapter 6.
3. The orientation of the delivery rolls has to be determined so, that the band width remains constant (cf. Eq. 4.2).
4. The tape may not fold up between the pay-out eye and the mandrel. The tape will fold up if the twist angle η, i.e. the angle between the binormal $\vec{b}$ on the mandrel and the axis of the delivery rolls $\vec{a}$, is too large (cf. Fig. 4.2). The twist angle η is therefore limited to a value[1] η_{max}. The free length must, in order to avoid folding of the tape, be larger than a minimum value l_{fm}.
5. The rotation ψ about the pay-out axis is limited to 360°, due to the stiffness of the chains and the limited displacement of the ends of the ladder.

[1] For the 25-mm wide glass fibre tape, the twist angle is limited to 100°. The minimum free length l_{fm} equals 100 mm.

6. The normal to the robot end flange must be directed vertically downwards. Due to the construction of the pay-out eye, the pay-out axis $\vec{v}$ is then horizontal. If no rotation is applied about the pay-out axis, the flexible ladder lies in a horizontal plane (Fig. 4.10).
7. The friction in the delivery rolls prevents the tape from rewinding into the pay-out eye. Rewinding occurs when the decrease of the free length is larger than the increase of the length of the wound fibre path. The tension will then drop to zero, causing errors in the tape placement, especially near the pin rings. No rewinding of the tape in the delivery rolls is allowed.
8. The angle between the tangent $\vec{t}$ to the fibre path and the pay-out axis $\vec{v}$ is, due to the limited accessibility of the delivery rolls, limited to about 90°.

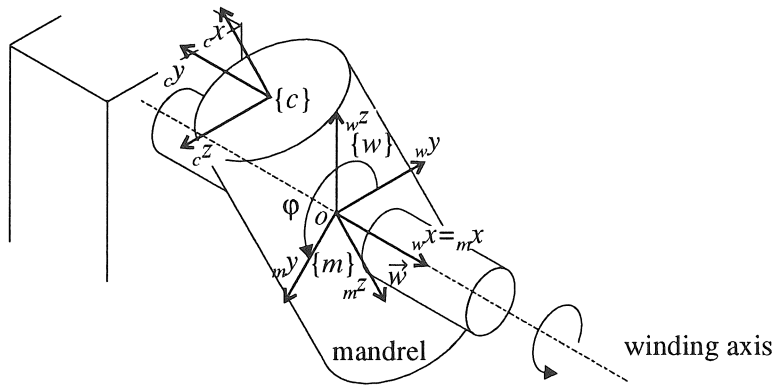

Figure 5.1: Coordinate systems used in the calculation of the robot path

Coordinate Systems and Frames The main coordinate systems are (Fig. 5.1) (cf. section 2.4.2) :

$\{c\}$ the *CAD-coordinate system.*

$\{m\}$ the *mandrel coordinate system*, which is attached to the mandrel. The x-axis corresponds to the (horizontal) winding axis $\vec{w}$. The origin o lies on the winding axis.

$\{w\}$ the *winding coordinate system*, which is fixed to the mandrel support structure. The x-axis is the winding axis $\vec{w}$, the z-axis

is directed vertically upwards. At the start of the motion, the mandrel and the winding coordinate system coincide. During the motion, the mandrel coordinate system rotates, together with the mandrel, about the winding axis $\vec{w}$.

$\{b\}$ the *robot base coordinate system.*

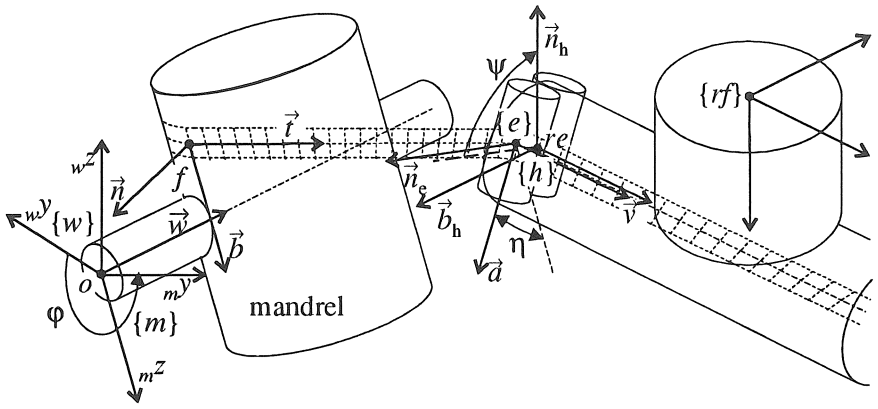

Figure 5.2: Frames during tape winding

A frame $\{a\} = \{a; \vec{t}_a, \vec{n}_a, \vec{b}_a\}$, has as origin the point a and consists of the three orthonormal vectors $\vec{t}_a, \vec{n}_a$ and $\vec{b}_a$ (cf. section 2.4.2 and the List of Symbols p. xxviii). In the frames, which are used during the calculation of the robot path, the x-axis ($\vec{t}_a$) corresponds to the length axis of the tape, the y-axis ($\vec{n}_a$) is normal to the tape, and the z-axis ($\vec{b}_a$) is the transverse axis of the tape. Some generally occurring vectors have been given special names, e.g. the pay-out axis $\vec{v}$.

The main frames are (Fig. 5.2) :

$\{f\} = \{f; \vec{t}, \vec{n}, \vec{b}\}$ the Frenet-trihedron in a point of the fibre path.

$\{e\} = \{e; \vec{v}, \vec{n}_e, \vec{a}\}$ the frame attached to the delivery point e, with as x-axis the pay-out axis $\vec{v}$ and as z-axis the axis of the delivery rolls $\vec{a}$.

$\{re\} = \{re; \vec{v}, \vec{n}_e, \vec{a}\}$ a frame in the reference delivery point re, parallel to the frame $\{e\}$. The reference delivery point is a fixed point in the pay-out eye, opposed to the actual delivery point e, the position of which depends on the orientation of the pay-out axis and the geometry of the delivery rolls.

$\{h\} = \{re; \vec{v}, \vec{n}_h, \vec{b}_h\}$ a frame in re. The tape is oriented as in the entry of the flexible ladder. The vector $\vec{n}_h$, which is normal

to the tape, is – in the winding coordinate system – directed vertically upwards.

$\{rf\}$ frame attached to the robot end flange

Calculation Steps (Fig. 5.3) For each point of the fibre path, the pose of the pay-out eye is calculated in the mandrel coordinate system : first, the position of the delivery point e and the pay-out axis $\vec{v}$ is calculated, and then the orientation of the axis of the delivery rolls $\vec{a}$. The position of the reference delivery point re is consecutively calculated. In the next step, the angular position φ of the winding axis is calculated, so that the axis of the pay-out eye is horizontal. Consecutively, the rotation angle ψ about the pay-out axis is calculated, so that the normal to the tape at the entry of the flexible ladder is directed vertically upwards. The angle ψ has to be limited to 360°. In a last step, the position of the robot end flange is derived.

5.2.1 Fibre Path

The fibre paths are calculated in the CAD-coordinate system $\{c\}$. The global fibre path consists of two parts : a linking path Γ_{i-1}^{i} behind the pin rings and a geodesic fibre path Γ_i on the part surface.

Many parts have planes or axes of symmetry, which allow to reduce the number of fibre paths to be calculated. Symmetry is, in the CAD-coordinate system, represented by a transformation matrix ${}_{c}\mathbf{S}$. The Frenet-trihedron $\{f\}$, which is attached to a point of the fibre path, is in the mandrel coordinate system then given by :

$$ {}^{m}_{f}\mathbf{T} = {}^{m}_{c}\mathbf{T}\ {}_{c}\mathbf{S}\ {}^{c}_{f}\mathbf{T} \tag{5.1} $$

5.2.2 Pose of the Pay-Out Axis in the Mandrel Coordinate System

For each point of the fibre path, the position of the delivery point e and the orientation of the pay-out axis $\vec{v}$ is calculated in the mandrel coordinate system $\{m\}$. First the method to define the motion Υ_i of the pay-out eye for the geodesic fibre path on the mandrel Γ_i is discussed, and then the linking motion Υ_{i-1}^{i} for the path Γ_{i-1}^{i} round the pin rings.

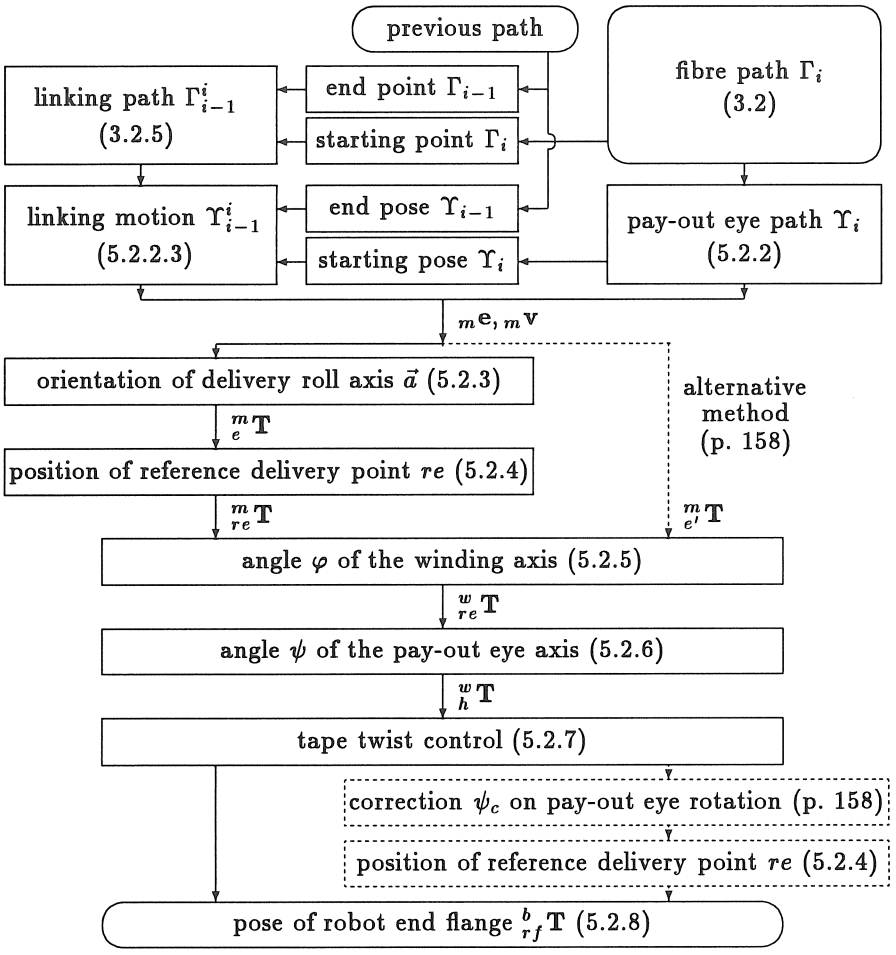

Figure 5.3: Consecutive steps in the calculation of the robot path
(for the dashed lines, see the alternative method on p. 158)

5.2.2.1 Position of the Delivery Point

The delivery point e must lie on the tangent to the fibre path. The position of the delivery point is normally uniquely defined for a winding machine with two degrees of freedom. If the machine has three degrees of freedom, the free length can be chosen freely. Two methods are used in literature to determine the position of the delivery point :

- The free length is kept constant [110].
- The delivery point is placed on an enveloping control surface, which circumscribes the mandrel [10, 47, 115].

A fixed free length is chosen. This method has the advantage that rewinding in the delivery point e is prohibited. The free length is fixed to a value, which is entered by the operator. The free length should be as small as possible to obtain an accurate fibre placement.

5.2.2.2 Orientation of the Pay-Out Axis

If the winding machine has more than three degrees of freedom, the orientation of the pay-out axis $\vec{v}$ can be chosen freely. The orientation of the pay-out axis in the mandrel coordinate system $\{m\}$ is defined with a strategy : the pay-out axis is aligned with the tangent to the fibre path, or the orientation of the pay-out axis is fixed. Several strategies will be discussed more in detail.

Aligning the pay-out axis with the fibre (Fig. 5.4a) The pay-out axis $\vec{v}$ equals the tangent $\vec{t}$ to the fibre path : $\vec{v} = \vec{t}$.

This strategy has the advantage that the number of fibre direction changes is reduced, and that the condition of constant band width (4.2) is always satisfied, so that the twist angle η is zero. This motion results in large motions of the entry of the pay-out eye, and in large variations of the fibre feed in the impregnation bath, especially when the winding angle is reversed at the ends of the mandrel. To prevent rewinding in the impregnation bath, a large fibre buffer is needed.

Fixed Orientation To reduce the fibre buffer, the pay-out axis $\vec{v}$ is placed in a plane $\mathcal{P}$ normal to the winding axis $\vec{w}$ (${}_m v_x = 0$). The ori-

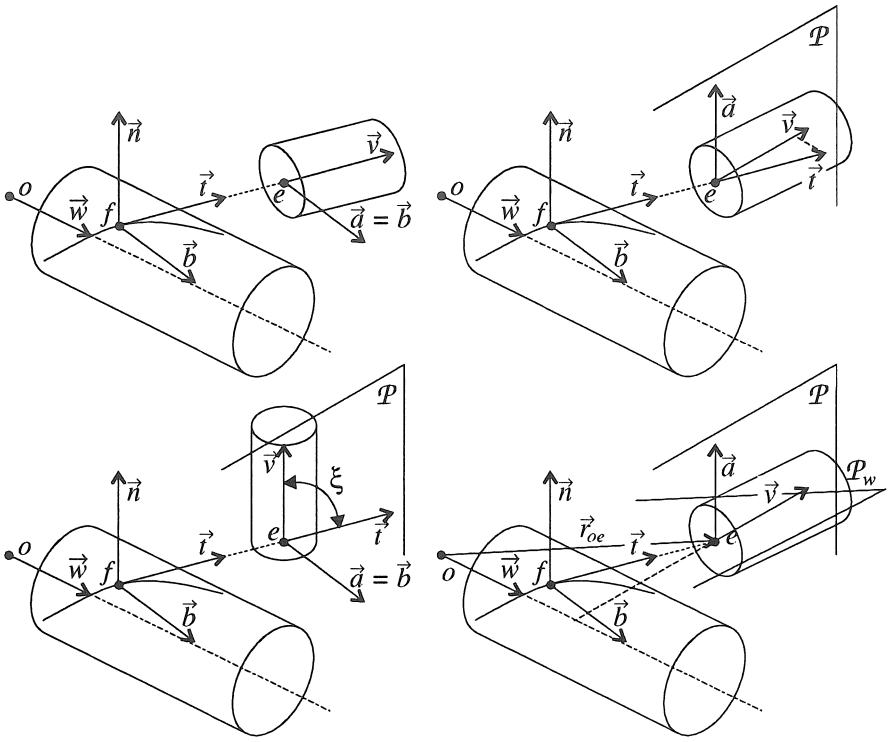

Figure 5.4: Strategies for the orientation of the pay-out axis
(a) Aligned (b) Projection
(c) Zero tape twist (d) Motion in plane

entation of the pay-out axis is fixed in the winding coordinate system, and equals[2] : ${}_w\mathbf{v} = [0 \quad \pm 1 \quad 0]^T$ (cf. Eq. 5.17).

Several strategies are possible to calculate the position of the pay-out axis in the plane $\mathcal{P}$, as projection, zero tape twist, and motion in a plane.

[2]The sign of the ${}_wv_y$ depends on the position of the robot with respect to the winding machine

Projection (Fig. 5.4b) The tangent $\vec{t}$ to the fibre path is projected on the plane $\mathcal{P}$ and normalized :

$$\vec{v} = \frac{\vec{t} - (\vec{t} \cdot \vec{w})\,\vec{w}}{\left\| \vec{t} - (\vec{t} \cdot \vec{w})\,\vec{w} \right\|} \quad \text{or} \quad {}_m\mathbf{v} = \frac{1}{\sqrt{{}_m t_y^2 + {}_m t_z^2}} \begin{bmatrix} 0 \\ {}_m t_y \\ {}_m t_z \end{bmatrix} \tag{5.2}$$

A singularity occurs when $\vec{t} = \vec{w}$.

Zero Tape Twist (Fig. 5.4c) The drawback of the previous strategy is that Eq. (4.2) is generally not satisfied, inducing a tape twist between the mandrel and the pay-out eye. The twist angle η is zero, when the axis of the delivery rolls $\vec{a}$ equals the binormal $\vec{b}$. The pay-out axis $\vec{v}$ is obtained by a rotation of $\vec{t}$ over an angle ξ about the binormal $\vec{b}$:

$$\vec{v} = \vec{t} \cos \xi + \vec{n} \sin \xi \tag{5.3}$$

The pay-out axis $\vec{v}$ lies in the plane $\mathcal{P}$ $({}_m v_x = 0)$:

$$\xi = \arctan\left(-\frac{{}_m t_x}{{}_m n_x} \right) \tag{5.4}$$

The angle ξ should be less than 90°, to limit the contact area with the rolls. This condition cannot be met if the sign of ${}_m n_x$, the x-coordinate of the normal changes : it is possible that the angle ξ keeps on increasing. This strategy gives only good results if the sign of ${}_m n_x$ does not change, as e.g. for a cylinder and a cone.

Motion in a Plane (Fig. 5.4d) The motion of the delivery point is (in the winding coordinate system) often restricted to the horizontal plane $\mathcal{P}_w$ through the winding axis [6, 115]. In the mandrel coordinate system, the pay-out axis is then directed along the normal to the winding axis $\vec{w}$ in the delivery point e :

$$\vec{v} = \frac{\vec{r}_{oe} - (\vec{r}_{oe} \cdot \vec{w})\,\vec{w}}{\left\| \vec{r}_{oe} - (\vec{r}_{oe} \cdot \vec{w})\,\vec{w} \right\|} \quad \text{or} \quad {}_m\mathbf{v} = \frac{1}{\sqrt{{}_m e_y^2 + {}_m e_z^2}} \begin{bmatrix} 0 \\ {}_m e_y \\ {}_m e_z \end{bmatrix} \tag{5.5}$$

5.2.2.3 Linking Motion

The fibre paths Γ_{i-1} and Γ_i on the part surfaces are linked by a path Γ^i_{i-1} behind the pin rings (cf. section 3.2.5). The path Γ^i_{i-1} is defined by the points $p_0, p_1, (p_{c_1}, p_{c_2}), p_2$ and p_e (Fig. 3.7).

The pose of the pay-out eye during the linking motion cannot be determined by one of the previous strategies, because the tangent to the fibre path is not always uniquely determined, e.g. at p_1 and p_2, at the edge of the pin ring. The linking motion Υ^i_{i-1} of the delivery point e is defined by a set of control points q_j (Fig. 5.5) :

1. Determination of q_0, the last position of the path Υ_{i-1}, corresponding to the point c_0 of the fibre path Γ_{i-1}. From c_0 onwards, the tangent to Γ_{i-1} intersects the pin ring. The calculation of the poses of Υ_{i-1} is stopped at c_0 to avoid that the fibre would be fixed behind a wrong pin.

2. Lay-down of the fibre path between c_0 and the pin at p_0, where the fibre has to be fixed. The control point q_1 lies on the line $c_0 p_{0e}$, with p_{0e} the end of the pin at p_0. Small errors can occur since the fibre may slip on the surface during the motion between q_0 and q_1.

3. The fibre is fixed behind the pin at p_0. The control point q_2 lies on the tangent to the fibre path Γ_{i-1} in p_0.

4. Lay-down of the path $p_0 p_1$ between the pins and the edge of the pin ring. The control point q_3 lies on the line $p_0 p_1$.

5. Lay-down of the fibre path on the pin ring end plane. The control point q_5 lies on the line $p_1 p_2$. If the fibre path makes contact with the end shaft of the pin ring, the delivery point is first put in q_{c_1}, on the line $p_1 p_{c_1}$, then the arc $p_{c_1} p_{c_2}$ round the pin ring shaft is wound, and the control point q_5 is placed on the line $p_{c_2} p_2$.

   In order to avoid collisions with the end plane of the pin ring, the delivery point is moved from q_3 over an intermediate point q_4 to q_5 (or q_{c_1}). The control point q_4 is obtained by translating q_5 (or q_{c_1}) over the radius of the pay-out eye away from the end plane of the pin ring.

6. The control point q_6 lies on the line $p_2 p_{ee}$, with p_{ee} the point at the edge of the pin in p_e.

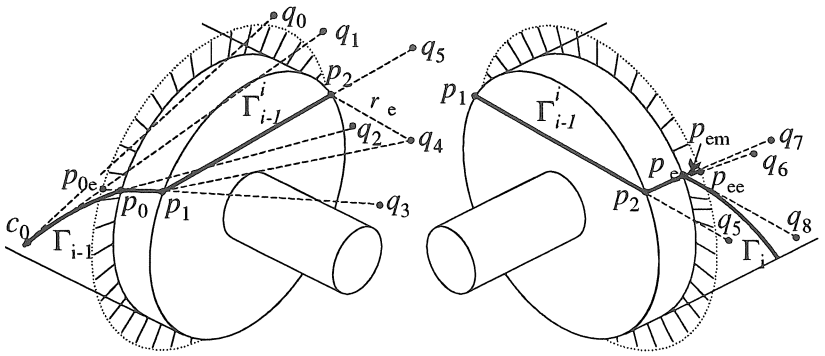

Figure 5.5: Control points of the linking motion (if Γ^i_{i-1} does not make contact with the end shaft of the pin ring)

7. The fibre is fixed behind the pin at p_e. The control point q_7 lies on the line p_2p_{em}, with p_{em} the point in the middle of the fixing pin, between p_e and p_{ee}.

8. The control point q_8 corresponds to the first point of the path Υ_i.

The distance between the control points q_j and the contact points on the mandrel must be as small as possible to obtain a correct tape lay-down (cf. p. 164). The motion between the points q_j is obtained by helical interpolation round the axis of the pin ring, or by linear interpolation if the pin ring has no end shaft. The orientation of the pay-out axis is obtained by applying one of the strategies, described in section 5.2.2.2. If the change in orientation between two consecutive control points q_j is too large, a via-pose is added.

The orientation of the Frenet-trihedra $\{f\}$ during the motion between the control points is not yet determined. The contact point on the pin ring remains constant during the motion between two control points. The tangent $\vec{t}$ is the unit direction vector of the line, which links the contact point on the pin ring and the delivery point e. The binormal $\vec{b}$ lies in the tangent plane to the surface, on which the fibre is placed.

5.2.3 Orientation of the Delivery Rolls

In order to maintain a constant band width, the axis of the delivery rolls $\vec{a}$ must be normal to the tangent $\vec{t}$ to the fibre path. Since the vector $\vec{a}$ is also normal to $\vec{v}$, the vector $\vec{a}$ equals :

$$\vec{a} = \pm \frac{\vec{t} \times \vec{v}}{\|\vec{t} \times \vec{v}\|} \tag{5.6}$$

The tangent $\vec{t}$ equals $\vec{n} \times \vec{b}$, so that $\vec{a}$ can be written as :

$$\vec{a} = \pm \frac{(\vec{n} \times \vec{b}) \times \vec{v}}{\|\vec{t} \times \vec{v}\|} = \pm \frac{(\vec{v} \cdot \vec{n})\,\vec{b} - (\vec{v} \cdot \vec{b})\,\vec{n}}{\sqrt{(\vec{v} \cdot \vec{n})^2 + (\vec{v} \cdot \vec{b})^2}} \tag{5.7}$$

The twist angle η between the binormal $\vec{b}$ and the roll axis $\vec{a}$ is :

$$\eta = \arctan\left(-\frac{\vec{v} \cdot \vec{b}}{\vec{v} \cdot \vec{n}}\right) + k_c \pi \tag{5.8}$$

with $k_c = -1, 0, 1$. The value of k_c is chosen so that the twist angle η is as small as possible.

If the twist angle becomes larger than the maximum value η_{max}, the vector $\vec{a}$ is reversed. This leads to a discontinuity in the path of the frame $\{e\} = \{e; \vec{v}, \vec{n_e}, \vec{a}\}$. These discontinuities pose problems during the calculation of the rotation angle ψ about the pay-out eye axis. To overcome this problem, the orientation of the delivery rolls (and the position of the reference delivery point) is calculated after the control of tape twists (dashed line in Fig. 5.3). Instead of the frame $\{e\}$, the frame $\{e'\} = \{e; \vec{v}, \vec{n_{e'}}, \vec{b_{e'}}\}$ is used for the calculations of the angle of the winding axis φ and the angle of the delivery rolls ψ. The frame $\{e'\}$ is constructed from the Frenet trihedron $\{f\}$ and the pay-out axis $\vec{v}$ by applying z-$y(-x)$-Euler angles [18] : the Frenet-trihedron $\{f\}$ is first rotated over an angle γ_z about the binormal $\vec{b}$, and then over an angle γ_y about the new vector $\vec{n}'$, until the vector $\vec{t}'$ corresponds to the pay-out axis $\vec{v}$. The frame $\{e\} = \{e; \vec{v}, \vec{n_e}, \vec{a}\}$ is obtained by rotating the frame $\{e'\} = \{e; \vec{v}, \vec{n_{e'}}, \vec{b_{e'}}\}$ over an angle ψ_c about the vector $\vec{v}$, so that $\vec{t}$ and $\vec{a}$ are perpendicular :

$$\vec{t} \cdot \vec{a} = \vec{t} \cdot (\vec{b}_{e'} \cos\psi_c - \vec{n}_{e'} \sin\psi_c) = 0 \tag{5.9}$$

or :

$$\psi_c = \arctan\left(\frac{\vec{t}\cdot\vec{b}_{e'}}{\vec{t}\cdot\vec{n}_{e'}}\right) + k_c\pi \tag{5.10}$$

5.2.4 Position of the Reference Delivery Point

The position of the delivery point e in the pay-out eye depends on the orientation of the tangent $\vec{t}$ in the frame $\{e\}$ and the geometry of the delivery rolls. The reference delivery point re is a fixed point in the pay-out eye, and lies on the rotating axis in the pay-out eye. For a set of rolls, the projection of the centre of the lower roll on the pay-out axis is chosen as reference delivery point re is (Fig. 5.6).

The position of the reference delivery point re in the mandrel co-ordinate system is :

$$_m\mathbf{re} = {}^m_e\mathbf{T}\ {}_e\mathbf{re} = -{}^m_e\mathbf{T}\ {}_{re}\mathbf{e} \tag{5.11}$$

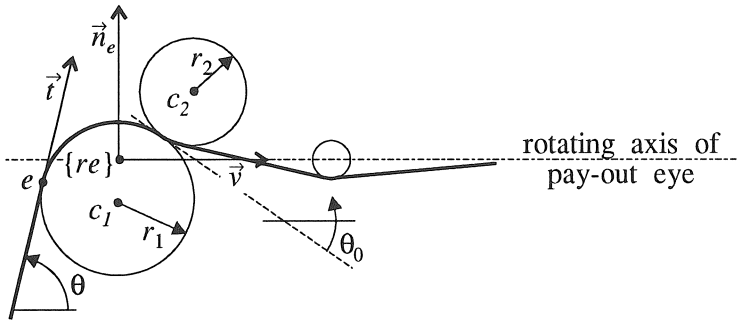

Figure 5.6: Contact point at the delivery rolls

The position of the actual delivery point e in the frame attached to the reference delivery point $\{re\}$ depends on the orientation of the tangent $\vec{t}$ in $\{re\} = \{re; \vec{v}, \vec{n_e}, \vec{a}\}$. Since $\vec{t}$ is normal to the vector $\vec{a}$ (Eq. 4.2), ${}_{re}\mathbf{t}$ can be written as $[\cos\theta \quad \sin\theta \quad 0]^T$. ${}_{re}\mathbf{e}$ equals (Fig. 5.6) :

$$\begin{array}{lll} \theta \le \theta_0 : & {}_{re}\mathbf{e} = & [-r_1\sin\theta \quad {}_{re}c_{1,y} + r_1\cos\theta \quad 0]^T \\ \theta < \theta_0 : & {}_{re}\mathbf{e} = & [{}_{re}c_{2,x} + r_2\sin\theta \quad {}_{re}c_{2,y} - r_2\cos\theta \quad 0]^T \end{array} \tag{5.12}$$

with r_1 the radius and ${}_{re}\mathbf{c}_1 = [0 \quad {}_{re}c_{1,y} \quad 0]^T$ the position of the centre c_1 of the lower roll, r_2 the radius and ${}_{re}\mathbf{c}_2 = [{}_{re}c_{2,x} \quad {}_{re}c_{2,y} \quad 0]^T$ the

position of the centre c_2 of the upper roll. The angle θ_0, at which the contact switches from roll equals :

$$\theta_0 = -\arctan\left(\frac{{}_{re}c_{2,x}}{{}_{re}c_{2,y} - {}_{re}c_{1,y}}\right) \tag{5.13}$$

5.2.5 Rotation about the Winding Axis

All the calculations in the previous sections have been performed in the mandrel coordinate system $\{m\}$, which is attached to the mandrel (cf. Fig. 5.3). The mandrel and the pay-out eye are rotated over an angle φ about the winding axis $\vec{w}$ so, that the pay-out axis $\vec{v}$ is horizontal.

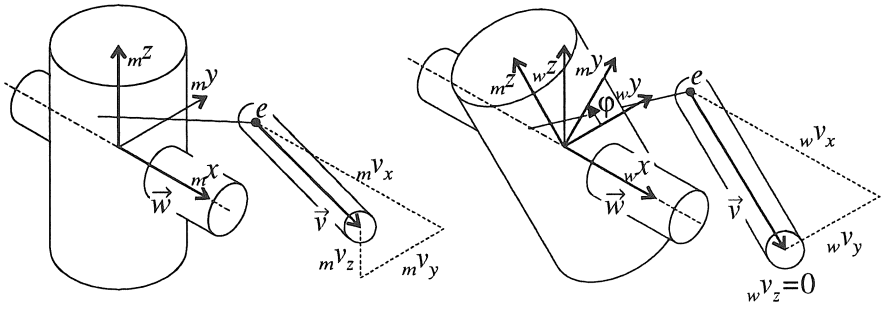

Figure 5.7: Pose of the pay-out eye in (a) the mandrel coordinate system and in (b) the winding coordinate system

The frame $\{re\} = \{re; \vec{v}, \vec{n_e}, \vec{a}\}$, which is attached to the delivery point, is in the winding coordinate system (Fig. 5.7) :

$${}^{w}_{re}\mathbf{T} = \mathbf{Rot}(x, \varphi)\, {}^{m}_{re}\mathbf{T} \tag{5.14}$$

with φ the angle of the winding axis. The pay-out axis $\vec{v}$ is horizontal, or ${}_{w}v_z = 0$:

$${}_{w}v_z = {}_{m}v_y \sin\varphi + {}_{m}v_z \cos\varphi = 0 \tag{5.15}$$

or :

$$\varphi = -\arctan\left(\frac{{}_{m}v_z}{{}_{m}v_y}\right) + k_\varphi \pi \tag{5.16}$$

The value of k_φ is derived from the previous angle. k_φ changes when the sign of ${}_{m}v_y$ changes, without ${}_{m}v_z$ changing sign. The angle φ between consecutive points should be less than 90° to avoid errors in the calculations.

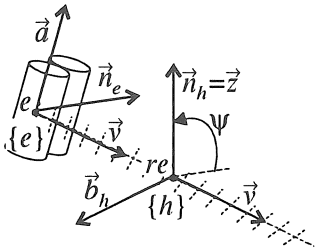

Figure 5.8: Rotation about the pay-out axis

The vector $\vec{v}$ equals in the winding coordinate system :

$$ {}_w\mathbf{v} = \begin{bmatrix} {}_m v_x \\ \pm\sqrt{{}_m v_y^2 + {}_m v_z^2} \\ 0 \end{bmatrix} \tag{5.17} $$

Two orientations are possible for $\vec{v}$ ($\pm {}_w v_y$), corresponding to two angles φ, which differ 180°. The corresponding positions of the delivery point are ${}_w\mathbf{e} = [{}_w e_x \quad {}_w e_y \quad {}_w e_z]^T$ and ${}_w\mathbf{e} = [{}_w e_x \quad -{}_w e_y \quad -{}_w e_z]^T$.

5.2.6 Rotation about the Pay-Out Axis

The tape lies in a horizontal plane at the entry of the flexible ladder. The orientation of the tape in the entry of the pay-out eye corresponds to the orientation of the frame $\{h\} = \{re; \vec{v}, \vec{n_h}, \vec{b_h}\}$ in re (Fig. 5.2). The frame $\{re\} = \{re; \vec{v}, \vec{n_e}, \vec{a}\}$ is rotated about the pay-out axis $\vec{v}$ to the frame $\{h\} = \{re; \vec{v}, \vec{n_h}, \vec{b_h}\}$, with $\vec{n}_h$ directed vertically upwards (Fig. 5.8) :

$$ {}^w_h\mathbf{T} = {}^w_{re}\mathbf{T}\ \mathbf{Rot}(x, \psi) \tag{5.18} $$

The vector $\vec{n}_h$ is directed vertically upwards :

$$ {}_w n_{h,z} = {}_w n_{e,z} \cos\psi + {}_w a_z \sin\psi = 1 \tag{5.19} $$

or :

$$ \psi = \arctan\left(\frac{{}_w a_z}{{}_w n_{e,z}}\right) + \frac{\pi}{2}[1 - \mathrm{sign}({}_w n_{e,z})] + 2k_\psi\pi \tag{5.20} $$

or, with (5.16) :

$$ \psi = \arctan\left(\frac{{}_m a_y \sin\varphi + {}_m a_z \cos\varphi}{{}_m n_{e,y} \sin\varphi + {}_m n_{e,z} \cos\varphi}\right) + \frac{\pi}{2}[1 - \mathrm{sign}({}_w n_{e,z})] + 2k_\psi\pi \tag{5.21} $$

The value of k_ψ changes when the sign of ${}_w n_{e,z}$ changes, while ${}_w a_z$ is negatiive. To avoid errors, the angle ψ between consecutive points should be less than 180°.

If not the frame $\{re\}$, but the frame $\{e'\}$ is used for the calculation of ψ, the value of ψ_c (Eq. 5.10) has to be subtracted from ψ.

The delivery rolls have to be rotated over an angle $-\psi$ about the pay-out axis so that the delivery rolls rotate from the frame $\{h\}$ towards the frame $\{re\}$.

5.2.7 Tape Twist Control

The rotation about the pay-out axis is, due to the construction of the flexible ladder, limited to 360°. Tape twists can however become larger during winding, e.g. when winding round a cylinder with an axis perpendicular to the winding axis. There are two ways to control tape twists : by storing excess twist behind the pin rings, and by means of an appropriate winding method.

5.2.7.1 Tape Twist Compensating Motion

When the tape twist becomes too large, it can be reduced by a synchronized rotation of both mandrel and pay-out eye about the winding axis. By a rotation of 360° degrees about the winding axis, a twist from e.g. 270° is reduced to −90° (Fig. 5.9). The rotation direction is derived from the sign of the numerator of the derivative of the main term in Eq. (5.21) :

$$\frac{d\psi}{d\varphi} = \frac{{}_m n_{e,z}\ {}_m a_y - {}_m n_{e,y}\ {}_m a_z}{({}_m a_y \cos\varphi - {}_m a_z \sin\varphi)^2 + ({}_m n_{e,y} \cos\varphi - {}_m n_{e,z} \sin\varphi)^2} \tag{5.22}$$

Such a rotation is only possible in an area where the robot is not hindered in its motions by the mandrel or by head- or tail-stock. Such an area does not exist if the mandrel is supported at both head- and tail-stock. If the mandrel is only supported at the headstock, a free area is available, which can be used to remove excessive twists (Fig. 5.10).

5.2.7.2 Storage of Excess Twists behind the Pin Rings

Excess tape twists can be stored behind the pin rings during the linking motion Υ_{i-1}^{i}, by a supplementary rotation of the delivery rolls. This

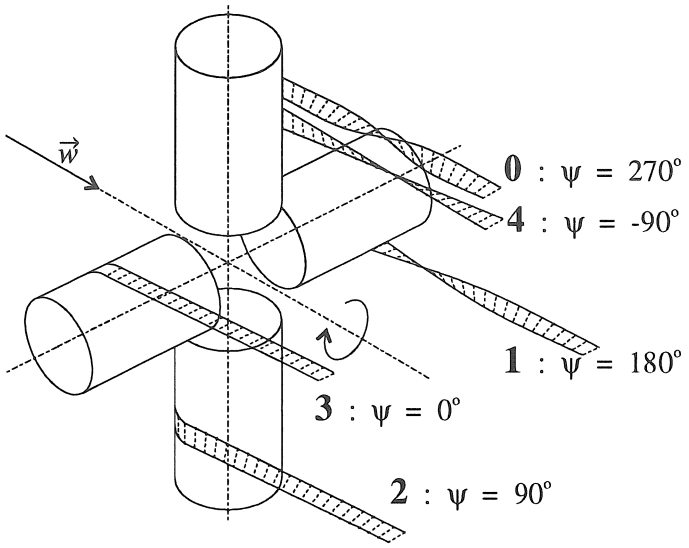

Figure 5.9: Twist compensating motion : a tape twist of 270° (situation **0**) is, by a rotation over 360° about the winding axis $\vec{w}$, reduced to −90° (situation 4)

"storage twist", which is a multiple of 180°, is preferably applied when that the pay-out axis is aligned with the tangent to the fibre path, in order to avoid slippage in the delivery rolls. The magnitude of the storage twist is calculated so, that the mean tape twist during the next motion Υ_i is as small as possible.

The storage twist will not be completely placed on the end plane of the pin ring, if the free length (during the motion between q_3 and q_5 – Fig. 5.5) is larger than the length of the linking path Γ_{i-1}^{i} on the

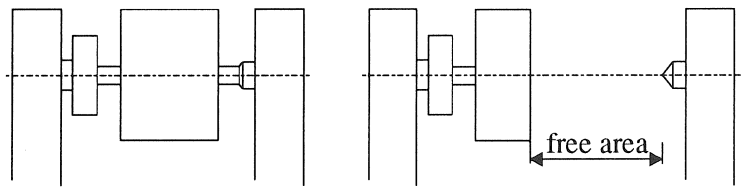

Figure 5.10: Set-up of the mandrel
(a) both head- and tailstock (b) only headstock

end plane. A residual twist remains in the tape after fixing the tape behind the pin ring. The tape can then be folded at the start of the next fibre path Γ_i. To prevent this, the free length should be as small as possible during the linking motion.

The side of the tape, which makes contact with the mandrel, is changed when the storage twist is not a multiple of 360°.

5.2.8 Pose of the Robot End Flange

The last step of the construction of the robot path is the calculation of the pose of the robot end flange (Fig. 5.3). The pose of the robot end flange in the robot base coordinate system is (cf. Eq. 2.11) :

$$ {}^{b}_{rf}\mathbf{T} = {}^{b}_{w}\mathbf{T}\,{}^{w}_{h}\mathbf{T}\,{}^{h}_{rf}\mathbf{T} \tag{5.23} $$

${}^{h}_{rf}\mathbf{T}$ is the transformation matrix from the frame $\{h\}$, which is attached to the pay-out eye in re to the robot end flange $\{rf\}$.

${}^{b}_{w}\mathbf{T}$ refers to the pose of the winding coordinate system in the robot base coordinate system. This transformation matrix is obtained from the calibration of the winding machine (cf. section 5.4.1).

5.3 Robot Trajectory

The robot path, which is calculated in the previous section, contains no information on velocity or time.

The ALTER-mode requires data at constant time intervals. This section discusses, after a short literature survey, the generation of the robot trajectory and the generation of the path control data for the ALTER-mode. The data are calculated on a VAX-computer, and are transmitted to the PC, that controls the filament winding process.

In order to obtain an optimal winding process, the global winding time should be as small as possible, while maintaining an optimal part quality.

Literature Survey The winding speed is limited due to the required minimum residence time of the fibres in the impregnation bath. Centrifugal forces on the fibre give rise to high splashing losses [72]. The winding speed is therefore limited to 1 m/s [72]. Accelerations are limited by the machine dynamics.

The two most common methods to calculate the velocity in filament winding are the application of a constant mandrel velocity and the application of a constant fibre pay-out rate.

Constant mandrel velocity, which is used in all the mechanical winding machines, offers good results for high angle helical and circumferential winding. It is advisable for large asymmetric cores, in order to reduce strains on the mandrel drives [47]. A constant mandrel velocity can result in large accelerations for the transversal carriage and the fibre in the pay-out eye, and cannot be used if the mandrel rotation direction changes during winding.

The application of a constant fibre feed decreases the accelerations of the pay-out eye and leads to a part with a more uniform quality [115]. This technique cannot be used if rewinding is necessary, e.g. when winding round the pin rings.

In robotics, research has been performed on the generation of time-optimal trajectories. The time-optimal trajectory has to be such that the maximum motor torques are not exceeded. Shin [87], Bobrow [5] and Pfeiffer [74] have developed algorithms to calculate the time-optimal trajectory, taking the robot dynamics into account.

Method Applied It is however difficult to calculate the dynamic parameters of a robot with six joints. A simpler model is therefore developed, in which not the joint torques but the joint accelerations are limited. If accelerations are limited instead of torques, the obtained trajectory is not optimal : the accelerations, which are allowed, are function of the pose and the velocity of the robot, and the maximum acceleration has therefore to be set to the minimum of the allowed accelerations. The model is based on joint accelerations, which results in a better performance than the use of cartesian accelerations. The maximum cartesian accelerations have to be set to the minimum of the allowed accelerations, which are low due to the presence of singularities.

Inputs for the robot trajectory module are the poses of the robot path and the angles of the winding axis and the pay-out axis, and the maximum joint velocities and accelerations and the maximum smoothing error. The output poses $\mathbf{b}_j$, which are sent to the robot at constant time intervals, have 8 components : 6 components for the robot pose, the angle of the winding axis and the angle of the pay-out eye axis.

The input poses $\mathbf{q}_i$ have one component more than the output poses : the fibre feed (measured at the impregnation bath or in the pay-out eye). The fibre feed is treated as an additional joint with a maximum velocity and acceleration.

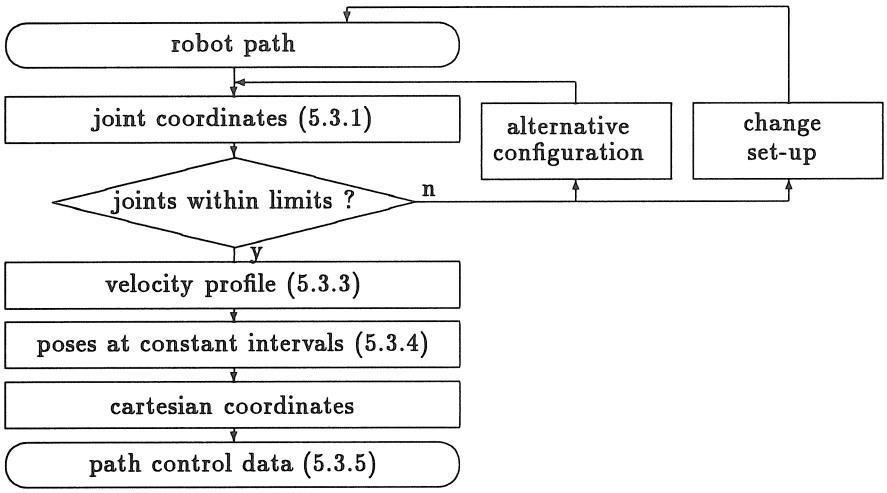

Figure 5.11: Consecutive steps in the calculation of the robot trajectory

The robot trajectory is calculated in several steps (Fig. 5.11) : first, a transformation from cartesian space towards the joint space of the robot is performed, then the maximum velocity and acceleration to trace the path are calculated, and the poses at constant time intervals are determined, followed by a transformation to the format required by the ALTER-mode. The poses which are sent to the robot are interpolated between the poses of the robot path. The original path is smoothed to allow higher velocities in the poses of the robot path. The smoothing of the path will be discussed in section 5.3.2.

5.3.1 Inverse Kinematics

The method requires the calculation of the joint values for each pose of the robot path. The solution of the inverse kinematics of a PUMA robot is described in [8, 18] and [89]. The geometric solution method of Pieper [8, 18] has been implemented to calculate the joint variables.

Eight solutions are possible for each pose in cartesian space, de-

pending on the initial configuration of the robot (arm left or right, elbow up or down, flip or noflip robot wrist [8]). By comparing all the points of the robot path, minimum and maximum joint values are obtained. The path cannot be wound if the limits of one or more joints are exceeded. In this case, an alternative initial configuration of the PUMA-762 can result in a feasible solution for all the joints. If not, the set-up has to be changed (cf. Fig. 5.11).

After calculation of the robot trajectory, the poses are transformed to cartesian space with forward kinematics [8, 18, 89].

5.3.2 Path Smoothing

The poses $\mathbf{b}_j$, which are sent at constant time intervals to the robot, are obtained by interpolation between the poses $\mathbf{q}_i$ of the original robot path in joint space, e.g. by linear interpolation :

$$\mathbf{b}_j = \mathbf{q}_i + \lambda_j(\mathbf{q}_{i+1} - \mathbf{q}_i) = (1 - \lambda_j)\,\mathbf{q}_i + \lambda_j \mathbf{q}_{i+1} \tag{5.24}$$

The relation between the poses $\mathbf{b}_j$ and $\mathbf{q}_i$ is given by the "setpoint" $\xi_j = i + \lambda_j$ with $0 \leq \lambda_j < 1$.

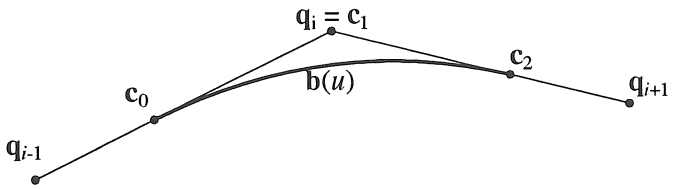

Figure 5.12: Parabolic Bézier curve

The maximum velocity, allowed to trace the linearly interpolated path, is very low due to the sharp edges. The path is smoothed by parabolic Bézier-curves in the edges. These Bézier-curves are defined by 3 control poses : $\mathbf{c}_0$ on the segment $\mathbf{q}_{i-1}\mathbf{q}_i$, $\mathbf{c}_1$ which coincides with $\mathbf{q}_i$, and $\mathbf{c}_2$ on the segment $\mathbf{q}_i\mathbf{q}_{i+1}$ (Fig. 5.12). The Bézier-curve starts tangentially at $\mathbf{q}_{i-1}\mathbf{q}_i$ and ends tangentially at $\mathbf{q}_i\mathbf{q}_{i+1}$, so that the tangent to the global path is continuous. The equation of the Bézier curve equals [81] :

$$\mathbf{q}(u) = (1 - u)^2\mathbf{c}_0 + 2u(1 - u)\mathbf{c}_1 + u^2\mathbf{c}_2 \tag{5.25}$$

with $0 \leq u \leq 1$. The control points $\mathbf{c}_0$ and $\mathbf{c}_2$ can, with χ_l and $1-\chi_r$ as parameters in Eq. (5.24), be written as :

$$\mathbf{c}_0 = \chi_l \mathbf{q}_{i-1} + (1-\chi_l)\mathbf{q}_i \quad (5.26)$$

$$\mathbf{c}_2 = (1-\chi_r)\mathbf{q}_i + \chi_r \mathbf{q}_{i+1} \quad (5.27)$$

The equation of the Bézier curve (5.25) is then :

$$\mathbf{q}(u) = (1-u)^2\chi_l \mathbf{q}_{i-1} + [1-(1-u)^2\chi_l - u^2\chi_r]\mathbf{q}_i + u^2\chi_r \mathbf{q}_{i+1} \quad (5.28)$$

If $\mathbf{q}_{i-1}$, $\mathbf{q}_i$ and $\mathbf{q}_{i+1}$ are collinear, the interpolation is equivalent with the linear interpolation, provided that $\mathbf{c}_1 - \mathbf{c}_0 = \mathbf{c}_2 - \mathbf{c}_1$.

The control poses $\mathbf{c}_0$ and $\mathbf{c}_2$ are chosen so, that for each joint k the smoothing error in $\mathbf{q}_i$ is less than the maximum allowed error $\epsilon_{M,k}$. To ease the calculations, the poses $\mathbf{q}_i$ are scaled to the poses $\mathbf{q}_i^s$, so that the maximum error for each joint in the scaled space equals ϵ_{max} :

$$\mathbf{q}_i^s = \left[q_{i,1}\frac{\epsilon_{max}}{\epsilon_{M,1}} \;\; q_{i,2}\frac{\epsilon_{max}}{\epsilon_{M,2}} \;\; \cdots \;\; q_{i,n}\frac{\epsilon_{max}}{\epsilon_{M,n}} \right]^T \quad (5.29)$$

with $n = 9$ the number of joints. The lengths[3] of the control segments $\mathbf{c}_0\mathbf{c}_1$ and $\mathbf{c}_1\mathbf{c}_2$ in the scaled space are taken equal : $l_c = \|\mathbf{c}_0^s\mathbf{c}_1^s\| = \|\mathbf{c}_1^s\mathbf{c}_2^s\|$. In this case, the pose at $u = 0.5$ (or $\xi = i$) is closest to $\mathbf{q}_i$. The error equals, with Eq. (5.25) (Fig. 5.13) :

$$\boldsymbol{\epsilon} = \mathbf{q}^s(0.5) - \mathbf{c}_1^s = \frac{1}{4}(\mathbf{c}_0^s + 2\mathbf{c}_1^s + \mathbf{c}_2^s) - \mathbf{c}_1^s = \frac{1}{4}(\mathbf{c}_2^s - \mathbf{c}_1^s) - \frac{1}{4}(\mathbf{c}_1^s - \mathbf{c}_0^s) \quad (5.30)$$

$(\mathbf{c}_1^s - \mathbf{c}_0^s)$ can be written as $l_c\mathbf{d}_{01}^s$, with $\mathbf{d}_{01}^s$ the unit vector in the direction of the segment $\mathbf{c}_0^s\mathbf{c}_1^s$. Eq. (5.30) is then :

$$\boldsymbol{\epsilon} = \frac{l_c}{4}(\mathbf{d}_{12}^s - \mathbf{d}_{01}^s) \quad (5.31)$$

For each joint k, it is required that $|\epsilon_k| \leq \epsilon_{max}$ (Fig. 5.13), so that the maximum length l_c of the control segments equals :

$$l_c = \frac{4\epsilon_{max}}{\max_{k=1,n} |d_{01,k}^s - d_{12,k}^s|} \quad (5.32)$$

[3]The length of the segment **ab** is, in analogy with the norm in $\mathbb{R}^3$, defined as :

$$\|\mathbf{ab}\| = \sqrt{(\mathbf{b}-\mathbf{a})^T(\mathbf{b}-\mathbf{a})}$$

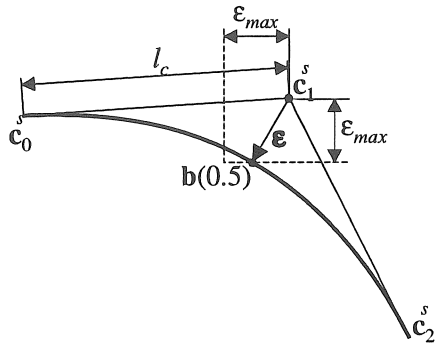

Figure 5.13: Smoothing error ($n = 2$)

The resolution of the robot joints is taken as the allowed smoothing error. Since data are only sent to the robot at regular intervals, a multiple of the robot cycle time, a supplementary error occurs due to the discretization of the path. Additional errors on the path are positioning errors of the robot ($\approx$ 2 mm for the PUMA-762 [70]), errors due to the flexibility of the tool, and errors in the fibre placement model.

5.3.3 Velocity Profile

The robot path must be traced so, that, for each joint, the maximum joint velocities $\dot{q}_{M,k}$ and accelerations $\ddot{q}_{M,k}$ are not exceeded, or :

$$\forall k \quad : \quad |\dot{q}_k(s)| \leq \dot{q}_{M,k} \tag{5.33}$$

$$\forall k \quad : \quad |\ddot{q}_k(s)| \leq \ddot{q}_{M,k} \tag{5.34}$$

To ease the calculations, the poses $\mathbf{q}_i$ are scaled to the poses $\mathbf{q}_i^*$ so, that the maximum accelerations for all joints in the scaled space equals A_{max} :

$$\mathbf{q}_i^* = \left[q_{i,1} \frac{A_{max}}{\ddot{q}_{M,1}} \quad q_{i,2} \frac{A_{max}}{\ddot{q}_{M,2}} \quad \cdots \quad q_{i,n} \frac{A_{max}}{\ddot{q}_{M,n}} \right]^T \tag{5.35}$$

The true arc length s in the scaled space is approximated by the arc length of the linearly interpolated path in the scaled space.

The velocity $\dot{\mathbf{q}}^*$ and the acceleration $\ddot{\mathbf{q}}^*$ are :

$$\dot{\mathbf{q}}^*(s) \quad = \quad v \frac{d\mathbf{q}^*}{ds} \tag{5.36}$$

$$\ddot{\mathbf{q}}^*(s) = a\frac{d\mathbf{q}^*}{ds} + v^2\frac{d^2\mathbf{q}^*}{ds^2} \tag{5.37}$$

with $v = \dot{s}$ and $a = \ddot{s}$

The maximum path velocity and acceleration are evaluated in the poses of the robot path $\mathbf{q}_i^*$. The maximum path velocity in the pose $\mathbf{q}_i^*$ is the minimum of the path velocity to trace the Bézier curve in $\mathbf{q}_i^*$ (section 5.3.3.1), and of the path velocity to reach $\mathbf{q}_{i+1}$ with maximum deceleration (section 5.3.3.2).

5.3.3.1 Maximum Path Velocity along a Bézier Curve

For the Bézier-segment with equal control lengths l, the arc length is $s = 2lu$. The derivative $\frac{d\mathbf{q}^*}{ds}$ and the second derivative $\frac{d^2\mathbf{q}^*}{ds^2}$ are derived from Eq. (5.25) :

$$\frac{d\mathbf{q}^*}{ds} = \frac{d\mathbf{q}^*}{du}\frac{du}{ds} = \frac{1}{l}[(u-1)\mathbf{c}_0^* + (1-2u)\mathbf{c}_1^* + u\mathbf{c}_2^*] = u\mathbf{d}_{12}^* + (1-u)\mathbf{d}_{01}^* \tag{5.38}$$

$$\frac{d^2\mathbf{q}^*}{ds^2} = \frac{d^2\mathbf{q}^*}{du^2}\left(\frac{du}{ds}\right)^2 = \frac{1}{2l^2}(\mathbf{c}_0^* - 2\mathbf{c}_1^* + \mathbf{c}_2^*) = \frac{1}{2l}(\mathbf{d}_{12}^* - \mathbf{d}_{01}^*) \tag{5.39}$$

with $\mathbf{d}_{01}^*$ the unit vector in the direction of the segment $\mathbf{c}_0^*\mathbf{c}_1^*$. The contribution of both terms in Eq. (5.37) is taken equal in the middle of the Bézier-curve ($u = 0.5$) : half of the maximum acceleration $\ddot{q}_M$ is used for the acceleration along the path (term in a) and half of $\ddot{q}_M$ is used for the path velocity (term in v). The maximum path velocity v_M along the Bézier curve in $\mathbf{q}_i^*$ is, with Eq. (5.39) :

$$v_{M,i} = \sqrt{\frac{l}{\max_{k=1,n}|d_{12,k}^* - d_{01,k}^*|}\frac{A_{max}}{2}} \tag{5.40}$$

The maximum path acceleration along the Bézier curve in $\mathbf{q}_i^*$ is, with Eq. (5.34) and Eq. (5.38) (for $u = 0.5$) :

$$a_{M,i} = \frac{2}{\max_{k=1,n}|d_{01,k}^* + d_{12,k}^*|}\frac{A_{max}}{2} \tag{5.41}$$

5.3.3.2 Maximum Path Velocity in a Point of the Path

The maximum path velocity $v_{M,i}$ in the poses $\mathbf{q}_i^*$ is calculated from the last pose of the path towards the beginning of the path.

The maximum path velocity $v_{M,i}$ in the pose $\mathbf{q}_i^*$ is the minimum of the path velocity to trace the Bézier curve in $\mathbf{q}_i^*$, as calculated with Eq. (5.40), and the path velocity, allowed to reach $\mathbf{q}_{i+1}^*$ at a path velocity of $v_{M,i+1}$ with maximum deceleration $-a_{M,i+1}$ (cf. Eq. 5.41). The latter velocity is calculated from the equations of constant deceleration :

$$l_i = \left\|\mathbf{q}_i^*\mathbf{q}_{i+1}^*\right\| = v_{M,i}t - \frac{a_{M,i+1}t^2}{2} \quad \text{with} \quad t = \frac{v_{M,i} - v_{M,i+1}}{a_{M,i+1}} \tag{5.42}$$

or :

$$v_{M,i} = \sqrt{v_{M,i+1}^2 + 2a_{M,i+1}l_i} \tag{5.43}$$

The maximum path velocity in the setpoint $\xi = i + \lambda$ equals :

$$v_M(\xi) = \sqrt{v_{M,i+1}^2 + 2a_{M,i+1}(1-\lambda)l_i} \tag{5.44}$$

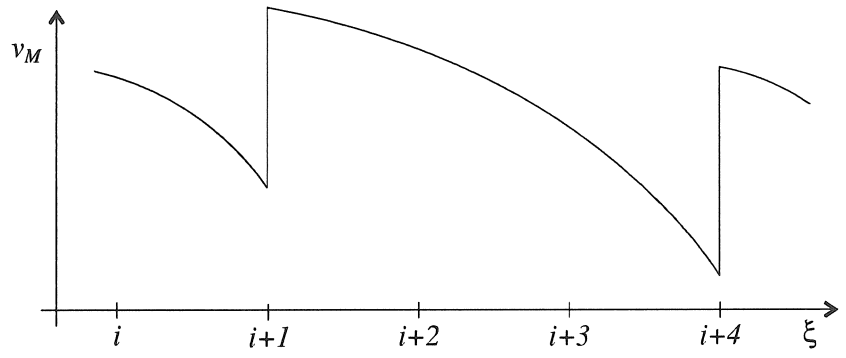

Figure 5.14: Velocity profile

The velocity profile is stepped (Fig. 5.14) : the maximum path velocity decreases, as long as the path velocity (5.43) is larger than the path velocity (5.40), allowed to trace the Bézier curve. After the Bézier curve, the maximum path velocity increases suddenly.

5.3.4 Generation of Setpoints

For each time interval j, the acceleration a is calculated, so that the maximum path velocity v_M and acceleration a_M and the maximum

joint velocities and accelerations are not exceeded. The length Δs_j of the path, traced during the j-th time interval equals :

$$\Delta s_j = v_{j-1}\Delta t + a\frac{(\Delta t)^2}{2} \tag{5.45}$$

with v_{j-1} the path velocity at the end of the $(j-1)$-th time interval, and Δt the time step. The setpoint at the end of the j-th time interval equals :

$$\xi_j = i + \lambda_j = \xi_{j-1} + \frac{\Delta s_j}{l_i} \tag{5.46}$$

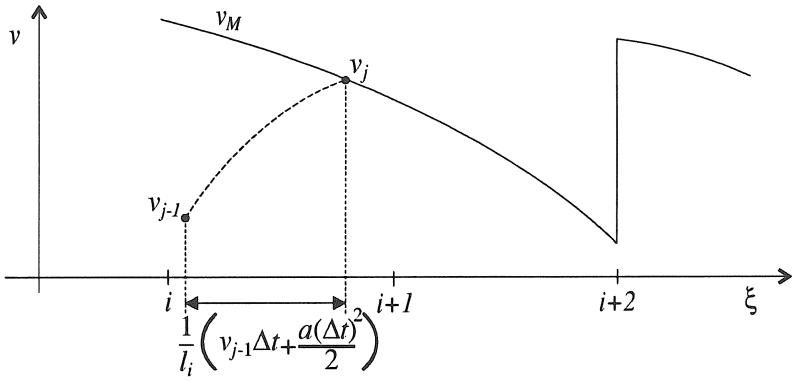

Figure 5.15: Maximum acceleration in a point

The path acceleration a is first calculated so that the maximum path velocity $v_M(\xi)$ at ξ_j is not exceeded (Fig 5.15) :

$$v_j = v_{j-1} + a\Delta t \leq v_M(\xi_j) \tag{5.47}$$

(5.44) in (5.47) results with (5.46) in :

$$\begin{aligned} a\Delta t \;\leq\; & -\left(v_{j-1} + \frac{a_{M,i+1}\Delta t}{2}\right) \\ & + \frac{1}{2}\sqrt{4v_{M,i+1}^2 + (a_{M,i+1}\Delta t)^2 + 8a_{M,i+1}\lambda_{j-1}l_i - 4a_{M,i+1}v_{j-1}\Delta t} \end{aligned} \tag{5.48}$$

The path acceleration a must be smaller than a_M. The maximum joint velocities may neither be exceeded (Eq. 5.33), or :

$$a\Delta t \leq \frac{\dot{q}^*_{M,k}}{\max_{k=1,n}\left|\frac{dq_k}{ds}\right|} - v_{j-1} \tag{5.49}$$

5.3.5 Path Control Data

The poses at constant time interval are calculated in the configuration space of the robot, and are transformed to cartesian space (Fig. 5.11). The path control data are then calculated (cf. p. 140).

The robot path and the robot trajectory are calculated on a VAX-computer. The data have to be transmitted to the PC, that controls the winding process (cf. section 4.4.2). Data are passed in binary format, to reduce the length of the data files and the time necessary to read the file. The data are converted to integers, to avoid problems in the interpretation between the C-compilers on the VAX-computer and the PC. The conversion factors, employed by ALTER (cf. p. 141) are used for the conversion of the robot coordinates to integers. For the external axes, the number of encoder pulses is used. Each robot coordinate requires 2 bytes for storage, and both external axes 4 bytes. The size of the data for the rotation of the pay-out eye axis are reduced to 2 bytes, since the total rotation is limited to 360°, while still maintaining enough accuracy.

The total number of stored data is limited, due to the limited memory available during execution of the program. During winding, two rotation components are zero, and can be omitted (cf. p. 141). This results in a reduction of 22 % of the required memory. If the maximum amount of data is exceeded, the time step Δt is increased, which results in a reduction of the number of path control data to be transmitted.

5.4 Construction of the Off-Line Winding Program with CAWAR

The robot program is constructed with the program `CAWAR`, which has been introduced in section 2.6. This section will describe the various steps in the construction of the winding program. As a case study, the tape winding of a T-piece will be discussed.

Fig. 5.16 shows the various steps in the construction of the off-line program.

The program `CAWAR` checks first if all the data, necessary to generate the models for collision control (e.g. pin rings, pay-out eye) (cf. section 6.3.2), and to calculate the robot path are available. For the

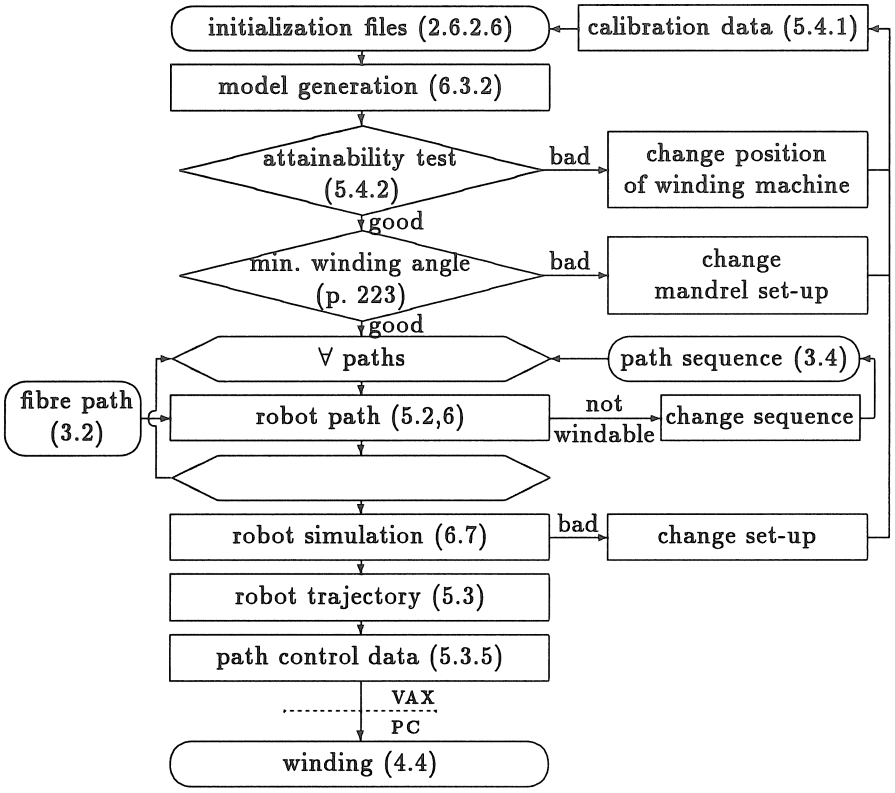

Figure 5.16: Steps in the generation of the winding program

calculation of the pose of the robot end flange, the transformation matrices ${}^{rf}_{h}\mathbf{T}$, the pose of the pay-out eye with respect to the robot end flange, and ${}^{b}_{w}\mathbf{T}$, the pose of the winding coordinate system in the robot base coordinate system, have to be known (cf. Eq. 5.23). The measurement of the position of the winding machine will be discussed in section 5.4.1.

Prior to the calculation of the robot path, the program checks the attainability of some points and the minimum winding angle (cf. section 5.4.2).

The program reads then the data of the fibre paths, in a predefined sequence, and calculates the points of the collision-free robot path. If a collision-free robot path cannot be constructed, the fibre path sequence is changed, and the program continued.

After the calculation of the robot path, the winding process can be simulated in a graphical robot simulation system. The simulation of the winding process will be discussed in section 6.7.

The next step is the calculation of the robot trajectory, followed by the generation of the path control data. These data are sent from the VAX-computer to the PC, which controls the winding process (cf. section 4.4). For parts, which have a symmetry about the winding axis, the robot program is repeated a number of times. Symmetry about the winding axis will be discussed in section 5.4.3.

5.4.1 Calibration

The pose of the robot end flange will only be calculated accurately if the transformation matrix ${}^{b}_{w}\mathbf{T}$ exactly maps the position of the winding machine in the robot base coordinate system. The position of the winding machine is derived from a set of reference points. The robot is used as a measuring device to determine the positions of these reference points. A measuring probe is mounted on the end flange and the robot is moved to the reference point. If the reference point is reached, the cartesian robot coordinates of the probe tip are read.

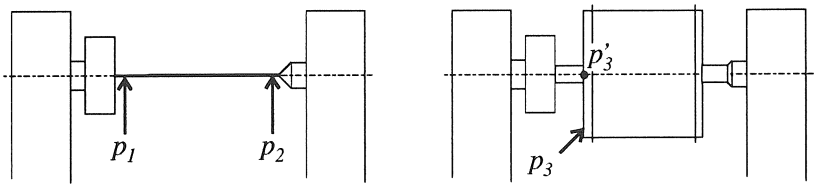

Figure 5.17: Calibration of the winding machine

In the winding process, the position of the winding coordinate system $\{w\}$ is measured in two phases :

- measuring the position of the winding axis. This is done by tightening a thin roving between the headstock and the tailstock and by measuring the position of two points p_1 and p_2 on this roving with the robot (Fig. 5.17). The winding axis $\vec{w}$ is in the coordinate system $\{b\}$:

$$ {}_{b}\mathbf{w} = \frac{1}{\sqrt{({}_{b}\mathbf{p}_2 - {}_{b}\mathbf{p}_1)^T({}_{b}\mathbf{p}_2 - {}_{b}\mathbf{p}_1)}}({}_{b}\mathbf{p}_2 - {}_{b}\mathbf{p}_1) \qquad (5.50) $$

with ${}_b\mathbf{p}_1$ the position of p_1 in the robot base coordinate system. The points p_1 and p_2 are preferably in the neighbourhood of the head- and tail-stock, to minimize the errors due to sagging of the roving.

- measuring the position of the mandrel. This is done by measuring the position of a point p_3 with known ${}_w x$-coordinate $({}_w p_{3,x})$ on the mandrel surface (Fig. 5.17). This point is projected on the winding axis (p'_3) :

$$ {}_b\mathbf{p'}_3 = {}_b\mathbf{p}_1 + [({}_b\mathbf{p}_3 - {}_b\mathbf{p}_1)^T \, {}_b\mathbf{w}] \, {}_b\mathbf{w} \tag{5.51} $$

The position of the origin o of the winding coordinate system in the robot base coordinate system $\{b\}$ is then :

$$ {}_b\mathbf{o} = {}_b\mathbf{p'}_3 - {}_w p_{3,x} \, {}_b\mathbf{w} = {}_b\mathbf{p}_1 + [({}_b\mathbf{p}_3 - {}_b\mathbf{p}_1)^T \, {}_b\mathbf{w} - {}_w p_{3,x}] \, {}_b\mathbf{w} \tag{5.52} $$

The z-axis of the winding coordinate system is directed vertically upwards.

Mandrel and winding coordinate system coincide at the start of the winding process. Therefore, the part has to be mounted correctly before starting to wind. No problem occurs when the part is axisymmetric. When the surface is asymmetric, positioning is done by using a feature of the part as reference or by adding a feature to the mandrel shaft, which serves as a reference.

5.4.2 Optimal Position of the Winding Machine

The optimal position of the mandrel with respect to the robot differs from part to part : for long parts the ends of the mandrel must still be attainable, for tape wound parts, where large tape twists can occur, the robot must be able to perform the twist compensation motion.

The distance between the mandrel and the robot centre b must be the smallest in the middle of the mandrel. This distance may not be too small to avoid collisions between the pay-out eye and the robot base. To check if the distance between mandrel and robot is not too large, attainability tests (cf. p. 224) are performed for critical poses, like the poses at the sides of the pin ring and the most extreme pose of the twist compensating motion.

The distance between the mandrel and both head- and tail-stock may not be too small, otherwise the minimum allowed winding angle (cf. p. 223) is too large.

5.4.3 Radial Symmetry

The use of radial symmetry, i.e. symmetry about the winding axis reduces the amount of data necessary to wind the part. Axisymmetric parts require only the calculation of the robot path for one winding circuit, which is repeated continuously.

A lot of asymmetric parts have a radial symmetry of 180°, as e.g. an elliptical cylinder. The data must then only be calculated for half of the fibre paths, that cover the mandrel. More generally, the angle of symmetry is $\theta_s = \frac{2\pi}{n_s}$ radians. After the completion of the robot path, the robot path is repeated, and an angle $\varphi_0 = 2k\pi + m\theta_s (0 < m < n_s$, m and n_s may not have a common divisor) is added to the angle of the winding axis. In case of an axisymmetric part, n_s equals n_p, the total number of fibre paths along the circumference. The value of m is then selected in function of the desired winding sequence (cf. section 1.5.1.2).

The angle of symmetry θ_s depends on the symmetry planes and axes of the mandrel and the set-up of the mandrel. Radial symmetry occurs if all symmetry transformation matrices ${}_c\mathbf{S}_i$, after a rotation over θ_s about the winding axis, are transformed into another symmetry transformation matrix ${}_c\mathbf{S}_j$, or :

$$ {}^m_c\mathbf{T}\ {}_c\mathbf{S}_i = \mathbf{Rot}(x, \theta_s)\ {}^m_c\mathbf{T}\ {}_c\mathbf{S}_j \tag{5.53} $$

or :

$$ {}^m_c\mathbf{T}\ {}_c\mathbf{S}_i\ {}_c\mathbf{S}_j^{-1}\ {}^m_c\mathbf{T}^{-1} = \mathbf{Rot}(x, \theta_s) \tag{5.54} $$

The robot poses are stored in two files : a starting file and a regime file. The starting file contains the data for the starting motion Υ_0^1, the regime file contains the rest of the data. The starting motion is executed once, the regime motion n_s times.

5.4.4 Case Study : Tape Winding of a T-piece

The T-piece, the design of which is discussed in section 3.3.3 is wound with tapes. This section will discuss the main steps in the production of the T-piece.

5.4.4.1 Mandrel

The mandrel must be removable. Hille [39] uses two solid cylinders and a flexible rubber material for the fillet. At PMA, a removable material

is used for the mandrel. Candidate materials are : sand, soluble salts, wax, plaster (cf. p. 41). The mandrel is first cast in a base mould and cured.

The base mould has been produced in two ways : a first mould has been made by welding steel tubes [82], a second mould has been machined on a CNC-machine. The welded mould is cut in two, along the axial symmetry plane, that contains the axes of all cylinders.

For the CNC-machined mould, the CAD-surfaces are intersected with the axial symmetry plane and only half the surface model is retained. The tool path is generated, and a CNC-program is generated in the CAD-system. The CNC-program is executed twice, to obtain both halves of the mould (Fig. 5.18).

The welded mould is less accurate than the machined mould, due to the thermal deformations during welding.

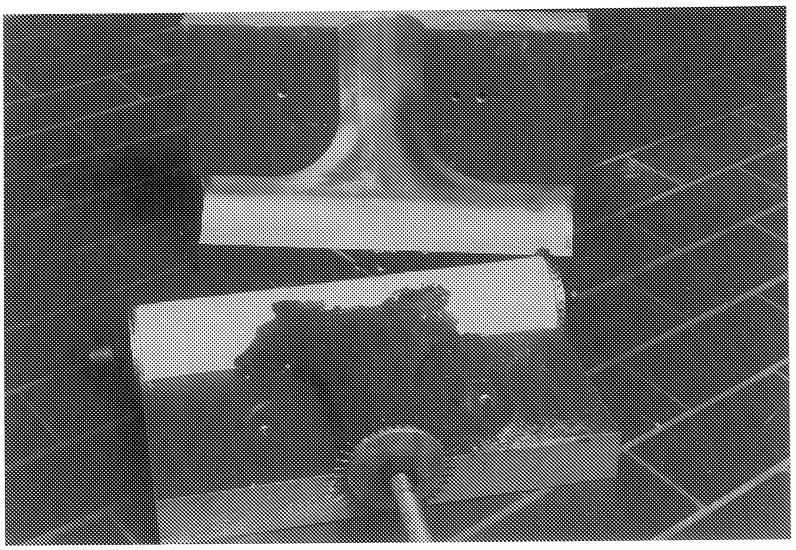

Figure 5.18: Base mould and the mandrel of the T-piece

Pin rings are mounted at the three ends of the T-piece. The pin rings are cylinders, in which holes are drilled at constant intervals (10°). Pens are placed in the holes in the pin ring. Two steel bars, placed along the axes of the cylinders 1-3 and 6, connect the pin rings which each other. One of the bars links the mandrel with the chuck. The pin rings keep, during casting, the cast material in the mould.

5.4.4.2 Set-up of the T-piece

The T-piece can be mounted in two ways : with two supports or with one support. In the former case the mandrel is supported at both head- and tail-stock and the winding axis coincides with the axis of the main cylinder (1-3) (Fig. 5.19a). In the latter case the mandrel is only supported at the tailstock, and the winding axis coincides with the axis of the transverse cylinder 6 (Fig. 5.19b).

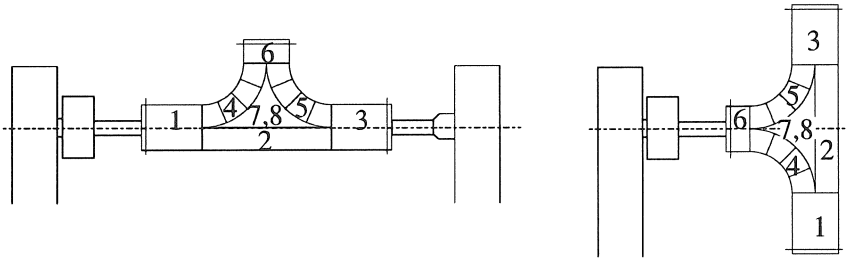

Figure 5.19: Set-up of the T-piece
(a) two supports (b) one support

The set-up with one support is the most advantageous. This set-up allows to control tape twists. During the winding motion round a cylinder perpendicular to the winding axis large tape twists occur. If the mandrel is only supported at the headstock, tape twists can be reduced with a twist compensating motion, as described in section 5.2.7.1. This is not possible when the T-piece is supported at both head- and tail-stock.

Another advantage of the set-up with one support is that the T-piece has a radial symmetry of 180° about the winding axis. The robot path must therefore only be calculated for half of the fibre paths, that cover the mandrel.

5.4.4.3 Calibration

The origin of the winding coordinate system $\{w\}$ is determined by measuring the pose of the winding axis and the position of a point on the mandrel with the robot (cf. section 5.4.1).

The planes 7 and 8 of the T-piece are used as reference for the starting position of the mandrel : at the start of the winding process

these planes should be vertical, which is checked by comparing the orientation of the plane with the vertical edge of the headstock.

5.4.4.4 Calculation of the Robot Path

The program **CAWAR** is used for the construction of the winding program. The main input parameters for the robot path calculation are (Fig. 5.20) :

desired free length : 200 mm
reinforcing material : 25-mm wide glass fibre tape
pay-out eye : flexible ladder
starting strategy : pay-out axis aligned with fibre

A test is performed to check if the most extreme point of the twist compensation motion is attainable. If this point cannot be attained, the program returns a warning and asks the user if the program must be continued :

```
Warning : Extreme Torsion Compensation point cannot be reached
Coordinates in Winding Coordinate System : 264.06 280.21 0.00
Position outside Working Envelope for 55.13 mm
```

If the point is not too far outside the working envelope of the robot (up to ca. 100 mm) mostly no problems occur in the twist compensation motion. Otherwise, the position of the winding machine has to be adapted, e.g. by slightly adapting the orientation of the winding axis, so that the zone, which is used to compensate tape twists, is nearer to the robot. After calibration, the program is executed again.

If the distance between the mandrel and the chuck (or the tailstock) is too small, low angle winding is not possible (cf. p. 223). The program **CAWAR** returns then a warning :

```
!!! Warning !!! Pin Ring 3 too close to chuck !!!
Distance between centre of pins and chuck   :   110.00 mm
Current Minimum Winding Angle               :    36.57 degrees
Minimum allowed distance to chuck           :   155.50 mm
i.e. min. free length (100.00 mm) + radius pay-out eye ( 46.50 mm)
     + width pin ring (  7.00 mm) + safety distance    (  2.00 mm)
Minimum allowed distance to headstock       :   335.50 mm
```

The distance between mandrel and chuck must be increased, if the winding angle at the end of the mandrel is smaller than (here) 36.57°.

During the calculations of the robot path, the program informs the user which paths are wound and shows the zones where collisions occur and the number of iterations during collision avoidance. If a path cannot be wound, the fibre path sequence is adapted, e.g.

```
============================ PROGRAM CAWAR ============================
 Tue Jun 23 15:41:05 1992

 --- Robot Program 1 ---

 --- Input Data ---
 Error mode                                    : Continue Program at Error
 Store points of robot path                    : YES
 Desired free length                           :  200.000 mm
 Minimum free length                           :  100.000 mm
 Material used                                 : Tape
 Band width                                    :   25.000 mm
 Pay-out eye                                   :    4
 Strategy for pay-out eye                      :  Aligned with Fibre
 Use symmetry about winding axis               : YES
 Immediate calculation of path control data    : NO
 Original sequence                             : 2

--- Filament Winding of Part 4 ---

 Repeatable Program
 Shift at end       :   180.000 degrees
 Output Robot Poses : mypool:sta001.crob (Starting File)
 Output Robot Poses : mypool:rob001.crob

 Start Vector (Mandrel) : -254.60 -165.00   10.00  0.0000 -1.0000  0.0000
 Simulation Origin      :  767.20 1215.56 -174.70  0.0000  0.0000 -60.4070

       ### 24 Fibre Paths Wound ###

  0 : File   1 -2 [pin 3 -> 1]  |  96  +  715  +  38 points |      0 ->   849
  1 : File   4  1 [pin 1 -> 3]  |  81  +  263  +  31 points |    849 ->  1224
  2 : File   3 -2 [pin 3 -> 1]  |  68  +  319  +  35 points |   1224 ->  1646
  3 : File  12  2 [pin 1 -> 2]  | 100  +  230  +  31 points |   1646 ->  2007
  4 : File   6 -2 [pin 2 -> 1]  |  69  +  284  +  30 points |   2007 ->  2390
  5 : File   1  1 [pin 1 -> 3]  |  60  +  718  +  40 points |   2390 ->  3208
   .
   .
 12 : File  12  1 [pin 1 -> 2]  | 100  +  230  +  31 points |   6171 ->  6532
 13 : File  11 -1 [pin 2 -> 1]  | 126  +  266  +  34 points |   6532 ->  6958
 14 : File   9 -2 [pin 1 -> 1]  |  98  +  381  +  29 points |   6958 ->  7466
 15 : File   6  1 [pin 1 -> 2]  |  74  +  292  +  35 points |   7466 ->  7867
 16 : File   7 -1 [pin 2 -> 1]  | 130  +  416  +  30 points |   7867 ->  8443
   .
   .
 21 : File   5  2 [pin 1 -> 2]  | 123  +  273  +  31 points |  10467 -> 10894
 22 : File  10 -2 [pin 2 -> 1]  |  75  +  467  +  32 points |  10894 -> 11468
 23 : File   8  2 [pin 1 -> 3]  | 119  +  348  + 117 points |  11468 -> 12052
 Total tape length :    23.779 m
=======================================================================
```

Figure 5.20: Log file for the robot path

```
--- Error in Robot Path  13 ---
Unable to wind path  13 : file   6 dir -1 [pin 2 -> 1]
Distance between contact point and
                intersection point on surface too small
Reversed       path  15 : file  11 dir  1 [pin 1 -> 2]
Reversed       path  14 : file   9 dir  2 [pin 1 -> 1]
Reversed       path  13 : file   6 dir -1 [pin 2 -> 1]
```

Data on the fibre paths, which are wound, are written in a log file (Fig. 5.20).

5.4.4.5 Simulation

The points of the robot paths are written to a file for simulation (cf. section 6.7.1). If collisions occur during simulation, the position of the winding machine has to be adapted, or the model has to be updated (cf. section 6.7.2).

5.4.4.6 Calculation of the Robot Trajectory

The operator enters the desired maximum velocities ($\dot{\mathbf{q}}_M$), accelerations ($\ddot{\mathbf{q}}_M$) and smoothing errors (ϵ_M) (cf. section 5.3). The program informs the operator on the maximum joint values, and returns the total number of points and the time necessary to wind the path. An example of such a log file is Fig. 5.20. In this example, joint 6 exceeds its upper limit. A valid solution is obtained by the use of an alternative configuration for the robot wrist (i.e. the "noflip" instead of the "flip" configuration [122])

Two output files are generated : the starting file `rt000.dat` and the regime file `rt001.dat`. The starting motion is performed once, the regime motion twice.

The time, necessary to wind the T-piece is relatively long. Especially the motion behind the pin rings at the ends of the cylinder, which is transverse to the winding axis, requires much time. The total time can be reduced by an optimization of the motion behind these pin rings.

5.4.4.7 Program Execution

Both the starting file and the regime file are copied from the VAX-computer to the PC.

```
--- Path Control Data ---

--- Input Data ---
Cycle Time                                    :   0.0288 s
Motion Axes                                   : Joints
Fibre Speed controlled at                     : Impregnation
Velocity (mm/s or deg/s)                      :
  88.1   88.1   95.5  100.0  100.0  186.2  200.0   88.0  100.0
Acceleration (mm/s2 or deg/s2)                :
 100.0  100.0  100.0  430.0  430.0  500.0  200.0  512.0  100.0
Tolerance (mm or degrees)                     :
0.0050 0.0035 0.0045 0.0125 0.0062 0.0134 0.1000 2.0000 10.0000
Output via                                    : NETWORK
Compressed Data Format                        : YES
Max. Number of Files                          :        1
Max. Number of Poses per File                 :    35000
Creation of VAL-II Program ALTER              : NO
Creation of Monitor File                      : NO


Maximum Increment                             :
   506    506    506    859    859    859     6068     3982
Start Position (VAL-II) :  556.38  641.11   -75.93 -60.407  90.000    0.000
Start Position (Joints) :  36.736 -49.203 -173.206   0.000  42.409  175.8567
Minimum Joint Values    :  -7.446 -72.538 -239.848   0.000  16.264   44.4166
Maximum Joint Values    :  52.761  -5.936 -144.871   0.000  87.790  276.7223
Joint 6 out of limits : 276.7223 (limit 270.0000)

--- Output Files ---
 -- Starting File --
 File mypool:rt000.dat :     200 points | time :   1 * cycle_time
 -- Regime File --
 File mypool:rt001.dat :   24684 points | time :   1 * cycle_time

   24684 (Regime) Points Generated
   Total (Regime) Time :  0 h 11 min 50 s
================================================================================
```

Figure 5.21: Log file for the robot trajectory

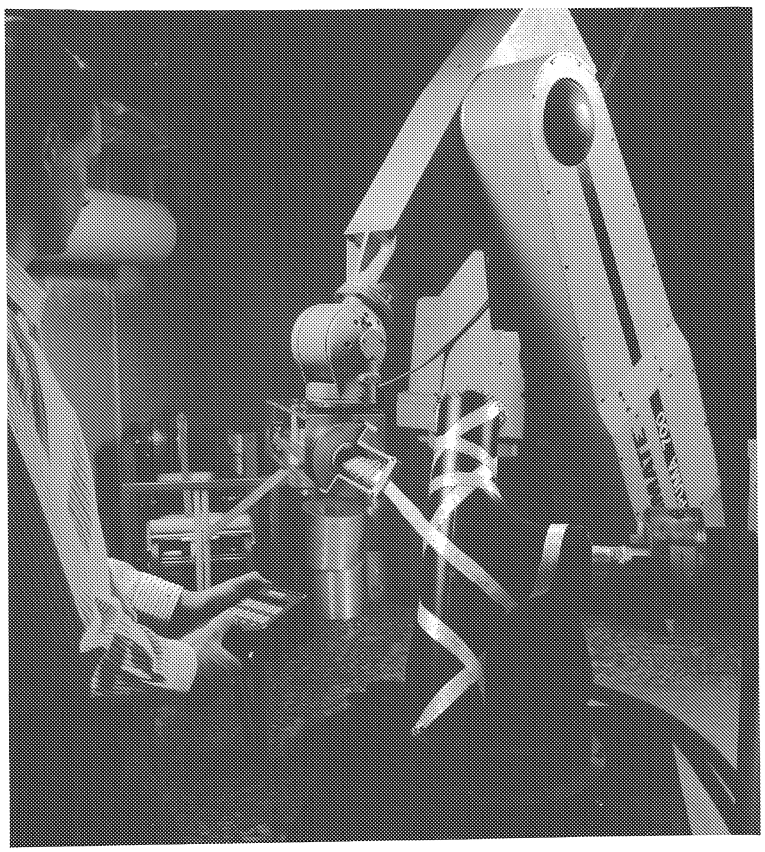

Figure 5.22: Dry winding of a T-piece

The winding process is prepared : the impregnation bath is filled with a mixture of resin and hardener, and the tape is pulled through the pay-out eye. The robot is moved to its starting pose, which can be read in the log file. Both external axes are placed in their starting position. The tape is fixed to the mandrel at the reference position, i.e. at the shaft connecting the mandrel with the headstock, next to the pin rings.

The operator starts first the control program on the PC. The program requests, after reading the starting and the regime file, the operator to start the VAL-II-program, that initiates the ALTER-mode (cf. p. 139), on the robot controller.

A T-piece has been wound, once dry (Fig. 5.23), and once with resin. No major problems occurred. However, the residual twist, which

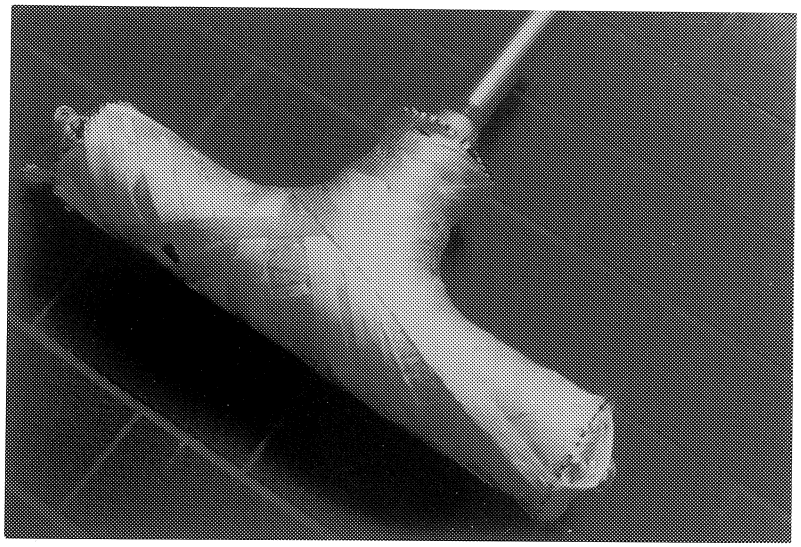

Figure 5.23: Dry wound T-piece

remains in the tape after applying the storage twist behind the pin rings (cf. p. 164), causes sometimes contraction of the tape just behind the pin rings.

5.5 Conclusions

This chapter described the calculation of the robot path and the robot trajectory. The points of the robot path are calculated so, that all the task requirements are fulfilled. Special attention has to be paid to the motion behind the pin rings and the reduction of tape twists. Tape twists are reduced by a combined rotation of the pay-out eye and the mandrel about the winding axis, and by storing excess tape twists behind the pin rings. Another important aspect is collision control, which will be treated separately in chapter 6.

The robot trajectory is calculated so, that the maximum joint velocities and accelerations are not exceeded. The data are converted to an integer format, and transmitted to the PC that controls the winding process.

The calculations have been validated by winding a T-piece.

Chapter 6

Collision Control

6.1 Introduction

Collisions may occur during the winding process in convex/concave parts of the mandrel, during winding around the ends of the mandrel, and if the free length is too small in areas with large radii of curvatures.

A heuristic collision control method has been developed for robotic tape winding. Collision control consists of two main parts : collision detection and collision avoidance. The collisions have to be avoided in such a way, that all the task requirements remain fulfilled.

This chapter describes how collision-free paths are generated. This chapter starts with a literature survey on collision handling in filament winding and robotic collision avoidance. The next section discusses the implementation of collision control in the calculation of the robot path. Collisions are controlled in two stages : in the first stage, collisions are controlled between the pay-out eye and the mandrel in the mandrel coordinate system, in the second stage, a.o. collisions between the robot wrist and the mandrel and collisions between the pay-out eye and the mandrel support structure, are controlled. Not all the collisions, which are possible, are modelled : some rarely occurring collisions are not modelled. To check if these collisions occur, the winding process can be simulated on a graphical robot simulation system.

Section 6.4 discusses the heuristic collision control method. This method consists of the following steps : collisions are checked for all the points of the path, the method, which will be used to avoid collisions, is selected, collision-free poses are calculated, and a smooth collision-free

path is generated. The next sections of this chapter apply this method to the two stages of collision control : first in the mandrel coordinate system, and then in the winding coordinate system. Section 6.7 deals with the simulation of the tape winding process in a robotic simulation system.

6.2 Literature Survey

This literature survey consists of two parts : the first part discusses how collisions are treated in filament winding, the second part gives an overview of collision avoidance in robot programming.

6.2.1 Collision Control in Filament Winding

Collision control in filament winding is mostly restricted to collision detection.

Wells [110] checks on collisions during filament winding by testing if the tangent to the fibre path intersects the mandrel. If an intersection is detected, the fibre path is rejected.

Barking [2] checks, for a surface of revolution, on collisions by checking the distance between the surface and the edge points of the pay-out eye, which moves in a horizontal plane through the winding axis. If this distance is smaller than a safety distance, the free length is increased.

Elliman [28] detects collisions in a robotic filament winding cell during graphical simulation and avoids collisions by the addition of via-points. These via-points will however alter the fibre path : the fibre will slip on the surface, since the fibre stability condition is not necessarily fulfilled.

A common method to determine the position of the delivery point, is to place it on an enveloping surface round the mandrel [47, 115]. Collisions between the mandrel and the pay-out eye cannot occur. But, if the surface has convex/concave parts, the tangent to the fibre path may intersect the mandrel before it intersects the enveloping control surface, so that a collision-free pose cannot be found.

6.2.2 Robotic Collision Avoidance

A lot of research has been done on robot motion planning. The basic problem handled is the *find path* or *generalized movers'* problem, which is the problem of moving a general robot, which can be an articulated robot or a mobile robot, between a starting and a goal pose in an environment filled with obstacles [53].

The problem is solved in the robot's configuration space. The configuration space of a robot with n degrees of freedom is a n-dimensional space, in which each dimension corresponds to a robot joint variable. The robot is represented as a point in its configuration space, and is defined by its joint variables.

The obstacles are expanded to n-dimensional volumes in the robot configuration space, which consist of all the possible robot configurations where collision with the obstacle occurs. The obstacles are mostly represented as closed convex polyhedra in cartesian space [101] to decrease calculation times.

In the configuration space, the problem of finding a path for the robot corresponds to the problem of planning the motion of a point between the "augmented" obstacles. A practical problem is that the dimension of the configuration space, and hence the complexity of the motion planning problem and the calculation time, grows with the number of joints.

Several methods have been developed to solve the find path problem. The methods are based on a few different general approaches : road-map, cell decomposition and potential field [53]. The first two approaches are global methods, and take the complete configuration space into account. The potential field method is a local approach, and needs only local information.

The road-map and the cell decomposition methods reduce the problem of finding a continuous free path to that of searching a graph by first checking the connectivity of the free space. The connectivity is represented in the *road-map* approach as a network of curves. Path planning consists of connecting the initial and the goal configurations to points in the network and by searching for a set of curves of the road-map between the initial and the goal pose [16]. An example of the road-map approach is the *visibility graph* method, in which the obstacles are described as polygons, and the visibility graph is constructed by connecting the vertices of the obstacles with straight lines. A graph

search algorithm is used to find the shortest path in the graph. The visibility graph method has a.o. been implemented for planning the path of a mobile robot at PMA by Song [92].

In the *cell decomposition* approach [9] the robot's free space is decomposed in simple regions, called cells. A connectivity graph, representing the adjacency relation between the cells, is then constructed. A channel, which consists of the consecutive cells of the path, is then searched between the initial and the goal pose [84].

In the *potential field* approach the robot is represented as a point, which moves in the configuration space under the influence of an artificial potential field, produced by the goal configuration and the obstacles. The goal pose generates an "attractive potential", which pulls the robot towards the goal, an obstacle produces a "repulsive potential", which pushes the robot away from it. This method has the disadvantage that it can get trapped in local minima of the potential function other than the goal configuration. The potential field method can be combined with a global method : the potential field method is employed at start and goal poses in the neighbourhood of obstacles, to move away from the obstacles, and a global method is employed to find a path in a low resolution configuration space between the new start and goal pose [60].

Extensions to the basic find path problem are needed in case of the occurrence of non-stationary obstacles, multiple robots, not fully known environment, kinematic constraints... In case of moving obstacles, with known motions, one dimension representing time is added to the configuration space. Multiple (non-cooperating) robots can be handled as one single multi-bodied robot which moves in a composite configuration space, or the motion of each robot is planned more or less independently, and the interactions among the paths are considered in a second phase of planning.

A second problem which is discussed in literature is the planning of redundant robots. The increased number of degrees of freedom can be used to avoid obstacles, while following a specified end-effector path. Solutions of this problem are based on inverse kinematics. Kirćanski [48] handles the collision avoidance problem by formulating an inverse kinematic solution which maximizes the distance between links and obstacles while following a specified path. Buchal [11] formulates the problem as the minimization of a cost functional, in which

violation of constraints and collisions are represented by penalty functions, as in the potential field approach. Nakamura [66] considers the control of redundant robots for a task with different orders of priority. The main task is to follow a path, collision avoidance is a subtask.

The above mentioned methods cannot be used when the end-effector has to make contact with the object, as e.g. during milling and surface measuring. Undesired collisions and the desired touch have to be accurately distinguished. Heuristics have been developed for collision avoidance in specific tasks. Yau [112] uses a heuristic method to plan the motion of the probe of a 3D-CMM-machine. Suh [90] developed a heuristic to avoid tool-surface collisions in four-axis milling.

6.3 Collision Control in Robotic Tape Winding

The main difference between the find path problem and filament winding is that the path between starting and goal pose cannot be chosen freely in case of filament winding.

The task requirements, which are described on p. 148, have to be fulfilled continuously during winding, to avoid changes in the fibre path. These requirements can be easily expressed in cartesian space, not in joint space. Motion planning is therefore performed in cartesian space.

The task requirements do not determine the position of the payout eye completely, but fix only three variables (two for the tangent and a third for the orientation of the delivery rolls). Three degrees of freedom (the free length and two rotations) can be used to avoid collisions.

A heuristic method has been developed to avoid collisions during the tape winding process. The method itself will be discussed in section 6.4. This section deals with the various collisions which are modelled, the modelling of the objects which can collide, and on the implementation of collision control in the tape winding process.

6.3.1 Types of Collisions Modelled

The robotic cell consists of two major structures : the robot and the mandrel structure. The robot structure consists of the robot trunk,

the robot elbow, the robot wrist and the pay-out eye. The mandrel structure can be divided in a rotating and a fixed structure. The rotating mandrel structure consists of the mandrel, the pin rings, the mandrel shaft, the chuck and the centre point (Fig. 6.1). The fixed mandrel structure consists of head- and tail-stock.

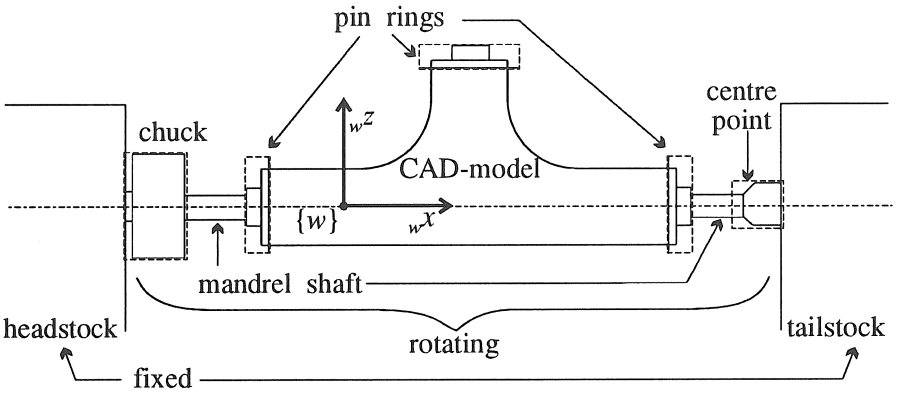

Figure 6.1: Model of the mandrel and the mandrel support structure

The collisions which are most likely to occur during tape winding are interactions between the robot structure and the mandrel structure. Other possible collisions are robot – tool interactions (e.g. between the entry of the pay-out eye and the arm or the trunk of the robot).

The collision control method, which is developed, is limited to the most frequently occurring collisions, viz. collisions between the robot structure (pay-out eye and robot wrist) and the mandrel structure (mandrel and head- and tail-stock). The robot arm and the trunk are not included in the model of the robot structure. Collisions between the robot arm or trunk with the mandrel or the pay-out eye are not modelled. These collisions can be checked by a simulation with a graphical simulation system, e.g. IGRIP.

6.3.2 Environment Model

A model of the filament winding machine and the mandrel is necessary for collision control. This model should be simple enough to avoid long calculation times. The model must be "safe", i.e. all the possible collisions, which the model takes into consideration, must be detected,

but, if a solution is possible in the real world, the program must always be able to find a solution,

Most approaches use polyhedra [53, 101] to model the environment. For rotating objects the use of cylindrical objects is however more appropriate.

The geometries which are employed in the collision control module include cylinders, planes and general surfaces.

6.3.2.1 Mandrel Model

The rotating mandrel structure is composed of (Fig. 6.1) :

- the surfaces of the CAD-surface model. The data of these surfaces are read from the IGES-file (cf. section 2.6.1).
- the pin rings, which are attached at the ends of the mandrel. The pin rings are represented as cylinders, with as length the distance between the pins and the outer edge of the mandrel, and as radius the outer radius of the pins.
- the mandrel shaft, that attaches the mandrel to the chuck and the centre point.
- the chuck and the centre point, which are modelled as cylinders.

The cylinders representing pin rings, chuck and centre point have also an end plane, which is taken into account during collision detection and avoidance.

6.3.2.2 Mandrel Support Structure Model

In the configuration, which is used in this work, the robot is positioned in the half space ${}_w y < 0$ (Fig. 6.2).

Head- and tail-stock are modelled as quarter spaces, and are defined by a front, a side and a top plane (Fig. 6.2). If the mandrel is only supported at the chuck, the tailstock can be removed. The geometry of the headstock is given by the inequalities : ${}_w x \leq x_{s1}$, ${}_w y \geq -y_s$, ${}_w z \leq z_s$. The geometry of the tailstock is : ${}_w x \geq x_{s2}$, ${}_w y \geq -y_s$, ${}_w z \leq z_s$. The edge of the headstock, nearest to the robot base, is given by the line $L_{s1} = (p_{s1}, -\vec{z})$ with ${}_w\mathbf{p}_{s1} = [x_{s1} \quad -y_s \quad z_s]^T$ and $\vec{z}$ directed vertically upwards $({}_w\mathbf{z} = [0 \quad 0 \quad 1]^T)$.

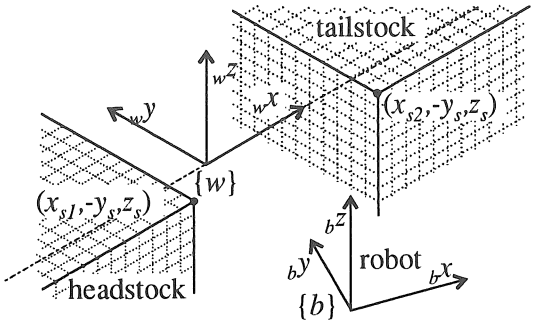

Figure 6.2: Head- and tail-stock

6.3.2.3 Pay-out Eye Model

The pay-out eye is modelled as a cylinder (Fig. 6.3). The pay-out eye resembles in reality more a beam, but a cylinder has the advantage that its geometry is not influenced by a rotation about its axis. As a consequence, the orientation of the delivery rolls does not influence the collision control. The position of the pay-out eye can therefore be described by a line.

The pay-out cylinder has as axis the line $L_e = (be, \vec{v})$ and as radius r_e. be is the base point of the pay-out cylinder, and lies on a distance d_r from the reference delivery point re (Fig. 6.3).

The dimensions of the pay-out cylinder are increased, to take the variations in the position of the delivery point e into account (cf. section 5.2.4). The pay-out eye radius r_e and the distance d_r are increased with the maximum deviations between the position of e and re.

6.3.2.4 Robot Model

The robot is not able to reach every point in space. The theoretical working envelope of the centre of the wrist rw of the PUMA-762 is a sphere, with center b and radius $r_r = 1263$ mm, a small cylinder round the base of the robot excluded [8]. The actual working envelope of the robot is smaller than the theoretical working envelope, due to the limits on the joints (Fig. 6.4). The limits on the joints are not taken into account for the collision control module.

The program can be adapted to other robots or winding machines, by adapting the routines for checking and controlling the attainability

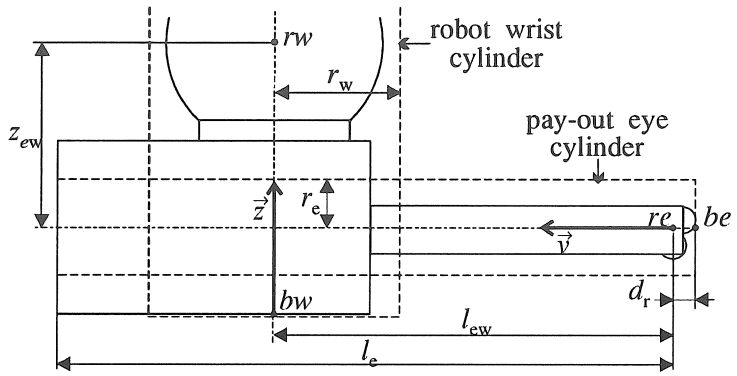

Figure 6.3: Model of the pay-out eye and the robot wrist

of the pay-out eye pose, and the direct and inverse kinematic routines, which are used for the calculation of the robot trajectory (section 5.3.1).

The robot wrist is modelled as a cylinder in the collision control module. The base of this cylinder is extended to the bottom of the attachment of the pay-out eye (point bw) (Fig. 6.3). The cylinder has as axis the line $L_w = (bw, \vec{z})$.

6.3.3 Two Stage Collision Control Strategy

The collisions, which are described in section 6.3.1, can be divided in two classes : collisions which are independent of the angle of the winding axis and collisions which are dependent of the angle of the winding axis. The first class consists of the collisions between the pay-out eye and the rotating mandrel structure, the second class of all the other collisions (collisions between robot wrist and mandrel, collisions with head- and tailstock,...).

The first class of collisions are the most frequent, since the delivery point of the pay-out eye e moves at a relative short distance from the mandrel. These collisions are the most critical : in the extreme case, the pay-out axis has to be aligned with the normal on the surface. These collisions are avoided in the mandrel coordinate system $\{m\}$.

The other collisions depend on the angle φ of the winding axis, and have to be avoided in the winding coordinate system $\{w\}$.

Collision control is therefore performed in two stages : first, colli-

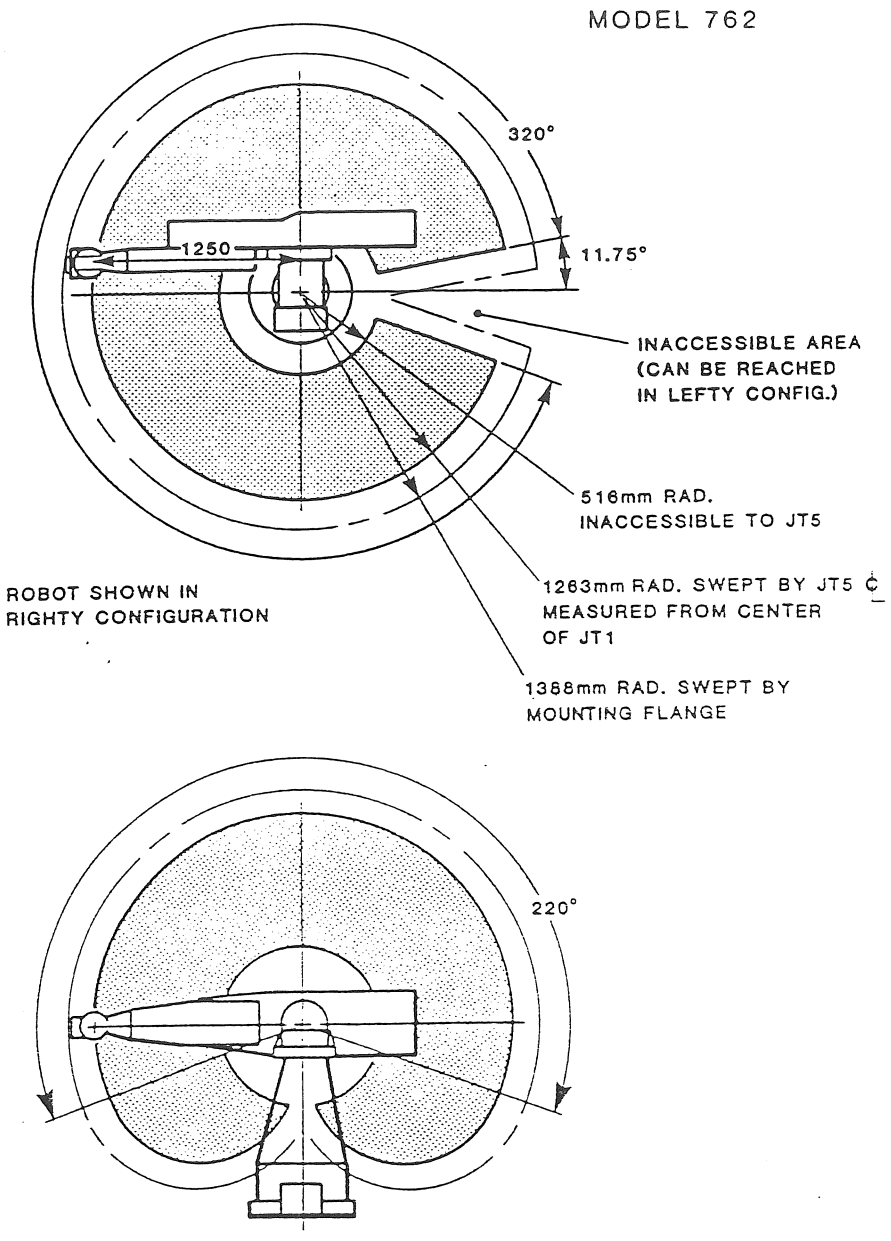

Figure 6.4: Working Envelope of the PUMA-762 (configuration with arm right)

sions between mandrel and pay-out eye are controlled in the mandrel coordinate system, then, after determining the angular position of the winding axis, the rest of the collisions are controlled in the winding coordinate system. After the calculation of the robot path, a robot simulation system can be used to check on collisions which are not comprised in the model.

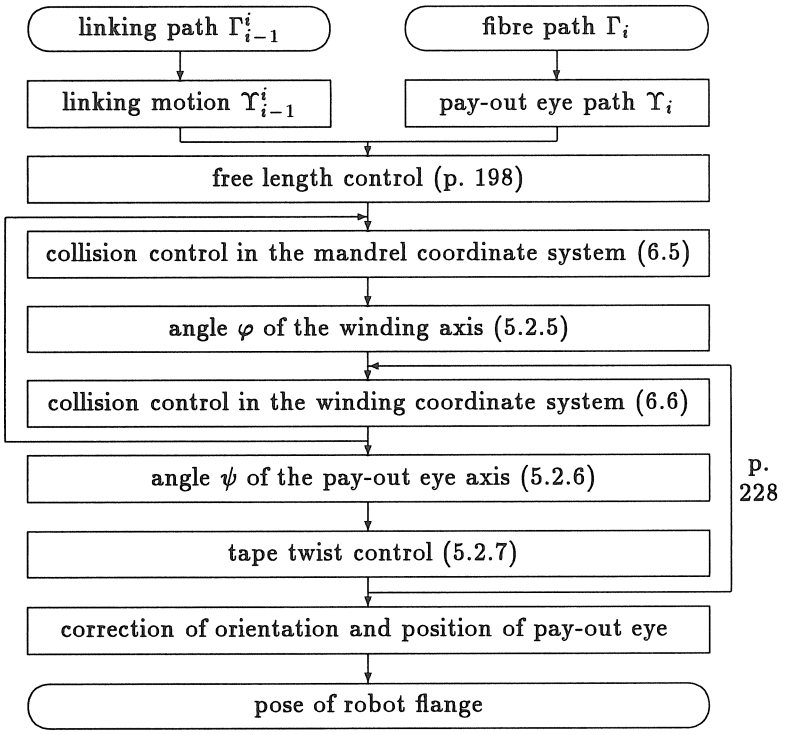

Figure 6.5: Consecutive steps in the calculation of the collision-free robot path

In the previous chapter, the consecutive steps in the calculation of the robot path are represented in Fig. 5.3, without taken collision control into account. Fig. 6.5 gives the consecutive steps in the construction of a collision-free robot path : the alternative method in Fig. 5.3 is used, and the collision control modules are added to the scheme.

6.3.3.1 Collision Control in the Mandrel Coordinate System

Collisions between the pay-out eye and the rotating mandrel structure (i.e. CAD-surfaces + pin rings + axis + chuck + centre point) are avoided in the mandrel coordinate system. The delivery point must always lie on the tangent to the fibre path. Collisions are avoided by changing the free length or the orientation of the pay-out eye. The free length l_f has a minimum value to avoid folding of the tape (cf. p. 148), and a maximum value, if the tangent to the fibre path intersects the mandrel. No rewinding is allowed. The angle between the tangent $\vec{t}$ and the pay-out axis $\vec{v}$ may not exceed 90° (or : the angles γ_z and γ_y (cf. p. 158) must be smaller than 90°).

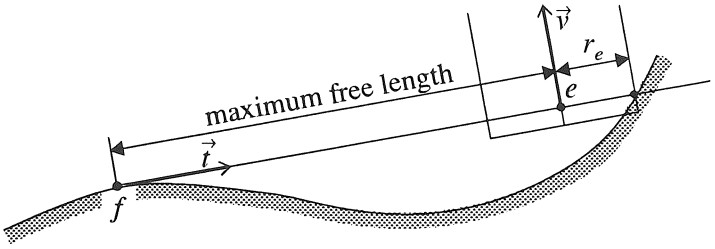

Figure 6.6: Maximum distance between the contact point on the mandrel f and the delivery point e

Before controlling collisions, the maximum free length is determined in each point of the fibre path. For each point, intersections between the tangent to the fibre path and the mandrel are checked. The maximum free length equals the distance between the point of the fibre path and the intersection point with the mandrel minus the pay-out eye radius r_e (Fig. 6.6). The free length in the previous points of the path is then also limited to avoid rewinding. If the proposed free length (cf. section 5.2.2.1) is larger than the allowed free length, a new pose for the pay-out eye is calculated. The free length in the end point of the robot path Υ_i is limited, to avoid rewinding during the next linking motion Υ_i^{i+1}.

6.3.3.2 Collision Control in the Winding Coordinate System

Collisions between the robot wrist and as well the rotating as the fixed mandrel structure (head- and tail-stock), and collisions between the

pay-out eye and both head- and tail-stock are avoided in the winding coordinate system. The pose of the pay-out eye is also adapted when the pose cannot be attained by the robot.

The delivery point e must lie on the tangent to the fibre path, and the pay-out axis must be horizontal (cf. p. 130). The pose of the pay-out eye is adapted by changing the free length, the orientation of the pay-out axis, or the angle of the winding axis.

After collision control in the winding coordinate system, the collision control in the mandrel coordinate system is repeated, to avoid collisions between the mandrel and the altered pay-out eye poses (Fig. 6.5).

The collision control in the winding coordinate system is also performed during the control of tape twisting, if excess twists have to be removed by a combined rotation of pay-out eye and mandrel about the winding axis (cf. p. 228).

The calculations of the orientation of the delivery rolls (angle ψ_c) and the position of the reference delivery point re are performed after twist control (cf. alternative method in Fig. 5.3).

6.4 Heuristic Collision Control Method

A heuristic collision control method has been developed. This section gives a general overview of the method, while the next sections will discuss the implementation of the method in the two stages of collision control : section 6.5 will discuss the collision control in the mandrel coordinate system, section 6.6 the collision control in the winding coordinate system.

Fig. 6.7 gives the different steps of the collision control method. First, each point is checked on collisions. The methods used to detect collisions, are described in section 6.4.1. For each zone of the path, where collision occurs, the collision mode, i.e. the method which will be used to avoid collisions, is determined. There are two main collision modes : scratching and perforating, which will be discussed in section 6.4.2. The next step is then the generation of collision-free poses. For all points collisions are checked. The geometrical information on the collisions is than further used to avoid the collisions. Collisions are classified in several types. For each collision type and each different avoidance method (adapting free length, adapting orientation of

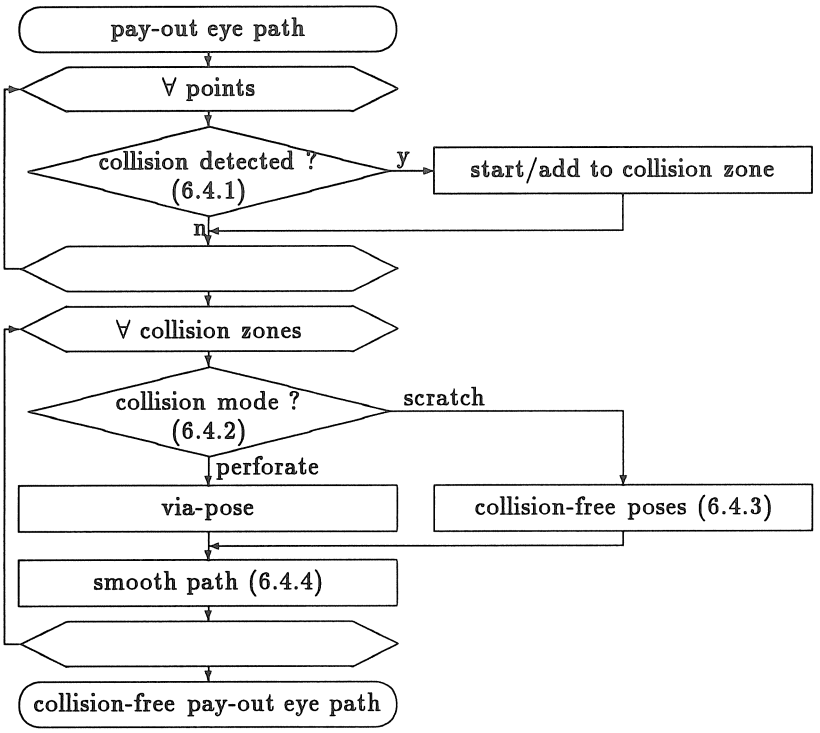

Figure 6.7: Consecutive steps in the heuristic collision control method

the pay-out eye, adapting the angle of the winding axis), a separate collision avoidance routine has been written. Collision avoidance will be discussed generally in section 6.4.3, and the individual collisions avoidance routines in section 6.5.3 for the mandrel coordinate system and in section 6.6.3 for the winding coordinate system. In the last step, a smooth collision-free path is generated. The generation of the smooth path is discussed in section 6.4.4.

6.4.1 Collision Detection Methods

Collisions are detected between, on the one hand, the pay-out eye or the robot wrist, and, on the other hand, the rotating or the fixed mandrel structure. Both pay-out eye and robot wrist are modelled as cylinders. This cylinder will further be called the tool. The tool is defined by its axis $L_1 = (p_1, \vec{v_1})$, and has as length l_1 and as radius r_1.

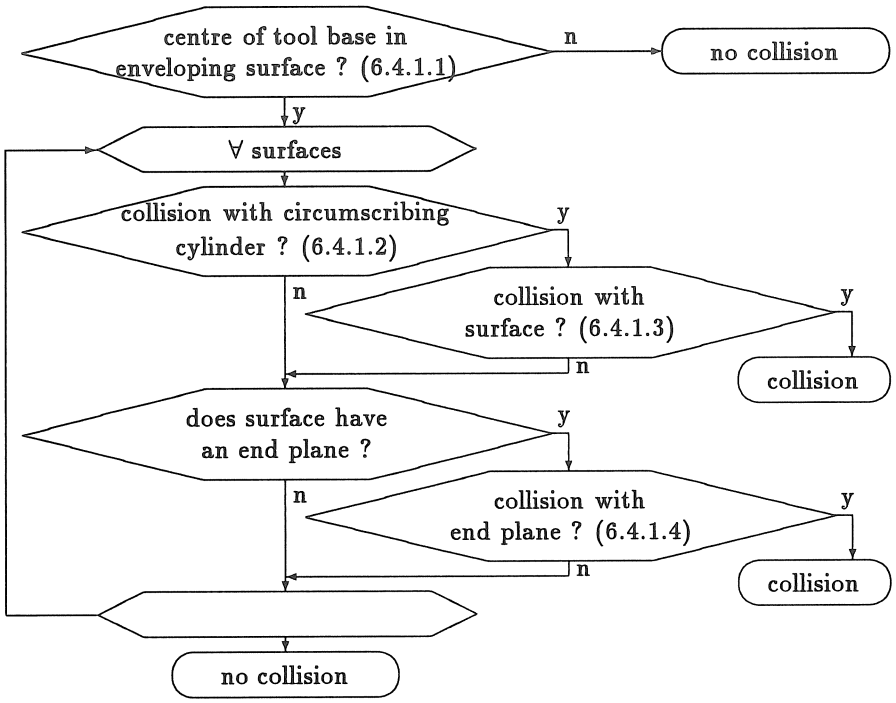

Figure 6.8: Steps in collision detection

Four steps can be distinguished in collision detection between the tool and the mandrel structure (Fig. 6.8) :

- Test if the centre of the tool base p_1 lies within an enveloping surface round the mandrel. If p_1 lies outside the enveloping surface, no collision can occur.
- Test if the tool axis intersects a rough model of the object, viz. a circumscribing cylinder.
- Test if the tool collides with an accurate model of the object.
- Test for collisions between the tool and an end plane of the surface (e.g. of a pin ring or chuck)

Collisions are characterized by the collision type (collision between tool base and mandrel surface, collision between tool base and end plane, collision between robot wrist and mandrel,...), the intrusion

depth d_c, the surface parameters u_c and v_c at the collision point and the tool parameter λ_c, i.e. the parameter along the axis of the tool[1]. The corresponding collision points are c_t on the tool axis and c_s on the surface.

6.4.1.1 Enveloping Surface

An enveloping surface around the mandrel is a surface, which is defined in such a way, that, if p_1, the starting point of the tool axis, lies outside the enveloping surface, no collisions can occur between the tool and the surface, and that, if p_1 lies in the enveloping surface, collisions can occur. An enveloping surface can only be constructed if the orientation of the vector $\vec{v_1}$ is limited, e.g. if $\vec{v_1}$ is normal to the winding axis. An enveloping surface can therefore not be constructed for the pay-out eye in the mandrel coordinate system, since its orientation can be chosen almost freely.

An enveloping surface can be constructed for the robot wrist, since the direction of the normal on the robot flange is fixed. The construction of this enveloping surface is discussed in section 6.6.1.2.

6.4.1.2 Collision between Tool and Circumscribing Cylinder

Collisions between the tool and a general surface is performed in two steps : first with a rough model, viz. the circumscribing cylinder of the mandrel, and then with the more accurate model (cf. Fig. 6.8).

Collisions between the tool (cylinder) and the circumscribing cylinder are tested by checking the distance between the axes of the two cylinders. The distance d between two lines $L_1 = (p_1, \vec{v_1})$ and $L_2 = (p_2, \vec{v_2})$ equals :

$$d = \|(\vec{r}_{p_1} + \lambda_1 \vec{v_1}) - (\vec{r}_{p_2} + \lambda_2 \vec{v_2})\| \tag{6.1}$$

$$\text{with} \quad \lambda_1 = \frac{(\vec{r}_{p_1} - \vec{r}_{p_2}) \cdot (\vec{v_1} - (\vec{v_1} \cdot \vec{v_2})\, \vec{v_2})}{(\vec{v_1} \cdot \vec{v_2})^2 - 1}$$

$$\lambda_2 = \frac{(\vec{r}_{p_1} - \vec{r}_{p_2}) \cdot ((\vec{v_1} \cdot \vec{v_2})\, \vec{v_1} - \vec{v_1})}{(\vec{v_1} \cdot \vec{v_2})^2 - 1}$$

with λ_1 and λ_2 the parameter along the line. If $\lambda_1 < 0$ or $\lambda_1 > l_1$, the distance between the two axes amounts to the distance between,

[1] in the mandrel coordinate system : $\lambda_c = 0$ in *be*, the base of the pay-out eye

respectively, the starting or end point[2] of L_1 and the line L_2.

If the distance d is smaller than the sum of the radii of the cylinders, the tool can collide with the surface, and the more accurate test is performed.

6.4.1.3 Collision between Tool and Surface

Collisions between the tool and a surface are checked by calculating the distance d_{ls} between the surface and the tool axis of the cylinder, measured normal to the tool axis[3]. Collision occurs if d_{ls} is smaller than r_1, the radius of the tool. The distance d_{ls} between the tool axis L_1 and a surface S equals the minimum of the distance between a point s on the surface S and its projection q on the tool axis L_1 (Fig. 6.9). The position of q is :

$$\vec{r}_q = \vec{r}_{p_1} + \lambda \vec{v}_1 \quad \text{with} \quad \lambda = (\vec{s}(u,v) - \vec{r}_{p_1}) \cdot \vec{v}_1 \tag{6.2}$$

The distance d_{ls} equals :

$$d_{ls}^2 = \min_{u,v} f(u,v) \tag{6.3}$$

$$\text{with} \quad f(u,v) = \|\vec{r}_{p_1} + \lambda \vec{v} - \vec{s}(u,v)\|^2 + g(\lambda) \tag{6.4}$$

$$\text{and} \quad g(\lambda) = \begin{cases} k\lambda^2 & \lambda < 0 \\ 0 & 0 \leq \lambda \leq l_1 \\ k(\lambda - l_1)^2 & l_1 < \lambda \end{cases}$$

The function $g(\lambda)$, with k a constant value[4], forces the solution towards the interval $0 < \lambda < l_1$. Due to $g(\lambda)$, $f(u,v)$ has continuous derivatives, and the minimum can numerically be searched with the routine E04LBF of the NAG-library. This routine uses a comprehensive modified Newton algorithm to find the minimum of a function of several variables [121].

6.4.1.4 Collision between Tool and End Plane

Some surfaces – viz. the pin rings, the chuck and the centre point – have a bounded end plane $\mathcal{P}$, the boundary of which is formed by the

[2] In this way, a half sphere at the ends of the cylinders is taken into account

[3] If the distance between the axis and the surface, measured normal to the surface would be calculated, a half sphere at the end of the tool would be taken into account

[4] in CAWAR : $k = 100$

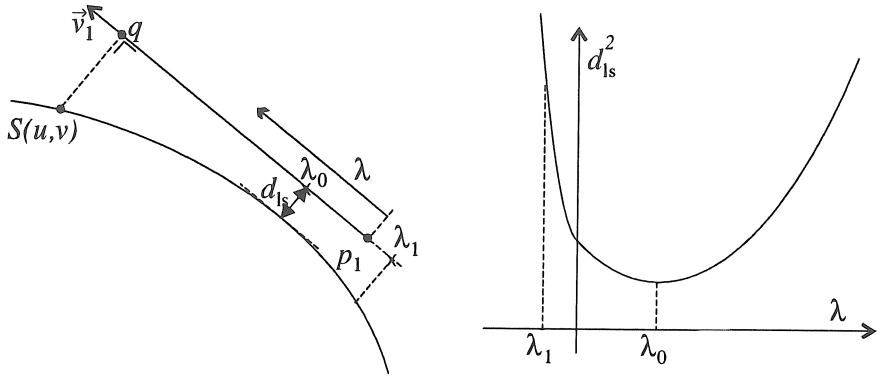

Figure 6.9: Distance between a line and a surface

edge of the surface. The points p of the end plane meet the equation $\vec{r}_p \cdot \vec{a} = b$ with $\vec{a}$ the (outwards directed) normal to the plane, and b a constant.

Several collisions can be distinguished between the tool, and the end plane $\mathcal{P}$:

- The tool axis $L_1 = (p_1, \vec{v_1})$ can cut the end plane prior to the CAD-surface. The intersection point c $(\vec{r}_c = \vec{r}_{p_1} + \lambda_c \vec{v_1})$ is defined by :

$$(\vec{r}_{p_1} + \lambda_c \vec{v_1}) \cdot \vec{a} = b \quad \text{or} \quad \lambda_c = \frac{b - \vec{a} \cdot \vec{r}_{p_1}}{\vec{a} \cdot \vec{v}_1} \tag{6.5}$$

  The intersection point must lie within the boundary of the end plane. The vector $\vec{v}_1$ has to be directed opposite to $\vec{a}$, so that the plane is cut first, or : $\vec{a} \cdot \vec{v}_1 < 0$.

- The tool mantle can hit the edge of the plane. This case is discussed in section 6.4.1.3.

- The base of the tool cylinder can hit the end plane. This is done by checking the distance between the plane and the point c, i.e. the point on the edge of the base plane which is the nearest to the plane (Fig. 6.10). The point c is given by :

$$\vec{r}_c = \vec{r}_{p_1} - r_1 \frac{\vec{a} - (\vec{a} \cdot \vec{v}_1)\,\vec{v}_1}{\|\vec{a} - (\vec{a} \cdot \vec{v}_1)\,\vec{v}_1\|} \tag{6.6}$$

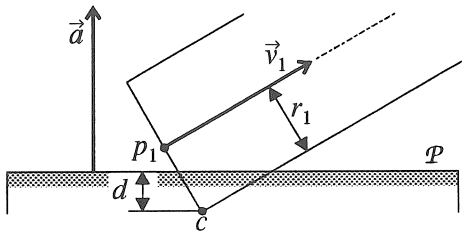

Figure 6.10: Intersection between the base of the tool and an end plane

with r_1 the radius of the tool. The distance between c and the plane equals :

$$d = \vec{r}_c \cdot \vec{r}_a - b \tag{6.7}$$

Collision occurs if $d < 0$ and if c lies within the boundary of the end plane (as in Fig. 6.10)

6.4.2 Selection of the Collision Avoidance Method

The first step in collision control is collision detection. Each point of the path is checked on collisions. This result in a set of collision zones (Fig. 6.7). Before searching for collision-free positions, the method which will be used to avoid collisions is determined.

6.4.2.1 Collision Modes : Scratching and Perforating

A distinction is made between scratching and perforating of an object (Fig. 6.11). Suppose that for each point of the collision zone, collision-free poses are calculated. The collision-free poses are linked by a path Υ^*.

If the path Υ^* is continuous, a collision-free path Υ^s can be obtained by smoothing the path Υ^*. This is the *scratching* mode.

In the *perforating* mode, the path Υ^* has a discontinuity in the middle of the collision zone. The path Υ^* is not collision-free in the discontinuity. Attempts to generate a smooth collision-free path, starting from the initial path Υ^*, will often result in an increasing deviation from the original path, failing to return to the original path. The perforating mode requires therefore the use of a via-pose in the middle of the collision zone.

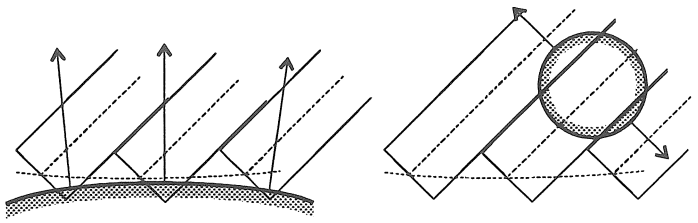

Figure 6.11: Collision modes
(a) Scratching (b) Perforating

In the mandrel coordinate system, perforating occurs when the tool moves through a surface. The pay-out eye can e.g. move through the shaft, which links the mandrel to the chuck, at the start of a fibre path at one of the (eccentric) pin rings (Fig. 6.12).

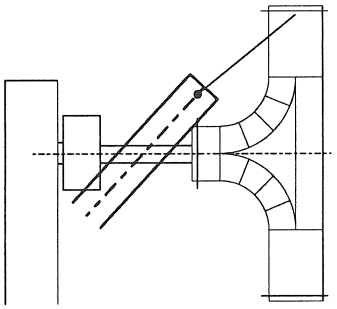

Figure 6.12: Collision between the pay-out eye and the mandrel shaft during the linking motion behind the pin rings of a T-piece

In the winding coordinate system, perforating occurs when the pay-out eye moves behind the mandrel (i.e. in the half space ${}_w y > 0$). Perforating is characterized by a discontinuity in the angle φ about the winding axis.

Perforating can, in the winding coordinate system, also lead to an additional rotation of 180° or 360° at the end of the collision zone.

6.4.2.2 Selection of the Adaptation Method

Collisions can be avoided by changing the free length, the orientation of the pay-out eye or the angle of the winding axis. The adaptation

method, which will be used to avoid collisions, has to be determined prior to the calculation of the collision-free poses.

During collision control in the mandrel coordinate system, a set of tests is used to determine the adaptation method (cf. section 6.5.2.2). During collision control in the winding coordinate system, adaptations are made hierarchical : first the orientation of the pay-out eye is adapted, then the angle of the winding axis, and then the free length (cf. section 6.6.2.2).

6.4.3 Collision Avoidance for a Single Pose

For each different type of collision (e.g. collision between the mantle of the pay-out cylinder and a surface, collisions between the robot wrist and the front plane of head- or tailstock,...) and each different adaptation method (e.g. adapt the free length, adapt the angle of the winding axis) a different collision avoidance routine is developed. These routines use the geometrical information of the collision and the surfaces to calculate a new pose. These routines change the position or the orientation of the pay-out eye so, that the distance between the pay-out eye and the (approximated) surface amounts to the safety distance δ_s. The different collision avoidance routines are discussed more in detail in section 6.5.3 for the collision control in the mandrel coordinate system and in section 6.6.3 for the collision control in the winding coordinate system.

Collisions are avoided iteratively. After the calculation of a new pose of the pay-out eye, collisions are checked again. If collision still occurs, a new pose is calculated, based on the new collision information. The safety distance δ_s is increased at each iteration. If after a maximum number of iterations[5] no solution has been found, the path is said to be unwindable, and the calculations of the path are stopped.

6.4.4 Generation of a Smooth Path

This section discusses the last step of the collision control method : the smoothing of the path (Fig. 6.7). The collision-free path Υ^s should be

[5]The maximum number of iterations is 20 during the collision control in the mandrel coordinate system and 5 during the collision control in the winding coordinate system

as smooth as possible, and remain as close as possible to the original path, or pass through the via-pose in the middle of the collision zone.

6.4.4.1 Correction

The deviations between the frames $\{e\}$ of the original path and the frames $\{e^*\}$ of the adapted path are characterized by the corrections c. The correction c has several components, which depend on the type of collision control.

During the collision control in the mandrel coordinate system the correction relates the pay-out axis to the Frenet-trihedron $\{f\}$. The correction has three components : the free length l_f, and the Euler angles γ_z and γ_y (cf. p. 158).

During the collision control in the winding coordinate system, the correction components are : the free length l_f, the angle τ for the orientation of the pay-out eye (cf. p. 224), and the angle φ of the winding axis.

6.4.4.2 Parabolic Path

In order to obtain a smooth path, a parabolic function is selected for the correction in function of the fibre path length s. In the most occurring case (and if only one component of the correction is considered), the correction path starts with a correction $c_{lim,-1} = 0$ with zero derivative, i.e. tangent to the original path Υ, reaches a maximum at $s = s_M$, and ends with a correction $c_{lim,1} = 0$ with zero derivative (Fig. 6.13). This path consists of 3 parabola (a convex parabol in the middle and two concave parabola at the ends).

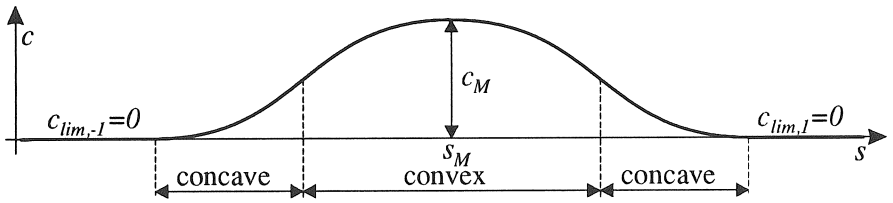

Figure 6.13: Parabolic smoothing path (in continuous domain and 1 correction component)

The parabolic path is discretized, and only evaluated at the points

j, which correspond to points with constant fibre path length interval Δs. The correction in a point j is (Fig. 6.14) :

$$\mathbf{c}_j = \mathbf{c}_{j-1} + \Delta\mathbf{c}_j = \mathbf{c}_{j-1} + \Delta\mathbf{c}_{j-1} + \Delta^2\mathbf{c}_j = \mathbf{c}_j^r + \Delta^2\mathbf{c}_j \qquad (6.8)$$

with $\Delta\mathbf{c}_j = \mathbf{c}_j - \mathbf{c}_{j-1}$ the difference in j, and $\Delta^2\mathbf{c}_j = \Delta\mathbf{c}_j - \Delta\mathbf{c}_{j-1}$ the second difference in j. The correction $\mathbf{c}_j^r = \mathbf{c}_{j-1} + \Delta\mathbf{c}_{j-1}$ is called the reference correction in j.

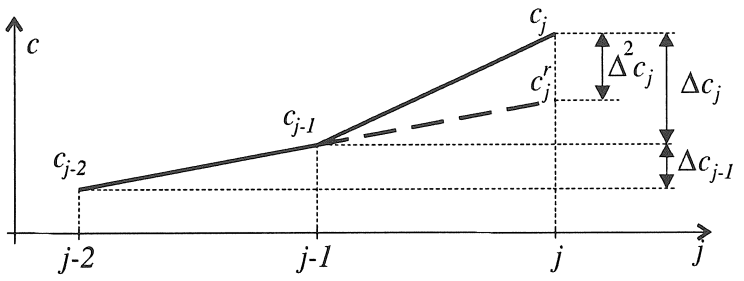

Figure 6.14: Correction path (if the correction has only 1 component)

The requirement that the second derivative in the continuous path is limited, is for the discrete path translated into the requirement that the second difference[6] is limited to ϵ, or, for all components k of the correction :

$$\forall k \;:\; |\Delta^2 c_{j,k}| \leq \epsilon_k \qquad (6.9)$$

This can, with (6.8), be written as :

$$\forall k \;:\; |c_{j,k} - c_{j,k}^r| \leq \epsilon_k \qquad (6.10)$$

From a starting point j_M onwards, the difference is in each point j increased with the maximum second difference ϵ, as long as the maximum difference $\Delta\mathbf{c}_{max}$, which is allowed to reach the limit values with minimum second difference $-\epsilon$, is not exceeded.

This will be illustrated for the most simple case : the correction $\mathbf{c}$ has only one component, the correction path starts (in positive direction) at the point j_M with a (positive) correction c_M and difference $\Delta c_M = 0$. The limit values are $c_{lim,1} = 0$ and $\Delta c_{lim,1} = 0$ (Fig. 6.15).

[6]The program CAWAR uses as maximum second difference : 8.10^{-5} m for the free length, $8.10^{-5}/l_{ew}$ for the rotation of the pay-out eye (with l_{ew} the distance (in meter) between re and the axis of the robot wrist cylinder (Fig. 6.3)) and $8.10^{-5}/l_{fu}$ for the angle of the winding axis (with l_{fu} the desired free length (in meter))

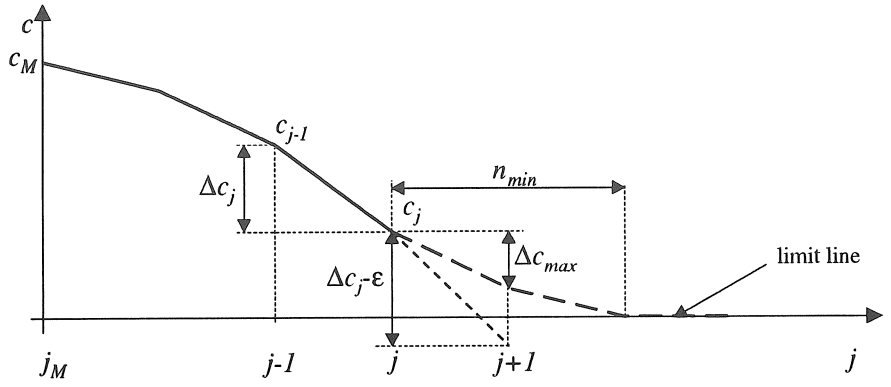

Figure 6.15: Parabolic smoothing path

At each point the difference is decreased with the maximum second difference ϵ. The correction c_j in j is then :

$$c_j = c_{j-1} + \Delta c_{j-1} - \epsilon \tag{6.11}$$

Or, if $j = j_M + n$:

$$c = c_M - \frac{n(n+1)}{2}\epsilon \tag{6.12}$$

The proposed difference in $j+1$ is $\Delta c_{j+1} = \Delta c_j - \epsilon = -(n+1)\epsilon$. This value is compared with the maximum difference Δc_{max} in $j+1$ allowed to reach the limit correction value $c_{lim,1} = 0$ with minimum second difference $-\epsilon$ (Fig. 6.15). The minimum number of points n_{min}, needed to reach $c_{lim,1}$ with zero difference, is derived from Eq. (6.12) (while replacing c_M by $c_{lim,1}$) :

$$n_{min} = \frac{1}{2}\left(-1 + \sqrt{1 + \frac{8|c_j|}{\epsilon}}\right) \tag{6.13}$$

The maximum (negative) difference is then :

$$\Delta c_{max} = -n_{min}\epsilon = -\frac{\epsilon}{2}\left(-1 + \sqrt{1 + \frac{8|c_j|}{\epsilon}}\right) \tag{6.14}$$

If the difference Δc_{j+1} is more negative than Δc_{max}, Δc_{max} is the new difference (Fig. 6.15).

In the previous example, the limit conditions were $c_{lim,1} = 0$ and $\Delta c_{lim,1} = 0$. During smoothing, a smoothing line $L_{j_o} = (c_{j_o}, \Delta c_{j_o})$ $(c_j = c_{j_o} + \Delta c_{j_o}(j - j_o))$ is often given as end conditions. Eq. (6.14) is (in positive direction) then replaced by :

$$(\Delta c - \Delta c_{j_o})_{max} = \frac{-\sigma_\Delta \epsilon}{2}\left(-1 + \sqrt{\frac{1 + 8|c_{j_o} - c_j + (j_o - 1 - j)\Delta c_{j_o}|}{\epsilon}}\right) \tag{6.15}$$

with $\sigma_\Delta = \text{sign}(c_{j_o} - c_j + (j_o - 1 - j)\Delta c_{j_o})$

6.4.4.3 Smoothing Algorithm

The path is smoothed with an iterative algorithm (Fig. 6.16). Starting from a set of starting conditions (the point j_M and its correction $\mathbf{c}_M$ and difference $\Delta\mathbf{c}_M$), a parabolic path is proposed, as discussed in the previous section. Each point is checked on collisions, and, if collision occurs, a new correction is proposed (Fig. 6.17). The path is calculated (both in positive ($\sigma = 1$) and negative ($\sigma = -1$) direction), until the end conditions are satisfied.

If, for each point of the path, the second difference lies within the allowed bounds (cf. Eq. 6.9), the smoothing process is halted. Else, a new iteration is performed.

During the first iteration, smoothing is performed towards the limit line $L_{lim,\sigma}$. For the next iteration, smoothing is performed towards the smoothing line $L_{opt} = L_{j_{o,\sigma}}$, formed by the correction $\Delta\mathbf{c}_{j_{o,\sigma}}$ and the difference $\Delta\mathbf{c}_{j_{o,\sigma}}$ in $j_{o,\sigma}$, the last point of the path where Eq. 6.9 is not fulfilled during the previous iteration (Fig. 6.16).

The smoothing routine takes all the task requirements into account, including the limitation of γ_z and γ_y to 90° and the ban on rewinding (cf. p. 198).

At each iteration loop the maximum second difference ϵ is increased, so that a collision-free path is easier to obtain.

Starting Conditions In the scratching mode, collision-free poses and the corresponding corrections $\mathbf{c}_j$ are calculated at each point j of the collision zone (Fig. 6.16). The point j_M, where the correction is maximal, is chosen as the starting point for the smoothing path. The starting correction corresponds to the correction $\mathbf{c}_M$ at the starting point. The limit conditions are always $L_{lim,-1} = L_{lim,1} = (\mathbf{0}, \mathbf{0})$.

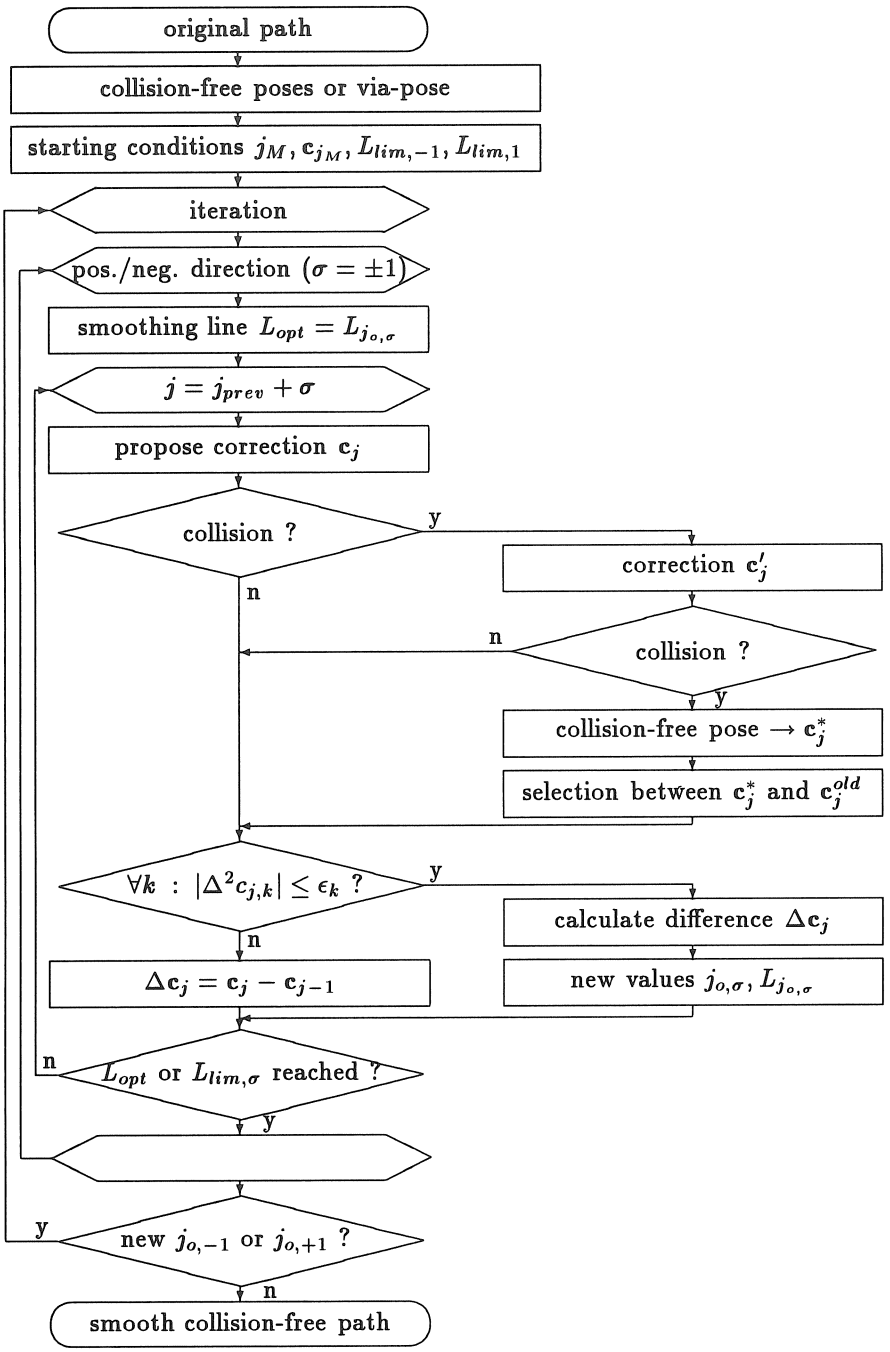

Figure 6.16: Smoothing Algorithm

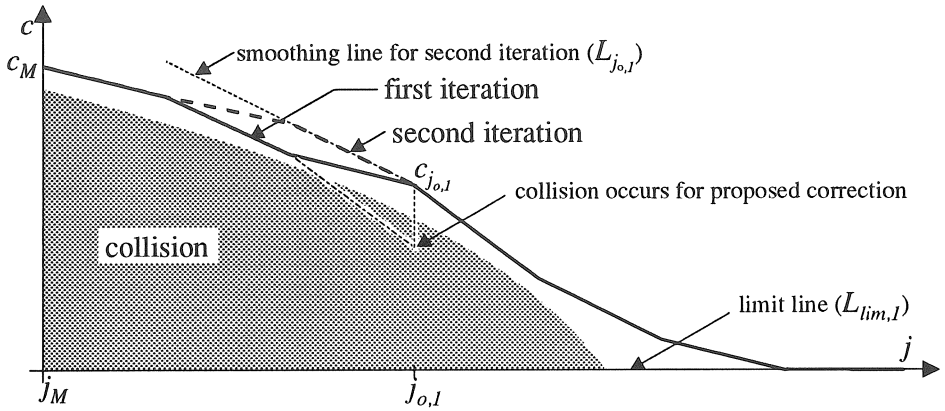

Figure 6.17: Smoothing path in positive direction $\sigma = 1$ (correction has 1 component)

If a via-pose is imposed (e.g. a rotation of the winding axis over an angle $\Delta\varphi_M$ or a fixed orientation of the pay-out eye), the correction in the via-pose is taken as starting correction. In the winding coordinate system, a rotation over an angle $\Delta\varphi$ ($\pm 180°$ or $\pm 360°$) can be implied at the end of the correction path.

The requirement (6.9) must not be fulfilled in the control points q_k of the linking motion Υ_{i-1}^{i} (cf. section 5.2.2.3), since the tangent to the original path is not continuous in the control points.

Adaptation of Correction For each correction $\mathbf{c}_j$, which is proposed, the corresponding pose is checked on collisions (Fig. 6.16). If collision occurs, a new correction $\mathbf{c}'_j$ is proposed, which is still within the tolerances (Eq. 6.10). The value of the new correction $\mathbf{c}'_j$ is based on $\mathbf{c}_j^{old}$, i.e. the correction in j from the previous iteration loop (or, during the first iteration, from the original collision-free pose) :

$$\forall k \;:\; c'_{j,k} = \begin{cases} c_{j,k}^{old} & |c_{j,k}^{old} - c_{j,k}^{r}| \leq \epsilon_k \\ c_{j,k}^{r} + \epsilon_k \text{sign}(c_{j,k}^{old} - c_{j,k}^{r}) & |c_{j,k}^{old} - c_{j,k}^{r}| > \epsilon_k \end{cases} \tag{6.16}$$

If collision still occurs, a collision-free pose is sought, by means of the collision avoidance routines, and $\mathbf{c}_j^*$, the correction corresponding to the collision-free pose, is derived (Fig. 6.16). For stability of the algorithm, the difference between the correction $\mathbf{c}_j^*$ and the refer-

ence correction $\mathbf{c}_j^r$ may not be larger than the difference between the (collision-free) correction $\mathbf{c}_j^{old}$ from the previous iteration loop and $\mathbf{c}_j^r$.

If the difference between the new correction $\mathbf{c}_j^*$ and the reference correction $\mathbf{c}_j^r$ is larger than ϵ (Eq. 6.10), a smooth path cannot be obtained in this iteration.

Calculation of the difference The difference $\Delta\mathbf{c}_j$ in the corrected point j has to be chosen so, that a smooth path can be obtained, both during the rest of the current iteration and during the next iteration. The difference $\Delta\mathbf{c}_j$ is first chosen proportional to the difference between the actual correction $\mathbf{c}_j$ and the smoothing correction $\mathbf{c}_{j_{o,\sigma}}$:

$$\Delta\mathbf{c}_j = \frac{\mathbf{c}_{j_{o,\sigma}} - \mathbf{c}_j}{j_{o,\sigma} - j} \tag{6.17}$$

The difference $\Delta\mathbf{c}_j$ must lie within the bounds to reach the smoothing line L_{opt} (Eq. 6.15) and the (original) limit line $L_{lim,\sigma}$ (Eq. 6.14). If these requirements are contradictory, the smoothing line is dropped, and smoothing is performed towards the limit line.

6.5 Collision Control in the Mandrel Coordinate System

Collisions between the mandrel and the pay-out eye are detected and avoided for each surface of the mandrel model (cf. section 6.3.2.1) separately. The scheme of Fig. 6.7 is then transformed into Fig. 6.18.

The surfaces which are tested first for collisions are the chuck and the pin rings, where collisions are most likely to occur. Then the CAD-surfaces are investigated. After avoiding collisions, the previously tested surfaces are checked on collisions in the zones where the pose of the pay-out eye is adapted.

This section will apply the method, which has been discussed in section 6.4, to the mandrel coordinate system. Section 6.5.4 discusses collision control during the linking motion.

6.5.1 Collision Detection

The method to detect collisions between the pay-out cylinder and a surface, has been discussed in section 6.4.1 (Fig. 6.8). An enveloping

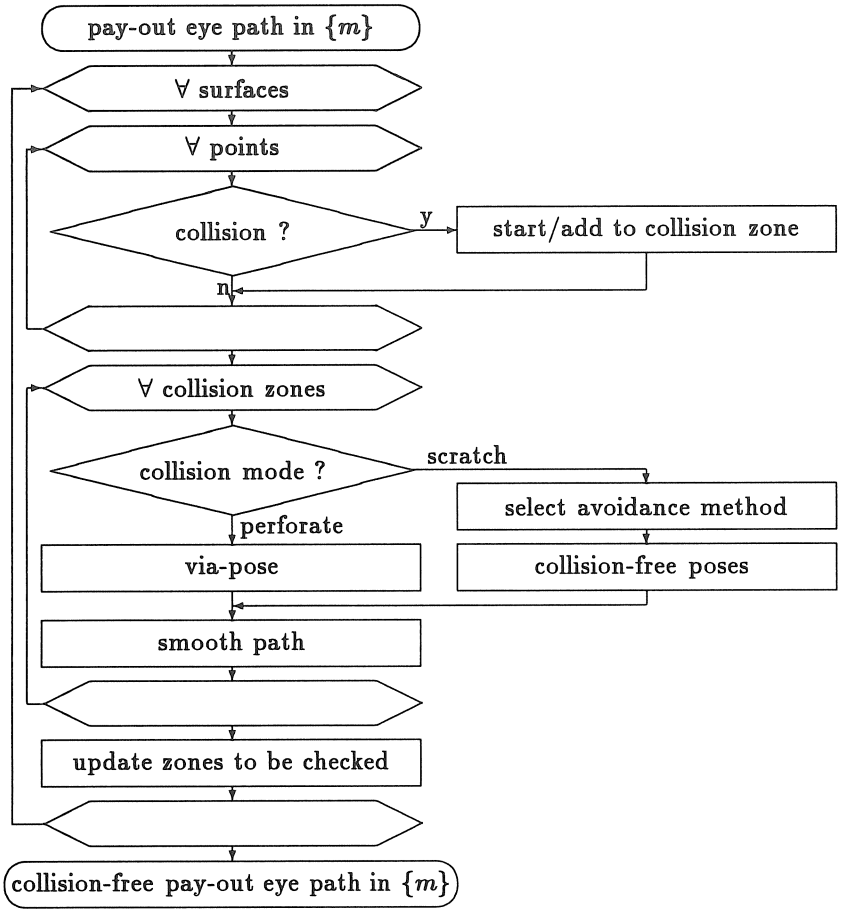

Figure 6.18: Collision control in the mandrel coordinate system

surface around the mandrel cannot be constructed for the pay-out eye, since the orientation of the pay-out axis can be chosen almost freely (cf. section 6.4.1.1). Collisions are detected for each surface separately (Fig. 6.18).

6.5.2 Selection of the Collision Avoidance Method

The first step in collision avoidance is the selection of the collision mode (scratching, perforating) and the adaptation method (adapt free length or adapt orientation) (cf. section 6.4.2).

6.5.2.1 Selection of the Collision Mode

If the pay-out axis intersects the surface, a test is performed to check if the pay-out eye moves through the surface (perforating) or only hits it (scratching). When the pay-out eye moves through a surface, the sign of the normal to the surface changes suddenly (Fig. 6.11b). When the surface is only scratched, the surface normal changes gradually (Fig. 6.11a). In the perforating mode, collisions occur with the axis of the pay-out cylinder, whereas scratching is mostly limited to collisions with the mantle or the edge plane of the pay-out cylinder (Fig. 6.11).

The perforating mode is selected when the variations in the direction of the normal, measured perpendicularly to the axis of the circumscribing cylinder $\vec{a}_c$ (Fig. 6.19), are larger than 135°.

In the via-pose, the pay-out axis is aligned with the axis $\vec{a}_c$ of the circumscribing cylinder. The free length is adapted if the distance between the pay-out axis and the surface axis is too small.

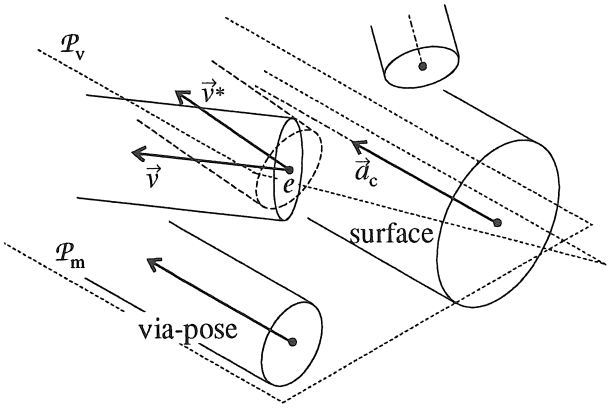

Figure 6.19: Adaptation of the orientation of the pay-out eye in the perforating mode

The motion of the pay-out eye must be so, that the orientation changes gradually from the orientation in the point at the start of the collision zone, over the orientation of the pay-out eye in the via-pose, to the orientation at the end of the collision zone. A test is performed to check if the orientation changes in the good direction. This test is characterized by a mid-plane $\mathcal{P}_m$, formed by the axis $\vec{a}_c$ of the circumscribing cylinder and the via-pose, and the side of the

mid-plane $\mathcal{P}_m$ at the start of the collision zone. The pay-out axis may not lie between the mid-plane $\mathcal{P}_m$, and the plane $\mathcal{P}_v$, formed by the axis $\vec{a}_c$ and the delivery point e (Fig. 6.19). If the pay-out axis $\vec{v}$ lies between these planes, it is projected on the plane $\mathcal{P}_v$ (vector $\vec{v}^*$ in Fig. 6.19).

6.5.2.2 Choice between Free Length and Orientation Adaptation

Two methods are possible to change the pose of the pay-out eye : changing the free length or changing the orientation of the pay-out eye.

For each collision zone the adaptations are evaluated at three points : at the start and the end of the collision zone and at the point with maximum intrusion. The following tests are consecutively made :

- if collision occurs with a pin ring during the linking motion, the free length is increased.
- else, if the pay-out axis intersects the surface, and the pay-out axis is aligned with the fibre, the orientation is adapted.
- if collision occurs with the base of the pay-out cylinder, a test is performed to check in which direction the free length has to be adapted. If these directions are not the same for the different points, the orientation is adapted.

To ensure the stability of the algorithm, the selected adaptation may not be contradictory with previous adaptations : if the free length has been decreased previously, an increase is not allowed.

If the avoidance method has not been selected yet, or, if a change of the free length has been selected, both orientation and free length changes are evaluated in the three points. If a change in orientation is needed for the adaptations of the free length, a change of the orientation is selected. Otherwise, the mode which gives the smallest adaptations is chosen.

6.5.3 Collision Avoidance for a Single Pose

This section discusses the avoidance routines in the mandrel coordinate system. As mentioned in section 6.4.3 collision avoidance is an iterative

process : the collision avoidance routines are executed until a collision-free position is found, or until the maximum number of iterations is exceeded.

Collisions are avoided by changing the free length or the orientation of the pay-out eye.

6.5.3.1 Adaptation of the Free Length

The free length can vary between a minimum value l_{fm} and a maximum value. If the minimum or maximum free length are attained, the orientation of the pay-out axis is changed.

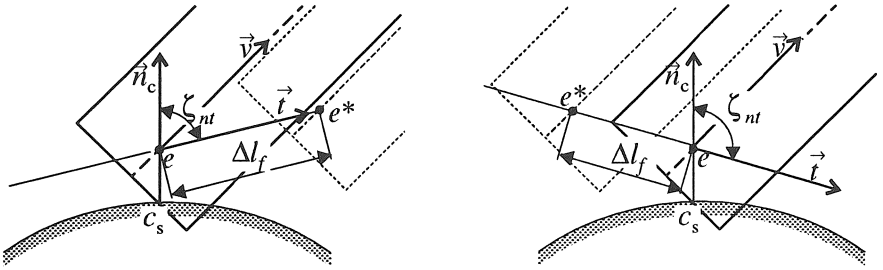

Figure 6.20: Selection of increase or decrease of the free length
(a) $\zeta_{nt} < 90° \Rightarrow \Delta l_f > 0$ (b) $\zeta_{nt} > 90° \Rightarrow \Delta l_f < 0$

Whether the free length has to be increased or decreased, depends on the magnitude of the angle ζ_{nt} between the tangent to the fibre path $\vec{t}$ and the normal $\vec{n}_c$ to the surface at the collision point on the mandrel. If $\zeta_{nt} > 90°$, the free length has to be decreased, since an increase of the free length would lead to an increase of the intrusion (Fig. 6.20b). If $\zeta_{nt} < 90°$, the free length must be increased (Fig. 6.20a).

If a collision occurs at the base of the pay-out eye ($\lambda_c = 0$), the free length is increased, so that the edge of the base of the pay-out eye is at a safety distance δ_s from the tangent plane $\mathcal{P}_c$ in the collision point c_s. The delivery point e has to be at a distance $r_e \sin\zeta_{nv} + d_r \cos\zeta_{nv} + \delta_s$ from the tangent plane, with ζ_{nv} the angle between the pay-out axis $\vec{v}$ and the normal $\vec{n}_c$ to the tangent plane. The change of the free length is (Fig. 6.21) :

$$\Delta l_f = \frac{r_e \sin\zeta_{nv} + d_r \cos\zeta_{nv} + \delta_s - h_c}{\cos\zeta_{nt}} = \frac{d_c \sin\zeta_{nv} + \delta_s}{\cos\zeta_{nt}} \qquad (6.18)$$

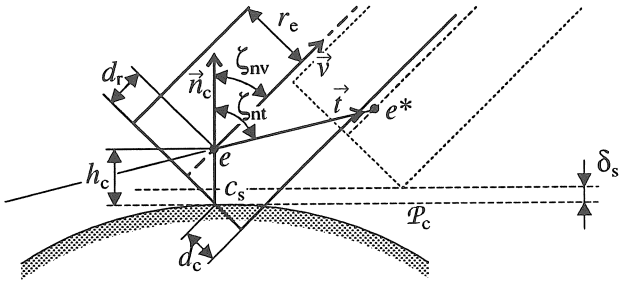

Figure 6.21: Increase of the free length at collision between pay-out eye and surface

with $h_c = (r_e - d_c)\sin\zeta_{nv}$, the distance between the delivery point e and the tangent plane $\mathcal{P}_c$.

If the surface has an end plane, the tangent plane is replaced by the end plane, and the test is also performed when collision occurs with the cylinder mantle ($\lambda_c > 0$).

The value of Δl_f is compared with the change of the free length necessary to put the base of the pay-out cylinder be on the circumscribed cylinder of the surface, the radius of which is increased with $\sqrt{r_e^2 + d_r^2} + \delta_s$.

6.5.3.2 Adaptation of the Orientation of the Pay-Out Eye

The angle ζ_{tv} between the pay-out axis $\vec{v}$ and the tangent to the fibre path $\vec{t}$ must be smaller than 90°. If no solution is found, for which the angle ζ_{tv} is smaller than 90°, the free length is changed until a valid solution is found.

The orientation of the pay-out axis $\vec{v}$ is adapted in two ways, dependent on the value of the tool parameter λ_c. Collisions near to the base of the pay-out cylinder are avoided by aligning the pay-out axis $\vec{v}$ with the normal to the surface. Collisions with the cylinder mantle are avoided by pushing the cylinder mantle away from the surface.

Collision with Mantle The pay-out eye is rotated in the plane, formed by the pay-out axis $\vec{v}$ and the normal $\vec{n}_c$ through the collision point c_t on the pay-out axis, so that the rotated collision point c_t^* is at a distance $d = \delta_s + r_e/\sin\zeta_{nv}$ of the tangent plane $\mathcal{P}$ in s_c, with s_c the projection of c_t on the surface (Fig. 6.22). The new angle ζ_{nv}^* between

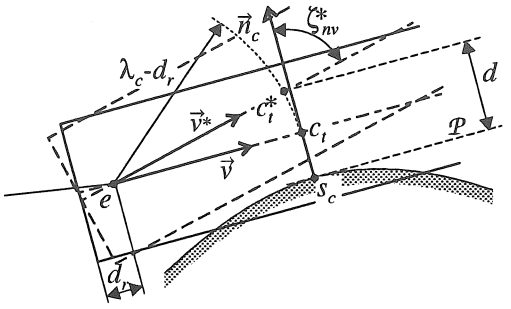

Figure 6.22: Change of the pay-out eye orientation at collision between the mantle of the pay-out eye and a surface

the normal $\vec{n}_c$ and the new pay-out axis $\vec{v}^*$ is :

$$\zeta^*_{nv} = \arccos\left[\frac{d - (\vec{r}_e - \vec{r}_{s_c}) \cdot \vec{n}}{\lambda_c}\right] \tag{6.19}$$

The new vector $\vec{v}^*$ equals :

$$\vec{v}^* = \cos\zeta^*_{nv}\vec{n}_c + \sin\zeta^*_{nv}\frac{\vec{v} - (\vec{v}\cdot\vec{n}_c)\,\vec{n}_c}{\|\vec{v} - (\vec{v}\cdot\vec{n}_c)\,\vec{n}_c\|} \tag{6.20}$$

If the angle ζ_{tv} between the tangent $\vec{t}$ and the new vector $\vec{v}^*$ is larger than 90°, ζ_{tv} is limited to 90°.

The definition of the normal is an important aspect of collision avoidance (Fig. 6.23). The normal $\vec{n}_p$, which is used for collision avoidance, through a point p is defined as the vector that links the point p and its nearest point s on the surface (e.g. point p_1 in Fig. 6.23). If this point s lies on the edge of the surface, the linking vector does not coincide with the surface normal $\vec{n}_s$ in s. For collision avoidance, the surface normal $\vec{n}_s$ is used at the boundary of two continuously linked surfaces or at the inner edge of a pin ring (p_2 in Fig. 6.23), and the linking vector is used when the edge is an outer edge of the part (p_3 in Fig. 6.23). If, in the latter case, the angle between $\vec{n}_s$ and the linking vector is larger than 90°, the normal to the end plane of the surface is used (p_4 in Fig. 6.23).

Collision with Pay-Out Cylinder Base The previous method becomes unstable when λ_c is too small (or : if the distance between

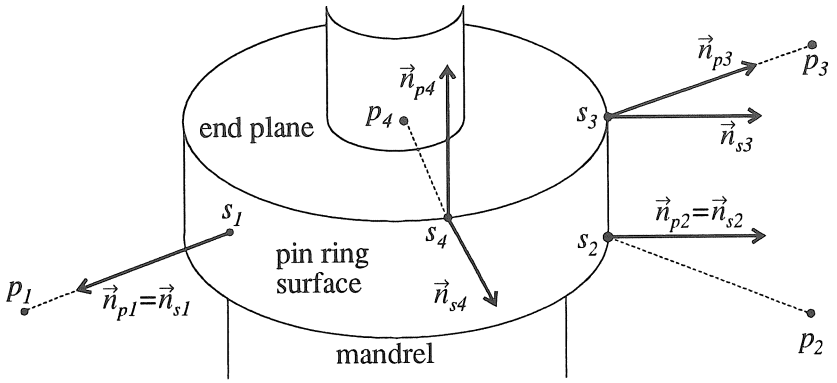

Figure 6.23: Normal on a Surface

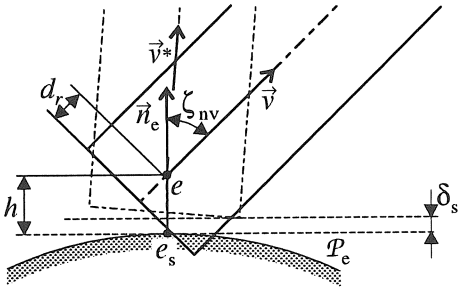

Figure 6.24: Rotation of the pay-out eye at collision between the base of the pay-out cylinder base and a surface

the delivery point e and the collision point c_t on the pay-out axis to the delivery point is too small). If collision occurs with the base of the cylinder, the pay-out axis is rotated so that the edge of the cylinder base is at a safety distance δ_s from the tangent plane at e_s, with e_s the projection of e at the surface (Fig. 6.24). The new angle ζ^*_{nv} between the normal to the surface $\vec{n}_e$ and the pay-out axis $\vec{v}$ is then :

$$\zeta^*_{nv} = \arcsin\left(\frac{h-\delta_s}{\sqrt{r_e^2+d_r^2}}\right) \tag{6.21}$$

with h the distance between e and the surface. If the height is too small ($h < d_r$), e.g. at the inner edge of a pin ring, the free length is adapted until the $h > d_r$.

If collision occurs, the value of δ_c is increased until a collision-free pose is found, or until the pay-out axis and the normal coincide.

If the angle ζ_{tv} between the tangent to the fibre path $\vec{t}$ and the pay-out axis $\vec{v}$ is larger than 90°, the angle is limited to 90°.

If the pay-out axis cannot be aligned with the normal without collision, the free length is varied between the minimum and the maximum free length and the pay-out axis is rotated, until a valid solution is found.

6.5.4 Collision Control during the Linking Motion

The collision control method, which has been discussed in the previous pages, does only take one surface into account. If collisions are avoided by changing the orientation of the pay-out eye, the angle between the pay-out axis and the normal on the surface is decreased. Problems arise when the normals to two surfaces are opposite : the pay-out eye is pushed away from one surface, so that it will collide with the opposite surface. This problem occurs often during the linking motion on e.g. a cylinder, where the pay-out eye must move between two planes, which normal to the winding axis, viz. the end plane of the pin ring and the end plane of the chuck (or centre point) (Fig. 6.25). The geometry of these surfaces is rather simple, and collisions can be avoided by applying some simple rules. Collisions are avoided during the creation of the robot path, without the iterative smoothing procedure.

During the first part of the linking motion, i.e. between the control points q_0 and q_5 (cf. section 5.2.2.3), collisions with head- and tailstock and the pin ring are checked and avoided. Collision control is performed in two steps : first the position of the delivery point is controlled, then the orientation.

6.5.4.1 Position Collision Control

The base of the pay-out cylinder may not intersect the end plane of the pin ring, nor the end plane of the chuck or tailstock. Collisions with the pin ring are likely to occur when the delivery point e lies in a cylinder with as base the end plane of the pin ring and a length of r_e. If the delivery point lies in this cylinder, the free length is increased. A similar cylinder can be defined for head- and tailstock : if the delivery point lies in a cylinder, with as base the end plane of the chuck and

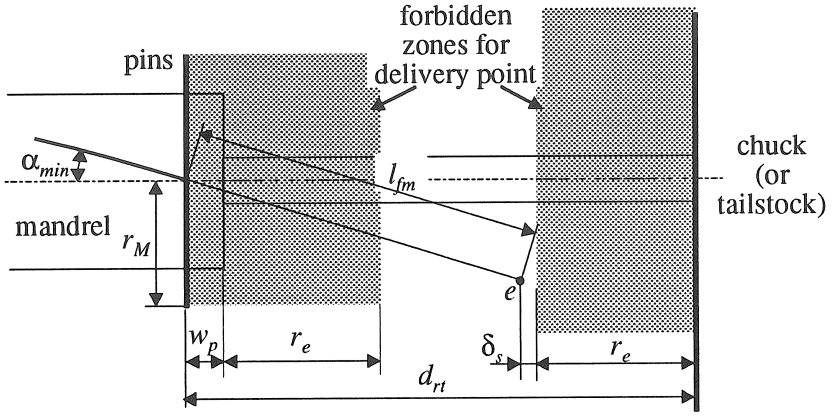

Figure 6.25: Minimum winding angle at end of the mandrel

length r_e, the free length is decreased.

If the distance d_{rt} between the chuck and the pin ring circle is too small ($d_{rt} < l_{fm} + r_e$), low angle winding is not possible. The minimum winding angle is, in function of the distance d_{rt} (Fig. 6.25) :[7]

$$\alpha_{min} = \arccos\left(\frac{d_{rt} - r_e - \delta_s}{l_{fm}}\right) \tag{6.22}$$

6.5.4.2 Orientation Collision Control

If the delivery point lies outside the above mentioned cylinders, a collision-free pose can always be found by aligning the pay-out eye with the normal to the winding axis. The orientation is adapted when collision with the end plane of chuck, tailstock or pin ring, or with the mandrel shaft. The pay-out axis $\vec{v}$ is made gradually more normal to the winding axis $\vec{w}$.

[7] Eq. (6.22) is not valid if the delivery point e lies inside the cylinder defined by the pin ring edge, i.e. when $l_{fm} \sin\alpha_{min} < r_M$ and $l_{fm} \cos\alpha_{min} < r_e + w_p$, with r_M the outer radius of the pin ring or $\sqrt{l_{fm}^2 - r_M^2} < d_{rt} - r_e < r_e + w_p$. The minimum winding angle is in this case :

$$\alpha_{min} = \arctan\left(\frac{r_M}{d_{rt} - r_e - \delta_s}\right)$$

6.6 Collision Control in the Winding Coordinate System

The collision control in the winding coordinate system is performed after the calculation of the angle φ of the winding axis (cf. Fig. 6.5). The collisions, which depend on the angle of the winding axis, i.e. collisions between the robot wrist and the rotating mandrel structure (i.e. mandrel, head- and tail-stock) as well as collisions between, on the one hand, pay-out eye and robot wrist and, on the other hand, head- and tail-stock, are detected and avoided. The position of the robot wrist must be attainable by the robot (cf. section 6.3.3).

This section will apply the heuristic collision control method to the winding coordinate system. The general scheme from Fig. 6.7 is transformed into Fig. 6.26.

The pay-out axis $\vec{v}$ lies in a horizontal plane. The orientation of the pay-out can be denoted in function of the angle τ : ${}_w\mathbf{v} = [\sin\tau \quad -\cos\tau \quad 0]^T$. The reference orientation ($\tau = 0$) is the orientation perpendicular to the winding axis (${}_w\mathbf{v} = [0 \quad -1 \quad 0]^T$).

6.6.1 Collision Detection

During collision detection in the winding coordinate system, the following tests are consecutively performed :

- test if the pose is attainable by the robot (section 6.6.1.1)
- test if a collision occurs between the robot wrist cylinder and the mandrel (section 6.6.1.2)
- test for collisions between as well robot wrist as pay-out eye and head- or tailstock (section 6.6.1.3)

6.6.1.1 Pose not Attainable by Robot

The centre of the robot wrist rw must lie in the working envelope, which corresponds to a sphere with radius r_r (cf. section 6.3.2.4). At the surface of the sphere, the arm of the robot is completely stretched. Due to small differences between the model and the actual configuration, a demanded pose may not be attainable. To avoid singularities, the radius r_r is decreased with $\delta_r = 50$ mm.

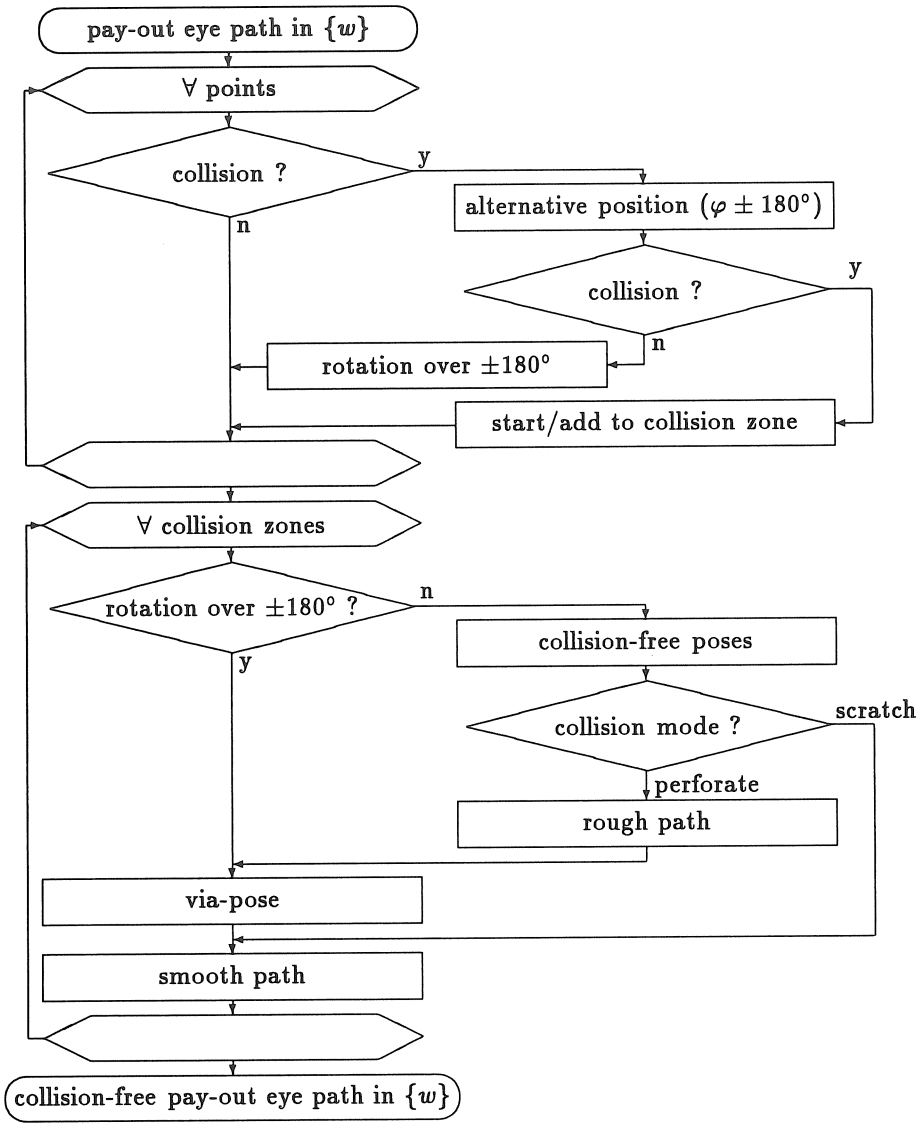

Figure 6.26: Collision control in the winding coordinate system

6.6.1.2 Collision between Robot Wrist and Mandrel

Collision detection between the robot wrist cylinder and the mandrel is performed as discussed in section 6.4.1. Collision detection is performed in two steps : first is checked if bw, the base of the robot wrist cylinder, lies in the enveloping surface round the mandrel. If this is the case, collisions between the robot wrist and the mandrel surfaces are checked (cf. Fig. 6.8).

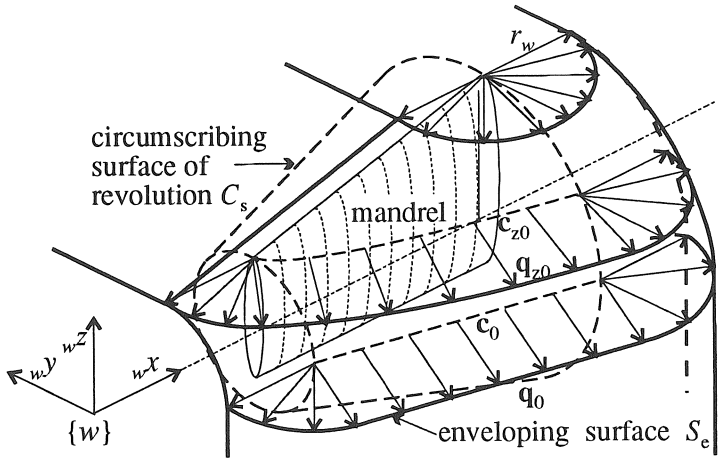

Figure 6.27: Enveloping surface round the mandrel for the robot wrist

An enveloping surface can be constructed for the robot wrist, because the normal to the robot flange is always directed vertically downwards. The enveloping surface is constructed for the line $L = (bw, \vec{z})$, with bw the basis of the attachment of the pay-out eye to the robot flange (Fig. 6.3). The enveloping surface is the surface formed by the positions of the point bw at which the robot wrist cylinder makes just contact with the mandrel.

The enveloping surface (Fig. 6.27) is constructed in two steps : first a circumscribing surface of revolution C_s of the mandrel round the winding axis is defined, then the enveloping S_e is constructed based on this circumscribing surface of revolution. The circumscribing surface of revolution is constructed by calculating for each point of the surface the distance r to the winding axis. The profile is stored as a list of ${}_w x$-coordinates with corresponding radii $r({}_w x)$. The enveloping surface S_e is, above the winding axis, constructed by offsetting the circum-

scribing surface of revolution over the radius of the robot wrist r_w in a horizontal plane. If the profile of C_s at the horizontal plane through the winding axis (${}_w z = 0$) is given by $\mathbf{c}_0({}_w x) = [{}_w x \quad -r({}_w x) \quad 0]^T$, the profile of C_s at ${}_w z = z_0$ is : $\mathbf{c}_{z_0}({}_w x) = \left[{}_w x \quad -\sqrt{r^2({}_w x) - z_0^2} \quad z_0\right]^T$. This curve is offset over r_w, i.e. each point is moved over the tool radius r_w along the normal $\mathbf{n}_{z_0}$ to the curve $\mathbf{c}_{z_0}({}_w x)$:

$$\begin{aligned} \mathbf{q}_{z_0}({}_w x) &= \mathbf{c}_{z_0}({}_w x) + r_w \mathbf{n}_{z_0}({}_w x) \qquad (6.23) \\ &= \begin{bmatrix} {}_w x \\ -\sqrt{r^2 - z_0^2} \\ z_0 \end{bmatrix} - r_w \sqrt{\frac{r^2 - z_0^2}{r^2\left[1 + \left(\frac{dr}{d_w x}\right)^2\right] - z_0^2}} \begin{bmatrix} r\frac{dr}{d_w x} \\ \sqrt{r^2 - z_0^2} \\ 0 \end{bmatrix} \end{aligned}$$

This surface requires however too much memory. Therefore, the surface is approximated by the surface of revolution with profile $\mathbf{q}_0({}_w x)$. Since no collisions between the robot wrist and the mandrel are possible if ${}_w bw_z > r_{max} = \max_x(r({}_w x))$, the part of the surface above ${}_w z = r_{max}$ is not taken into account. Below the winding axis ($z_0 < 0$) is $\mathbf{q}_{z_0}({}_w x) = \mathbf{q}_0({}_w x)$. The enveloping surface is generated at the start of the calculations of the robot path.

6.6.1.3 Collision with Head- and Tail-stock

Head- and tail-stock are modelled as quarter spaces (section 6.3.2.2). The following collisions are checked consecutively :

- The delivery point can lie inside head- or tail-stock. In this case the free length has to be decreased.
- The base of the robot wrist cylinder bw can lie inside head- or tail-stock.
- Collisions can occur between the pay-out eye and the edge of the stocks. This is checked by calculating the distance between the pay-out axis and the edge of the stock.
- Collisions can occur between the robot wrist cylinder and the edge of the stock. This is checked by calculating the distance between rw and the stock edge.
- Collisions can occur between the pay-out eye and the front plane of the stock (${}_w y = -y_s$).
- Collisions can occur between the robot wrist and the front plane of the stock.

6.6.2 Selection of the Collision Avoidance Method

Each pose is checked on collisions. If collision occurs, the alternative robot pose (cf. p. 161) is checked on collisions. If this pose is collision-free, the winding axis has to be rotated over 180° (Fig. 6.26). If not, a collision zone is constructed, and the method which will be used to avoid collisions has to be determined. Collision-free poses are generated, and from these collision-free poses the collision mode (scratching or perforating) is derived (Fig. 6.26). In the case of perforating, a via-pose is calculated. A smooth path is generated by smoothing of the path, which links the collision-free poses, or through the via-pose (Fig. 6.26).

If the twist compensating motion is used to remove excess tape twists (cf. section 5.2.7.1), the desired final rotation (±360°) is inputted to the collision control module, in order to obtain a smooth collision-free path.

6.6.2.1 Collision Mode : Scratching or Perforating

If the path, which links the collision-free poses, has a discontinuity in the angle φ of the winding axis, a smooth path cannot be constructed starting from the calculated collision-free poses, and a final rotation or a via-pose has to be imposed. A rough path is constructed to investigate the different alternatives : a supplementary rotation over ±360° and a via-rotation over ±180°. This rough path is based on three poses in the collision zone. The first and the third pose are rotated over +90° and −90°, the second pose over 180°, and collision-free poses are calculated (Fig. 6.28). This rough path may not intersect the horizontal plane through the winding axis at positive ${}_w y$-values, since the pay-out eye would otherwise move through the mandrel. The corrections in the three points of the path should be as small as possible. If a via-motion is selected, the angle $\Delta\varphi$ of the winding axis for which the corrections are as small as possible is calculated.

If a final correction or a via-correction is imposed, the orientation τ of the pay-out axis and the angle $\Delta\varphi$ of the winding axis are coupled. The coupling is given by the equation (Fig. 6.29) :

$$\tau = \tau_0 + (1 - \cos\Delta\varphi)(\sigma\frac{\pi}{2} - \tau_0) \tag{6.24}$$

with τ_0 the orientation angle before additional rotation and $\sigma = \pm 1$

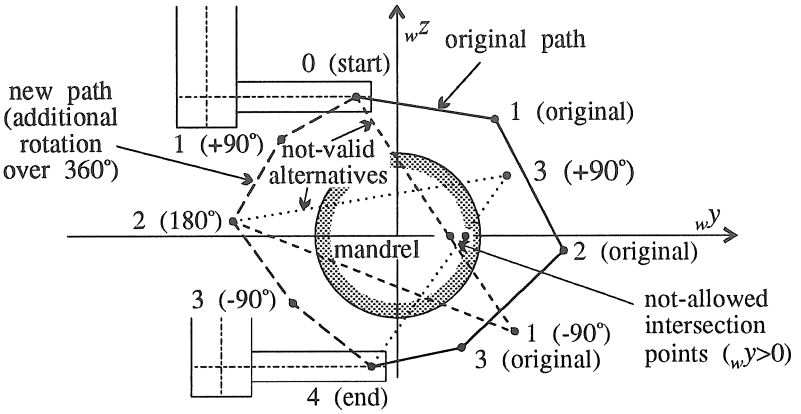

Figure 6.28: Rough path with rotation about the winding axis

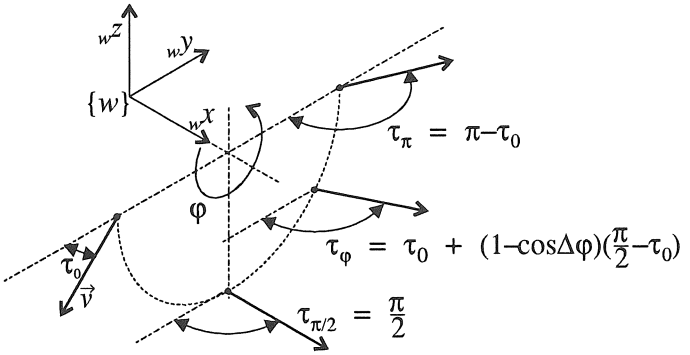

Figure 6.29: Coupling between the angle of the winding axis $\Delta\varphi$ and the orientation of the pay-out eye τ

the direction of orientation change, which is defined at the start of the collision zone. The value of σ corresponds to the most occurring sign of the $_w x$-component of the tangent $\vec{t}$ to the fibre path in the collision zone.

6.6.2.2 Selection of the Adaptation Method

During collision control in the winding coordinate system, adaptations are made hierarchically : first the orientation of the pay-out eye is changed, until the reference orientation is obtained, or until no further improvement can be found. Consecutively, the angular position of the

winding axis is changed, and, if again no solution has been found, the free length.

6.6.3 Collision Avoidance for a Single Pose

Collisions can be avoided by changing the orientation of the pay-out axis, by rotating the winding axis, or by changing the free length.

6.6.3.1 Adaptation of the Orientation of the Pay-Out Eye

The pay-out axis $\vec{v}$ can only rotate in a horizontal plane. The orientation may only vary between two limit orientations, which are, at the start of the calculations, $\tau = 0$ (${}_w\mathbf{v} = [0 \quad -1 \quad 0]^T$) and $\tau = \pm\pi$ (${}_w\mathbf{v} = [0 \quad 1 \quad 0]^T$). The sign of the orientation τ is not allowed to change. A change is called stable when the orientation is changed towards the reference orientation.

The position of the centre of the robot wrist rw with respect to the frame $\{re\}$ in the (reference) delivery point re is given by : ${}_{re}\mathbf{rw} = [l_{ew}\cos\zeta_{ew} \quad l_{ew}\sin\zeta_{ew} \quad z_{ew}]^T$.

Pose not Attainable by Robot The centre of the robot wrist rw describes a circle in a horizontal plane $\mathcal{P}$ when the orientation of the pay-out axis changes, with as centre e', the projection of the delivery point e on $\mathcal{P}$, and as radius l_{ew}. The intersection of the working envelope of the robot with the horizontal plane $\mathcal{P}$ is a circle with as center b', the projection of b on $\mathcal{P}$, and radius $r'_r = \sqrt{(r_r - \delta_r)^2 - ({}_wrw_z - {}_wb_z)^2} - \delta_s)$. The new orientation τ^* of the pay-out axis is derived from the intersection of the two circles (Fig. 6.30) :

$$\tau^* = \tau_{eb} \pm \arccos\left(\frac{l_{ew}^2 + r_{eb}^2 - r_r'^2}{2l_{ew}r_{eb}}\right) + \zeta_{ew} \qquad (6.25)$$

with τ_{eb} the angle corresponding to the line $e'b'$ and r_{eb} the distance between e' and b'. The sign has to be chosen so that the sign of the orientation τ does not change and that the orientation change is stable.

Collision Between Robot Wrist and Mandrel The base of the robot wrist bw moves on a circle in a horizontal plane $\mathcal{P}$ with as centre the projection of the delivery point e on $\mathcal{P}$ and with radius l_{ew}.

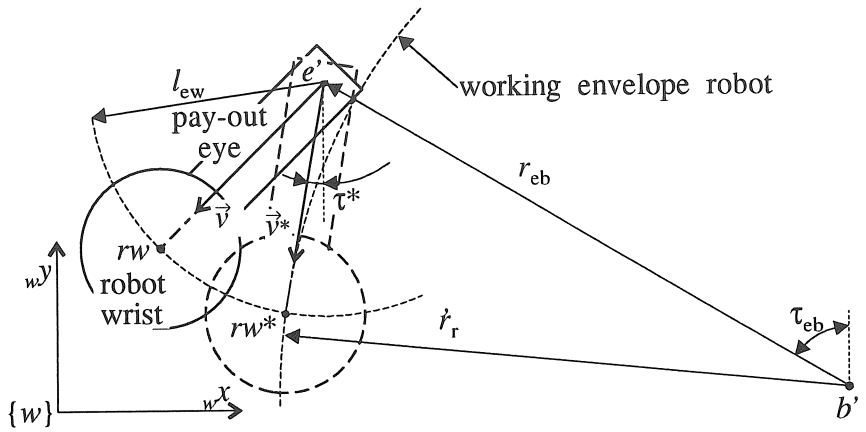

Figure 6.30: Change of the orientation of the pay-out axis if the position is not attainable by the robot

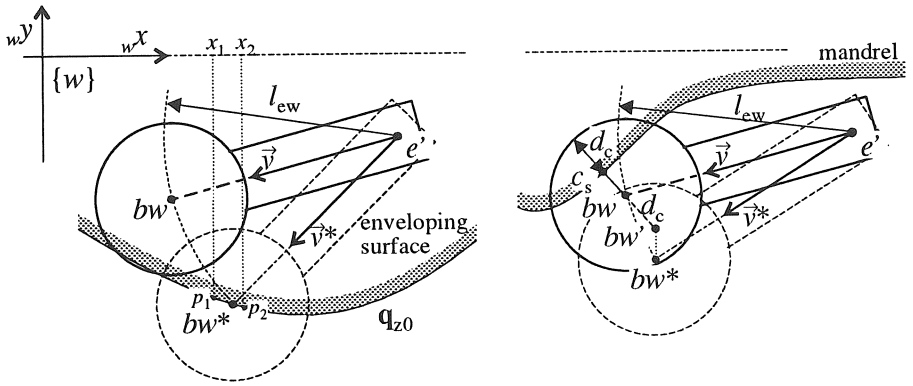

Figure 6.31: Change of the orientation of the pay-out axis with use of the enveloping surface

The point bw^* is placed on the intersection of this circle with the enveloping surface. For each ${}_w x$-coordinate, the intersection point p_x of the enveloping surface and the plane $\mathcal{P}$ is calculated, and the distance between p_x and e. This distance has to equal l_{ew}. The new point bw^* is interpolated between the intersection points (Fig. 6.31a). First a solution is searched in the stable rotation direction, and then, if no solution has been found, in the unstable direction. An unstable solution is only allowed, when the reference orientation ($\tau = 0$) is not collision-free.

The method discussed above can lead to large adaptations. To decrease the adaptations, an alternative solution is sought. The point bw is moved over the collision distance d_c along the line, which links the collision point on the surface c_s and the point bw to the point bw' (Fig. 6.31a). Only the ${}_w x$-coordinate of the new point bw' is used, since the distance between bw^* and the delivery point e must be constant. The obtained orientation must remain in the orientation limits. The solution closest to the original orientation is selected from the two alternatives.

Collision with Head- or Tail-stock Each of the collisions, described in section 6.6.1.3, is solved in a different way.

Collisions between the Pay-Out Eye and the Front Plane The end point of the pay-out cylinder is put at a distance $r_e + \delta_s$ from the front plane (${}_w y = -y_s$). The new orientation is then (Fig. 6.32) :

$$\tau^* = \sigma \arccos\left(\frac{{}_w e_y + (y_s + r_e + \delta_s)}{l_e}\right) \tag{6.26}$$

with $\sigma = 1$ for the tailstock and $\sigma = -1$ for the headstock.

Collision between the Pay-Out Eye and the Stock Edge The pay-out axis has to be at a distance $r_e + \delta_s$ from the edge of the stock (Fig. 6.33) :

$$\tau^* = \tau_{es} - \sigma \arcsin\left(\frac{r_e + \delta_s}{l_{es}}\right) \tag{6.27}$$

with τ_{es} the orientation of the line, which links the delivery point e and the stock edge, and l_{es} the distance, measured in a horizontal plane, between the delivery point and the stock edge.

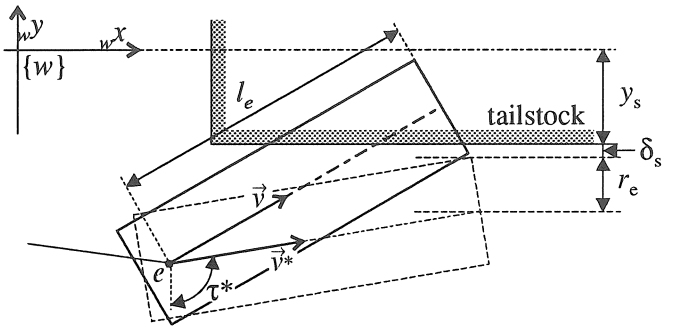

Figure 6.32: Change of the orientation of the pay-out axis at collision between the pay-out eye and the front plane of the tailstock

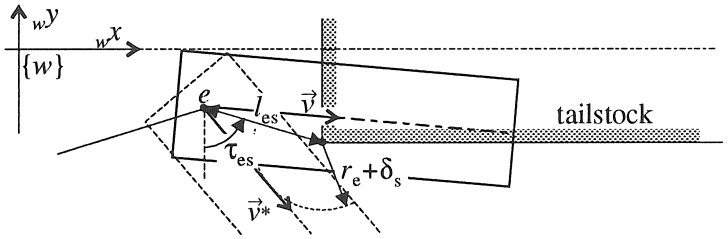

Figure 6.33: Change of the orientation of the pay-out axis at collision between the pay-out eye and the edge of the tailstock

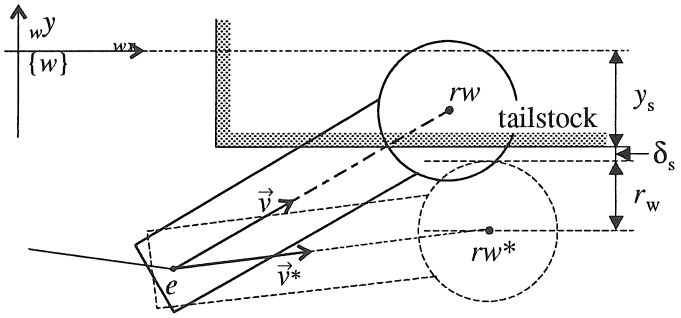

Figure 6.34: Change of the orientation of the pay-out axis at collision between the robot wrist and the front plane of the tailstock

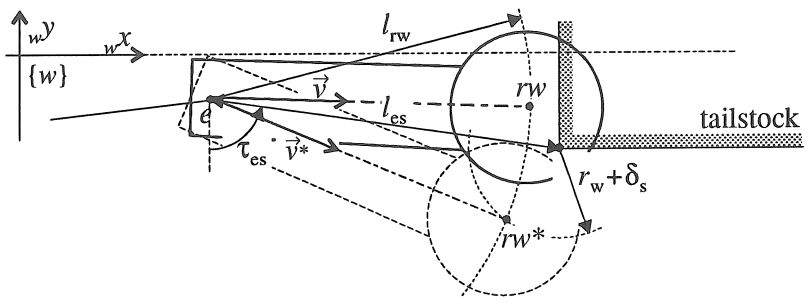

Figure 6.35: Change of the orientation of the pay-out axis at collision between the robot wrist and the edge of the tailstock

Collisions between the Robot Wrist and the Front Plane The centre rw of the robot wrist is put at a radius $r_w + \delta_s$ from the front plane (Fig. 6.34) :

$$\tau^* = \sigma \arccos\left(\frac{{}_w e_y + (y_s + r_w + \delta_s)}{l_{ew}}\right) + \zeta_{ew} \qquad (6.28)$$

Collisions between the Robot Wrist and the Stock Edge The centre rw of the robot wrist is placed at a distance $r_w + \delta_s$ from the edge of the stock (Fig. 6.35) :

$$\tau^* = \tau_{es} - \arccos\left(\frac{l_{es}^2 + l_{ew}^2 - (r_w + \delta_s)^2}{2 l_{es} l_{ew}}\right) + \zeta_{ew} \qquad (6.29)$$

6.6.3.2 Adaptation of the Angle of the Winding Axis

The pay-out eye and the mandrel are rotated over an additional angle $\Delta\varphi$, while maintaining the orientation of the pay-out axis $\vec{v}$.

The delivery point e moves on a circle with centre o and radius ρ_e in a vertical plane $\mathcal{P}_e$ normal to the winding axis. Since the orientation of the pay-out axis remains constant, the centre of the robot wrist rw describes also a circle with radius ρ_e in a vertical plane $\mathcal{P}_w$. The centre of the circle is shifted over $\vec{x} = \vec{r}_{rw} - \vec{r}_e$ towards o'.

Pose not Attainable by Robot The intersection of the working envelope of the robot with the vertical plane $\mathcal{P}_w$, in which rw moves, is a circle with as radius $r'_r = \sqrt{(r_r - \delta_r)^2 - ({}_w rw_x - {}_w e_x)^2} - \delta_s$ and

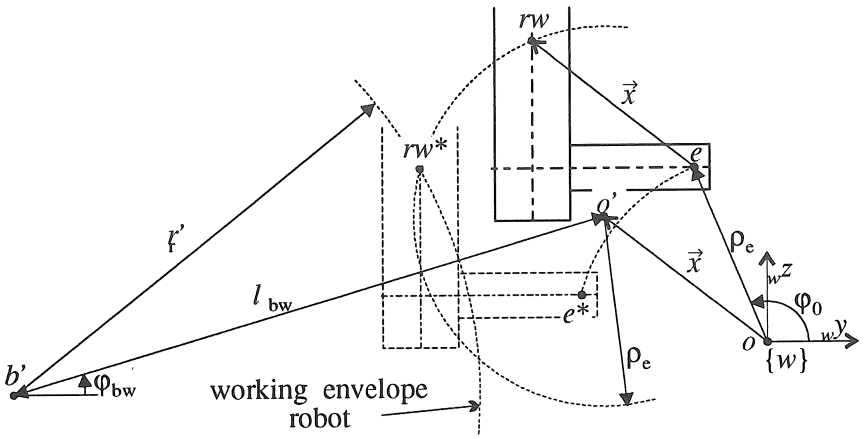

Figure 6.36: Rotation about the winding axis if the position is not attainable by the robot

is a circle with as radius $r'_r = \sqrt{(r_r - \delta_r)^2 - ({}_w rw_x - {}_w e_x)^2} - \delta_s$ and as centre b', the projection of b on $\mathcal{P}$. The new angle of the winding axis is derived from the intersection of the two circles (Fig. 6.36) :

$$\Delta\varphi = \pm \arccos\left(\frac{\rho_e^2 + l_{bw}^2 - r_r'^2}{2r'_r\rho_e}\right) + \varphi_{bw} + \pi - \varphi_0 \qquad (6.30)$$

with l_{bw} the distance between b' and rw, φ_{bw} the corresponding angle and φ_0 the original angle of the winding axis. The smallest value of $\Delta\varphi$ is selected.

Collision between Robot Wrist and Mandrel Both mandrel and delivery point are rotated until the distance, measured in a horizontal plane, between the rotated collision point on the surface c_s^* and the rotated robot wrist rw^* equals the radius of the robot wrist $r_w + \delta_s$. The distance in the ${}_w y$-direction between the collision point c_s^* and the robot wrist rw^* has then to equal $d_y = \sqrt{(r_w + \delta_s)^2 - {}_w o'^2_x}$. Thus (Fig. 6.37) :

$$({}_w c_y \cos\Delta\varphi - {}_w c_z \sin\Delta\varphi) - ({}_w e_y \cos\Delta\varphi - {}_w e_z \sin\Delta\varphi + {}_w o'_y) = d_y \qquad (6.31)$$

or :

$$({}_w c_y - {}_w e_y)\cos\Delta\varphi - ({}_w c_z - {}_w e_z)\sin\Delta\varphi = d_y + {}_w o'_y \qquad (6.32)$$

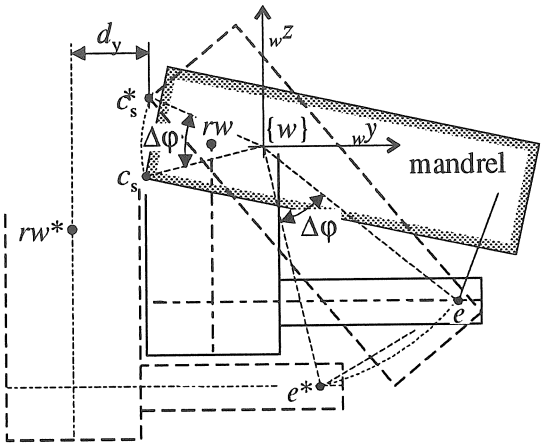

Figure 6.37: Rotation about the winding axis at collision between the robot wrist and the mandrel

This is a linear goniometric equation with solution :

$$\Delta\varphi = \pm \arccos\left(\frac{d_y + {}_w o'_y}{\sqrt{({}_w c_y - {}_w e_y)^2 + ({}_w c_z - {}_w e_z)^2}}\right) - \arctan\left(\frac{{}_w c_z - {}_w e_z}{{}_w c_y - {}_w e_y}\right) \tag{6.33}$$

The smallest value of $\Delta\varphi$ is selected.

Collisions with Head- or Tail-stock The winding axis is rotated until the delivery point e or the base of the robot wrist bw are at a constant distance from the top or the front plane of the head- or tail-stock. This result in searching the intersection between a circle and a line, so in the solution of a linear goniometric equation, as in the previous case.

6.6.3.3 Adaptation of the Free Length

Collision with Head- or Tail-stock If the delivery point lies inside the stocks or if the tangent to the fibre path intersects the stock, the free length is decreased. The new position of the delivery point e^* is the intersection between the tangent to the fibre path and a plane at a distance $r_e + \delta_s$ from the side plane of the stock.

If the tangent to the fibre path does not intersect the stock, the free length may be increased, unless it has previously been decreased.

If the free length is increased, an intersection is sought with a plane at a distance $r_e + \delta_s$ from the front plane.

If the free length is decreased, the orientation is also adapted.

Pose not Attainable by Robot The free length is changed if a rotation about the winding axis gives no solution. The new centre of the robot wrist rw^* lies on the line $L = (rw, \vec{t})$, with $\vec{t}$ the tangent to the fibre path. The centre of the robot wrist lies also on a sphere with radius $r'_r = r_r - \delta_r - \delta_s$ and centre b. The new position of the robot wrist is the intersection point of the line L with the sphere. The distance between rw^* and b equals in this point r'_r, or (Fig. 6.38) :

$$\left\| \vec{r}_{rw} + \Delta l_f \vec{t} - \vec{r}_b \right\| = r'_r \tag{6.34}$$

or :

$$\Delta l_f = -\vec{t}.(\vec{r}_{rw} - \vec{r}_b) + \sqrt{[\vec{t}.(\vec{r}_{rw} - \vec{r}_b)]^2 - [(\vec{r}_{rw} - \vec{r}_b) \cdot (\vec{r}_{rw} - \vec{r}_b) - r'^2_r]} \tag{6.35}$$

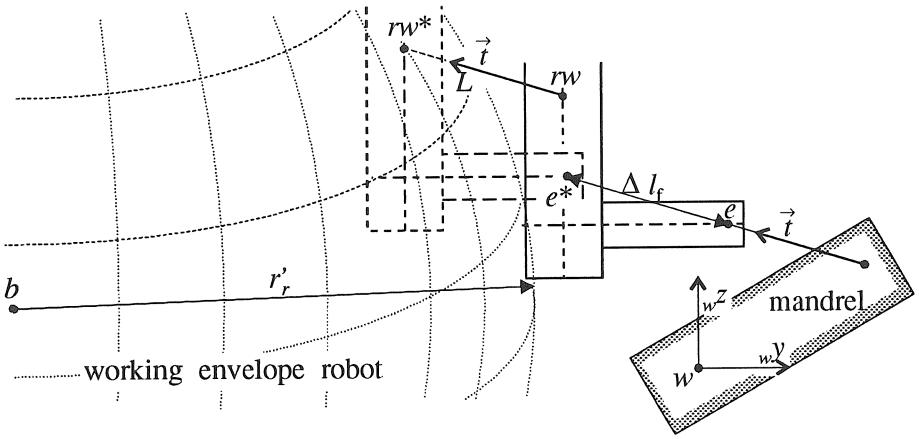

Figure 6.38: Change of the free length if the position is not attainable by the robot

Collision between Robot Wrist and Mandrel The free length is increased until the base of the robot wrist cylinder bw lies on the enveloping surface.

6.7 Simulation

Robot simulation systems have been developed for the design and programming of robot systems without needing the actual workcell. These systems include off-line programming and graphical simulation capabilities, allowing to display the motion of the robot through computer graphical animation [88]. Simulation systems have a CAD-system for 3D-modelling, based on polygonized solids [6, 88]. Robot simulation systems allow to check on collisions between the robot and peripheral devices. Robot programs are written in a generic robot language and converted by a postprocessor into the robot native language. Robot programming becomes in this way independent of the robot and programs can be loaded into different robot types [71]. The generic language has the possibilities of a classic robot language, including motion commands, I/O-communication between devices, monitoring,...

If collision is detected during the simulation of a robot task, the simulation system indicates the polygons which make contact. The operator adapts then the robot path manually by the addition of viapose or by changing the orientation of the end-effector. If the task of the robot is defined with respect to a path on a surface, these viapoints have to be chosen in such a way that the task requirements are fulfilled, which can be, as e.g. for the tape winding process, very difficult.

If the possibility of collisions is large, an automatic collision avoidance method is desired to reduce the work of the operator. Routines have then to be programmed, which change the position or the orientation of the end-effector in function of the collision information in the system's database. This requires an open software environment : the programmer should have direct access to the system's database and be able to add routines to the simulation system.

6.7.1 Simulation of the Tape Winding Process

The filament winding process is simulated to check if all collisions are avoided. Not all the possible collisions have been modelled in the heuristic collision control method, e.g. collisions between the pay-out eye and the joints of the robot are not checked. The filament winding cell is simulated in the simulation system IGRIP (Deneb Robotic Systems).

6.7.1.1 Workcell Layout

The workcell consists of three cooperating machines : the robot, the winding axis and the pay-out axis (Fig. 6.39). The robot is placed in the origin, so that the robot base coordinate system corresponds to IGRIP's world coordinate system. The mandrel support structure is defined in the winding coordinate system, which is attached to the world coordinate system.

The geometry of the mandrel is transmitted from the CAD-system to IGRIP by means of an IGES-file. IGRIP converts surfaces of revolution to polygons. Problems may occur due to this polygonization, as e.g. non-continuous linked polygons or wrongly directed polygon normals.

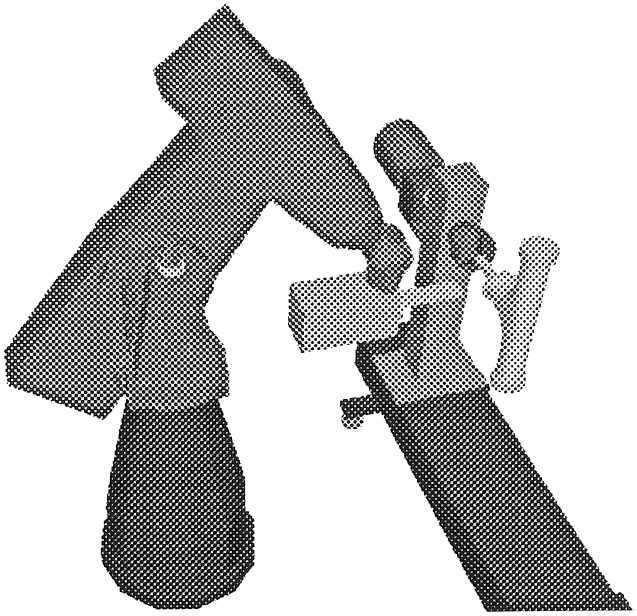

Figure 6.39: Filament winding cell in IGRIP

6.7.1.2 Simulation Program

The motion of the robot and the two external axes is simulated. The program `CAWAR` writes the poses of the robot and the external axes to a file. A program, written in the GSL-language of IGRIP, is loaded in each of the cooperating devices : `WIKKEL_PUMA` in the PUMA-762, `WIKKEL_AS`

in the winding axis and `WIKKEL_OOG` in the pay-out eye. The program `WIKKEL_PUMA` reads the poses of all variables in the file, sends a start-of-motion command to both the winding axis and the pay-out eye, moves the robot, and waits for an end-of-motion command of the winding axis and the pay-out eye before proceeding to read the file. `WIKKEL_OOG` and `WIKKEL_AS` wait continuously for a start-of-motion command, move to the demanded position, and return an end-of-motion command.

It would also be possible to simulate the placement of the tape and the motion of the tape, in order to check on interferences between the fed tape and the robot. The tape should then be programmed two times as a device with three degrees of freedom (variable length and two rotations[8]), once between the impregnation bath and the pay-out eye, and once between the pay-out eye and the mandrel. The values of these additional degrees of freedom should be provided by the user, or be derived from the motion of the robot and the contact point on the mandrel. The latter option requires that the inverse kinematics of the tape devices is programmed in the simulation package.

6.7.2 Action at Collisions

The heuristic collision control method takes only the most frequently occurring collisions into account. It is a compromise between the complexity of the problem and the ability to predict all collisions.

Collisions which occur rarely are collisions between the robot arm (joint 3) and the mandrel, collisions between the entry of the pay-out eye and the robot arm (joint 2) or the robot trunk, collisions between the entry of the pay-out eye and the mandrel support structure.

If IGRIP detects a collision during filament winding, three different actions can be taken : the collision can be added to the heuristic collision control method, resulting in an increase of the algorithm's complexity, the dimensions of the objects in the model can be adapted, or the position of the winding machine can be altered.

6.7.2.1 Add Collision to Heuristic Collision Avoidance Algorithm

This solution is the most time-consuming. If a collision has to be included in the collision control algorithm, routines have to be written

[8]The twisting of the tape is not taken into account

for collision detection and collision avoidance by (in the winding coordinate system) changing, respectively, the orientation of the pay-out axis, the angular position of the winding axis, and the free length.

Collisions which require unstable solutions (cf. p. 230) are hard to implement, and will not always lead to success. Collisions between e.g. the entry of the pay-out eye and the robot arm occur mainly when the pay-out eye is normal to the winding axis ($\tau \approx 0$). To avoid this collision, the pay-out eye is made more parallel with the winding axis, thus in an unstable direction. At this moment, collisions can occur between the pay-out cylinder or the robot wrist and the mandrel. The pay-out eye will than be made more normal to the winding axis. New collisions between the entry of the pay-out eye and the robot arm must then be avoided by a rotation about the winding axis or by decreasing the free length. Success is however not guaranteed for these two methods, since a solution has to be sought in the (in this case narrow) area between robot arm and mandrel.

6.7.2.2 Model Adaptation

The dimensions of the objects in the model are adapted to avoid two types of collisions :

- Collisions between the end of the robot arm of the PUMA-762 (joint 3) and the mandrel. These collisions are avoided by increasing the radius r_w of the robot wrist cylinder.

- Collisions between the entry of the pay-out eye and the mandrel support structure. These collisions are not modelled : the pay-out eye is modelled as a cylinder, which circumscribes the delivery section, over the whole length of the pay-out eye. The dimensions of the entry section of the pay-out eye are however much larger (Fig. 6.3). The first part of this larger section, where most collisions occur, is however incorporated in the model of the robot wrist.

  The entry of the pay-out eye collides in practice only with head- or tail-stock, if $|\tau| > 90°$ (or ${}_w v_y > 0$). To avoid these collisions the geometry of the stocks (value y_s) is increased.

6.7.2.3 Change the Set-Up

If a collision occurs between the entry of the pay-out eye and the robot arm, there are two possible actions : to take an alternative configuration of the robot (e.g. arm right instead of arm left) or to change the position of the winding machine. To check the influence of an alternative robot configuration, the simulation program is run again.

A collision between the entry of the pay-out eye and the robot arm occurs mostly when the winding machine is to close to the robot. The winding machine is than moved away from the robot, the machine is calibrated and the robot path recalculated. This has, until now, always led to a positive result.

6.8 Conclusions

This chapter discussed the heuristic method which has been developed to avoid collisions during tape winding. Collisions between the robot structure (pay-out eye and robot wrist) and the mandrel structure (mandrel and mandrel support structure) are checked and avoided. Collisions are avoided in two steps : collisions between the pay-out eye and the mandrel are avoided in the mandrel coordinate system, the other collisions in the winding coordinate system.

The heuristic method consists of four steps : collision detection, selection of the collision mode and the avoidance method, collision avoidance, and path smoothing. A distinction is made between scratching and perforating. In the scratching mode, the path obtained by linking the collision-free positions is smoothed. In the perforating mode, a via-pose is defined.

A collision-free position is sought by changing the free length, the orientation of the pay-out axis or the angle of the winding axis. The method to calculate the new position of the pay-out eye depends on the type of collision and the adaptation method. The pose of the pay-out eye is changed so, that the distance between the pay-out eye and the (approximated) surface amounts to the safety distance δ_s.

For the collisions which are not incorporated in the model, a simulation is performed. If collisions occur, the geometry of the model is adapted, e.g. by increasing the radius of the robot wrist. If collisions

between the entry of the pay-out eye and the robot trunk occur, the position of the winding machine has to be altered.

Conclusions and directions of further research

Filament winding is a production technique for fibre reinforced plastics in which the fibres are laid along prescribed directions.

A computer integrated environment has been developed round the filament winding process, encompassing design, production and quality control.

Design

The design of a wound part is an integrated process, in which three subtasks are coordinated : the design of the geometry in a CAD-system, strength calculations with finite element analysis and the calculations of the fibre paths. A computer program CAWAR has been developed for the calculation of fibre paths on parts, which have been designed in a CAD-system. The optimal fibre angles can be derived from a finite element analysis and imported into the program CAWAR. The data of the fibre paths can then be used to generate the laminate lay-up in the finite element model.

The fibre paths cannot be chosen freely, but must meet some stability criteria. If independently tensioned rovings are used to wind the part, the fibres may not slip on the surface. This leads to the requirement that the fibre path must correspond to a semi-geodesic, i.e. that the slippage tendency must be smaller than the friction coefficient. If tapes are used, the tapes may not wrinkle or contract, and the fibre path must correspond to a geodesic.

The fibre paths must be selected so, that the mandrel is uniformly covered, and that the part is as strong and as light as possible. In

order to obtain an optimal strength, the fibres are aligned with the principal stress directions.

A methodology has been developed to cover a mandrel uniformly with fibre paths. This methodology is not restricted to tubelike (or almost-axisymmetric) parts, but applies also to completely asymmetric parts. For axisymmetric and tubelike parts, a winding pattern, that covers the mandrel uniformly, can be generated by repeating a basic fibre path over the circumference. A winding pattern, that covers the mandrel completely cannot be found for asymmetric parts. In order to cover asymmetric parts uniformly, fibre paths are placed as parallel as possible to each other, over as large areas as possible

Since filament winding allows deviations of the geodesics, the fibre paths can be better aligned with the optimal fibre directions than the paths in a tape wound part, and a uniformly covered part is easier to obtain.

Directions for further research

In a tubelike part, the fibre paths, from which the patterns are generated, have to be selected so, that the part has an optimal strength and a minimal weight. Lossie [59] has studied the optimal design of geodesically wound axisymmetric parts, but this research should be extended towards the optimal design of semi-geodesically wound tubelike (and asymmetric) structures. The optimal design of filament wound parts requires multiple interactions between the FEA-program and the fibre path calculations : the fibre path must be designed, based on the results of the finite element analysis, and the material data for the finite element model are derived from the trajectory of the fibre path. Fibre path calculations and finite element analysis should therefore be thoroughly integrated.

The design of a wound part should however not be restricted to the design of the fibre paths, but must also include the design of the geometry of the part. The geometry should be such that the part is easily windable (e.g. by avoiding concavities as much as possible). A technique which can be used for the optimization of part geometry, is netting analysis, which is used for the calculation of end domes of pressure vessels [59]. A simultaneous design of shape and fibre paths can lead to a more optimal part. The optimal design of filament wound parts is the subject of the Ph.D. thesis of Jonas de Carvalho.

Production

A robotic tape winding unit has been developed, consisting of a PUMA-762 robot with 6 degrees of freedom and 2 external axes : the mandrel drive and the rotation of the delivery rolls in the pay-out eye. The rotation of the delivery rolls allows to maintain a constant band width. The robotic cell is controlled with the ALTER-mode of VAL-II : an external PC sends every robot cycle (28.8 ms) motion commands to both the robot and the external axes.

The basic material is a 25-mm wide unidirectional glass fibre tape. Tension is applied at the unwinding rolls. The tape is impregnated during the winding process.

Tapes are very sensitive to transversal forces, so that special attention has to be paid to tape guidance and tape twisting. A flexible ladder in the pay-out eye allows tape twists up to 360° without wrinkling. The drawback of the ladder is however that friction forces are very high.

The robotic cell has in total 8 degrees of freedom : three degrees of freedom are fixed by the task requirements, and three others are needed to avoid collisions efficiently. Two degrees of the freedom of the robot wrist are not used : the normal on the end flange of the robot is always directed vertically downwards, and the axis of the pay-out eye is horizontal. Since two degrees of freedom are not used, the six-axis robot could be replaced by a cheaper four-axis robot. A ceiling-mounted robot would be more appropriate than a floor-mounted robot, since it allows a more optimal position of the impregnation unit and a more optimal use of the working envelope of the robot.

An off-line robot program is generated, starting from the data of the fibre paths. The robot path is calculated so, that all the task requirements are fulfilled. The major problems which occur during the calculations of the robot path are the control of tape twists and collision control. Tape twists are controlled by an appropriate winding method and by lay-down of excess tape twists behind the pin rings, which are mounted at the ends of the mandrel and which are cut away after curing.

Collisions between the robot structure (robot wrist and pay-out eye) and the mandrel structure (mandrel and head- and tailstock) are checked and avoided by means of a heuristic method : a collision-free position is sought, based on the collision information and a selected

adaptation method. A smooth collision-free path is then generated. The winding process can be simulated in a graphical robot simulation system, to check on the collisions, which are not modelled. Actually, the only collisions which occur in the simulation are interactions between the robot and the pay-out. These collisions can be avoided by changing the set-up or the position of the winding machine.

The robot trajectory is determined so, that the maximum joint velocities and accelerations and the maximum winding speed and acceleration are not exceeded. The data are then converted to the format, required by the ALTER-mode, and transferred to the PC, which controls the winding process.

Tape winding has, compared with filament winding, several drawbacks : the design of a tape wound part is limited to geodesics and during winding special attention has to be paid to tape twisting and tape guidance. The investment cost of a tape winding machine is, compared with a filament winding machine for wide roving bundles, less, since only one tension control unit is necessary.

Design and Production of a Tape Wound T-piece

A tape wound T-piece has been designed and produced.

Fibre bridging occurs for a high amount of the geodesics on the T-piece. The main problem in the design of the T-piece is therefore the complete coverage of the mandrel with bridging-free fibre paths.

For axisymmetric and tubelike parts, one pattern can be found that covers the mandrel completely. It is not possible to cover the tape wound T-piece with only a few patterns : two main patterns can be found to cover the main parts of the T-piece, but still a number of additional geodesics is required to cover isolated spots. This results in a rather irregular outside surface (Fig. 5.23). In filament winding, the basic patterns could cover larger areas of the T-piece, by deviating from the geodesics, and could perhaps even cover the mandrel completely.

Finite element analysis is only used as a validation tool. Strength calculations indicated that the strength of the part is not sufficient at the planes, so that additional reinforcements have to be added. Tape winding may therefore not be the most appropriate way to produce the T-piece, and other fabrication methods should be evaluated.

The T-piece has been wound successfully. The residual twists, which remain in the tape after the motion behind the pin rings, cause

sometimes contraction of the tape just behind the pin rings. The time necessary to wind the T-piece is relatively long. Especially the motion behind the pins rings, at the ends of the cylinder transverse to the winding axis, requires much time. The speed can be increased by a more optimal design of the pay-out eye (transmission ratio of the gears), and by an optimization of the motion behind the pin rings.

Possible improvements of the program CAWAR

The program CAWAR has been developed to be able to design and to wind T-pieces.

At this moment, the program is limited to "simple" CAD-surfaces, like surfaces of revolution and ruled surfaces. More general surfaces, like B-spline surfaces, need to be implemented in order to make the program more general. For the addition of new surfaces, routines have to be included to read the data in the IGES-file and to evaluate the surface.

No major problems are expected for winding other parts than T-pieces. For most parts, the risk of collisions is much smaller than for the T-piece. All pin rings in the T-piece have a circular cross section, and can be modelled as cylinders. When the cross section is not circular, the pin ring has to be modelled as a tabulated cylinder. Some adaptations are then required for the calculation of the fibre path on the pin ring, and the linking motion.

The interaction between CAWAR and the CAD-system is currently minimal. The CAD-system is only used for the design of the part and the representation of the fibre paths. All the other input is entered interactively in CAWAR. The user-friendlyness of the program should be increased (and the risk of errors decreased) if the capabilities of the CAD-system would be used for the generation of the model of e.g. the pin rings and the set-up.

Directions for further research

One of the major drawbacks of wet filament winding is the difficult control of fibre-resin content and interlaminar pressure. To obtain a constant interlaminar pressure, the fibre tension should be inverse proportional to the path curvature. For a complex part the fibre tension should therefore be computer-controlled. The desired value of the fibre

tension must be calculated at each point of the machine path and sent to the tension controller, which should control the tension in a point, which should be as near as possible to the delivery point.

The influence of the different process and material parameters and the choice of the optimal parameters for winding cylinders is the subject of a Brite/Euram program which is about to start at K.U.Leuven.

Thermosetting resins are still the major matrix material for composites. Thermoplastics have many interesting properties, such as an improved damage tolerance and short processing cycles. Compared to thermoset filament winding, larger deviations from geodesics are allowed, since the incoming material is welded directly to the substrate. As for thermoset filament winding, a robot could be used to guide the pay-out eye. Both the heating system (e.g. inert gas torch) and the consolidation roller must be attached to the end flange of the robot. The heat must be concentrated near the consolidation point, and the consolidation roller must be normal to the surface. These requirements determine six degrees of freedom, so that only one degree of freedom can be chosen freely, and be used to avoid collisions.

Quality Control

A robotic ultrasonic C-scanning cell has been developed for quality control of curved composite parts. A pulse-echo method with water jet transmission is used. Starting from a CAD-model of the part, the positions of the robot are calculated, and transferred to the PC, that controls the scanning process. After scanning, the ultrasonic measuring data are sent to a VAX-workstation for an image analysis. The robotic ultrasonic C-scanning works well for curved laminated structures with a constant thickness. The results obtained by scanning filament wound parts, which had no additional finishing, are however not so good, due to the variations in the thickness.

Directions for further research

Off-line programming requires an accurate CAD-model and calibration data. The generation of these data is very time-consuming. An alternative would be to start from a rough model and to adapt the robot path during scanning. This could be performed by the application of force control : a force sensor is mounted between the squirter and the

end flange of the robot, and the position of the robot is adapted in function of the sensor data.

Bibliography

[1] R. AERTGEERTS, W. GEERAERTS, *Geleidingseenheid voor het Wikkelen met Thermoplasten* – Design Project 90MO13, Faculty of Applied Sciences, Division PMA, K.U.Leuven, 1990

[2] H.L. BARKING, *Steuerungskonzepte für das Präzisionswickeln von faserverstärkten Kunststoffen* – Ph.D. Dissertation, Rheinisch-Westfälische Technische Hochschule, Aachen, 1977

[3] J.R. BARTH, *Fabrication of Complex Composite Structures Using Advanced Fiber Placement Technology* – 35th International SAMPE Symposium, April 2-5, 1990, pp. 710-720

[4] O.K. BERGSMA, *Deep Drawing of Fabric Reinforced Thermoplastics* – Manufacture and In Service Behaviour of Composites, European Postgraduate Education in Polymer and Composites Engineering (EUPOCO), K.U.Leuven, 1992, Module 5.4.4

[5] J.E. BOBROW, S. DUBOWSKY, J.S. GIBSON, *Time-optimal Control of Robotic Manipulators along Specified Paths* – International Journal of Robotics Research, 4/3, Fall 1985, pp. 3-17

[6] F. BONTE, K. MEERSMANS, *Geodetisch Wikkelen van Komposietmaterialen* – Engineering Thesis 88E07, Faculty of Applied Sciences, Division PMA, K.U.Leuven, 1988

[7] W. BRAUN, *A Control System for Filament Winding Equipment as a Pre-requisite for Automation* – 1st International Conference Automated Composites, PRI, Nottingham, September 10-12, 1986, pp. 11/1-11/11

[8] D. BROCHIER, J. HAVERHALS, *Studie voor On-line Toepassing van Inverse Kinematica en Dynamica* – Engineering Thesis 88E16, Faculty of Applied Sciences, Division PMA, K.U.Leuven, 1988

[9] R.A. BROOKS, *Planning Collision-Free Motions for Pick-and-Place Operations* – International Journal of Robotics Research, 2/4, 1983, pp. 19-44

[10] S. BRYON, O. VAN AELST, *Robotsturing voor het Wikkelen van Composietstukken* – Engineering Thesis 87E06, Faculty of Applied Sciences, Division PMA, K.U.Leuven, 1987

[11] R.O. BUCHAL, D.B. CHERCHAS, *An Iterative Method for Generating Kinematically Feasible Interference-free Robot Trajectories* – Robotica, 7/2, 1989, pp. 119-127

[12] F. BULLOCK, S. KOWALSKI, R. YOUNG, *Automated Prepreg Tow Placement for Composite Structures* – 35th International SAMPE Symposium, April 2-5, 1990

[13] G. BURKHARDT, *Eigenschaften den Verbundwerkstoffe* – Wickeltechnik für Faserverbundbauteile – Auslegung – Fertigung – Prüfung, Aachener Demonstrationszentrum für Faserverbundkunststoffe, October 15-16, 1990, pp. 33-76

[14] E.P. CALIUS *Filament Winding of Composite Cylinders* – Ph.D. Dissertation, Stanford University, 1989

[15] J.H. CAMPBELL, J.L. KITTELSON, *The Tape Winding Process and Applications* – 36th International SAMPE Symposium, San Diego, April 15-18, 1991, pp. 791-805

[16] J.F. CANNY, *The Complexity of Robot Motion Planning* – Ph.D. Dissertation, MIT, Cambridge, Mass., 1987

[17] S. COPPENS, D. DURT, *Sturing van een Twee-assige Wikkelmachine* – Engineering Thesis 90EP22, Faculty of Applied Sciences, Division PMA, K.U.Leuven, 1990

[18] J.J. CRAIG, *Introduction to Robotics – Mechanics & Control* – Addison-Wesley, Reading, 1986

[19] PH. DE BIE, S. SERRIEN, *Sturen van een Robot met door CAD Gegenereerde Gegevens* – Engineering Thesis 86E24, Faculty of Applied Sciences, Division PMA, K.U.Leuven, 1986

[20] J. DE CARVALHO, *Fibre Path Optimisation Based on Non-geodesic Winding*, Master's Thesis 92EP26, Faculty of Applied Sciences, Division PMA, K.U.Leuven, 1992

[21] R. De Samblanx, *Bijdrage tot het Gerobotiseerd Wikkelen met Glasvezelbanden* – Ind. Eng. Thesis, Instituut De Naeyer, Mechelen, 1991

[22] J. De Schutter, *An Introduction to PID Control and its Application to Motion Control* – Computer Controlled Motion and Robotics - Lecture Notes of the Integrated European Course in Mechatronics, K.U.Leuven, June 1991, pp. 77-110

[23] F. Dings, V. Eerlingen, *Realisatie van een Real-time PC Sturing van Robots* – Engineering Thesis 88E25, Faculty of Applied Sciences, Division PMA, K.U.Leuven, 1988

[24] G. Di Vita, M. Marchetti, P. Moroni, P. Perugini, *Designing Complex Shape Filament-Wound Structures* – Composites Manufacturing, 3/1, 1992, pp. 53-58

[25] F.S. Dominguez, *Unidirectional Tape Prepregs* – Engineered Materials Handbook, Vol. 1, Composites, ASM International, 1987, pp. 143-145

[26] D.R. Dreger, *The Challenge of Manufacturing Composites* – Machine Design, October 22, 1987, pp. 92-98

[27] T.L. Elegante, *Filament Winding* – Mechanical Engineering, December 1986, pp. 32-36

[28] D.G. Elliman, P. Sorenti, L. Brown, M. Shearing, V. Middleton, M.J. Owen, *A Cell for the Manufacture of Composite Components by Filament Winding* – Advanced Manufacturing Engineering, Vol. 1, October 1990, pp. 15-20

[29] M.L. Enders, *The Fiber-Placement Process* – Proceedings of the 8th International Conference on Composite Materials, Honolulu, July 15-19, 1991, pp. 14.B.1-14.B.11

[30] G.J. Evans, *The Processing of Pre-impregnated Composite Materials* – 2nd International Conference : Automated Composites '88, PRI, Noordwijkerhout, September 26-28, 1988, pp. 8/1-8/6

[31] I.D. Faux, M.J. Pratt, *Computational Geometry for Design and Manufacture* – Ellis Horwood Publishers, Chichester, 1979

[32] G.F. Franklin, J.D. Powell, M.L. Workman, *Digital Control of Dynamic Systems* – Addison Wesley, Reading, 1990

[33] A. GILBU, *The Drostholm Continous Filament Winding Process* – 26th Annual Technical Conference, Reinforced Plastics/Composites Division, The Society of Plastics Industry, 1971, pp. 16.D.1-16.D.6

[34] M. GOEDEL, *Vorstellung verschiedener Wickelmaschinen und Wickelvorrichtungen* – Wickeltechnik für Faserverbundbauteile – Auslegung – Fertigung – Prüfung, Aachener Demonstrationszentrum für Faserverbundkunststoffe, October 15-16, 1990, pp. 133-171

[35] M. GOEDEL, *Fasertränkung und Rovingführung* – Wickeltechnik für Faserverbundbauteile – Auslegung – Fertigung – Prüfung, Aachener Demonstrationszentrum für Faserverbundkunststoffe, October 15-16, 1990, pp. 211-249

[36] W.B. GOLDSWORTHY, *Two-stage Tape Placement System* – Progress in Advanced Materials and Processes : Durability, Reliability and Control, Elsevier, 1985, pp. 211-222

[37] M.T. HARVEY, *Thermoplastic Matrix Processing* – Engineered Materials Handbook, Vol. 1, Composites, ASM International, 1987, pp. 544-553

[38] D.E. HAUBER, L.A. HILL, *Automated Fiber Placement of Thermoplastic Components on Complex Shapes* – Fabricating Composites '90, Arlington, October 8-11, 1990, SME technical paper EM90-658

[39] E.A. HILLE, *Faserwickeltechnik – Methoden zur Herstellung Geometrish Komplizierten Bauteile* – Ph.D. Dissertation, Rheinisch-Westfälische Technische Hochschule, Aachen, 1981

[40] B.E. HOSKIN, A.A. BAKER, *Composite Materials for Aircraft Structures* – AIAA Educational Series, New York, 1986

[41] J. HÜMMLER, S.K. LEE, K.V. STEINER, *Recent Advances in Thermoplastic Robotic Filament Winding* – 36th International SAMPE Symposium, San Diego, April 15-18, 1991

[42] M. JEHRKE, *Bauteilbeispiele zur Anwendung von Faserverbundwerkstoffe aus dem Bereich der Wickeltechnik* – Wickeltechnik für Faserverbundbauteile – Auslegung – Fertigung – Prüfung, Aachener Demonstrationszentrum für Faserverbundkunststoffe, October 15-16, 1990, pp. 6-30

[43] P. KESTELOOT, S. BELAEN, J.P. KRUTH, *Final Report of Development Group M0 : System Independent Programming Interface* – Brite Modesti – Project 1391 : Mould Design and Manufacturing Optimisation by Development, Standardisation and Integration of CAD/CAM Procedures, 1990

[44] P. KESTELOOT, J.P. KRUTH, *CAD-Data Exchange by means of Neutral Format Interfaces. Analysis of the Existing Standards (IGES, VDAFS, SET)* – 1988 Integrated European Course in Mechatronics, K.U.Leuven, May 30 - June 3, 1988

[45] J.L. KITTELSON, *Tape Winding : A Logical Progression and Alternative to Filament Winding* – SAMPE Journal, 26/1, 1990, pp. 37-42

[46] J.L. KITTELSON, J.H. CAMPBELL, *Method and Apparatus for Tape Winding on Irregular Shapes* – U.S. Patent 4,909,880 (to General Dynamics Corp.), 1990

[47] K.W. KIRBERG, *Konzept zur Prozeßsimulation der Faserwickeltechnologie* – Ph.D. Dissertation, Rheinisch-Westfälische Technische Hochschule, Aachen, 1988

[48] M. KIRĆANSKI, M. VUKOBRATOVIĆ, *Contribution to Control of Redundant Robotic Manipulators in an Environment with Obstacles* – The International Journal of Robotics Research, 5/4, 1986, pp. 112-119

[49] F.K. KO, *Braiding* – Engineered Materials Handbook, Vol. 1, Composites, ASM International, 1987, pp. 519-528

[50] J.F. KOBER, *Automated Fiber Placement – Process Creativity* – 30th National SAMPE Symposium, March 19-21, 1985, pp. 1238-1245

[51] G.A. KORN, T.M. KORN, *Mathemathical Handbook for Scientists and Engineers* – McGraw-Hill, 1968

[52] M. KROLEWSKI, T. GUTOWSKI, *Automation of Advanced Composite Fabrication Processes on Part Cost* – Proceedings of the 18th SAMPE Technical Conference, October 1986, pp. 83-97

[53] J.C. LATOMBE, *Robot Motion Planning* – Kluwer Academic Publishers, Boston, 1991

[54] S.Y. LEE, *Filament Winding Process Model* – Ph.D. Dissertation, Stanford University, 1989

[55] X.L. Li, D.H. Lin *Non-Geodesic Winding Equations on a General Surface of Revolution* – Proceedings of the 6th International Conference on Composite Materials, London, 1987, pp. 1.152-1.160

[56] X. Liao, *Control of a Filament Winding Machine* – Master's Thesis 87E19, Faculty of Applied Sciences, Division PMA, K.U.Leuven, 1987

[57] E. Linclau, J. Rousseau, *Een Krachtsensor voor de PUMA-robot* – Engineering Thesis 89E07, Faculty of Applied Sciences, Division PMA, K.U.Leuven, 1989

[58] D.G. Lloyd-Thomas, G.C. Eckold, G.M. Wells, *Asymmetric Filament Winding* – 2nd International Conference : Automated Composites '88, PRI, Noordwijkerhout, September 26-28, 1988, pp. 12/1-12/12

[59] M. Lossie, *Production Oriented Design of Filament Wound Composites* – Ph.D. Dissertation 90D5, Faculty of Applied Sciences, Division PMA, K.U.Leuven, 1990

[60] T. Lozano-Pérez, J.L. Jones, E. Mazer, P.A. O'Donnell, *Task-Level Planning of Pick-and-Place Robot Motions* – IEEE Computer, March 1989, pp. 21-29

[61] W.T. McCarvill, *Filament Winding Resins* – Engineered Materials Handbook, Vol. 1, Composites, ASM International, 1987, pp. 135-138

[62] W. Michaeli, U. Rosenbaum, *Structural Braiding of Complex FRP Parts - A New Approach for Higher Productivity* – 34th International SAMPE Symposium, May 8-11, 1989, pp. 1834-1842

[63] W. Michaeli, M. Wegener, *Einführung in die Technologie der Faserverbundwerkstoffe* – Carl Hanser Verlag, Munich, 1989

[64] V. Middleton, M.J. Owen, D.G. Elliman, M. Shearing, *Developments in Non-axisymmetric Filament Winding* – 2nd International Conference : Automated Composites '88, PRI, Noordwijkerhout, September 26-28, 1988, pp. 10.1-10.15

[65] M. Munro, *Review of Manufacturing of Fiber Composite Components by Filament Winding* – Polymer Composites, 9/5, 1988, pp. 352-359

[66] Y. NAKAMURA, H. HANAFUSA, T. YOSHIKAWA, *Task-Priority Based Redundancy Control of Robot Manipulators* – The International Journal of Robotics Research, 6/2, 1987, pp. 3-15

[67] H. NOLLET, PH. VERHEYEN, *Ontwerp van een Geleidingseenheid voor het Wikkelen van Kunststofbanden* – Design Project 89MO13, Faculty of Applied Sciences, Division PMA, K.U.Leuven, 1989

[68] H. NOLLET, PH. VERHEYEN, *Gerobotiseerd Wikkelen van Cilinders met Glasvezelbanden* – Engineering thesis 90EP04, Faculty of Applied Sciences, Division PMA, K.U.Leuven, 1990

[69] B. O'NEILL, *Elementary Differential Geometry* – Academic Press, New York, 1966

[70] W. PERSOONS, *Robot Performance tests on KUKA IR 363/08/15 - Measurements report*, Report 92R2, Division PMA, K.U.Leuven, 1991

[71] W. PERSOONS, *New Trends in Off-Line Programming* – Symposium Robotica in België, Twaalf Jaren Later, Zellik, April 1, 1992

[72] K. PETERS, G. GREENING, *Filament Winding of Preimpregnated Rovings* – BASF, 1989

[73] S.T. PETERS, W.D. HUMPHREY, R.F. FORAL, *Filament Winding - Composite Structure Fabrication* – SAMPE, Covina, 1991

[74] F. PFEIFFER, R. JOHANNI, *A Concept for Manipulator Trajectory Planning* – IEEE Journal of Robotics and Automation, RA-3/2, 1987, pp. 115-123

[75] R.J. PHILPOT, *Finishing and Coating Techniques for Filament Wound Composite Structures* – 35th International SAMPE Symposium, April 2-5, 1990, pp. 721-733

[76] H.V. REVIE, W.M. BANKS, *Experimental Stress Analysis of Glass Reinforced Plastic Pipes with Tee Pieces* – 44th Annual Conference, Composites Institute, The Society of the Plastics Industry, February 6-9, 1989, pp. 13.C.1-13.C.6

[77] J.H.C. ROWAN, *Advanced Filament Winding : Evolution and Revolution* – Metals and Materials, May 1988, pp. 280-284

[78] P.A. ROY, *Tube Rolling* – Engineered Materials Handbook, Vol. 1, Composites, ASM International, 1987, pp. 569-574

[79] A.E. SAMUEL, C.R. BURVILL, *Tracing Surfaces with a Robot Manipulator* – ICAR '91, pp. 493-499

[80] D. SCHILDERMANS, P. VAN GENECHTEN, *Geodetisch Wikkelen van Rotatiesymmetrische Komposietstructuren* – Engineering Thesis 88E08, Faculty of Applied Sciences, Division PMA, K.U.Leuven, 1988

[81] J. SCHOLLIERS, K. BARTHOLOMÉ, *Computergesteund Ontwerpen en Fabriceren van Complexe Oppervlakken* – Engineering Thesis 86E02, Faculty of Applied Sciences, Division PMA, K.U.Leuven, 1986

[82] J. SCHOLLIERS, M. LOSSIE, H. VAN BRUSSEL, *Wikkelen van T-stukken* – Report 89R13, Faculty of Engineering, Division PMA, K.U.Leuven, 1989

[83] M.M. SCHWARTZ, *Composite Materials Handbook* – McGraw-Hill Book Company, New York, 1983

[84] M. SHARIR, *Algorithmic Motion Planning in Robotics* – IEEE Computer, March 1989, pp. 9-20

[85] D.E. SHAW-STEWART, *Filament Winding – Materials and Engineering* – Materials and Design, 6/3

[86] D.E. SHAW-STEWART, *Pullwinding* – 2nd International Conference : Automated Composites '88, PRI, Noordwijkerhout, September 26-28, 1988, pp. 15/1-15/14

[87] K.G. SHIN, N.D. MCKAY, *Minimum-Time Control of Robotic Manipulators with Geometric Path Constraints* – IEEE Transactions on Automatic Control, AC-30/6, 1985, pp. 531-541

[88] P. SIMKENS, *Graphical Simulation of Sensor Controlled Robot* – Ph.D. Dissertation 90D6, Faculty of Applied Sciences, Division PMA, K.U.Leuven, 1990

[89] J. SIMONS (Ed.), *Mathemathica, Programmatie en Controle van Industriële Robots* – K.U.Leuven, July 4-5, 1983

[90] S.H. SUH, K.S. LEE, *Solving Toll-Interference Problem for Four-Axis NC-Machining* – Proceedings of the 1992 IEEE In-

ternational Conference on Robotics and Automation, Nice, May 12-15, 1992, pp. 981-986

[91] B. SMITH, K. BRAUNER, P. KENNICOTT, M. LIEWALD, J. WELLINGTON, *Initial Graphics Exchange Specification (IGES) version 2.0* – National Bureau of Standards Report, US Department of Commerce, Washington, 1983

[92] K.T. SONG, *Planning and Control of a Mobile Robot Based on an Ultrasonic Sensor* – Faculty of Applied Sciences, Division PMA, K.U.Leuven, 1989

[93] B.E. SPENCER, *Tooling Considerations for the Filament Winding Process* – Productive Filament Winding Technology for Manufacturing Engineers and Technologists, Los Angeles, August 23-25, 1988, SME – Technical Paper MS88-800

[94] K.V. STEINER, *Development of a Robotic Filament Winding Workstation for Complex Geometries* – 35th International SAMPE Symposium, April 2-5, 1990, pp. 757-766

[95] A.B. STRONG, *Fundamentals of Composites Manufacturing – Materials, Methods and Applications* – Society of Manufacturing Engineers, Dearborn, 1989

[96] K. SUBRAMANIAN, J.L. ROSE, *C-Scan Testing for Complex Parts* – Advanced Materials & Processes, 87/2, pp. 40-43

[97] Y.M. TARNOPOLS'KII, A.I. BEIL', *Problems of the Mechanics of Composite Winding* – Fabrication of Composites, Handbook of Composites, Volume 4, Elsevier, Amsterdam, 1983, pp. 45-108

[98] S. TORNINCASA, R. IPPOLITO, N. BELLOMO, *New Trends in Robotics : the Robotized Lay Up of Carbon Fiber Tapes on Surfaces with Large Curvature* – Proceedings 21th Symposium on Industrial Robotics, IFS, October 1990, pp. 215-220

[99] S.W. TSAI, *Composites Design* – Think Composites, Dayton, 1988

[100] J.T.S. TZENG, *A Model of the Winding and Curing Processes for Filament Wound Composites*, Ph.D. Dissertation, Virginia Polytechnic Institute and State University, 1988

[101] S.M. UDUPA, *Collision Detection and Avoidance in Computer Controlled Manipulators* – Ph.D. Dissertation, California Insitute of Technology, 1977

[102] H. VAN DER AUWERAER, *Development and Evaluation of Advanced Measurement Methods for Experimental Modal Analysis* – Ph.D. Dissertation 87D3, Faculty of Applied Sciences, Division PMA, K.U.Leuven, 1987

[103] H. VAN BRUSSEL, *Evaluation and Testing of Robots* – Cirp Annals 90 – Manufacturing Technology, (39)2, 1990, pp. 657-664

[104] TH. VAN DER WAETEREN, *Servomechanismen en Regeltechniek* – VTK, Leuven, s.d.

[105] D. VEREECKE, F. VANDEWALLE, *Gerobotiseerd C-scannen van Composietvoorwerpen* – Engineering thesis 90EP03, Faculty of Applied Sciences, Division PMA, K.U.Leuven, 1990

[106] W.J.P. VINK, N.H.R. VERSLUIS, *Niet Destructief Onderzoek* – Vereniging voor studie- en studentenbelangen, Delft, 1980

[107] E. VON GELLHORN, *Die Fertigung von Technischen Teilen im Wickelverfahren* – Ph.D. Dissertation, Rheinisch-Westfälische Technische Hochschule, Aachen, 1985

[108] P.M. WACKERLE, R. WETTER, *Range of Applications in Filament Winding* – Industrial and Production Engineering, 10/3, 1986, pp. 37-45

[109] M. WECK, H. ZENDER, F. HERBERG, *Automatisierte Fertigung von Faserverbundbauteilen im Wickelverfahren* – VDI-Z, 131/5, 1989, pp. 47-52

[110] G.M. WELLS, K.F. MCANULTY, *Computer Aided Filament Winding Using Non-Geodesic Trajectories* – Proceedings of the 6th International Conference on Composite Materials, London, 1987, pp. 1.161-173

[111] J.A.S. WHITING, *Automated Manufacture of Advanced Thermoplastic Composites* – Paper presented at Automated Composites '88, Noordwijkerhout, September 26-28, 1988

[112] H.T. YAU, C.H. MENG, *Path Planning for Automated Dimensional Inspection Using Coordinate Measuring Machines*, Proceedings of the 1991 IEEE International Conference on Robotics and Automation, Sacramento, April 1991, pp. 1934-1939

[113] N., *Robot Filament-Winds Asymmetrical Parts* – Modern Plastics International, Nov. 1986, pp. 24-25

[114] N., *Servo-Fadenspannungsregler STC* – Josef Baer, Weingarten, s.d.

[115] N., *En-Tec's FiberGrafix Software* – En-Tec, Salt Lake City, s.d.

[116] N., *En-Tec Filament Winding Machines – Wimax Control System* – En-Tec, Salt Lake City, s.d.

[117] N., Technical Data-Sheet Woven Tapes – Eurocarbon Tilburg B.V., s.d.

[118] N., *General Purpose Motion Control IC HCTL-1000 Data Sheet* – Hewlet Packard, 1985

[119] N., *AUSS-V, Automated Ultrasonic Scanning System, Technical Description* – McDonnell Douglas, 1989

[120] N., *MAUS, Mobile Automated Ultrasonic Scanner, Technical Description* – McDonnell Douglas, 1990

[121] N., *The Nag Fortran Library Manual, Mark 15* – Oxford, 1991

[122] N., *Unimate Industrial Robots – Puma 700 Series Mark III – Val II (Models 761/762) Equipment Manual 398Z1* – Unimation, Danbury, 1985

[123] N., *User's Guide to VAL II – Programming Manual* – Unimation, Danbury, 1984

[124] N., *VDA-Flächenschnitstelle (VDAFS) Version 2.0* – Verband der Automobilindustrie (VDA), Frankfurt, 1987

Appendix A

Calculation of Particular Fibre Paths

A.1 Fibre Path on a Surface of Revolution

In this section the equations for a semi-geodesic on a surface of revolution are derived. These equations are translated into the equation of Clairaut (1.9) for geodesics.

A.1.1 Path on a Surface of Revolution

The equation of a surface of revolution is :

$$\mathbf{s}(x,\theta) = [x \quad r(x)\cos\theta \quad r(x)\sin\theta]^T \tag{A.1}$$

with x the axial coordinate and θ the circumferential coordinate. The normalized derivatives in x- and θ-direction are :

$$\mathbf{s}_x = \left[\frac{1}{A} \quad \frac{r'}{A}\cos\theta \quad \frac{r'}{A}\sin\theta\right]^T \tag{A.2}$$

$$\mathbf{s}_\theta = [0 \quad -\sin\theta \quad \cos\theta]^T \tag{A.3}$$

with $r' = \frac{dr}{dx}$ and $A = \sqrt{1+r'^2}$.

The tangent $\vec{t}$ to the fibre path $\Gamma(s) = [x(s)\ \theta(s)]^T$ can be written as the derivative of (A.1) :

$$\mathbf{t} = \left[\frac{dx}{ds} \quad r'\frac{dx}{ds}\cos\theta - r\frac{d\theta}{ds}\sin\theta \quad r'\frac{dx}{ds}\sin\theta + r\frac{d\theta}{ds}\cos\theta\right]^T \tag{A.4}$$

or, with the winding angle, i.e. the angle between the tangent to the fibre path and the generatrix of the surface, measured in the tangent plane to the surface (cf. p. 34) :

$$\mathbf{t} = \mathbf{s}_x \cos\alpha + \mathbf{s}_\theta \sin\alpha = \frac{1}{A}\begin{bmatrix} \cos\alpha \\ r'\cos\theta\cos\alpha - A\sin\theta\sin\alpha \\ r'\sin\theta\cos\alpha + A\cos\theta\sin\alpha \end{bmatrix} \tag{A.5}$$

By comparing (A.4) and (A.5) the relation between $\frac{d\theta}{ds}$ and $\frac{dx}{ds}$ and the winding angle α can be derived :

$$\frac{d\theta}{ds} = \frac{\sin\alpha}{r} \tag{A.6}$$

$$\frac{dx}{ds} = A\cos\alpha = \frac{\cos\alpha}{\sqrt{1+r'^2}} \tag{A.7}$$

The normal $\vec{n} = -\vec{s}_x \times \vec{s}_\theta$ on the surface equals :

$$\mathbf{n} = \left[\frac{-r'}{A} \quad \frac{1}{A}\cos\theta \quad \frac{1}{A}\sin\theta\right]^T \tag{A.8}$$

The binormal $\vec{b} = \vec{t} \times \vec{n}$ equals :

$$\mathbf{b} = \frac{1}{A}\begin{bmatrix} -\sin\alpha \\ -A\sin\theta\cos\alpha + r'\cos\theta\sin\alpha \\ -r'\sin\theta\sin\alpha - A\cos\theta\cos\alpha \end{bmatrix} \tag{A.9}$$

The curvature vector $\vec{c}$ is calculated by differentiating $\vec{t}$ to s.

The slippage tendency λ is defined by Eq. (3.5) :

$$\lambda = \frac{\vec{c}\cdot\vec{b}}{-\vec{c}\cdot\vec{n}} \tag{A.10}$$

This equation becomes, with (A.5),(A.8) and (A.9), after simplification :

$$\lambda = \frac{A^2 r'\sin\alpha + A^3 r\frac{d\alpha}{ds}}{A^2\sin^2\alpha - rr''\cos^2\alpha} \tag{A.11}$$

or, in function of $\frac{d\alpha}{ds}$:

$$\frac{d\alpha}{ds} = \frac{\lambda(A^2\sin^2\alpha - rr''\cos^2\alpha) - A^2 r'\sin\alpha}{A^3 r} \tag{A.12}$$

Eq. (A.12) becomes, with (A.7) :

$$\frac{d\alpha}{dx} = \frac{\lambda(A^2\sin^2\alpha - rr''\cos^2\alpha) - r'A\sin\alpha}{rA^2\cos\alpha} \tag{A.13}$$

A.1.2 Equation of Clairaut

Eq. (A.13) becomes for a geodesic :

$$\frac{d\alpha}{dx} = -\frac{r\sin\alpha}{r'\cos\alpha} \tag{A.14}$$

or :

$$r\cos\alpha\frac{d\alpha}{dx} + \frac{dr}{dx}\sin\alpha = \frac{d(r\sin\alpha)}{dx} = 0 \tag{A.15}$$

or :

$$r\sin\alpha = c_c \tag{A.16}$$

with c_c a constant. Eq. (A.16) is called the equation of Clairaut [59].

A.1.3 Calculation of Geodesics on a Surface of Revolution

The relation between the radial parameter $d\theta$ and the axial parameter dx is given by combining (A.6) and (A.7) :

$$d\theta = \frac{\tan\alpha}{Ar}dx = \frac{\tan\alpha}{r}\sqrt{1+r'^2}dx \tag{A.17}$$

With the equation of Clairaut (A.16) :

$$d\theta = \frac{c_c}{r}\sqrt{\frac{1+r'^2}{r^2-c_c^2}}dx \tag{A.18}$$

Integration over the axial coordinate x :

$$\theta(x) = \theta(x_0) + c_c\int_{x_0}^{x}\frac{1}{r(u)}\sqrt{\frac{1+r'^2(u)}{r(u)^2-c_c^2}}du \tag{A.19}$$

A.1.3.1 Geodesic on a Cylinder

For a cylinder is $r(x)$ constant. Eq. (A.19) is then :

$$\theta(x) = \theta_0 + \frac{c_c(x-x_0)}{r\sqrt{r^2-c_c^2}} = \theta_0 + (x-x_0)\tan\alpha \tag{A.20}$$

A.1.3.2 Geodesic on a Cone

The radius of a cone is given by $r(x) = r_0 + kx$. Eq. (A.19) is :

$$\theta(x) = \theta_0 + c_c \int_{x_0}^{x} \frac{1}{r_0 + ku} \sqrt{\frac{1+k^2}{(r_0+ku)^2 - c_c^2}} du \tag{A.21}$$

u is replaced by $v = \frac{r_0+ku}{c_c}$. Eq. (A.21) becomes :

$$\theta = \theta_0 + \frac{\sqrt{1+k^2}}{k} \int_{\frac{r_0+kx_0}{c_c}}^{\frac{r_0+kx}{c_c}} \frac{1}{v} \sqrt{\frac{1+k^2}{v^2-1}} dv \tag{A.22}$$

v is replaced by $z = \frac{1}{v}$:

$$\theta = \theta_0 + \frac{\sqrt{1+k^2}}{k} \int_{\frac{c_c}{r_0+kx_0}}^{\frac{c_c}{r_0+kx}} \frac{-dz}{\sqrt{1-z^2}} \tag{A.23}$$

or [2] :

$$\theta = \theta_0 + \frac{\sqrt{1+k^2}}{k} \left[\arccos\left(\frac{c_c}{r_0+kx}\right) - \arccos\left(\frac{c_c}{r+kx}\right) \right] \tag{A.24}$$

or, in function of the winding angle (with Clairaut : $\sin\alpha = \frac{c_c}{r}$) :

$$\theta = \theta_0 + (\alpha_r - \alpha_0) \frac{\sqrt{1+k^2}}{k} \tag{A.25}$$

A.1.4 Path with Constant Slippage Tendency on a Cylinder

Consider a cylinder, with radius r and length L. The derivative $r' = 0$. Eq. (A.13) becomes :

$$\frac{d\alpha}{dx} = \frac{\lambda \sin^2\alpha}{r\cos\alpha} \tag{A.26}$$

The relation between the winding angle and the radial coordinate θ is with (A.6) and (A.7) :

$$\frac{d\alpha}{d\theta} = \frac{\frac{d\alpha}{dx}\frac{dx}{ds}}{\frac{d\theta}{ds}} = \lambda \sin\alpha \tag{A.27}$$

A.1.4.1 Path with a constant slippage tendency

For a semi-geodesic with constant slippage tendency λ, that starts at $x = 0$ and $\theta = 0$, is the x-coordinate in function of the winding angle, that changes from α_0 to α_e, given by :

$$x = \frac{r}{\lambda} \int_{\alpha_0}^{\alpha_e} \frac{\cos\gamma}{\sin^2\gamma} d\gamma \tag{A.28}$$

By substituting $t = \tan\frac{\alpha}{2}$:

$$x = \frac{r}{\lambda} \int_{\tan\frac{\alpha_0}{2}}^{\tan\frac{\alpha_e}{2}} \frac{1-t^2}{2t^2} dt \tag{A.29}$$

or :

$$x = \frac{r}{2\lambda} \left[\left(\frac{1}{\tan\frac{\alpha_0}{2}} + \tan\frac{\alpha_0}{2} \right) - \left(\frac{1}{\tan\frac{\alpha_e}{2}} + \tan\frac{\alpha_e}{2} \right) \right] \tag{A.30}$$

In function of the radial parameter θ :

$$\theta = \frac{1}{\lambda} \int_{\alpha_0}^{\alpha_e} \frac{d\alpha}{\sin\alpha} = \frac{1}{\lambda} \left[\ln\left(\tan\frac{\alpha_e}{2}\right) - \ln\left(\tan\frac{\alpha_0}{2}\right) \right] \tag{A.31}$$

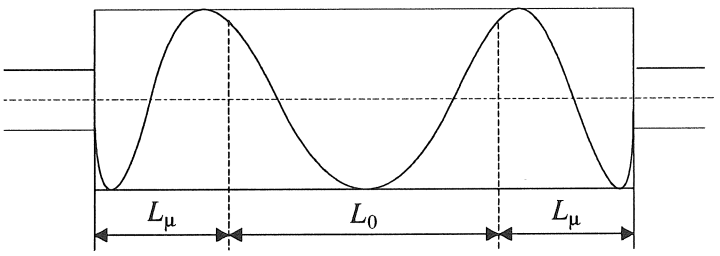

Figure A.1: Fibre path on a cylinder with return at ends

A.1.4.2 Application : Winding a cylinder with return of the fibre path at the end

The cylinder can be divided in three parts : a part with length L_0, which is wound with a constant winding angle α_0, and two end parts with length L_μ where winding with a constant slippage tendency is

applied (Fig. A.1). The winding angle changes in the end parts from α_0 to 90°. The length of the end parts is derived from Eq. (A.30) :

$$L_\mu = \frac{r}{2\lambda}\left[\left(\frac{1}{\tan\frac{\alpha_0}{2}} + \tan\frac{\alpha_0}{2}\right) - \left(\frac{1}{\tan 45°} + \tan 45°\right)\right] \quad (A.32)$$

$$= \frac{r}{2\lambda}\left[\frac{1}{\tan\frac{\alpha_0}{2}} + \tan\frac{\alpha_0}{2} - 2\right] \quad (A.33)$$

and the radial span of the end parts from Eq. (A.31) :

$$\Delta\theta_\mu = \frac{1}{\lambda}\left[\ln(\tan 45°) - \ln\left(\tan\frac{\alpha_0}{2}\right)\right] = -\frac{1}{\lambda}\ln\left(\tan\frac{\alpha_0}{2}\right) \quad (A.34)$$

The global span $\Delta\theta$ equals :

$$\Delta\theta = \Delta\theta_0 + 2\Delta\theta_\mu = \frac{L_0}{r}\tan\alpha_0 - \frac{2}{\lambda}\ln\left(\tan\frac{\alpha_0}{2}\right) \quad (A.35)$$

The slippage tendency $|\lambda| \leq \mu$ has to be selected in function of the winding strategy (cf. section 1.5.1.2). If the next winding circuit has to be adjacent to the previous winding circuit, the span $2\Delta\theta$ for one winding circuit (one fibre path at $+\alpha$ and one fibre path at $-\alpha$) equals :

$$2\Delta\theta = 2\pi n \pm \Delta\theta_w = 2\pi n \pm \frac{w}{r\cos\alpha} \quad (A.36)$$

with $\Delta\theta_w$ the span corresponding with the width of the fibre band.

Numerical example If the radius of the cylinder is 100 mm, the winding angle is 45° and the maximum coefficient of friction equals 0.2, then the minimum length of the end parts is 207 mm. So, if the constant length should be 1000 mm, a mandrel with a minimum length of 1414 mm is necessary, 40 % more than the useful length of the mandrel. Winding with return of the fibre path is only advisable for high winding angles, and relatively long mandrels.

A.2 Geodesics on a Developable Surface

A developable surface is a surface which can be developed in a plane, or, in other words, which is shaped from a plane without any in-plane forces. This surface can be seen as the mapping of a rectangular grid

without in-plane deformation of the grid. The following conditions are met :

$$\vec{s}_u \cdot \vec{s}_u = \vec{s}_v \cdot \vec{s}_v = 1 \tag{A.37}$$
$$\vec{s}_u \cdot \vec{s}_v = 0 \tag{A.38}$$

By derivation of these equations :

$$\frac{d(\vec{s}_u \cdot \vec{s}_u)}{du} = 2\vec{s}_u \cdot \vec{s}_{uu} = 0 \tag{A.39}$$
$$\frac{d(\vec{s}_u \cdot \vec{s}_u)}{dv} = 2\vec{s}_u \cdot \vec{s}_{uv} = 0 \tag{A.40}$$
$$\frac{d(\vec{s}_v \cdot \vec{s}_v)}{dv} = 2\vec{s}_v \cdot \vec{s}_{vv} = 0 \tag{A.41}$$
$$\frac{d(\vec{s}_v \cdot \vec{s}_v)}{dv} = 2\vec{s}_v \cdot \vec{s}_{vv} = 0 \tag{A.42}$$
$$\frac{d(\vec{s}_u \cdot \vec{s}_v)}{du} = \vec{s}_u \cdot \vec{s}_{uv} + \vec{s}_v \cdot \vec{s}_{uu} = \vec{s}_v \cdot \vec{s}_{uu} = 0 \tag{A.43}$$
$$\frac{d(\vec{s}_u \cdot \vec{s}_v)}{dv} = \vec{s}_v \cdot \vec{s}_{uv} + \vec{s}_u \cdot \vec{s}_{vv} = \vec{s}_u \cdot \vec{s}_{vv} = 0 \tag{A.44}$$

The geodesic is solved by solving the set of equations (3.12). This set of equations equals, after dropping the variables which are zero :

$$\frac{d\vec{t}}{ds} \cdot \vec{s}_u = \frac{d^2u}{ds^2} = 0 \tag{A.45}$$
$$\frac{d\vec{t}}{ds} \cdot \vec{s}_v = \frac{d^2v}{ds^2} = 0$$

Since both second order derivatives are zero, the geodesic on a developable surface is the image of a line in the developed surface.

A.3 Thickness of a Filament Wound Part

A.3.1 Thickness of a Tubelike Part

In a tubelike part the number of fibres in a cross section is always constant. If the spine direction of the surface $S(u, v)$ corresponds to the u-direction, and the circumferential direction to the v-parameter, the

fibre paths $\Gamma_i(s) = [u_i(s)\ v_i(s)]^T$, obtained by circumferential shifting of a basic fibre path $\Gamma_0(s) = [u_0(s)\ v_0(s)]^T$, are :

$$\begin{cases} u_i(s) &= u_0(s) \\ v_i(s) &= v_0(s) + \frac{iV}{n_p} \end{cases} \tag{A.46}$$

with V the total span in the v-direction and n_p the number of fibre paths in each cross section.

The distance d_v between two fibres, measured along a curve with constant v-parameter, equals :

$$d_v = \int_v^{v+\frac{V}{n_p}} \vec{s}_v(u,\nu)d\nu \approx \|\vec{s}_v\| \frac{V}{n_p} \tag{A.47}$$

The distance d_w, measured perpendicular to the fibre path, equals (with ζ_{tv} the angle between the tangent $\vec{t}$ and $\vec{s}_v$) :

$$d_w = d_v \sin\zeta_{tv} = \frac{V}{n_p}\sqrt{(\vec{s}_v \cdot \vec{s}_v)^2 - (\vec{t} \cdot \vec{s}_v)^2} \tag{A.48}$$

The thickness t_w of the wound pattern is inversely proportional with the distance between the fibres :

$$t_w = \frac{wt}{d_w} = \frac{n_p wt}{V\sqrt{(\vec{s}_v \cdot \vec{s}_v)^2 - (\vec{t} \cdot \vec{s}_v)^2}} \tag{A.49}$$

with t and w respectively the thickness and the width of the impregnated fibre bundle.

A.3.2 Thickness of a Surface of Revolution

For a surface of revolution is $\vec{s}_u$ always perpendicular to $\vec{s}_v$. The angle ζ_{tv} equals $\frac{\pi}{2} - \alpha$, with α the winding angle. The distance d_v equals $\frac{2\pi r}{n_p}$. The perpendicular distance between two fibres is then :

$$d_w = \frac{2\pi r}{n_p}\cos\alpha = \frac{2\pi}{n_p}\sqrt{r^2 - c_c^2} \tag{A.50}$$

The thickness :

$$t_w = \frac{n_p wt}{2\pi r\cos\alpha} = \frac{n_p wt}{2\pi\sqrt{r^2 - c_c^2}} \tag{A.51}$$

The most common filament wound part is, (apart from a cylinder) the pressure vessel. Most pressure vessels have two equal polar openings with a radius r_0 and a cylindrical part with radius r_u (Fig. A.2). The fibre path starts tangentially to the polar openings, perpendicular to the axis and the generatrix. Consequently, the starting winding angle equals 90°, or :

$$r_0 \sin 90° = r_0 = c_c \tag{A.52}$$

The winding angle in the cylindrical part is then, by combining (1.9) and (A.52) :

$$\alpha = \arcsin\left(\frac{r_0}{r_u}\right) \tag{A.53}$$

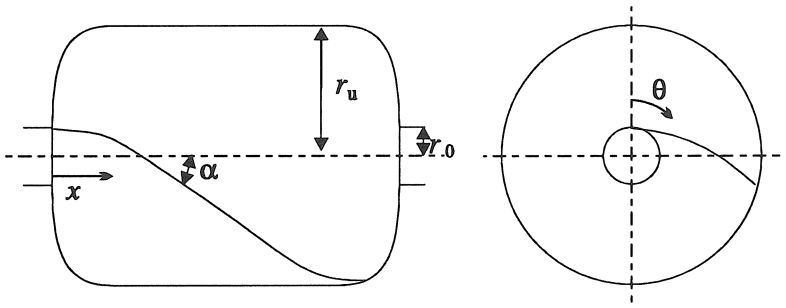

Figure A.2: Pressure vessel

The number of fibres n_p necessary to cover the complete mandrel with one layer equals according to Eq. (A.51) (with $t_w = t$ and $r = r_u$) :

$$n_p = \frac{2\pi}{w}\sqrt{r_u^2 - r_0^2} \tag{A.54}$$

The thickness of the part depends on the radius r. For one complete winding (i.e. one layer at $+\alpha$ and one layer at $-\alpha$) the thickness t_w of the wound part equals :

$$t_w = \frac{n_p w t}{\pi\sqrt{r^2 - r_0^2}} \tag{A.55}$$

The thickness increases with smaller radius. At the return radius the theoretical thickness is infinite.

Appendix B

Two-axis Filament Winding Machine

B.1 Design of the Machine

A small low-cost two-axis filament winding machine has been developed at PMA to wind axisymmetric parts with single rovings [59]. The first axis of this machine is the mandrel drive, the second an oscillating arm. The oscillating arm rotates in a vertical plane parallel to the winding axis (Fig. 1.21). A toroidal eyelet is mounted at the end of the arm. The length of the oscillating arm can be adjusted in function of the dimensions of the mandrel. The inertia of the arm is very small compared with the inertia of the carriage in a conventional cartesian filament winding machine, so that higher winding speeds can be obtained.

The machine is designed to wind axisymmetric parts, but in principle every asymmetric shape can be wound, provided that the fibre paths do not intersect the mandrel.

In the first design of the machine, the spindle rotates at a constant speed, and the oscillating arm is controlled as a slave of the spindle. In a second design, the velocities of both the spindle and the oscillating arm are computer controlled.

The spindle and the arm are controlled by a PC. An interface board has been developed by Liao [56] for the communication between a PC and one or two DC-motors. This interface board [56] sends signals to the motor amplifiers and reads the positions of the encoders. This

board converts, for both axes, the digital output signal of the control program on the PC with a 12-bit DAC into a voltage for the motor amplifier (Fig. B.1). The encoder signal is counted by a 16-bit TCTL-2000 - IC, and stored in a register which is read by the control program.

Data are sent under interrupt. Interrupts are generated at constant time intervals. The interrupt time Δt can be selected by the operator.

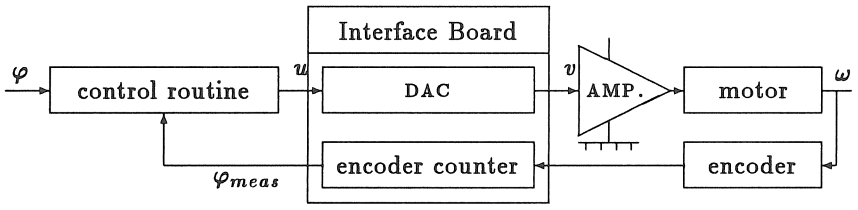

Figure B.1: Interface board

B.2 Calculation of the Fibre Path

A PC-program has been written for the calculation of geodesics on axisymmetric surfaces with a central mid-plane and return at the end domes [59]. Half the mandrel geometry is entered as a number of cylindrical, conical, toroidal and spherical surfaces. These surfaces are subdivided in a number of conical segments. A conical segment i is characterized by the starting radius r_{i-1}, the end radius r_i and the axial coordinates x_{i-1} and x_i of the starting and the end plane [59].

The geodesic starts at the end of the mandrel ($i = 0$) with a winding angle $\alpha_0 = 90°$. For each each x_i, the corresponding winding angle α_i and span θ_i are calculated. If the winding angle at x_{i-1} equals α_{i-1}, the winding angle at x_i equals, according to the equation of Clairaut (A.16) :

$$\alpha_i = \arcsin\left(\frac{r_{i-1}}{r_i}\sin\alpha_{i-1}\right) \tag{B.1}$$

The radial span θ_i equals, according to Eq. (A.25) :

$$\theta_i = \theta_{i-1} + (\alpha_{i-1} - \alpha_i)\sqrt{1 + \left(\frac{x_i - x_{i-1}}{r_i - r_{i-1}}\right)^2} \tag{B.2}$$

The tangent to the fibre path is given by Eq. (A.4).

B.3 Position of the Pay-Out Eye

The pay-out eye moves on a circle in the vertical plane[1] ${}_w y = y_0$, with as centre c : ${}_w\mathbf{c} = [x_0 \quad y_0 \quad z_0]^T$ and as radius r_a. The position of the delivery point e is given by (Fig. B.2) :

$$ {}_w\mathbf{e} = \begin{bmatrix} 1 & 0 & 0 \\ 0 & \cos\varphi & -\sin\varphi \\ 0 & \sin\varphi & \cos\varphi \end{bmatrix} \begin{bmatrix} {}_m p_x + l_f\ {}_m t_x \\ {}_m p_y + l_f\ {}_m t_y \\ {}_m p_z + l_f\ {}_m t_z \end{bmatrix} = \begin{bmatrix} x_0 + r_a \sin\psi \\ y_0 \\ z_0 + r_a \cos\psi \end{bmatrix} \tag{B.3} $$

or :

$$ {}_m p_x + l_f\ {}_m t_x = x_0 + r_a \sin\psi \tag{B.4} $$

$$ ({}_m p_y + l_f\ {}_m t_y)\cos\varphi - ({}_m p_z + l_f\ {}_m t_z)\sin\varphi = y_0 \tag{B.5} $$

$$ ({}_m p_y + l_f\ {}_m t_y)\sin\varphi + ({}_m p_z + l_f\ {}_m t_z)\cos\varphi = z_0 + r_a \cos\psi \tag{B.6} $$

with φ the rotation of the mandrel and ψ the rotation of the arm.

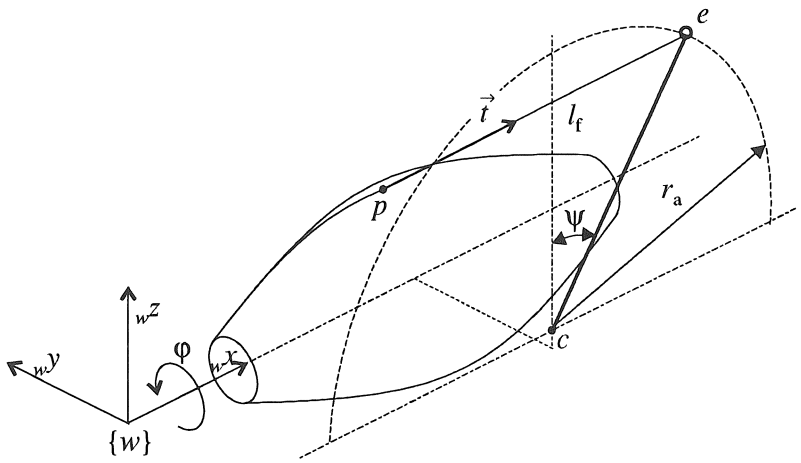

Figure B.2: Position of the pay-out eye in the two-axis machine

By summing the squares of (B.5) and (B.6) and replacing $r_a \cos\psi = \sqrt{r_a^2 - r_a^2 \sin^2\psi}$ by (B.4), and squaring the result, a fourth order equation in l_f is obtained, which is solved iteratively. The angle ψ is obtained from Eq. (B.4) and φ from Eq. (*B*.5).

[1] The prefix w refers to the winding coordinate system $\{w\}$ (cf. section 2.4.2)

Another solution is to propose a value for φ and to calculate the value of l_f with Eq. (B.5). The distance between the new position of the delivery point and the centre of the arm circle is calculated, and the angle φ adapted until a solution is found [59].

The angles of the winding axis φ and the oscillating arm ψ are stored in a table. This table gives the angle ψ of the oscillating arm at equidistant angles φ of the winding axis. The table is smoothed to avoid abrupt variations in the motion of the arm [80], which are caused by the discontinuities between the conical segments [17].

B.4 Pay-Out Eye Trajectory

The generation of the trajectory depends on the machine. In the first design, the spindle rotates at a constant speed, and the arm is computer controlled. In the second design both spindle and arm are computer controlled.

The PC sends data to the axes to be controlled at constant time intervals.

B.4.1 Constant Spindle Speed

The control is performed by a PC under interrupt. The encoders of spindle and arm are read at constant time intervals (e.g. 6 ms). The next spindle position is determined, assuming that the speed of the spindle remains constant. The corresponding position of the oscillating arm is determined by linear interpolation in the table. The control of the oscillating arm is based on a combination of position feedforward and P-I feedback control.

The sign of the angle ψ is changed for the return path.

B.4.2 Variable Spindle Speed

If the speed of the spindle is constant, high accelerations occur in the oscillating arm and fibre feed in zones where the mandrel geometry changes suddenly. These accelerations can be decreased by the application of a variable spindle speed. The calculation of the trajectory is then similar to the calculation of the trajectory for the robotic winding cell (cf. section 5.3).

Two files are generated, which contain the positions of the spindle and the arm at constant time intervals, taking the limitations of accelerations and velocities into account. The starting file contains the data for the first winding circuit, the regime file contains the data for the next winding circuits. The velocity at the end of the starting file corresponds to the velocity at the start and at the end of the regime file.

The application of a variable spindle speed allows to obtain higher winding speeds. As an example, the times necessary to wind one fibre path are given [17] :

	Pressure vessel	Spinning pot
Constant spindle speed	8.70 s	77.54 s
Variable spindle speed	1.91 s	10.08 s

B.5 Control of the Two-axis Machine

The control of the axes is based on position-feedforward, combined with feedback control (Fig. B.3). The purpose of the feedforward control is to reduce tracking errors, based on a knowledge of the system dynamics and the desired output trajectory [22]. The feedforward control is based on an estimation of the system's transfer function and does not take the actual position of the axes into account. The errors, which occur due to errors in the model and noise, are minimized by means of a feedback control. The output signal u of the control program is the sum of the feedforward signal u_{ff} and the feedback signal u_{fb}.

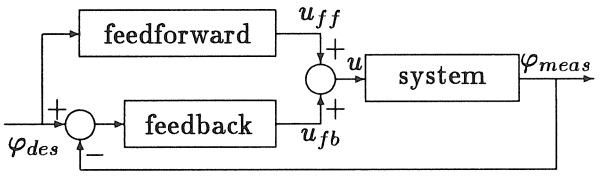

Figure B.3: Control of the two-axis machine

B.5.1 Feedforward Control

As feedforward control, the inverse dynamic model of the system, which has to be controlled, is taken. The input of the system is the output signal from the control program u_{ff}, the output is the position φ_{meas}, as measured by the encoder counters. The system has an internal velocity feedback loop by the tachogenerator.

The transfer function of the system $\frac{\Phi(s)}{U(s)} = H(s)$ consists of three parts : the transfer function $H_1(s)$ from the DAC, the transfer function $H_2(s)$ between the output voltage and the velocity of the axis, and the transfer function $H_3(s)$, which relates the velocity to the encoder position.

The frequency response function $H_2(j\omega)$ has been measured with the Data Harvester [102]. The Data Harvester sends a sinusoidal voltage to the system. Comparison of the input and the output signal gives the amplitude and the phase at the signal's frequency. The signal from the Data Harvester is inputted to the motor amplifier, the output signal is the signal returned by the tachogenerator [17]. Fig. B.4 shows the Nyquist plot for the spindle.

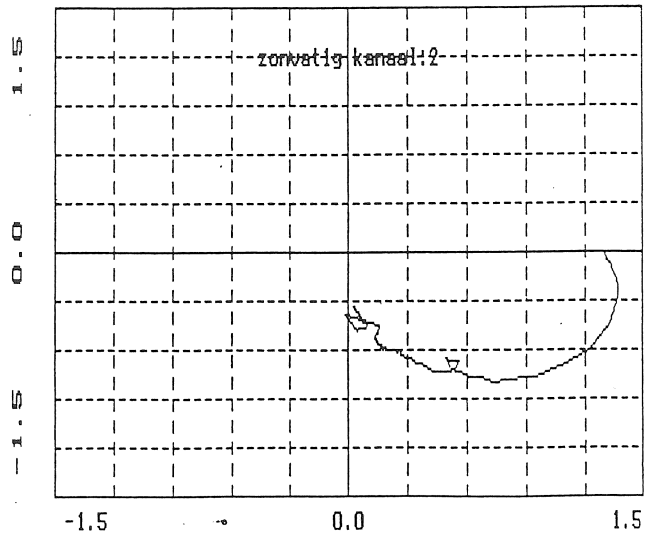

Figure B.4: Nyquist plot for the spindle [17]

The Nyquist plot for the spindle describes a quarter of a circle in the fourth quadrant. This corresponds to the Nyquist plot of a linear

system with one time constant. For the arm motor, a similar result is obtained [17] :

$$H_2(s) = \frac{A_2}{\tau s + 1} \tag{B.7}$$

The global transfer function $H(s)$ in the continuous time domain is :

$$H(s) = H_1(s)H_2(s)H_3(s) = A_1 \frac{A_2}{(\tau s + 1)} \frac{1}{s} = \frac{A}{s(\tau s + 1)} \tag{B.8}$$

The gain A is determined by measuring the static relation between the signal y sent to the DAC and the velocity $w_{calc} = \frac{\Delta\varphi_{meas}}{T}$. The time constant τ is derived from the phase plot, from the frequency where the phase equals $-45°$ ($\tau = \frac{1}{2\pi f_{45}}$) [104]. The results are [17] :

	τ (ms)	A
Spindle	6.6	97.7
Arm	1.8	98.1

The transfer function is transformed from the Laplace domain to the discrete z-domain [32] :

$$H(z) = \frac{A\Delta t z(1 - e^{-\frac{\Delta t}{\tau}})}{(z - e^{-\frac{\Delta t}{\tau}})(z - 1)} \tag{B.9}$$

with Δt the sampling (or interrupt) time.

The inverse of the transfer function is used for the feedforward control :

$$H^{-1}(z) = \frac{U_{ff}(z)}{\Phi(z)} = \frac{(z - e^{-\frac{\Delta t}{\tau}})(z - 1)}{A\Delta t z(1 - e^{-\frac{\Delta t}{\tau}})} \tag{B.10}$$

Replacing the z-variable by q, the forward shift operator ($qy(k) = y(k + 1)$), yields :

$$H^{-1}(q) = \frac{q^2 - (1 + e^{-\frac{\Delta t}{\tau}})q + e^{-\frac{\Delta t}{\tau}}}{At_s(1 - e^{-\frac{\Delta t}{\tau}})q} = \frac{u_{ff}(k)}{\varphi(k)} \tag{B.11}$$

or :

$$At_s(1 - e^{-\frac{\Delta t}{\tau}})u_{ff}(k) = q\varphi(k) - (1 + e^{-\frac{\Delta t}{\tau}})\varphi(k) + q^{-1}e^{-\frac{\Delta t}{\tau}} \tag{B.12}$$

The following recursive relation can be derived :

$$u_{ff}(k) = b(\varphi(k + 1) + a_0\varphi(k) + a_1\varphi(k - 1)) \tag{B.13}$$

with :

$$\begin{aligned} a_0 &= -(1+e^{-\frac{\Delta t}{\tau}}) \\ a_1 &= e^{-\frac{\Delta t}{\tau}} \\ b &= \frac{1}{A\Delta t(1-e^{-\frac{\Delta t}{\tau}})} \end{aligned}$$

The value of A is slightly adapted in function of the linearly increasing error during pure feedforward control [17].

If the sample time Δt equals 6 ms, the variables are :

	Spindle	Arm
a_0	-1.403	-1.036
a_1	0.403	0.036
b	0.00284	0.00176

B.5.2 Feedback Control

A proportional-plus-integral control is selected. A discrete equivalent of the PI-control is [17] :

$$u_{fb}(k) = k_p \left(e(k) + \frac{1}{\tau_i} \sum_{j=0}^{k} \Delta t e(j) \right) \tag{B.14}$$

with $e(k) = \varphi_{des}(k) - \varphi_{meas}(k)$ the error between the measured and the desired angle. The proportional gain is inversely proportional to the sampling time Δt. Eq. (B.14) can then be written as :

$$u_{fb}(k) = u_{fb}(k-1) + k_p(e(k) - e(k-1)) + \frac{k_p \Delta t}{\tau_i} e(k) \tag{B.15}$$

The values of k_p and τ_i are determined experimentally :

	k_p (ms/ms)	τ_i (ms)
Spindle	$8/\Delta t$	105
Arm	$8/\Delta t$	115

The control has been tested during the winding of pressure vessels and spinning pots (Fig. B.5). For the spindle the maximum error is $4'$ (17 encoder pulses[2]) for the pressure vessel and $9'$ (41 encoder pulses)

[2]The conversion factors are : 97400 encoder pulses per revolution for the spindle and 60680 encoder pulses per revolution for the arm

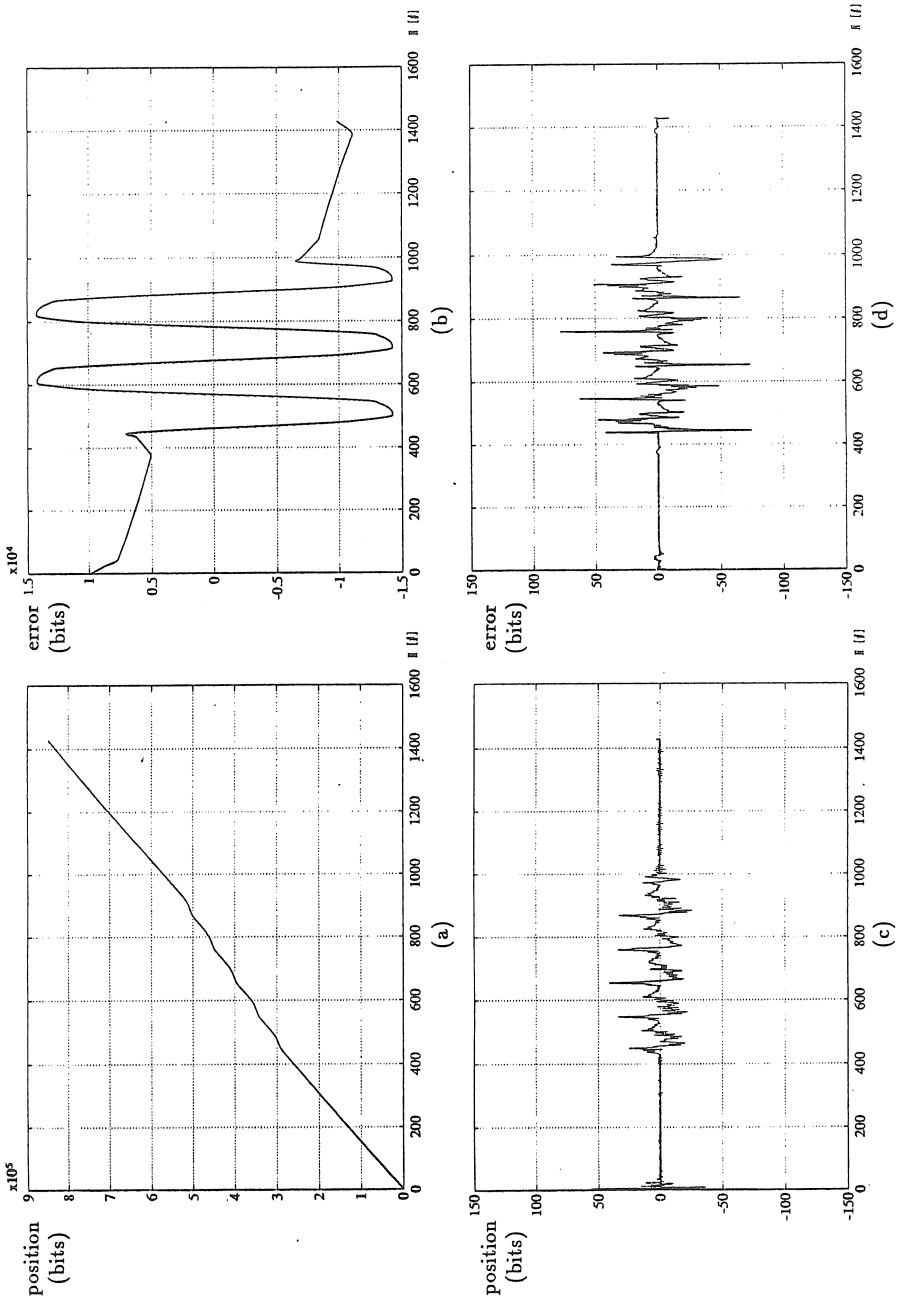

Figure B.5: Accuracy of the control of the two-axes winding machine for the winding of a spinning pot

(a) Trajectory spindle (b) Trajectory arm

(c) Error spindle (d) Error arm

for the spinning pot. For the arm the maximum error is 2'30" (7 encoder pulses) for the pressure vessel and 28' (78 encoder pulses) for the spinning pot. This large error is due to sudden direction changes in the motion of the oscillating arm [17].

B.5.3 Control of the Robotic Winding Cell

The control of the external axes (winding axis and pay-out eye axis) in the robotic cell is similar to the control of the axes of the two-axis filament winding machine. The major difference is that the interrupt time is fixed at 28.8 ms.

The frequency response of the pay-out eye motor cannot be measured in the same way as discussed in the previous section, since this motor does not have a tachogenerator.

The variables for the control of the winding axis are derived from the results in the previous section :

a_0	-1.012
a_1	0.012
b	0.000360
k_p	0.278

Due to the large cycle time, no integration is used.

KATHOLIEKE UNIVERSITEIT LEUVEN
FACULTEIT DER TOEGEPASTE WETENSCHAPPEN
DEPARTEMENT WERKTUIGKUNDE
AFDELING PRODUKTIETECHNIEKEN,
MACHINEBOUW EN AUTOMATISERING
Celestijnenlaan 300B - B-3001 Leuven (Heverlee), Belgium

ROBOTIC FILAMENT WINDING OF ASYMMETRIC COMPOSITE PARTS

Promotor :
Prof.dr.ir. H. VAN BRUSSEL

Proefschrift voorgedragen tot
het behalen van het doctoraat
in de toegepaste wetenschappen

door

Johan Scholliers

92D5 December 1992

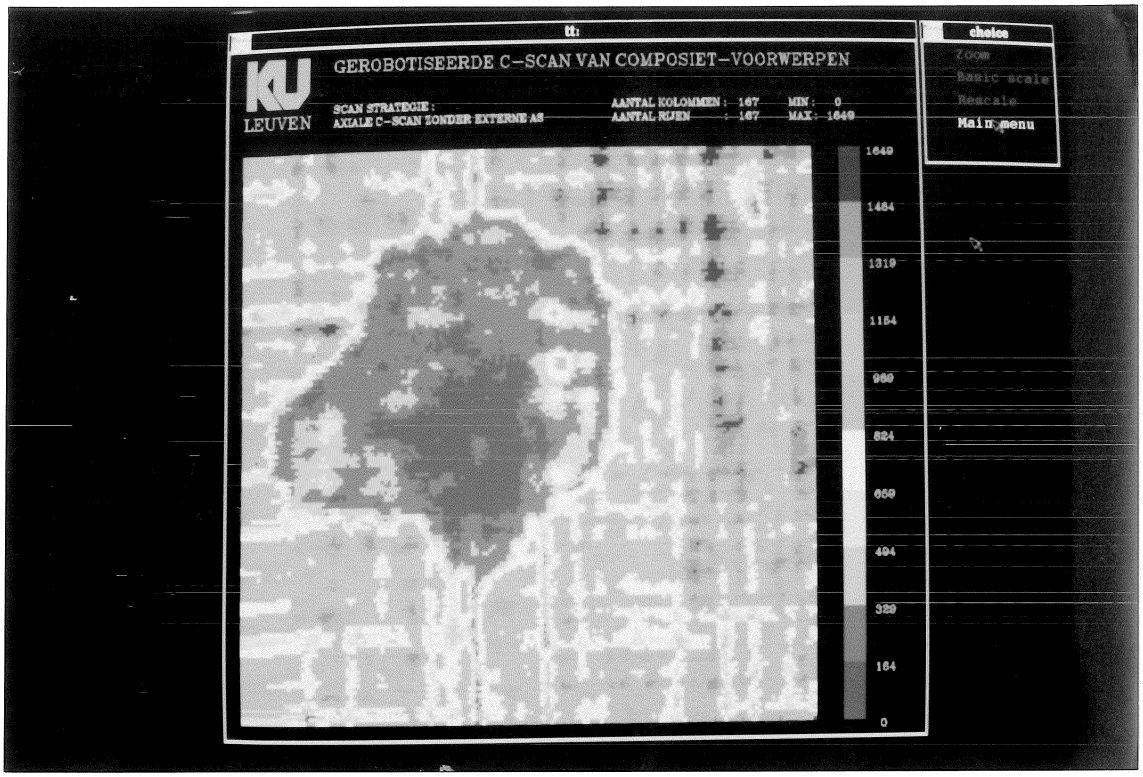

Figure 2.19: Colour plot of impacted plate [105]

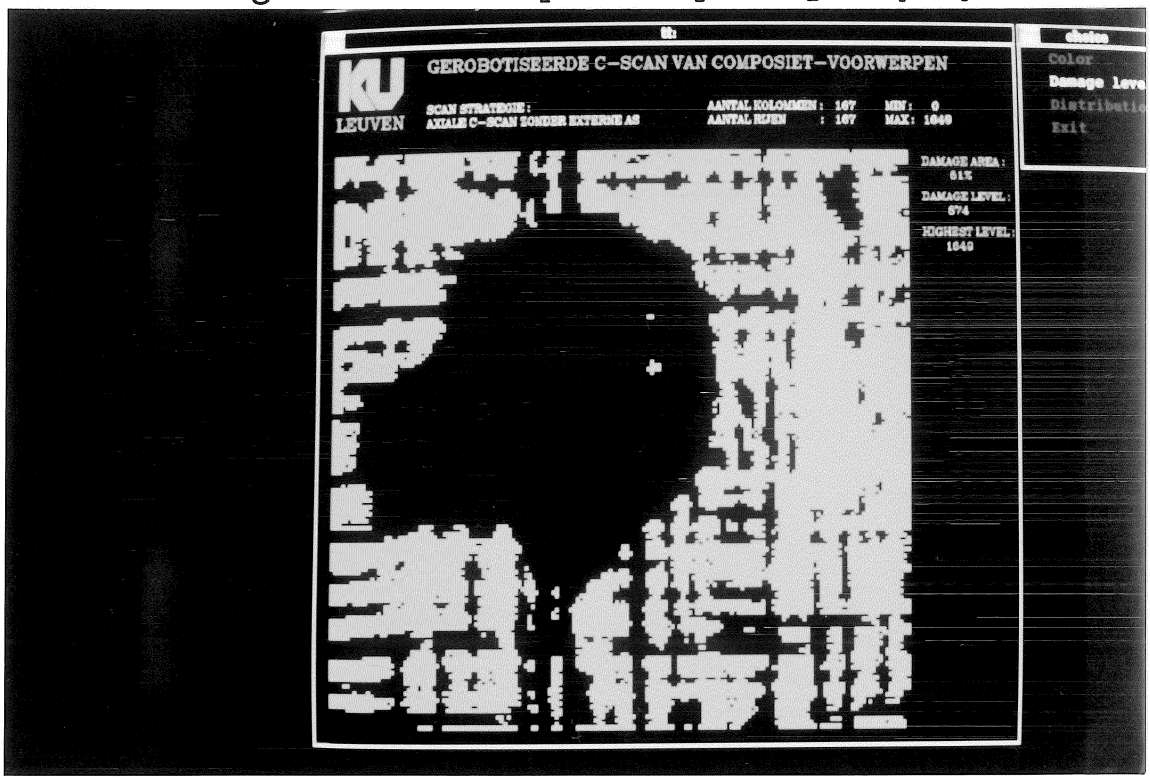

Figure 2.20: Damage level plot of impacted plate [105]

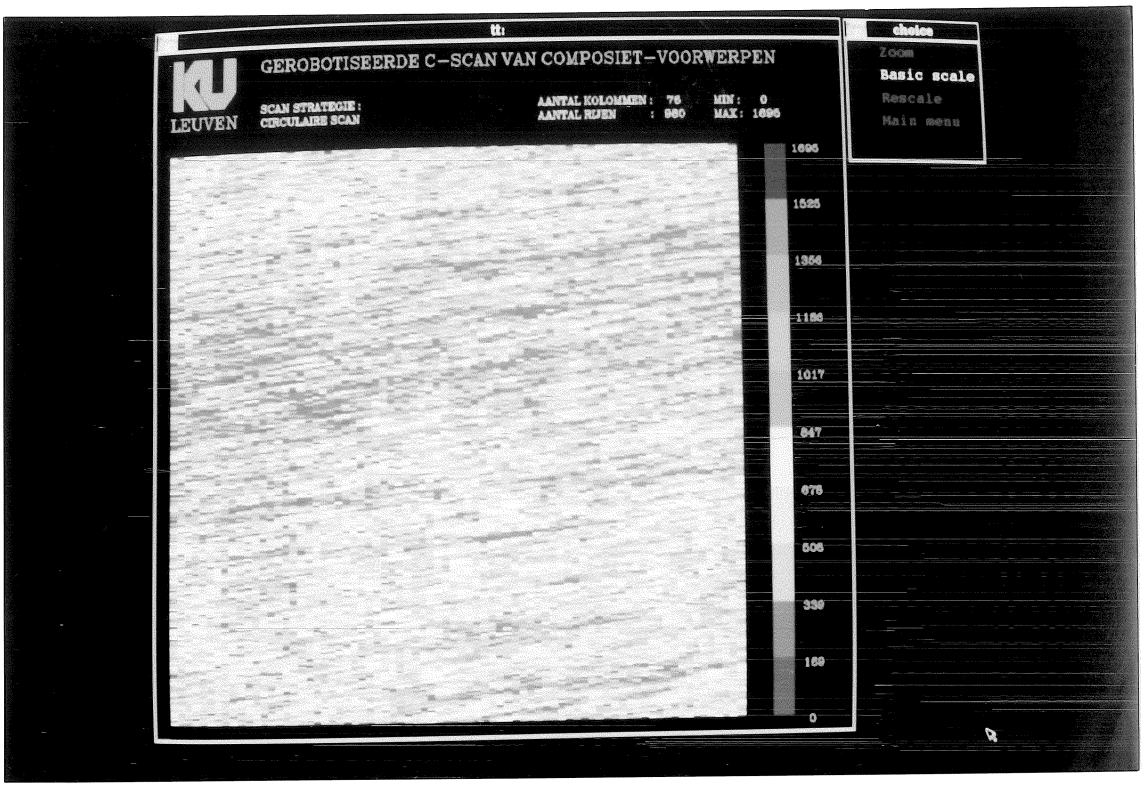

Figure 2.21: Colour plot of wound cylinder [105]

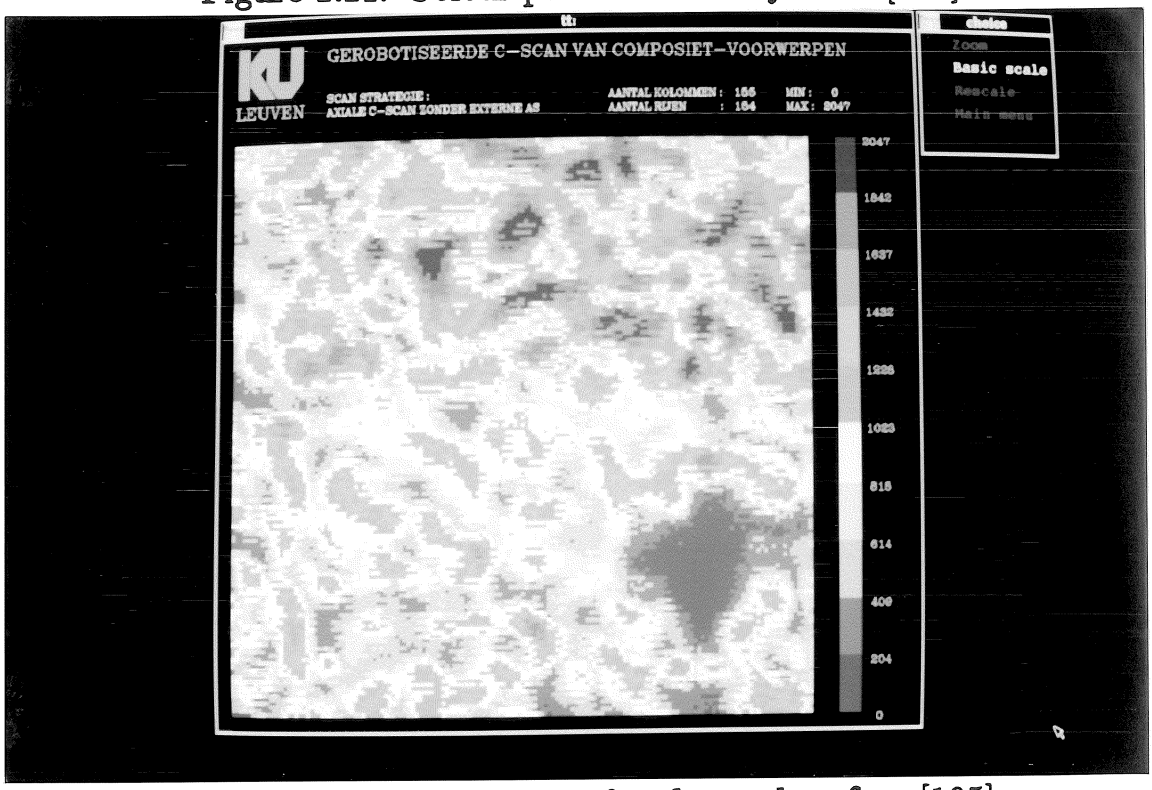

Figure 2.22: Colour plot of sculptured surface [105]

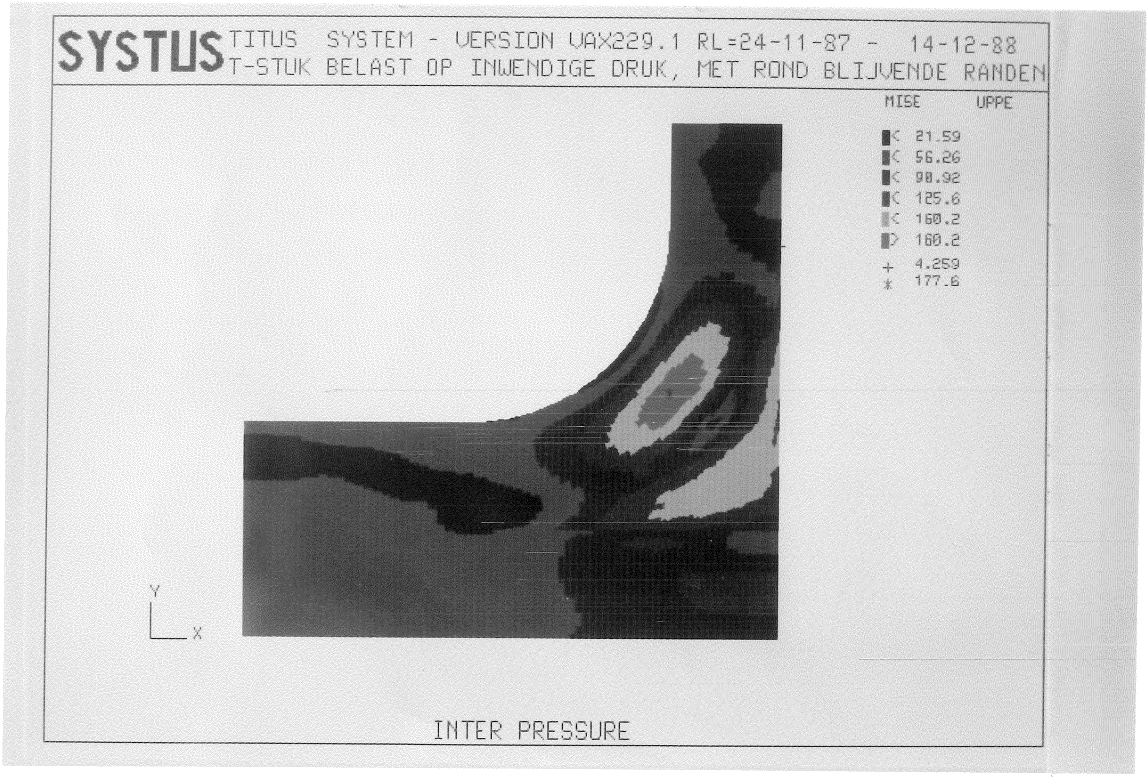

Figure 3.14: Von Mises stresses in a quarter of the T-piece, loaded with a 1 MPa internal pressure (clamped end sections)[59]

3.3.3.3 Trajectory Maps

Trajectory maps are generated for the lower edge of cylinder 6 and the right edge of cylinder 1 as starting curve. Fig. 3.15 shows a trajectory map with the lower edge of the vertical cylinder 6 as a starting curve. Geodesics are calculated for different combinations of starting positions and winding angles. The starting position needs only to be varied over a quarter of the complete circumference, due to the symmetry planes of the T-piece. The geodesics are represented by their surface sequence (cf. Table 3.1) If fibre bridging occurs, the geodesic must be excluded and its symbol in Fig. 3.15 is shaded. Three main families of trajectory types can be distinguished (Fig. 3.16) :

- The trajectory types K,L (surface sequence : 6 4 (7 2) 1 – Fig. 3.16a) and U,V (6 4 7 5 (8 2) 3 – Fig. 3.16b), that start at cylinder 6, and follow the inner ring of one of the torus segments towards the cylinder 1 or 3. Fibre bridging occurs in most of these geodesics.